Investigating the Origins of IgG1 Pan-Neurofascin Antibodies in a Severe Subtype of Autoimmune Neuropathy

Claire Elizabeth Bergstrom Johnson, BS

A thesis submitted for the degree of Doctor of Philosophy

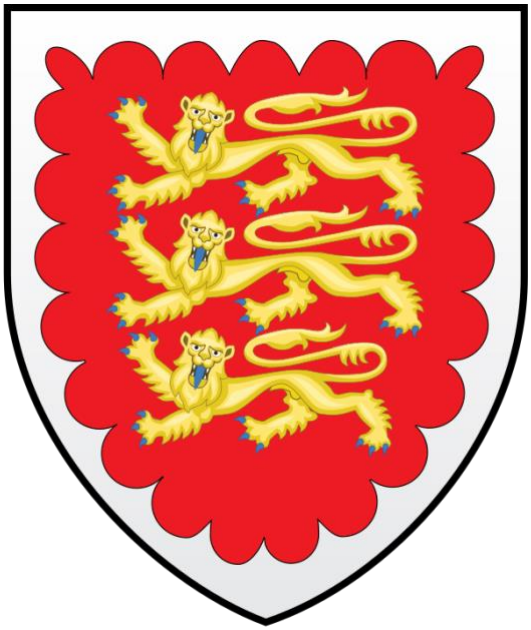

Oriel College

University of Oxford

Trinity Term 2025

“The struggle is nature’s way of strengthening it.”

- John Locke

“The Moth”
Season 1, Episode 7
Lost

Abstract

Investigating the origins of IgG1 pan-neurofascin antibodies in a severe subtype of autoimmune neuropathy by Claire Elizabeth Bergstrom Johnson, Oriel College, a thesis submitted for the degree of Doctor of Philosophy, Trinity Term 2025.

IgG1 pan-neurofascin autoimmune nodopathy (pan-NF AN) is a rare and fulminant form of autoimmune neuropathy characterised by IgG1 antibodies targeting both neurofascin-155 (NF155) and neurofascin-186 (NF186), often resulting in severe sensorimotor and autonomic involvement, and poor responses to standard immunotherapies. While B-cell depletion therapy can lead to improvement, relapse and long-term disability remain common, underscoring the need to better understand the origins and regulation of the autoreactive B-cell responses in this disease.

In this thesis, I developed and applied a suite of immunological tools to dissect the neurofascin-specific B-cell response in pan-NF AN. A peripheral blood mononuclear cell (PBMC) culture system was optimised to induce robust immunoglobulin secretion, enabling the isolation, screening, and B-cell receptor (BCR) sequencing of 480 single $CD27^{+}IgD^{-}$ memory B cells from a patient with severe pan-NF AN. Neurofascin reactivity was detected in 16 wells (3.3%); unexpectedly, IgM-secreting clones outnumbered IgG by approximately four to one. Recombinant monoclonal antibodies generated from three autoreactive clones confirmed stronger antigen binding when expressed as IgM compared to IgG1, despite identical variable regions. These results suggest that the multivalency of IgM may compensate for lower intrinsic affinity. Sequencing revealed minimal somatic hypermutation in the IgG-expressing autoreactive clones despite their memory surface phenotype, suggesting that autoreactive B cells may emerge via extrafollicular or germinal centre-independent pathways.

Evidence of dual IgM and IgG transcript expression in some autoreactive clones, together with the post hoc detection of serum IgM autoantibodies in all 13 IgG1 pan-NF AN patients screened, supports the hypothesis that IgM-class autoreactivity is a generalisable and previously unrecognised feature of the disease. To facilitate future investigation and clinical translation, biotinylated antigen “bait” tetramers were developed for NF155 and NF186, capable of binding patient autoantibodies and will enable future antigen-specific B-cell enrichment.

Together, these findings support a model in which both central and peripheral tolerance defects contribute to the generation of neurofascin-reactive B cells in IgG1 pan-NF AN, with early IgM responses giving rise to class-switched IgG via limited or non-canonical pathways. The characterisation of an IgM component has implications for diagnosis and therapy, providing a rationale for isotype-inclusive testing and antigen-specific therapeutic targeting of autoreactive B cells in pan-NF AN.

Acknowledgements

First, I would like to acknowledge and thank my twin sister, Maegan, without whom I wouldn't be at Oxford in the first place, conducting this research and writing this thesis. I remember, just barely, when you were first diagnosed with CIDP and how scary it was for all of us. But you fought for your life and have always been the best friend I've never taken for granted. As you gave up your entire childhood, adolescence, and teens battling CIDP and its aftermath – including cancer – it was your tenacity and relentless curiosity about what was going on biologically that inspired me to dedicate my career to inflammatory neuropathy research. I know you didn't have much of a choice – but I want you to know that your sacrifice was not in vain. You've inspired an entire career aimed at preventing even one patient, one family, from going through what we did. Thank you also to my older sister, Rachael, for fiercely loving and protecting me. Both of you have always been my biggest cheerleaders – just a phone call away, ready to offer love and support without judgement, no matter what. I love you, and I couldn't have done this without either of you.

To my supervisors – Dr Simon Rinaldi, Dr Alexander Davies, and Dr Sarosh Irani – thank you. Over the past four years, you have each challenged me to grow, to level up, and to become someone I barely recognise from the rather intimidated new DPhil student who joined in late 2021. Each of you have met me with a kind of kindness, appreciation, and insight that was, at the time, unfamiliar in academia – but has since become my norm.

Sarosh, though we only worked near one another for a year before you moved to Mayo, your belief in me and encouragement (even before we'd met!) meant more than I can say. Thank you for your continued support.

Alex, as the sole postdoc (and soon-to-be UKRI Future Leaders Fellow!) in Simon's lab when I joined, you took me under your wing, patiently answering countless questions and guiding me through the many early mistakes. Since then, you've been a thoughtful and generous mentor – always asking the right questions, never making me feel like I couldn't ask the wrong ones (which do exist, and of which I still have many).

Simon, you believed in me at a time when few others did, when I was applying in 2021/21, still shaken by over 10 PhD rejections three years prior. Your belief made the difference. You endured my endless chasing after funding (I still suspect this is how I won a Clarendon – you were all too tired of me pestering you and pulled strings just to get me off your back!). Your supervisory style has made me a more independent, stubbornly persistent scientist. You encouraged me to think for myself, speak up and share ideas, become a confident presenter of my work, and explore new horizons. You also (re-?)introduced me to my chaotic side – reminding me that things don't have to be

perfect, that no one is perfect, and that life is to be enjoyed, with surprises around every corner when you dare to just go for it. At the risk of sounding dramatic, I would say you have fundamentally changed me – but let's keep it to a British "not bad." Thank you.

To others in the lab who've supported me:

Dr Mateusz Makuch – thank you for all your help with flow cytometry, sorting, sequencing, and for your steady moral support when I needed it most. You are one of the most knowledgeable scientists I know, and your calm, kind presence has been an anchor throughout this DPhil. I look forward to working more with you.

Dr Bo Sun and Dr Sofija Paneva – thank you for your many insights into B-cell work and for saving me more than once with reagents and technical help. Thanks, in particular, also goes to Dr Sun for your help in making the large-scale antigen baits possible (as well as Mr Andrew Fower) and generously helping me with endless troubleshooting.

To my lab mates in the Rinaldi group – Janev, Roberto, Mariya, Luana, Nicolas – thank you. Not just for the professional support, but for being there personally. You've given me space to process thoughts, frustrations, and hopes, always with kindness and generosity. It's rare to build a lab family like this, and I look forward to working (and dancing!) with each of you in one way or another for years to come. To the broader Bennett group, thank you for patiently listening to me go on about B cells and autoantibodies for four years and supporting me professionally and morally at the bench and TC hood. Your support has meant the world.

To my dear friends outside the lab – particularly Idalien, Clara, Ellen, and Saheli – thank you for listening, celebrating, crying, and simply loving me through it all. I'm so grateful for you.

Finally, to my parents and family – thank you for your unwavering support on what has been a long, winding academic journey. It has not been a straight path, and I've faced many, many doubts. But whatever I've chosen to pursue, you have always stood by me with good questions and unconditional love. You fostered in me a love for learning and a singular persistence and grit that has truly made this DPhil possible. You knew nearly a decade ago that I wouldn't be returning to the US for my career, and though I know you'd love me to be closer (and I'd love that sometimes too), you have never made me feel guilty for following my passions, wherever they may take me. I love you.

Und zu guter Letzt: Danke, Gregor. Ich bin mir nicht sicher, ob sich das perfekt übersetzen lässt, aber lass es uns versuchen. Du warst einer der ersten Menschen, die ich in Oxford kennengelernt habe, und ich fühlte mich sofort irgendwie zu Hause. Ich habe mich noch nie so wohl gefühlt, ich selbst zu sein, zusammenzubrechen, einfach *mit* jemandem zusammen zu sein, ohne Vorurteile und ohne Angst. Du hast die erstaunliche

Fähigkeit, mich über den dümmsten, seltsamsten Scheiß zum Lachen zu bringen, mehr als jeder andere, den ich je getroffen habe, und das macht mich glücklich. Du hältst mich, wenn ich glücklich, müde, oder verängstigt bin. Wir haben nicht immer gewusst, wie wir am besten miteinander kommunizieren, aber du hast nie aufgehört, mich zu lieben, auch wenn ich deine Gnade wahrscheinlich nicht verdient habe. Du hast mich gerettet, als ich zu ertrinken drohte – und das mehrfach – und hast mich in einigen der schwierigsten Phasen meines Lebens über Wasser gehalten. Das werde ich nie vergessen. Du hast so viel Talent, Intelligenz und Ehrgeiz, aber nichts davon zählt ohne deine Freundlichkeit. Bitte verliere nie das, was dich ausmacht, dich selbst. Egal, was passiert, für den Rest meines Lebens wirst du für mich immer so wertvoll sein.

Table of Contents

Abstract 3

Acknowledgements 4

Table of Contents 7

List of Figures 11

List of Tables 16

Abbreviations 18

1 Introduction 23

1.1 Autoimmune inflammatory neuropathies 24

1.2 Immunoglobulins in health and disease 29

1.3 B cells and humoral immunity 35

1.4 Immune tolerance and autoimmunity 45

1.5 Pan-neurofascin autoimmune nodopathy 50

1.6 Summary and aims 54

2 Methods 56

2.1 Participants 56

2.2 Solutions 59

2.3 PBMC processing 72

2.4 PBMC cultures 73

2.5 ELISAs 76

2.6 Plasmid midi prep 80

2.7 Live CBA 82

2.8 Flow cytometry 88

2.9 FACS 91

2.10 B-cell receptor complementary DNA synthesis and amplification of variable domain heavy and light chain sequences 95

2.11 Twist Bioscience cloning and mAb production 110

2.12 Antigen bait production 111

3 Development and Optimisation of PBMC Cultures for *In Vitro* Antibody Production 130

3.1 Introduction and rationale 130

3.2 Initial healthy control PBMC culture trials 131

3.3 ASC generation in culture and its relationship to IgG output 143

3.4 Flow cytometry development and bulk sorting experiments 154

3.5 Discussion and limitations 166

3.6 Summary and future directions 182

4 Single-Cell Sorting and Sequencing to Isolate Rare Pan-Neurofascin-Reactive Clones 187

4.1 Introduction 187

4.2 Experimental overview 188

4.3 Antibody production in bulk cultures 191

4.4 Single-cell cultures and antibody production 196

4.5 Single-cell sequencing and monoclonal antibody production 200

4.6 Discovery of predominant IgM reactivity 204

4.7 Functional characterisation of IgM monoclonal antibodies 209

4.8 IgM screen of pan-NF^+ and $CNTN1^+$ AN patients 214

4.9 Summary and interpretation of findings 215

5 Development of NF155 and NF186 Antigen Baits for Enrichment of Pan-Neurofascin-Reactive B Cells 227

5.1 Introduction 227

5.2 Antigen bait approach, design, and plasmid production 229

5.3 Proof-of-concept small-scale production of antigen baits 232

5.4 Large-scale production of antigen baits 254

5.5 Tetramerisation of large-scale antigen baits 261

5.6 Discussion and limitations 266

5.7 Summary and future directions 271

6 Discussion 273

6.1 Overview of key findings 273

6.2 Mechanisms of tolerance failure and B-cell origins 275

6.3 The role of autoantibody isotype and subclass 277

6.4 Technical and methodological considerations 283

6.5 Clinical and scientific implications 286

6.6 Future directions 292

7 Conclusion 296

8 Appendix 299

8.1 List of primers 299

8.2 Cloning vector sequences 303

8.3 Antigen bait sequences 304

8.4 Antigen bait tetramerisation protocol 309

Reference List 310

List of Figures

Figure 1: Structure, sub-regions, and molecular landscape of the node of Ranvier 23

Figure 2: Immunoglobulin (antibody) structure schematic 29

Figure 3: Structural diversity of human IgG subclasses 34

Figure 4: B-cell development, maturation, and tolerance checkpoints 37

Figure 5: Pathogenic mechanisms of NF155 and NF186 antibodies 53

Figure 6: Schematic overview of the experimental workflow utilised in this thesis. 55

Figure 7: Culture strategy for PBMCs 74

Figure 8: ASC/plasmablast gating strategy 91

Figure 9: Bulk sort gating strategy used to bulk sort PBMCs 94

Figure 10: B-cell receptor (BCR) sequencing pipeline for mAb production 95

Figure 11: NF155 and NF186 antigen bait constructs 112

Figure 12: Dose-dependent increase in total IgG production with increasing PBMC seeding density, but no enhancement from additional pro-inflammatory cytokines 133

Figure 13: Effect of sCD40L addition and extended culture duration on total IgG production in healthy control PBMCs 135

Figure 14: Addition of TNFα and IFNγ does not enhance total IgG production in PBMC cultures, but extension of culture duration from 6 to 14 days does 137

Figure 15: Total IgG production across three healthy donors after 14 days of culture with R848, IL-2, and sCD40L in scBCM 139

Figure 16: Total IgG production from stimulated and unstimulated 14-day PBMC cultures in patients with autoimmune nodopathy and a healthy control 142

Figure 17: Initial testing of fluorophore panel for ASC identification at baseline 145

Figure 18: In vitro ASC generation and cumulative IgG secretion in healthy donor PBMC cultures 146
Figure 19: Stimulation-dependent ASC differentiation in healthy control PBMC cultures over time 147
Figure 20: Correlation between ASC frequency and total IgG production in vitro in healthy donor PBMC cultures 149
Figure 21: CD38 PE fails to fully resolve $CD27^{++}CD38^{++}$ ASCs from $CD38^{intermediate}$ B cells after stimulation 151
Figure 22: CD38 PE-Cy7 enables clearer separation of $CD27^{++}CD38^{++}$ ASCs following stimulation 152
Figure 23: Flow cytometry gating strategy for subset sorting of PBMCs from an $NF155^{+}$ AN patient 158
Figure 24: Immunoglobulin secretion from FACS-isolated memory B-cell subsets cultured at varying input densities 160
Figure 25: Impact of enhanced cytokine stimulation on total IgG production by sorted B-cell subsets from a healthy donor 164
Figure 26: Total IgM production by sorted B-cell subsets from a healthy donor cultured under standard versus enhanced stimulation conditions 165
Figure 27: Donor-to-donor variability in total IgG production from stimulated PBMC cultures 171
Figure 28: Summary of factors tested and the main findings at each stage of the iterative PBMC bulk unsorted culture refinement process 182
Figure 29: Relative frequencies of canonical B-cell subpopulations among $CD19^{+}$ B cells sorted from peripheral blood of individual donors 190

Figure 30: Total IgG production in 14-day cultures of bulk unsorted PBMCs from a pan-NF^{+} and CASPR2^{+} patient 192
Figure 31: Total IgG production in 14-day bulk sorted PBMC cultures from pan-NF^{+} and CASPR2^{+} patients 194
Figure 32: Total IgG production and antigen-specific IgG detection in bulk-sorted B-cell subpopulations from a pan-NF^{+} patient following 14-day stimulation..... 196
Figure 33: Total IgG production in CASPR2^{+} single-cell cultures 197
Figure 34: CBA screening for antigen-specific IgG in CASPR2^{+} single-cell cultures 197
Figure 35: Heat maps showing total IgG production from five 96-well plates of CD27^{+}IgD$^{–}$ memory B cells single-sorted from a pan-NF^{+} patient..... 198
Figure 36: CBA images of three CD27^{+}IgD^{-} single memory B-cell clones from a pan-NF AN patient showing antigen-specific IgG reactivity to neurofascin isoforms 199
Figure 37: Total IgG ELISA confirming functional IgG mAbs 204
Figure 38: Detection of IgM reactivity to neurofascin in vitro by CBA from single CD27^{+}IgD^{-} memory B cells from a pan-NF AN patient 206
Figure 39: Detection of IgG1 and IgM subclass reactivity against NF186 in clone 4G2 by live CBA 206
Figure 40: Representative images from re-screening of 480 single-cell culture supernatants for IgM reactivity to NF155 and NF186 208
Figure 41: Live CBA testing of recombinant IgM mAbs derived from pan-NF^{+} clones 210
Figure 42: Head-to-head comparison of three IgG1 and IgM mAbs on live CBA. 211
Figure 43: Comparison of positive binding concentration ranges for IgG1 and IgM recombinant mAbs against NF155 and NF186 212

Figure 47: Detection of neurofascin expression in small-scale bait supernatants by Western blotting (Trials 2 and 3)..... 235
Figure 45: Coomassie-stained gel following streptavidin pull-down of Trial 4 cobalt-purified eluates 238
Figure 46: ELISA comparison of in-house antigen baits versus commercial proteins for NF155 and NF186 autoantibody detection..... 239
Figure 47: SDS-PAGE analysis of Trial 4 cobalt resin purification and buffer exchange fractions and antigen baits 240
Figure 48: Coomassie-stained SDS-PAGE gel of Trial 5 E1 fractions of NF155 and NF186 bait proteins following Ni-NTA purification 242
Figure 49: Western blots probing for neurofascin expression and biotinylation in Trial 5 bait proteins 243
Figure 50: ELISA using Trial 5 NF155 and NF186 baits coated onto ELISA plates to assess autoantibody binding from pan-NF^{+} and $NF155^{+}$ patient sera 244
Figure 51: Neurofascin and biotin Western blots for Trial 6 bait proteins (produced using unpurified BirA)..... 246
Figure 52: Western blot assessing neurofascin expression in supernatant and lysate fractions from the antigen baits of Trial 7 248
Figure 53: Repeat Western blot on Trial 7 NF186 bait supernatant and lysate samples using maximal volume loading..... 248
Figure 54: 6×His tag Western blot on Trial 7 baits to confirm neurofascin expression249
Figure 55: Re-analysis of Trial 5 bait proteins with increased loading volumes on Western blot..... 250

Figure 56: Re-analysis of Trial 6 bait proteins (non-biotinylated) using increased loading volume on neurofascin Western blot probed with chicken anti-neurofascin antibody 251
Figure 57: Western blots showing successful expression and biotinylation of NF155 and NF186 baits using freshly midi-prepped BirA and low-passage HEK293T cells as the final validation of Trial 8 baits 252
Figure 58: ELISA comparing Trial 8 small-scale antigen baits to commercial NF155 and NF186 protein coats for detection of pan-NF^{+} autoantibodies 253
Figure 59: Streptavidin pull-down assay to assess biotinylation of large-scale antigen baits..... 259
Figure 60: ELISA comparing autoantibody binding to Trial 8 small-scale and large-scale baits..... 260
Figure 61: Streptavidin-PE competition Western blot to assess biotin-to-antigen ratio in large-scale NF155 and NF186 antigen baits..... 261
Figure 62: Overview of assessing the amount of biotinylated antigen bait, producing the control tetramer, and tetramerising the antigens 309

List of Tables

Table 1: Participant demographics of patients and healthy controls 58

Table 2: AN participant clinical features 59

Table 3: Cell culture media components and cytokines 60

Table 4: ELISA secondary antibodies 64

Table 5: CBA primary, secondary, and tertiary antibodies 88

Table 6: Flow cytometry fluorophores 90

Table 7: Bulk and single sort flow panel fluorophores 92

Table 8: Thermocycler conditions for cDNA synthesis during Sanger sequencing 98

Table 9: Sanger sequencing nested PCR1 thermocycler conditions 99

Table 10: Sanger sequencing nested PCR2 thermocycler conditions 100

Table 11: Molecular weights and inferred molar extinction coefficients of bait proteins, control protein, and fluorophores 117

Table 12: Western blotting antibodies 122

Table 13: Fluorophores and dilutions used for initial ASC panel development 143

Table 14: Fluorophore-conjugated antibodies and titration dilutions used for the finalised B-cell bulk sorting panel 156

Table 15: Immunogenetic characteristics of antigen-reactive and non-reactive B-cell clones 201

Table 16: Frequency of neurofascin-reactive clones by isotype and antigen specificity among supernatants of 480 single $CD27^{+}IgD^{-}$ memory B-cell clones from a pan-NF AN patient 207

Table 17: Summary of neurofascin-specific IgM and IgG reactivity across single-cell supernatants and corresponding mAbs 214

Table 18: Summary of small-scale NF155 and NF186 antigen bait production trials . 230

Abbreviations

AA	antibiotic-antimycoctic
ADCC	antibody-dependent cellular cytotoxicity
AF	AlexaFluor®
AID	activation-induced cytidine deaminase
AN	autoimmune nodopathy(ies)
APC	allophycocyanin
APRIL	a proliferation-inducing ligand
ASC	antibody-secreting cell
AQP4	aquaporin-4
BAFF	B-cell activating factor
BCDT	B-cell depleting therapy(ies)
BCR	B-cell receptor
BirA	biotin ligase
b-ME	β-mercaptoethanol
BSA	bovine serum albumin
BSC	biosafety cabinet
BV	brilliant violet
C1q	complement component 1q
CAR	chimeric antigen receptor
Caspr	contactin-associated protein
CBA	cell-based assay
CD	cluster of differentiation
CD40L	cluster of differentiation 40 ligand
CDC	complement-dependent toxicity
cDNA	complementary DNA
CDR	complementarity-determining region
CIDP	chronic inflammatory demyelinating polyradiculoneuropathy
CNS	central nervous system
CNTN1	contactin-1
CSF	cerebrospinal fluid
CSR	class-switch recombination

CTLA-4	cytotoxic T-lymphocyte-associated protein 4
CXCL	C-X-C motif ligand
D	diversity
DAPI	4’,6’-diamidino-2-phenylindole
DMEM	Dulbecco’s Modified Eagle medium
DMSO	dimethyl sulfoxide
DNA	deoxyribonucleic acid
dNTP	deoxyribonucleotide triphosphate
DPBS	Dulbecco’s phosphate-buffered saline
DTT	dithiothreitol
ECL	enhanced chemiluminescence
EDTA	ethylenediaminetetraacetic acid
ELISA	enzyme-linked immunosorbent assay
Fab	fragment antigen binding
FBS	foetal bovine serum
Fc	fragment crystallisable
FcγR	Fc gamma receptor
FcR	Fc receptor
FcRn	neonatal FcR
FDC	follicular dendritic cell
FITC	fluorescein isothiocyanate
FMO	fluorescence-minus-one
GBS	Guillain-Barré Syndrome
GC	germinal centre
GM1	monosialotetrahexosylganglioside
HEPES	4-(2-Hydroxyethyl)piperazine-1-ethanesulfonic acid
HEK293T	human embryonic kidney 293T cells
His	hexahistidine
HLA	human leukocyte antigen
HRP	horseradish peroxidase
ICOS	inducible T-cell co-stimulator
ICOSL	ICOS ligand
IFNγ	interferon-gamma

Ig	immunoglobulin
IgA	immunoglobulin A
IgD	immunoglobulin D
IgG	immunoglobulin G
IgH	immunoglobulin heavy chain
IgL	immunoglobulin light chain
IgM	immunoglobulin M
IL	interleukin
IMAC	immobilised metal affinity chromatography
IMDM	Iscove's Modified Dulbecco's Medium
iPSC	induced pluripotent stem cell
IVIg	intravenous immunoglobulin
J	joining
L	litre
LDS	lithium dodecyl sulfate
LLPC	long-lived plasma cell
M	molar
mAb	monoclonal antibody
mCD40L	membrane-bound cluster of differentiation 40 ligand
MG	myasthenia gravis
MHC-II	major histocompatibility complex type II
MOPS	3-(N-morpholino)propanesulfonic acid
mRNA	messenger ribonucleic acid
mRs	Modified Rankin Scale
MWCO	molecular weight cut-off
NF155	neurofascin-155
NF186	neurofascin-186
NGS	next-generation sequencing
NK	natural killer
Ni-NTA	nickel-nitrilotriacetic acid
nm	nanometre
NMDA	N-methyl-D-aspartate
NMOSD	neuromyelitis optica spectrum disorder

NMS	normal mouse serum
OANG	Oxford Autoimmune Neurology Group
OD	optical density
OPD	o-phenylenediamine dihydrochloride
PAGE	polyacrylamide gel electrophoresis
pan-NF	pan-neurofascin
PBMC	peripheral blood mononuclear cell
PBS	phosphate-buffered saline
PCR	polymerase chain reaction
PCKS9	proprotein convertase subtilisin/kexin type 9
PD-1	programmed cell death protein 1
PDL	poly-D-lysine
PE	phycoerythrin
PEI	polyethylenimine
PFA	paraformaldehyde
PIC	protease inhibitor cocktail
PLEx	plasma exchange
PNS	peripheral nervous system
pg	picograms
PLL	poly-L-lysine
P/S	penicillin/streptomycin
PVDF	polyvinylidene fluoride
R848	Resiquimod
RA	rheumatoid arthritis
RIPA	radioimmunoprecipitation assay
RNA	ribonucleic acid
rpm	revolutions per minute
RT	reverse transcription
S	switch (region)
SA	streptavidin
scBCM	single-cell B-cell medium
sCD40L	soluble cluster of differentiation 40 ligand
SD	standard deviation

SDS	sodium dodecyl sulfate
SHM	somatic hypermutation
SLE	systemic lupus erythematosus
SOC	Super Optimal broth with Catabolite repression
T1	transitional 1 B cell
T2	transitional 2 B cell
TC	tissue culture
TBS	tris-buffered saline
TE	Tris-EDTA
Tfh	T follicular helper
Tfr	T follicular regulatory
TGF-β	transforming growth factor-beta
TLR	Toll-like receptor
TMB	3,3',5,5'-Tetramethylbenzidine
TNFα	tumour necrosis factor alpha
Treg	regulatory T cell
V	variable
VH	variable region heavy chain
VL	variable region light chain
v/v	volume/volume
V(D)J	variable (diversity) joining
xg	times gravity

1 Introduction

The maintenance of peripheral nerve integrity depends on highly specialised cellular and molecular structures, particularly the node of Ranvier and adjacent paranodal junctions, which enable rapid saltatory conduction (Figure 1). Disruption of these domains has emerged as a critical mechanism in a subset of inflammatory neuropathies collectively termed *autoimmune nodopathies* (AN), wherein the immune system targets nodal and paranodal adhesion molecules such as contactin-1 (CNTN1), Caspr1, and neurofascin isoforms.[1]

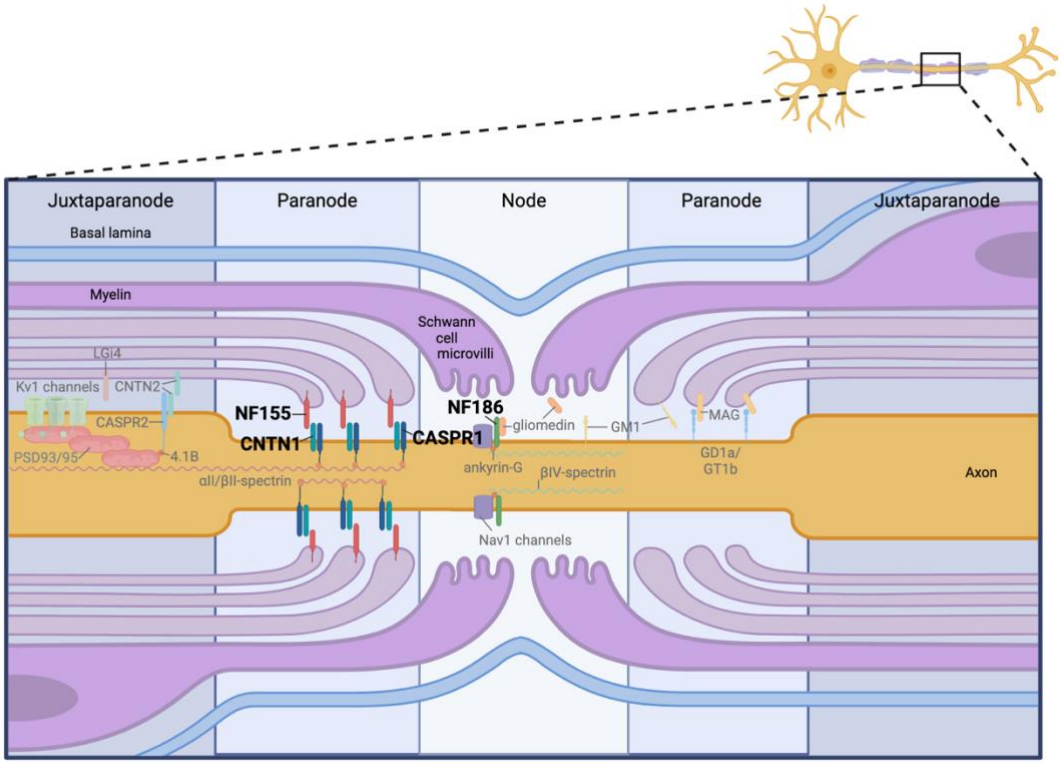

Figure 1: Structure, sub-regions, and molecular landscape of the node of Ranvier. *Established antigenic targets for the autoimmune nodopathies are shown in bold. (NF: neurofascin, CASPR: contactin-associated protein, Nav: voltage-gated sodium channel, Kv: voltage-gated potassium channel, MAG: myelin-associated glycoprotein). From Bergstrom Johnson et al (2025).*[1]

A particularly severe variant within this spectrum is associated with antibodies against both neurofascin-186 (NF186) and neurofascin-155 (NF155), termed *pan-neurofascin* (pan-NF) antibodies. These define a clinically aggressive subtype of autoimmune

neuropathy, pan-NF AN, distinguished by profound motor and sensory impairment, autonomic involvement, and high treatment resistance. While rare, this condition has challenged conventional diagnostic frameworks for chronic inflammatory demyelinating polyradiculoneuropathy (CIDP) and Guillain-Barré Syndrome (GBS), highlighting a need for tailored immunotherapeutic strategies.[1,2]

Of particular interest is the subset of patients with pan-NF AN who harbour IgG1 subclass antibodies. While most existing studies on AN have focused on cases associated with IgG4 antibodies,[3–7] IgG1 pan-NF AN appears to follow a notably more aggressive clinical course, with greater disability, treatment refractoriness, and worse overall outcomes.[1,2] Despite its severity, this variant remains understudied, and little is known about the immunological events that underlie its development. Focusing on IgG1 pan-NF AN therefore provides an opportunity to better understand a distinct and clinically important form of autoimmune neuropathy that has not been adequately characterised at the immunological level.

1.1 Autoimmune inflammatory neuropathies

1.1.1 General overview and classification

Inflammatory neuropathies comprise a heterogeneous group of disorders characterised by immune-mediated injury to the peripheral nervous system (PNS). These conditions manifest with diverse patterns of nerve involvement, clinical severity, and underlying immunopathogenic mechanisms. Broadly, they can be classified into acute and chronic forms: acute presentations include GBS, while chronic forms encompass CIDP and its variants.[4] While traditionally viewed as T-cell- and macrophage-mediated demyelinating processes,[8,9] recent research has expanded our understanding of the

diverse immune mechanisms involved in these disorders. In particular, the role of IgG antibodies and complement activation has garnered increasing attention, as evidenced by the emergence of therapeutic approaches targeting these pathways – such as complement inhibitors, neonatal Fc receptor (FcRn) inhibitors, and IgG-degrading enzymes (eg, imlifidase) – in both GBS and CIDP. These developments underscore a broader appreciation of humoral immunity and Fc-mediated effector functions in the pathogenesis of inflammatory neuropathies.

Inflammatory neuropathies can be distinguished by their clinical course, predominant features, electrophysiological findings, and immunopathological characteristics. GBS typically presents with rapidly progressive weakness and is associated with antibody- or cell-mediated attacks on peripheral nerve components. Subtypes such as acute motor axonal neuropathy (AMAN) and acute motor and sensory axonal neuropathy (AMSAN) differ by the pattern of nerve involvement and the presence of specific autoantibodies.[10] Chronic forms, including CIDP and multifocal motor neuropathy (MMN), generally feature a relapsing-remitting or slowly progressive course with demyelination, often reflected in distinct electrophysiological patterns.[4] The spectrum also includes paraneoplastic and vasculitic neuropathies, where immune responses target nerve antigens due to malignancy or result in vascular inflammation.[11] This classification underscores the heterogeneity of inflammatory neuropathies and the importance of integrating clinical, serological, and neurophysiological data for diagnosis and management.

1.1.2 Clinical features, diagnosis, and disease progression

Inflammatory neuropathies present with a spectrum of clinical features, reflecting underlying immune-mediated disruption of nerve integrity. Patients may exhibit symmetrical limb weakness, sensory disturbances, and reduced or absent tendon reflexes. Symptom severity ranges from mild, slowly progressive neuropathies to rapidly evolving conditions with life-threatening complications, such as respiratory failure. Autonomic dysfunction, though less common, may manifest as orthostatic hypotension, gastrointestinal dysmotility, or urinary retention, complicating clinical presentation.[7,12]

Diagnosis involves a combination of clinical, electrophysiological, and serological assessments. Nerve conduction studies may show features of demyelination or axonal loss, including prolonged distal latencies, conduction block, and reduced amplitudes of motor or sensory nerves. Cerebrospinal fluid (CSF) analysis may reveal albuminocytologic dissociation, particularly in GBS.[13] However, overlapping features with other neuropathic disorders can complicate diagnosis. Serological testing for disease-specific autoantibodies (eg, against neurofascin isoforms, CNTN1, or Caspr1) has become a crucial adjunct, particularly in atypical or treatment-refractory cases.[1,14]

The disease course of inflammatory neuropathies is equally heterogeneous. Some patients experience a monophasic illness with gradual recovery, while others endure relapses or progression to chronic forms, notably in CIDP or AN. Disease progression is influenced by factors including autoantibody subclass, with IgG1 and IgG3 subclasses often associated with more severe phenotypes due to their capacity to activate complement and engage Fc gamma receptors (FcγRs).[15] Early recognition and treatment

are critical, as delays can lead to irreversible nerve damage and long-term disability. This dynamic disease spectrum underscores the importance of serial clinical assessments and monitoring of serological markers to guide treatment decisions.

1.1.3 Therapeutic approaches and challenges

Management of inflammatory neuropathies involves therapies aimed at suppressing aberrant immune responses and promoting nerve repair. First-line treatments include corticosteroids and intravenous immunoglobulin (IVIg), which modulate immune activity and provide symptomatic relief. IVIg, in particular, has demonstrated efficacy in conditions such as CIDP and GBS, where it is thought to act through numerous mechanisms, including saturating Fc receptors, modulating complement activity, and altering cytokine signalling.[4] Plasma exchange (PLEx) is also an established option, and is thought to act mainly by rapidly reducing circulating pathogenic antibodies.[12]

However, treatment responses vary depending on disease subtype, severity, and immunopathogenic mechanisms. While many patients respond well to standard therapies, others – particularly those with atypical or antibody-mediated variants – may be refractory or prone to relapse. These cases have prompted growing interest in targeted immunomodulatory strategies, including B-cell depletion therapies (BCDT) and complement inhibitors.[16] Understanding the cellular and humoral drivers of treatment resistance remains a major clinical and research challenge.

1.1.4 Pan-NF AN as a distinct clinical entity

Among the spectrum of autoimmune neuropathies, pan-NF AN has emerged as a clinically distinct and especially severe subtype. Patients typically present with a rapidly progressive phenotype marked by profound motor weakness, sensory loss, and often

autonomic dysfunction. Unlike classical CIDP or other types of AN, pan-NF AN is notable for its poor prognosis and limited responsiveness to first-line immunotherapies such as IVIg and corticosteroids. BCDT, including rituximab, may offer clinical benefit in some cases, yet responses are often delayed, incomplete, or followed by relapse – highlighting a critical need for an improved understanding of the disease's underlying immunopathology.[1]

Given these clinical challenges, attention has increasingly turned to the role of B cells in the immunopathogenesis of pan-NF AN. In addition to their capacity for antibody production, B cells participate in antigen presentation and immune regulation, placing them at the nexus of adaptive immune responses. Failures in B-cell tolerance – well-documented in systemic autoimmune diseases – may also be operative in pan-NF AN, enabling the survival and activation of autoreactive clones that give rise to pathogenic antibodies.[1] While subclass differences have been explored in other AN forms, the mechanisms driving IgG1-dominant responses in pan-NF AN remain unclear.[6,17] This thesis therefore focuses on pan-NF AN patients specifically harbouring IgG1-subclass pan-NF antibodies, which are associated with a particularly aggressive disease course yet remain poorly understood. Elucidating the B-cell mechanisms underlying IgG1 pan-NF AN may yield vital insights for developing targeted diagnostic and therapeutic strategies in this life-threatening condition.

1.2 Immunoglobulins in health and disease

1.2.1 Overview of immunoglobulin structure and diversity

Immunoglobulins (Ig) are glycoproteins secreted by B cells and plasma cells, central to the humoral immune response. Structurally, antibodies are composed of two identical heavy chains (IgH) and two identical light chains (IgL), linked by disulfide bonds to form a Y-shaped molecule (Figure 2). The variable regions at the N-termini of these chains confer antigen specificity, while the constant regions determine the antibody's isotype (IgM, IgG, etc) and mediate effector functions through interactions with Fc receptors and complement proteins.[18]

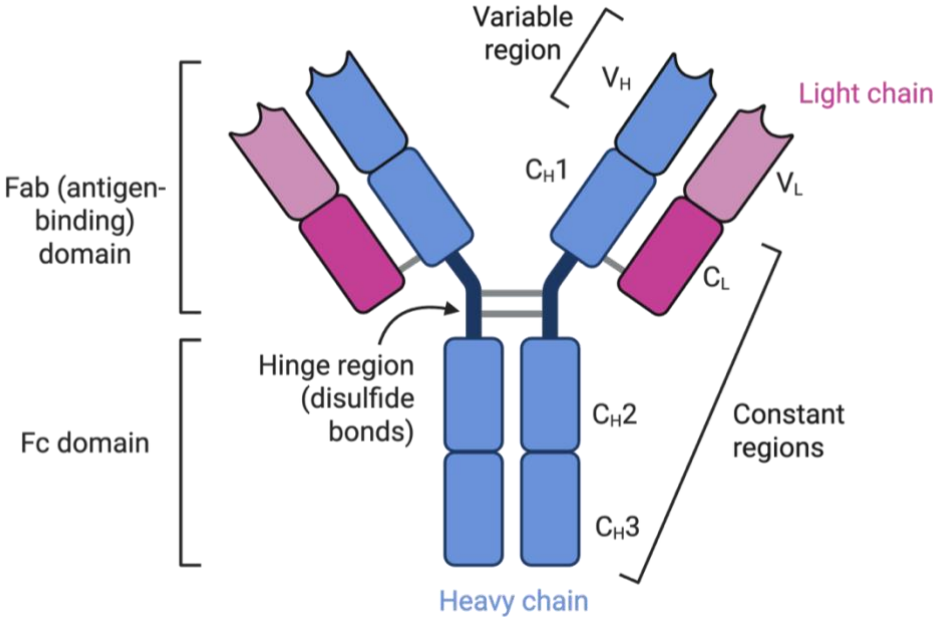

Figure 2: Immunoglobulin (antibody) structure schematic. *Each immunoglobulin (Ig) molecule consists of two identical heavy chains (blue) and two identical light chains (pink), connected by disulfide bonds. The variable regions at the tips of the Y-shape (comprising V_L and V_H) form the antigen-binding sites within the Fab (fragment antigen-binding) domains. The hinge region provides flexibility and contains inter-chain disulfide bonds. The Fc (fragment crystallisable) domain comprises the constant regions of the heavy chains (C_H2 and C_H3), mediating interactions with Fc receptors and complement. The light chains contain one variable and one constant domain, while the heavy chains include one variable and multiple constant domains, determining the antibody isotype. Together, these structural elements enable both antigen recognition and immune effector functions.*

The generation of antibody diversity begins during B-cell development in the bone marrow, where a process called *variable (diversity) joining (V(D)J) recombination*

(section 1.3.1.1) assembles gene segments encoding the IgH and IgL chains. This process creates a vast repertoire of B-cell receptors (BCRs) capable of recognising a wide range of antigens. Upon antigen encounter, B cells become activated, typically with support from T follicular helper (Tfh) cells, leading to proliferation and differentiation into memory B cells, antibody-secreting cells (ASCs), or long-lived plasma cells (LLPCs). Plasma cells specialise in producing antibodies, while memory B cells enable rapid and robust responses upon re-exposure to the same antigen.[19–21]

Class-switch recombination (CSR; section 1.3.3.5) further refines the humoral response, enabling B cells to switch from producing IgM antibodies to other isotypes such as IgG, IgA, or IgE. This process is orchestrated by cytokines and co-stimulatory signals within specialised structures called *germinal centres* (GCs; section 1.3.3.1), ensuring that antibody responses are tailored to the nature of the antigenic challenge. The Fc portion of antibodies engages with FcγRs on effector cells and complement components, triggering functions including phagocytosis, antibody-dependent cellular cytotoxicity (ADCC), and modulation of inflammatory responses.[4]

The Fc-mediated effector functions of antibodies are determined not only by their isotype but also by the subclass and glycosylation status of the Fc region. These Fc-dependent activities modulate phagocytosis, ADCC, and cytokine release by immune effector cells, such as natural killer (NK) cells, macrophages, and neutrophils.[4] Dysregulation of FcγR signalling, particularly the balance between activating and inhibitory FcγRs, is a feature of antibody-mediated autoimmune diseases, including pan-NF AN.[7,22–26]

Regulation of antibody production is crucial for maintaining immune homeostasis and preventing autoimmunity. Checkpoints during B-cell development and activation ensure the deletion or silencing of self-reactive clones. However, failure of these mechanisms may permit the survival and expansion of autoreactive B cells, leading to loss of tolerance and the production of pathogenic autoantibodies (section 1.4). Tfh and T follicular regulatory (Tfr) cells help shape the magnitude and specificity of antibody responses, providing an additional layer of control over humoral immunity.

The ability of B cells to produce distinct antibody isotypes is governed by CSR and modulated through interactions with Tfh cells. Pan-NF autoantibodies encompassing all IgG subclasses (IgG1-4) have been identified,[6,7,27] and case reports describe subclass switching of these autoantibodies in patients with AN.[7] However, there are no known reports of autoantibody class switching (eg, from IgM to IgG) in pan-NF AN, and the pathogenic significance of B cell-driven subclass selection, particularly the emergence of IgG1 antibodies, remains unexplored.

1.2.2 Immunoglobulin classes and their biological roles

Immunoglobulins exhibit structural and functional diversity, enabling recognition and neutralisation of a vast array of antigens. They are classified into five major isotypes – IgM, IgD, IgG, IgA, and IgE – each with unique structural features and effector functions tailored to distinct immunological contexts. The class-switching process, mediated by activation-induced cytidine deaminase (AID), allows B cells to transition from producing IgM and IgD to isotypes like IgG, IgA, or IgE, conferring specialised roles in immunity and tolerance.[28] The following sections highlight the isotypes most relevant to the current work.

1.2.2.1 IgM and early immune responses

IgM, the first antibody isotype produced during adaptive immune responses, plays a pivotal role in early pathogen clearance. Its pentameric structure, stabilised by a joining (J) chain, affords high avidity, compensating for relatively low intrinsic affinity.[29] This configuration facilitates efficient activation of the classical complement pathway and the formation of immune complexes, promoting antigen clearance and phagocytosis.[28]

During initial antigen exposure, naïve B cells primarily secrete IgM before CSR to other isotypes.[30] CSR, initiated by AID, subsequently enables the production of isotypes with more refined effector functions, such as IgG or IgA. Early IgM responses also shape later immunity by enhancing antigen presentation and promoting GC formation, where B cells undergo affinity maturation (section 1.3.3.4).[31]

Notably, the stochastic nature of V(D)J recombination generates a repertoire that includes self-reactive IgM-producing clones. Central and peripheral tolerance checkpoints usually ensure deletion or anergy of such cells, thereby safeguarding against autoimmunity.[32] However, failures in these checkpoints can permit the persistence of autoreactive IgM-secreting B cells, potentially contributing to autoimmune pathogenesis.[29]

1.2.2.2 IgD and its role in B-cell development

IgD emerges during early B-cell maturation, marking the transition from immature to mature naïve B cells. Co-expressed with IgM through alternative mRNA splicing, IgD is a hallmark of mature naïve B cells and plays a role in modulating BCR signalling thresholds.[32] While its precise function remains incompletely understood, IgD may fine-

tune B-cell responsiveness to antigen, contributing to peripheral tolerance and the prevention of autoreactivity.[33]

As B cells migrate to peripheral lymphoid organs, IgD expression delineates functional maturation and readiness to engage in adaptive immunity. Within secondary lymphoid tissues, IgD^+ naïve B cells localise to follicles, positioning them for interactions with antigen-presenting cells and Tfh cells, which are essential for GC entry and differentiation into memory or plasma cells.[19]

Anergic B cells that retain surface IgD but are functionally silenced represent an important peripheral checkpoint. These cells fail to respond to BCR or Toll-like receptor (TLR) signals, reflecting a multilayered mechanism of tolerance.[32] Their positioning within lymphoid follicles facilitates antigen surveillance while maintaining functional anergy, representing a key peripheral tolerance checkpoint.

Thus, IgD expression not only marks B-cell maturation but also contributes to the fine-tuning of immune activation and tolerance thresholds. Its role in both central and peripheral selection highlights its relevance in preventing autoreactive B-cell activation while maintaining antigen responsiveness.

1.2.2.3 IgG subclasses and their differential effector functions

IgG, the most prevalent antibody isotype in human serum, comprises four subclasses – IgG1, IgG2, IgG3, and IgG4 – each with structural differences that directly influence effector functions (Figure 3; de Taeye et al, 2019).[34] These differences arise primarily from variations in the constant regions of the heavy chain, particularly in the hinge and Fc domains, which affect flexibility, complement activation, and binding to FcγRs.[4,6]

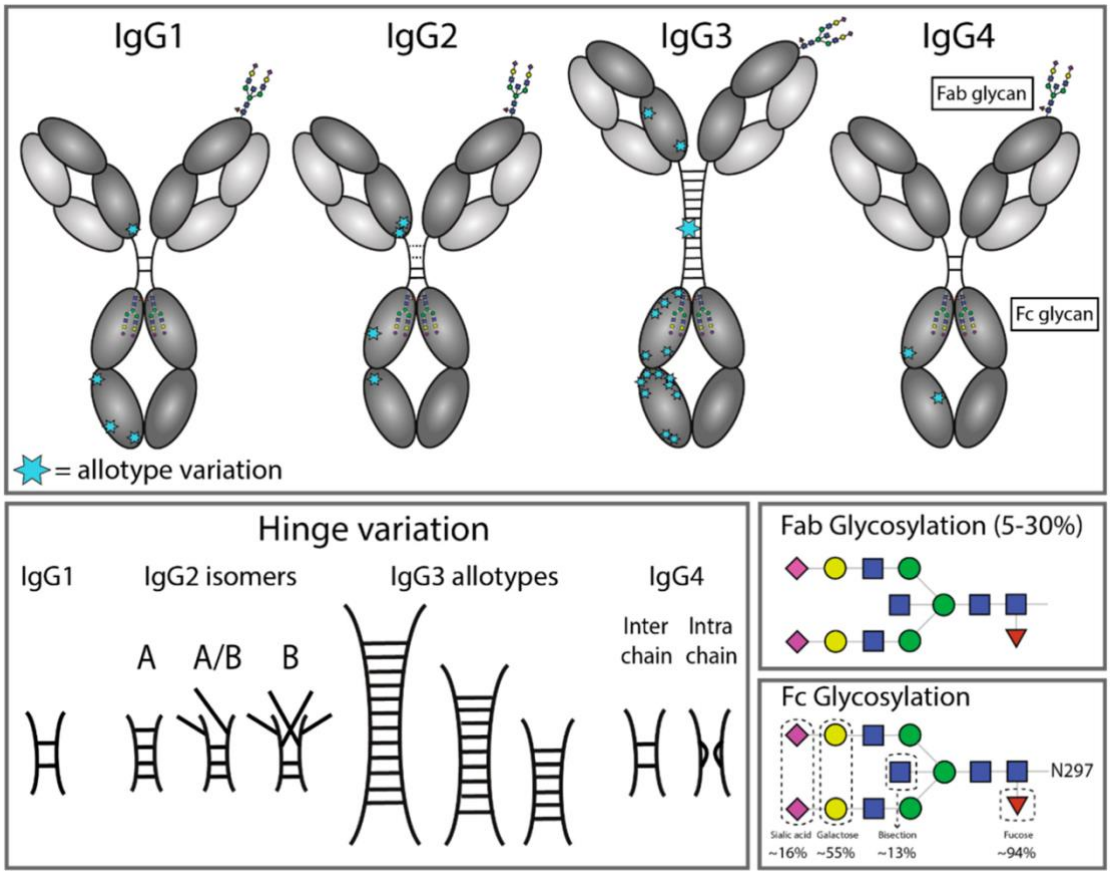

Figure 3: Structural diversity of human IgG subclasses. *This figure illustrates the structure of the immunoglobulin G (IgG) subclasses, highlighting key areas of variation, including allotype polymorphisms, differences in hinge length, and glycosylation patterns. Blue stars denote sites of amino acid variation within the constant region of the heavy gamma (IgHG) chain, with most stars indicating single-residue differences except for one, which marks hinge length variation in IgG3 allotypes. Fab glycosylation is depicted, which occurs in approximately 5–30% of serum antibodies depending on subclass and antigen specificity. The N297 glycan in the Fc region shows high glycoform variability, with the relative frequencies of different glycan moieties found in human serum indicated. From de Taeye, 2019.*[34]

IgG1, the most abundant subclass, features a flexible hinge and high affinity for activating FcγRs. This allows potent effector functions, including ADCC, phagocytosis, and robust complement activation via the protein *complement component 1q* (C1q). Consequently, IgG1 autoantibodies – like those observed in IgG1 pan-NF AN – are typically associated with complement-mediated damage and severe clinical phenotypes.[7,15]

IgG3, while less abundant, has the longest hinge region, allowing broader antigen engagement but also increased susceptibility to proteolysis. It shares IgG1's high complement activation potential but is less frequently implicated in neuropathies.[4]

IgG2, with a shorter and more rigid hinge, preferentially targets carbohydrate antigens and exhibits limited FcγR binding and complement activation, making it less relevant in most autoimmune neuropathies.[4]

IgG4 is unique among subclasses due to its capacity for Fab-arm exchange, producing bispecific, functionally monovalent antibodies.[6] This structural rearrangement, alongside poor C1q binding and preferential interaction with the inhibitory FcγRIIb, imparts an anti-inflammatory profile. In AN, IgG4 autoantibodies typically disrupt protein-protein interactions at neural junctions without triggering direct tissue injury.[4,35]

CSR, influenced by cytokine signals and microenvironmental cues, governs subclass distribution during B-cell maturation. In autoimmune neuropathies, subclass profiles correlate with both clinical severity and therapeutic responses. For example, pan-NF autoantibodies dominated by IgG1 indicate complement-mediated pathology, while IgG4-driven responses in other AN forms typically reflect non-inflammatory, disruption-based mechanisms (section 1.5.1).[6,7]

1.3 B cells and humoral immunity

B cells, or B lymphocytes, are a specialised subset of white blood cells central to the adaptive immune system, mediating humoral immunity through the production of antigen-specific antibodies. Originating from haematopoietic stem cells in the bone marrow, B cells undergo a complex process of development and selection to establish a

diverse repertoire of immunoglobulin receptors on their surface. These receptors must retain the ability to recognise foreign antigens while avoiding self-reactivity, a balance achieved through mechanisms of central and peripheral tolerance.[20] These BCRs serve both as antigen sensors and initiators of intracellular signalling upon antigen engagement and are eventually secreted in soluble form as antibodies.

Upon encountering their cognate antigen, B cells can differentiate into a variety of longer-lived cell types, contributing to both immediate and long-term immunity.[15,20,21] In addition to antibody secretion, B cells function as antigen-presenting cells, internalising and processing antigens for presentation to $CD4^+$ T cells via major histocompatibility complex class II (MHC-II) molecules. This interaction, particularly within GCs, is essential for affinity maturation and CSR, which refine and tailor antibody responses to pathogens or, in pathological settings, to self-antigens.[15]

The BCR complex, comprising a membrane-bound immunoglobulin and associated signalling proteins (Igα and Igβ), orchestrates B-cell activation upon antigen binding.[36] V(D)J recombination in the bone marrow and somatic hypermutation (SHM) in GCs (section 1.3.3.4) confer remarkable antigenic diversity to the BCR repertoire, enabling the immune system to detect a broad array of epitopes. BCR engagement with antigen triggers intracellular signalling cascades that promote proliferation, CSR, and the expansion of B cells bearing high-affinity BCRs within GCs.[20] Regulatory kinases and phosphatases modulate these signals to prevent excessive activation, dysregulation of which has been implicated in autoimmune pathogenesis.[32] The BCR's dual role in antigen recognition and intracellular signalling underpins both protective humoral

immunity and the potential for autoantibody-mediated pathology, as observed in autoimmune neuropathies.

An overview of B-cell development and maturation, and key immunological checkpoints including V(D)J recombination, CSR, and SHM, is shown in Figure 4 (from Sun et al, 2020) to contextualise the subsections that follow.[21]

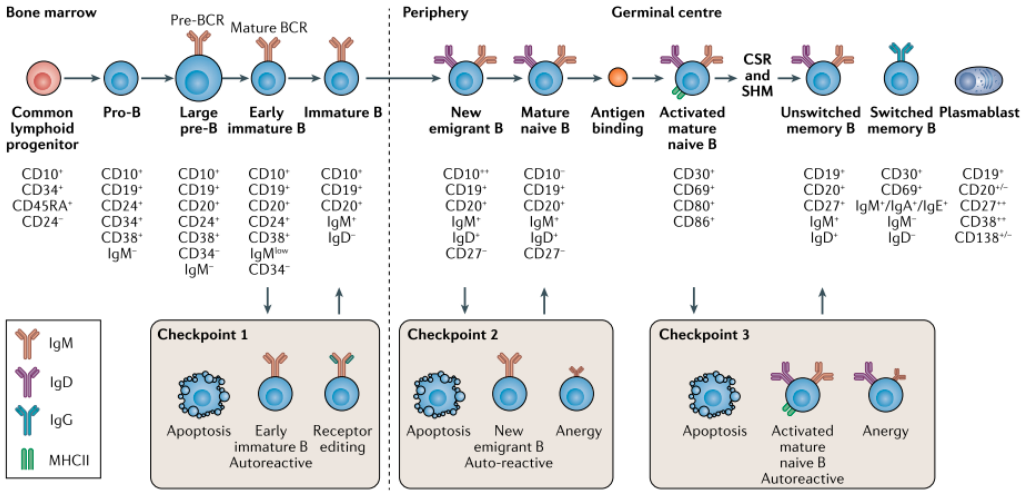

Figure 4: B-cell development, maturation, and tolerance checkpoints. *B cells originate from common lymphoid progenitors, progressing through pro-B and pre-B cell stages where IgH genes are rearranged and paired with a surrogate light chain to form the pre-BCR. In early immature B cells, the surrogate light chain is replaced with a true light chain, resulting in the expression of surface IgM. This stage represents the first tolerance checkpoint (Checkpoint 1), where self-reactive BCRs are eliminated via apoptosis or corrected through receptor editing. Successfully selected B cells exit the bone marrow as new emigrants and undergo further negative selection (Checkpoint 2) as they transition into mature naive B cells in the periphery. Upon encountering specific antigens, mature naive B cells can enter germinal centres where they undergo somatic hypermutation (SHM) and class-switch recombination (CSR) to produce high-affinity antibodies and switch isotypes. Within germinal centres, B cells expressing autoreactive or low-affinity BCRs are subject to further tolerance mechanisms, including apoptosis or anergy (Checkpoint 3). Some cells may persist as unswitched IgM+ memory B cells or differentiate into class-switched memory B cells or antibody-secreting plasma cells. From Sun et al (2020).*[21]

1.3.1 Early B cells

B-cell development begins in the bone marrow from multipotent common lymphoid progenitor cells, which give rise to pro-B cells under the influence of IL-7 and stromal cell signals. In the pro-B cell stage, IgH D and J gene segments undergo rearrangement, initiating antigen receptor formation. Successful D-J joining permits progression to the

large pre-B cell stage, where a “pre-BCR” comprising the newly rearranged IgH and a surrogate IgL is expressed. This complex signals for proliferation and allelic exclusion at the IgH locus, ensuring clonal identity. Following multiple rounds of division, large pre-B cells become small pre-B cells, initiating IgL V-J rearrangement.[21]

Assembly of a functional IgL and IgH pair results in a mature IgM BCR, marking the early immature B-cell stage. These cells undergo selection to eliminate strongly self-reactive clones. B cells that pass this checkpoint become immature B cells and migrate into the periphery for further maturation.

1.3.1.1 V(D)J recombination

V(D)J recombination is a site-specific DNA recombination process occurring during early B-cell development. It assembles the V, D, and J gene segments of the IgH locus and the V and J segments of the IgL locus, enabling the generation of an enormous BCR repertoire.[37]

Combinatorial diversity, arising from random selection of V, D, and J gene segments, is further expanded by junctional diversity, which results from imprecise joining and non-templated nucleotide additions at coding joints. These mechanisms together create a highly polyclonal repertoire, where each B cell expresses a unique BCR.[38]

Tight regulation of V(D)J recombination is essential, as mistargeted recombination events can induce genomic instability, contributing to lymphoid malignancies.[39] The diversity generated through this process underlies the capacity for antigen specificity but also creates the potential for autoreactivity. When tolerance checkpoints fail (see

section 1.4), autoreactive B cells emerging from V(D)J recombination may persist and produce pathogenic antibodies.[38,40]

1.3.2 New emigrant B cells

New emigrant (transitional) B cells exit the bone marrow and enter the periphery, representing an essential checkpoint between immature and fully mature naïve B cells. These transitional B cells are subclassified into transitional 1 (T1) and transitional 2 (T2) stages based on surface marker expression and survival characteristics. T1 B cells, distinguished by high IgM and low CD23/CD21 expression, are especially susceptible to deletion due to elevated autoreactivity. In contrast, T2 B cells upregulate CD23 and CD21, exhibit improved survival, and respond to B-cell activating factor (BAFF), thereby becoming more competent for entry into the mature naïve pool.[32]

At this stage, BCR signals are tightly regulated: strong self-reactivity results in deletion or anergy, while appropriate tonic signalling (low-level, antigen-independent BCR signalling required for survival) promotes positive selection. T2 cells, once selected, express high surface IgD and transition into circulating mature naïve B cells, capable of antigen encounter and activation.[21]

1.3.3 Mature naïve B cells and germinal centre development

Mature naive B cells, identified by surface co-expression of IgM and IgD, represent the reservoir of antigen-inexperienced lymphocytes. These cells circulate through peripheral lymphoid tissues, continuously scanning for antigens. Upon encountering their cognate antigen within secondary lymphoid structures, and in the presence of T-cell help, B cells initiate GC responses that drive functional diversification.

1.3.3.1 Germinal centres: structure and function

GCs are specialised microenvironments in secondary lymphoid tissues that support affinity maturation and CSR. Their open architecture facilitates dynamic migration of B cells between the "dark zone", where they undergo rapid proliferation and SHM, and the "light zone", where selection for high-affinity clones occurs through interactions with follicular dendritic cells (FDCs) and Tfh cells.[20]

CSR occurs in parallel with SHM and selection, enabling isotype switching while preserving antigen specificity. Together, these processes yield high-affinity, isotype-switched antibodies adapted to the immunological context.

1.3.3.2 Tolerance mechanisms within GCs

While GCs promote protective immunity, they also serve as critical checkpoints against autoreactivity. B cells bearing low-affinity or self-reactive BCRs are eliminated through apoptosis or rendered anergic.[21] GC tolerance failure may permit the survival of autoreactive clones, which can differentiate into memory B cells or LLPCs producing autoantibodies – a feature implicated in systemic autoimmunity and autoimmune neuropathies.[41]

Ectopic GC-like structures may form in non-lymphoid tissues, including the central nervous system (CNS), enabling local affinity maturation and sustained autoantibody production. Elevated C-X-C motif ligand 13 (CXCL13) in CSF, for example, is a biomarker of GC activity in N-methyl-D-aspartate (NMDA) receptor antibody encephalitis.[21]

1.3.3.3 Regulation of B-cell responses in GCs

GC responses are shaped by cytokines, chemokines, and cell-cell interactions.[20] IL-21, produced by Tfh cells, promotes GC maintenance and supports both SHM and CSR.[19] Co-stimulatory interactions such as inducible T-cell co-stimulator (ICOS)-ICOS ligand (ICOSL), cytotoxic T-lymphocyte-associated protein 4 (CTLA-4), and programmed cell death protein 1 (PD-1) guide B-cell selection and positioning.[31] Complement receptors and antigen delivery via subcapsular sinus macrophages further modulate GC responses.[20]

Tfr cells act within GCs to suppress excessive or autoreactive B-cell activation.[31] Dysregulation of these pathways promotes extrafollicular plasmablast differentiation and autoantibody production.[42]

1.3.3.4 SHM and affinity maturation

SHM introduces point mutations into the BCR variable region during GC reactions. High-affinity variants are selected, while deleterious or autoreactive variants are culled.[21,28] However, these processes are not completely error-proof: up to 20% of IgG^+ memory B cells retain autoreactivity.[43–45] Dysregulation of SHM or CSR, under the influence of cytokines or tissue-derived factors, can produce high-affinity, class-switched autoantibodies, as seen in systemic lupus erythematosus (SLE).[41]

Single-cell transcriptomic analyses reveal that lymphoid tissue architecture and Tfh-B cell dynamics strongly influence the efficiency and fidelity of these processes.[20,46]

1.3.3.5 Class-switch recombination

CSR diversifies antibody function by replacing the IgH μ constant region with downstream regions (eg, γ, α, ε), allowing the production of IgG, IgA, or IgE respectively while retaining antigen specificity. CSR is catalysed by AID, which introduces DNA breaks at switch (S) regions.[47,48] Repair via non-homologous end joining leads to recombination.

CSR is regulated by CD40-CD40 ligand (CD40L) interactions and cytokines including IL-4, IL-10, and transforming growth factor-β (TGF-β), which direct isotype fate.[47] Epigenetic factors, including the IgH 3' regulatory region, modulate chromatin accessibility at S regions.[49] Aberrant CSR contributes to autoimmunity by promoting production of complement-fixing IgG and mucosal IgA autoantibodies.[48] Understanding CSR regulation is therefore key to addressing B-cell dysregulation in antibody-mediated disease.

1.3.4 Memory B cells

Memory B cells are long-lived, antigen-experienced cells primed for rapid reactivation upon re-exposure to cognate antigen. They arise from GC reactions and typically undergo SHM and CSR.[48] Upon restimulation, they rapidly differentiate into ASCs or re-enter secondary GCs for further maturation.[20,21]

Memory B cells exhibit clonal persistence and are categorised as unswitched (IgD^+/IgM^+) or switched ($IgG^+/IgA^+/IgE^+$), with distinct effector potential. These subsets differ in activation threshold, cytokine responsiveness, and contribution to inflammatory responses. Dysregulation of memory B-cell maintenance or activation plays a role in chronic autoantibody production in disease.[48]

1.3.4.1 Unswitched memory B cells

Unswitched memory B cells (typically $CD27^{+}IgD^{+}$) retain IgD/IgM expression and may arise from either GC or extrafollicular pathways. Though their precise origins remain under investigation, they persist long-term and can mount rapid secondary responses.[50] They may re-enter GCs or differentiate into IgM-secreting plasmablasts, with roles in both host defence and autoreactive potential under dysregulated conditions.[51]

Unswitched memory B cells also demonstrate increased BCR responsiveness and elevated IL-6 production during inflammation. In infections like SARS-CoV-2, their depletion correlates with poor outcomes, and their altered activation status has been linked to increased autoantibody production.[50]

1.3.4.2 Switched memory B cells

Switched memory B cells have undergone CSR and express IgG, IgA, or IgE. They exhibit high levels of SHM and rapidly differentiate into ASCs upon restimulation.[21] Their isotype reflects cytokine exposure during GC selection.

Switched memory B cells are particularly relevant in autoimmunity due to their ability to produce high-affinity, class-switched autoantibodies. Evidence suggests that expansion of these cells and their differentiation into LLPCs may contribute to sustained autoantibody production in some autoimmune diseases such as SLE.[21] Single-cell repertoire studies reveal clonal relationships between switched memory B cells and ASCs, indicating ongoing antigen-driven selection.[52]

1.3.5 Plasmablasts and ASCs

Plasmablasts are short-lived, proliferative ASCs arising early in immune responses, either via extrafollicular activation or GCs.[42] They generally secrete low-affinity antibodies and can differentiate into LLPCs with sustained production capability.[53]

ASCs are pivotal in both protective immunity and pathogenic autoimmunity. In autoimmune diseases, dysregulated ASC differentiation results in chronic autoantibody production.[54] Failures in tolerance checkpoints allow autoreactive B cells to mature into ASCs, fuelling inflammation.[55] Dysfunctional regulatory B cells may fail to restrain ASC activity, enabling disease progression.[56]

1.3.6 LLPCs and sustained antibody production

LLPCs are terminally differentiated, non-dividing cells that primarily secrete high-affinity antibodies. Generated primarily in GCs, they migrate to bone marrow niches where survival depends on signals including a proliferation-inducing ligand (APRIL), BAFF, and IL-6.[21] These cytokines prevent apoptosis and support sustained antibody production over months to years.

In autoimmunity, autoreactive LLPCs persist independently of antigen and are not directly targeted by anti-CD20 BCDT like rituximab, as they lack CD20.[57] Their niche localisation and survival pathways pose a barrier to therapeutic depletion, necessitating LLPC-directed approaches such as proteasome inhibitors or IL-6/APRIL blockade.

1.4 Immune tolerance and autoimmunity

1.4.1 Principles of immune tolerance

1.4.1.1 Central tolerance checkpoints

Immune tolerance is a fundamental process that ensures self-reactive lymphocytes are either eliminated or rendered functionally silent, thereby preventing autoimmunity and shaping the BCR repertoire. In B cells, central tolerance operates in the bone marrow, where immature B cells expressing high-affinity BCRs for self-antigens undergo clonal deletion, receptor editing, or induction of anergy (Figure 4). Clonal deletion involves apoptotic removal of strongly self-reactive B cells, particularly those recognising multivalent or membrane-bound self-antigens. Receptor editing allows certain autoreactive clones to revise their specificity by rearranging IgL genes, potentially generating a non-autoreactive BCR. Anergic B cells, though functionally silenced, may escape into the periphery and persist within the mature B-cell pool.[21,29] The effectiveness of central tolerance is modulated by both genetic and environmental factors that shape the diversity and reactivity of the developing BCR repertoire.[21,42]

1.4.1.2 Peripheral tolerance checkpoints

Peripheral tolerance provides an additional safeguard, eliminating or controlling self-reactive B cells that evade central tolerance. Mechanisms include maintenance of anergy, deletion of activated autoreactive clones, and modulation of activation thresholds by cytokines and co-stimulatory signals. Tfr cells play a crucial role in restraining GC responses and limiting the development of high-affinity autoreactive antibodies.

In addition to cellular mechanisms, molecular checkpoints and genetic polymorphisms influence tolerance. Variants in genes regulating BCR signalling thresholds, receptor editing efficiency, or antigen presentation can modulate tolerance stringency.[58] The convergence of these intrinsic and extrinsic factors ultimately determines whether autoreactive B cells are deleted, silenced, or permitted to differentiate into ASCs.[46,58]

1.4.2 Failures of tolerance in autoimmunity

Despite this multi-tiered architecture, immune tolerance is not absolute. In both human autoimmune diseases and animal models, tolerance mechanisms can be bypassed, allowing autoreactive B cells to persist, differentiate, and contribute to pathogenic antibody production. Although central tolerance aims to delete, edit, or anergise self-reactive B cells in the bone marrow, these checkpoints are frequently "leaky"; studies show that polyreactive and autoreactive clones routinely escape deletion or receptor editing and enter the periphery, even in healthy individuals.[59]

Peripheral tolerance mechanisms – including sustained anergy, cytokine-mediated regulation, and suppression by regulatory T cells (Tregs) and Tfr cells – form a second line of defence. However, these too may be compromised by genetic mutations, pro-inflammatory signals, or environmental exposures. For instance, infections can trigger epitope spreading, bystander activation, and molecular mimicry, promoting inappropriate B-cell activation.[60] Age-related immunosenescence, microbiome alterations, and the formation of chronic inflammatory niches such as tertiary lymphoid structures can further facilitate survival of autoreactive clones.[61]

In some antibody-mediated autoimmune diseases, autoreactive B-cell clones have been observed to express IgM with limited SHM, consistent with development through

extrafollicular pathways rather than GCs. This may reflect early failures of central or peripheral tolerance that allow naïve or unswitched memory B cells to persist and participate in autoantibody production without stringent affinity maturation or selection.[62]

1.4.2.1 BCR repertoire skewing in autoimmunity

A hallmark of failed tolerance is skewing of the BCR repertoire. In healthy individuals, BCR diversity, generated through V(D)J recombination, SHM, and CSR, supports broad antigen recognition. In contrast, autoimmune disorders often display oligoclonal or monoclonal B-cell expansions, reflecting antigen-driven selection and persistent autoreactivity.[63]

In conditions like SLE, rheumatoid arthritis (RA), and autoimmune neuropathies, repertoire analyses demonstrate expansion of either hypomutated polyclonal IgG^+ B cells or clonally restricted memory populations, suggesting ongoing stimulation by self-antigens. While infections often induce polyclonal responses, autoimmunity often results in focused expansions due to impaired deletion or editing.[59]

Importantly, repertoire architecture has diagnostic and therapeutic implications. Monoclonal expansions are often associated with high-affinity, complement-fixing autoantibodies that drive tissue pathology. They may also serve as biomarkers of disease activity or therapeutic response, particularly in B-cell-targeted strategies.[60]

1.4.3 HLA associations in autoimmune nodopathies

Emerging evidence suggests that specific HLA class II haplotypes may confer susceptibility to certain antibody-defined forms of AN. For example, $NF155^+$ AN has

been associated with HLA-DRB1*15 alleles in both European and Japanese cohorts, with reported odds ratios as high as 20 in comparison to seronegative CIDP and healthy controls.[64,65] Additionally, HLA-DRB1*06 has also been implicated in Japanese $NF155^+$ patients, while a more modest association has been observed between DRB1*11 alleles and $CNTN1^+$ AN. These haplotypes are neither necessary nor sufficient to trigger disease, but appear to act as risk alleles that enhance the likelihood of mounting an autoreactive response to specific nodal/paranodal antigens. This aligns with the broader hypothesis that class II HLA-mediated antigen presentation to T-helper cells is integral to the pathogenesis of AN. *In silico* modelling supports this mechanism, identifying high-affinity binding of relevant neurofascin- and contactin-derived peptides to their associated HLA alleles. To date, however, no HLA associations have been specifically described for patients with pan-NF antibodies, and this remains an important area for future investigation.

1.4.4 Restoration and modulation of immune tolerance

Therapeutic strategies to restore tolerance in autoimmunity focus on repairing dysregulated checkpoints that permit the survival and activation of autoreactive B cells. A central target is BAFF, which supports transitional and mature B cells, including autoreactive clones. BAFF inhibition, using agents like belimumab, has been shown to reduce autoreactive B-cell subsets and restore anergy, particularly in SLE and warm autoimmune hemolytic anemia.[66] More recently, BAFF-receptor-specific chimeric antigen receptor (CAR)-T cell therapies have demonstrated selective depletion of autoreactive B cells and plasma cells in murine SLE models, suggesting a novel approach for durable immunomodulation.[67]

Parallel strategies seek to enhance Treg/Tfr-mediated tolerance, for example by expanding Treg populations or enhancing their suppressive capacity. Co-stimulatory modulation using therapeutics like abatacept (CTLA-4-Ig) has been tested to suppress aberrant T-B interactions and reinforce tolerance. However, studies such as the TOLERA trial in RA suggest that sequential T- and B-cell targeting (eg, rituximab plus abatacept) does not reliably eliminate autoantibodies, underlining the complexity of tolerance restoration.[68]

In this context, the immunoglobulin isotype may influence both the pathogenic potential of autoantibodies and the capacity of B-cell clones to escape regulation. Structural features unique to IgM, such as pentameric avidity and reduced dependence on affinity maturation, may enable autoreactive clones to retain antigen-binding capacity outside of GCs.[69] Therapies that target early B-cell activation pathways – including extrafollicular responses – may therefore offer additional routes to restore immune tolerance in diseases driven by class-unswitched autoreactive clones.

Whether tolerance mechanisms are compromised in conditions like IgG1 pan-NF AN remains unclear. The developmental origins of NF186 and NF155 autoantibodies found in pan-NF AN patients and the B-cell subsets responsible for their production remain to be elucidated. Given the parallels with other neurological autoimmune diseases in which tolerance breakdown plays a central role,[60] it is plausible that similar defects in B-cell selection or regulation may contribute to the emergence and persistence of IgG1 pan-NF autoantibodies.

1.5 Pan-neurofascin autoimmune nodopathy

As previously introduced, pan-NF AN represents a rare but devastating subtype of autoimmune neuropathy, defined by autoantibodies targeting both neurofascin isoforms: NF155 and NF186. Clinically, it is notable for its fulminant onset, profound motor and sensory deficits, and frequent autonomic involvement. Unlike classical CIDP or isolated nodal/paranodal antibody syndromes, pan-NF AN frequently displays refractoriness to conventional immunotherapies such as IVIg and corticosteroids, highlighting the need for mechanistic insight into its distinct immunopathogenesis.[1]

Emerging evidence from serological and histopathological studies implicates a humoral immune signature characterised by high-titre IgG1 pan-NF antibodies.[1] These complement-fixing antibodies likely mediate tissue damage via both CDC and ADCC, facilitated by FcγR engagement on immune effector cells.[57,70,71] This contrasts with other AN variants, such as CNTN1- or Caspr1-associated IgG4 AN, where antibodies primarily disrupt protein-protein interactions without inducing overt inflammation.[6,7,57] The observation of mixed IgG1/IgG4 subclass profiles in some pan-NF AN patients raises the possibility of an evolving immune response, potentially driven by cytokines such as IL-21 that promote GC formation and CSR toward IgG1 isotypes.[19,72]

1.5.1 Autoantibody profiles in pan-NF AN

NF155 and NF186 autoantibodies in pan-NF AN disrupt axoglial integrity essential for saltatory conduction.[1] While direct evidence of complement activation in IgG1 pan-NF is still emerging, IgG1 antibodies are classically associated with strong C1q binding and potent FcγR-mediated effector functions,[73] features that likely contribute to an aggressive clinical phenotype. In contrast, IgG4 antibodies – which are structurally

monovalent due to Fab-arm exchange and exhibit reduced C1q binding – are more typical of less inflammatory forms of AN, interfering with adhesion rather than inducing cytotoxicity.[6]

Since the initial characterisation of pan-NF antibodies approximately five years ago, studies have reported distinct subclass profiles in different patient cohorts. In the earliest report by Fehmi et al (2020), all eight identified patients exhibited IgG1-restricted pan-NF antibodies, with no evidence of IgG3 or IgG4 involvement.[2] However, reports from cohorts in Germany have reported IgG3 and IgG4 predominance with little or no IgG1 reactivity.[72,74,75] This inter-cohort variability may reflect regional differences in immune priming, technical variation in subclass detection, or temporal evolution of humoral responses. Nonetheless, the repeated observation of IgG1-predominant responses in some pan-NF AN cohorts remains clinically significant, given IgG1's potent effector functions via complement activation and FcγR engagement.

The detection of IgG1, IgG4, and sometimes IgG3 autoantibodies within individual AN patients may reflect epitope spreading, subclass switching, or temporal evolution of the immune response. Longitudinal studies in other types of AN report shifts in subclass dominance over time,[76] though its clinical implications remain poorly understood, and no longitudinal subclass profiling has yet been conducted in IgG1 pan-NF AN. Nonetheless, persistent IgG1-dominated responses have emerged as potential biomarkers of disease severity, warranting their close monitoring in clinical practice.[2,7]

1.5.2 Mechanisms underlying antibody-mediated nerve damage

Pan-NF antibodies likely mediate nerve damage through direct disruption of the nodal/paranodal architecture, impeding action potential propagation. IgG1-mediated

complement activation and FcγR engagement recruit macrophages and NK cells, resulting in axonal degeneration, demyelination, and sustained inflammation (Figure 5).[77,78] Biopsy studies have reported complement deposition at sites of nerve injury in pan-NF AN, a feature not observed in IgG4-dominant cases, suggesting distinct immune effector pathways.[6,7]

A

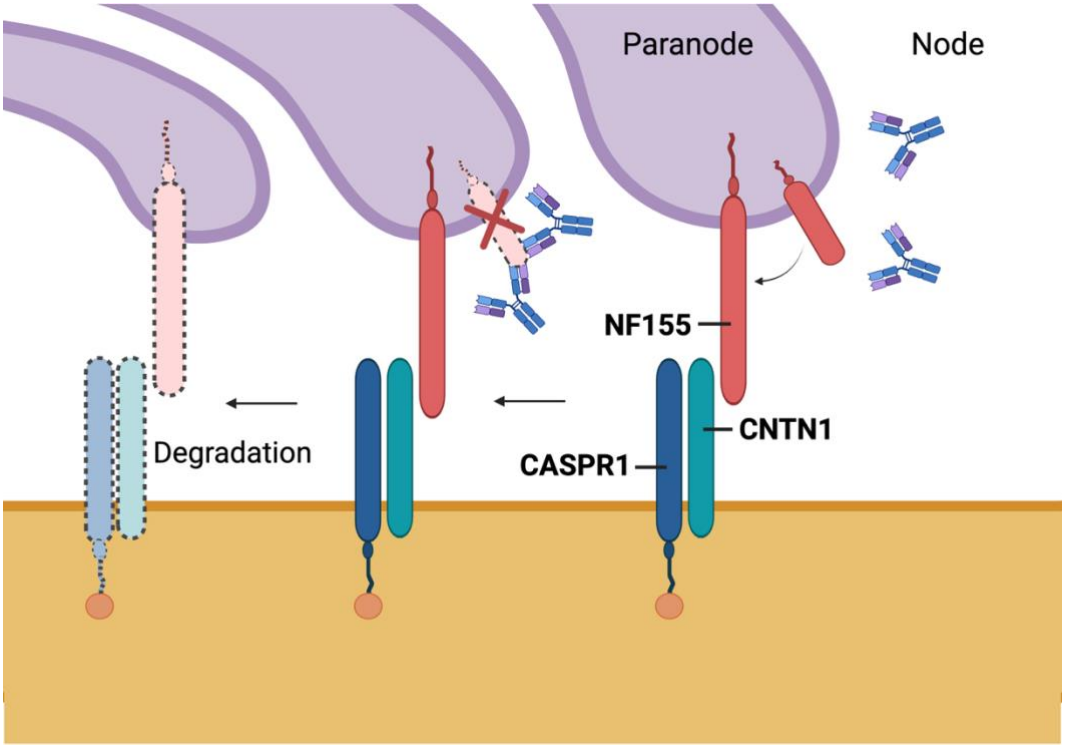

B

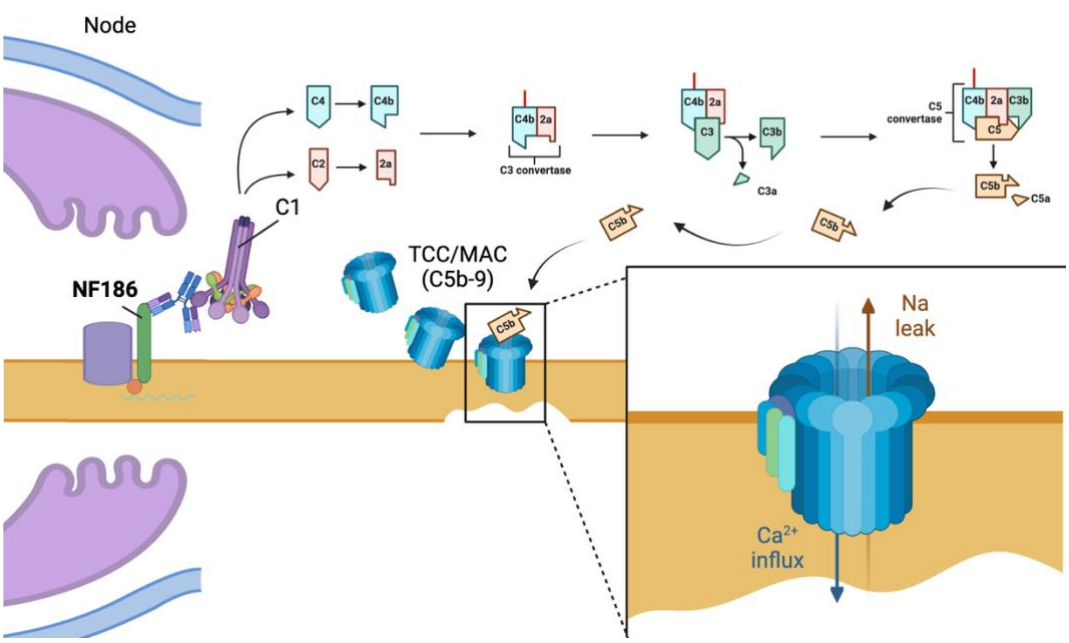

Figure 5: Pathogenic mechanisms of NF155 and NF186 antibodies. ***(A)*** *IgG1/3 subclass pan-NF antibodies likely target NF186 at the node, where they are bound by C1q and activate the complement cascade, ultimately leading to the formation of the terminal complement component (TCC) C5b-9. Inserted into the axolemma, this pore can act as a non-specific ion channel, causing reduced membrane resistance/current leak, leading to conduction block and calcium influx, activating calcium dependent proteases and leading to axonal degeneration.* ***(B)*** *In contrast, bivalent/monospecific NF155 antibodies bind to their target antigen outside of the paranode, on the nodal/abaxonal Schwann cell membrane, and prevent integration into the paranodal complex, leading to its degradation. From Bergstrom Johnson et al (2025).*[1]

The dual targeting of both NF186 and NF155 in pan-NF AN likely exacerbates nodal pathology relative to monospecific forms of AN, contributing to rapid functional decline and elevated mortality.[6] Comparative analysis with GBS and CIDP highlights overlapping effector mechanisms, but underscores the unique combination of subclass potency and dual antigen specificity in pan-NF AN.[4,56,79–85]

1.5.3 Therapeutic implications

The aggressive course of pan-NF AN necessitates immunotherapeutic strategies beyond conventional B-cell depletion. Although rituximab (anti-CD20 monoclonal antibody (mAb)) has shown clinical efficacy in some patients, its action is delayed, and it has demonstrated limited capacity to induce lasting remission. Furthermore, LLPCs, which

are $CD20^-$, reside in bone marrow niches supported by IL-6, APRIL, and BAFF, and are resistant to most frontline B-cell therapies.[86]

Consequently, new therapeutic strategies are under investigation. These include anti-CD38 mAbs and proteasome inhibitors such as bortezomib, both capable of targeting LLPCs in autoantibody-mediated diseases.[87] BAFF-blocking therapies like belimumab may also restore peripheral tolerance by reducing survival signals for autoreactive new emigrant and mature B cells, a strategy with potential relevance to pan-NF AN, given its immunopathological parallels with systemic autoimmunity.[88]

1.6 Summary and aims

Despite these advances, the origin and maintenance of IgG1 pan-NF antibodies remain poorly understood. This thesis therefore investigates the developmental trajectory of the B-cell clones producing these autoantibodies, which is essential for elucidating disease mechanisms and informing targeted interventions.

Specifically, this thesis addresses two primary questions:

1. Which B-cell subset(s) is/are predominantly responsible for producing IgG1 pan-NF antibodies?
2. How do defects in B-cell tolerance checkpoints facilitate the emergence and persistence of autoantibody responses in pan-NF AN?

To investigate these questions, a methodological approach involving peripheral blood mononuclear cell (PBMC) culture, differentiation into ASCs, immunoglobulin characterisation, BCR sequencing, mAb generation, and detailed functional analyses was employed (Figure 6).

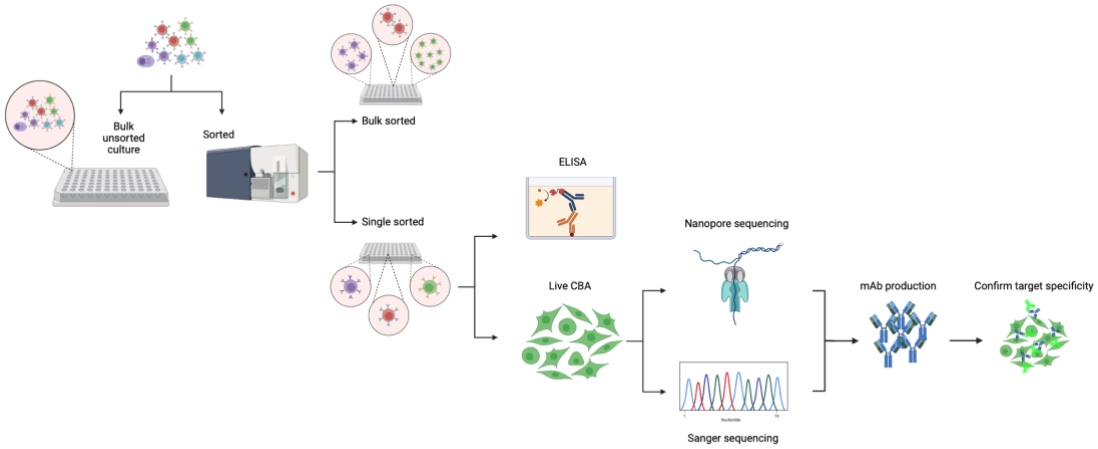

Figure 6: Schematic overview of the experimental workflow utilised in this thesis. *Key methodological steps included working from cell culture through to immunoglobulin sequencing and mAb production and analysis.*

By addressing these central questions, this work seeks to clarify some of the critical immunological events underlying pan-NF AN, potentially informing improved diagnostic tools and targeted therapeutic strategies.

2 Methods

2.1 Participants

Participant demographics and clinical features are summarised in Table 1 & Table 2, respectively. In total, 17 samples were included: eight patient-derived samples from seven patients and nine healthy control samples from eight donors.

2.1.1 Patient demographics

The patient cohort consisted of ten individuals with pan-neurofascin (pan-NF), two with neurofascin-155 (NF155), and six with contactin-1 (CNTN1) antibodies. Within the pan-NF AN cohort, sample SR834, collected on 04/08/2020, was from the oldest patient (72 years), while the youngest patient, Bio-121 (SR2348), was 18 years old at the time of sample collection. $CNTN1^{+}$ patients ranged from 15 to 77 years old.

2.1.2 Healthy control demographics

The control cohort included nine samples from eight healthy donors, with ages ranging from 20 to 43 years. Two samples (Con-017 and Con-019) were derived from the same donor.

Patient ID	Sample ID	Age	Sex	Autoantibodies	Serum titre (IgG subclass relative binding strength)			IgM score (NF155/ NF186)	Date sample collected (DD/MM/YY)	Prior Treatment
					NF155	NF186	CNTN1/ Caspr1			
Patients										
Bio-007	SR391	33	M	NF155$^+$	1:6400 4>1=2>3	Neg	Neg		02/07/19	Post-corticosteroids
	SR1495				1:800 4=1>2	Neg	Neg	1	29/11/21	
Bio-081	SR392	46	M	NF155$^+$	>1:6400 4>1>2	Neg	Neg	0	08/07/19	Pre-treatment
	SR581				1:800 4>1>2	Neg	Neg	0	14/01/20	Corticosteroids, IVIg, IA
	SR1409				1:150 1>4	Neg	Neg	0	01/10/21	Post-rituximab
	SR1383				1:150 1>4	Neg	Neg	0	01/10/21	
Bio-099	SR963	58	M	pan-NF$^+$	>1:800 1>2>3	>1:800 1>2>3	Neg		10/12/20	None
	SR964 (CSF)				Neg	Neg	Neg	0	10/12/20	None
	SR1053				1:400 1	1:600 1	Neg	1/0	15/02/21	Post-IVIg, PLEx, corticosteroids
	SR1076				1:800 1>2	>1:800 1>2	Neg	1.5/0.5	01/03/21	Post-rituximab
	SR1077				1:300 1>2	1:400 1>2	Neg	4/4	02/03/21	Post PLEx (second round)
	SR1091				1:200 1>2	1:400 1>2	Neg	0.5/3	09/03/21	
	SR1092				1:200 1>2	1:400 1>2	Neg	1.5/1.5	09/03/21	
	SR1114				1:800 1>2	1:800 1>2	Neg	0/1.5	29/03/21	Post-rituximab (26/12/20 and 19/1/21) and post-pulsed corticosteroids (18/1-22/1/21)
SR834	SR834	72	M	pan-NF$^+$	>1:800 1>3	>1:800 1>3	Neg		04/08/20	Post-IVIg, corticosteroids and PLEx, pre-rituximab
Bio-091	SR745	68	M	pan-NF$^+$	1:400 1>>3	1:400 1>>3	Neg		25/05/20	Post-IVIg, pre-rituximab
Bio-121	SR2348	18	F	pan-NF$^+$	>1:3200 1>2	1:3200 1>2	Neg	4/3	23/01/23	Post-IVIg, PLEx, cyclophosphamide; pre-rituximab
Bio-149	SR3148	45	F	pan-NF$^+$	1:3200 1>2	1:6400 1>2	Neg	3/3	08/01/24	Post-IVIg, PLEx
Bio-151	SR3161	21	M	pan-NF$^+$	1:800 1>4	1:400 1>4	Neg	0/3	04/01/24	Post-IVIg
SR2416	SR2416	69	F	pan-NF$^+$	1:200 1=4	1:200 1=4	Neg	1.5/0	13/02/23	Unknown
SR2167	SR2167	66	M	pan-NF$^+$	1:200 1>4	1:100 1>4	Neg		14/11/22	Post-IVIg, PLEx; pre-rituximab
	SR2432				1:100 1	1:100 1	Neg	1.5/0	20/02/23	Post-rituximab
SR2988	SR2988	44	F	pan-NF$^+$	1:1600 1>4=2	1:1600 1>4/2	Neg	2/2.5	23/10/23	Post-IVIg, corticosteroids
SR3001	SR3001	67	M	pan-NF$^+$	1:1200 1>4	1:800 1>4	Neg	0.5/1	16/10/23	Post-IVIg

Bio-138	SR259	64	M	CNTN1^{+}	Neg	Neg	1:1600 4>1>2	0.5	20/02/19	Post-IVIg, PLEx, corticosteroids, MMF
	SR366	65			Neg	Neg	Neg	0	19/06/19	
	SR835	66			Neg	Neg	>1:320 1=4	0	19/08/20	
	SR974	66			Neg	Neg	>1:800 1>3>2	0	04/12/20	Post-rituximab
	SR2996	69			Neg	Neg	Neg	0.5	23/10/23	
	SR3212	69			Neg	Neg	Neg	0	13/02/24	
	SR3340	69			Neg	Neg	Neg	0	03/04/24	
SR211	SR211	72	M	CNTN1^{+}	Neg	Neg	1:1600 1=4	0	30/11/18	Post-IVIg, corticosteroids
	SR323	73			Neg	Neg	Neg	0.5	08/05/19	Post-rituximab
	SR443	73			Neg	Neg	Neg	0	02/10/19	
SR144	SR251	15	M	CNTN1^{+}	Neg	Neg	1:6400 4=1>3>2	0	20/02/19	Post-IVIg, corticosteroids
	SR408	16			Neg	Neg	Pos	0	07/08/19	
	SR765	17			Neg	Neg	1:160 1>4	0	15/06/20	
	SR3108	20			Neg	Neg	1:3200 1/4>2/3	1	27/12/23	
Bio-069	SR056	71	M	CNTN1^{+}	Neg	Neg	1:6400 4	1	07/02/18	Post-IVIg
	SR3337	77			Neg	Neg	Neg	0.5	03/04/24	
SR2273	SR2273	20	F	CNTN1^{+}	Neg	Neg	1:1600 1>2=3	0	23/02/23	Post-IVIg, corticosteroids, MMF
	SR2647				Neg	Neg	1:100 1	0	30/05/23	
SR2732	SR2732	77	M	CNTN1^{+}	Neg	Neg	>1:3200 1=4>2>3	1	19/04/23	Post-IVIg, PLEx, corticosteroids
Healthy donors										
Con-010		38	M	N/A	-	-			10/10/21	
Con-011		25	F	N/A	-	-			10/10/21	
Con-012		42	M	N/A	-	-			06/12/21	
Con-013		38	F	N/A	-	-			16/03/22	
Con-014		20	M	N/A	-	-			16/03/22	
Con-015		43	M	N/A	-	-			16/03/22	
Con-017*		31	M	N/A	-	-			26/05/22	
Con-018		24	F	N/A	-	-			27/05/22	
Con-019*		31	M	N/A	-	-			28/05/22	

Table 1: Participant demographics of patients and healthy controls, *including age, sex, autoantibody status, endpoint titres, IgG subclasses present and their relative binding strengths, IgM reactivity, sample collection dates, and any treatment received. IgM reactivity was quantified qualitatively based on relative immunofluorescence intensity on a scale of 0.5-4, with 4 being the highest binding strength. No value in this column means IgM was not tested. Pan-NF: pan-neurofascin. CSF: cerebrospinal fluid. CNTN1: contactin-1. IVIg: intravenous immunoglobulin. PLEx: plasma exchange. IA: immunoadsorption. MMF: mycophenolate mofetil. *Same donor*

Pt ID	Antibodies	Acute/subacute onset	Ataxia	Tremor	Pain	Cranial nerve palsies	Autonomic dysfunction	Respiratory compromise	Nephrotic syndrome	Nadir mRs
Bio-007	**NF155$^+$**	Y	N	Y	N	N	N	N	N	2
Bio-081	**NF155$^+$**	N	Y	N	N	N	N	N	N	2
Bio-091	**pan-NF$^+$**	Y	N	N	Y	Y	N	Y	N	6
Bio-099	**pan-NF$^+$**	Y	N	N	Y	Y	Y	Y	N	6
Bio-121	**pan-NF$^+$**	Y	Y	N	N	Y	N	N	Y	5
Bio-149	**pan-NF$^+$**	Y	N	N	N	Y	N	Y	Y	5
SR834	**pan-NF$^+$**	Y	Y	N	N	Y	Y	Y	N	5

Table 2: AN participant clinical features. *NF155$^+$ patients (green) presented with milder disease, both reaching a nadir modified Rankin scale (mRs) score of 2, and exhibited features such as tremor and ataxia without cranial, autonomic, or respiratory involvement. In contrast, pan-NF$^+$ patients (salmon) exhibited a more severe clinical phenotype, with acute or subacute onset in all cases and higher mRS scores (5-6). Common features among pan-NF$^+$ patients included cranial nerve palsies (5/5) and respiratory compromise (4/5), consistent with a more aggressive disease course. Data were collected at initial clinical evaluation and prior to sample acquisition.*

2.2 Solutions

2.2.1 Cell culture media

2.2.1.1 RPMI 1640 cell culture media

Cell culture media was prepared by supplementing 500 mL of RPMI 1640 medium (chosen for its suitability for lymphocyte culture due to its balanced nutrient

composition; Gibco 21875-034) with 50 mL of heat-inactivated foetal bovine serum (FBS; Gibco 10082147) and 5 mL of antibiotic-antimycotic solution (AA; Gibco 15240-062). To create supplemented RPMI 1640 media for bulk peripheral blood mononuclear cell (PBMC) cultures, cytokines listed in Table 3 were added as required. Prepared media was stored at 4°C and used within three months of preparation.

Reagent	Make	Cat. #	Final Concentration
Bulk culture cytokines (unsorted and sorted)			
Resiquimod (R848)	Tocris Bioscience	3B/263565	2.5 μg/mL
IL-2	PeproTech	200-092-1mg	50 ng/mL
sCD40L	Miltenyi Biotec	130-096-712	50 ng/mL
IFNγ	PeproTech	300-02	20 ng/mL
TNFα	PeproTech	300-01A	1 ng/mL
IL-1β	PeproTech	200-01B	1 ng/mL
IL-21	PeproTech	200-21	50 ng/mL
Single B-cell culture cytokines			
BAFF	R&D Systems	2149-BF	10 ng/mL
IL-2	PeproTech	200-02	50 ng/mL
IL-21	PeproTech	200-21	10 ng/mL
IL-4	PeproTech	200-04	10 ng/mL

Table 3: Cell culture media components and cytokines *used in RPMI 1640 cell culture media, bulk sort cell culture media, and single-cell B-cell media (scBCM). Cat. #: catalogue number.*

2.2.1.2 Freezing media

Freezing media was made by preparing a solution of 80% heat-inactivated FBS and 20% dimethyl sulfoxide (DMSO; Sigma-Aldrich D8418).

2.2.1.3 MS40L media

To prepare MS40L media, 450 mL of IMDM without phenol red (Thermo Fisher Scientific 21056023) was supplemented with 50 mL of heat-inactivated FBS, 5 mL of penicillin/streptomycin (P/S; Gibco 15140-122), and 0.5 mL of β-mercaptoethanol (b-ME; 1:280 dilution; Gibco 11508-916).

2.2.1.4 Single-cell B-cell media (scBCM)

The base single-cell B-cell media (scBCM) was prepared by combining 500 mL of RPMI without phenol red (Gibco 32404-014) with 50 mL of qualified FBS (Gibco 10270-106), 5 mL of P/S, 5 mL of Glutamax (Gibco 35050-061), 5 mL of 1 M HEPES (Gibco 15630-080), 5 mL of MEM non-essential amino acids (Gibco 11140-035), 5 mL sodium pyruvate (Gibco 11360-070), and 0.5 mL of 50 mM b-ME (Gibco 11508-916). The corresponding cytokines listed in Table 3 were then added, depending on the culture context (bulk unsorted, bulk sorted, or single B cells). This solution was stored at 4°C for up to three months.

2.2.2 Bethyl Total IgG enzyme-linked immunosorbent assay (ELISA) reagents

All reagents were prepared fresh on the day of use unless otherwise specified.

2.2.2.1 Plate Coating Solution

110 µL of kit Capture Antibody was diluted in 11 mL of 0.05 M carbonate-bicarbonate coating buffer (pH 9.6).

2.2.2.2 Wash Solution

2 L of Tris-buffered saline (TBS; 50 mM Tris, 0.14 M NaCl, pH 8.0) was mixed with 1 mL of Tween-20 (Sigma P7949).

2.2.2.3 Blocking Solution

40 mL of TBS was supplemented with 0.4 g of bovine serum albumin (BSA; Sigma-Aldrich A8412) to yield a 1% BSA solution.

2.2.2.4 Sample Diluent

10 mL of Blocking Solution was combined with 5 µL of Tween-20 to create a 0.05% Tween-20 solution.

2.2.2.5 Horseradish peroxidase (HRP) Detection Antibody

A 1 µL aliquot of HRP Detection Antibody was pre-diluted in 199 µL of Sample Diluent. From this solution, 11 µL was diluted into 11 mL of Sample Diluent to reach a final 1:200,000 dilution.

2.2.2.6 Stop Solution

0.99 mL of 4 M sulphuric acid (H_2SO_4) was mixed with 10.01 mL of Milli-Q water.

2.2.3 Invitrogen Total IgG and IgM ELISA reagents

All reagents were prepared fresh on the day of use unless otherwise stated.

2.2.3.1 Capture Antibody Solution

Capture antibody from the kit was diluted 1:250 in kit 1X Coating Buffer.

2.2.3.2 Wash Buffer

1X PBS was combined with Tween-20 to yield a 0.05% Tween-20 solution.

2.2.3.3 Detection Antibody Solution

The Detection Antibody concentrate supplied in the kit was diluted 1:250 in 10 mL of kit 1X Assay Buffer per 96-well plate.

2.2.3.4 Stop Solution

Equal parts of 2 M H_2SO_4 and Milli-Q water were combined to create a 2 N solution.

2.2.4 Neurofascin commercial proteins

2.2.4.1 NF155

50 µg of recombinant human, HEK293-derived neurofascin protein (R&D Systems 8208-NF) was reconstituted in 500 µL of 0.01 M PBS to create a 100 µg/mL stock solution. Aliquots were stored at -80°C.

2.2.4.2 NF186

20 µg of human recombinant NF186 protein (Origene SC327705) was reconstituted in 200 µL of 0.01 M PBS, yielding a 100 µg/mL stock solution. Aliquots were stored at -80°C.

2.2.5 NF155 and NF186 ELISA reagents

All reagents were prepared fresh on the day of use unless stated otherwise.

2.2.5.1 Plate Coating Solution

Reconstituted NF155 or NF186 commercial protein was diluted to 1 µg/mL in PBS (10 µL of 100 µg/mL stock per mL).

2.2.5.2 Blocking Solution

A 5% solution of non-fat milk (Sigma-Aldrich M7409) in 0.01 M PBS was prepared the day before use and stored overnight at 4°C.

2.2.5.3 Secondary Antibody Solutions

HRP-conjugated goat anti-human secondary antibodies (Table 4) were diluted in Blocking Solution.

Host	Specificity	Conjugate	Manufacturer	Cat. #	Dilution
Goat anti-human	IgG (Fc-specific)	HRP	Sigma	A0170	1:3000
Goat anti-human	IgG (κ light chains – bound and free)	HRP	Sigma	A7164	1:500
Goat anti-human	IgG (λ light chains – bound and free)	HRP	Sigma	A5175	1:500
Goat anti-human	IgM (μ-chain specific)	HRP	Sigma	A0420	1:3000

Table 4: ELISA secondary antibodies, *including host species, antibody specificity, conjugate, manufacturer, catalogue number, and working dilution. All antibodies were goat-derived and conjugated with HRP for detection. Both Fc-specific and light-chain specific antibodies for IgG, as well as an IgM-specific antibody, are included. Cat. #: catalogue number.*

2.2.5.4 O-phenylenediamine dihydrochloride (OPD) Substrate

One gold and one silver SigmaFast OPD tablet (SigmaFast P9187) were dissolved in 20 mL of distilled water and shaken vigorously to ensure complete dissolution immediately before use.

2.2.6 IgM GM1 ELISA reagents

All reagents were made fresh on the day of use. GM1 stock (Sigma G9652-1MG) and working solutions were sonicated for 3 minutes before use to ensure homogeneity. Working solutions were prepared by diluting the stock GM1 in methanol to a final concentration of 2 μg/mL and used immediately.

2.2.7 Plasmid midi prep reagents

2.2.7.1 LB agar

16 g of LB agar (Invitrogen 22700025) was dissolved in 500 mL of Milli-Q water in a 500 mL Duran bottle and autoclaved for 15 minutes at 121°C. If the agar solidified before use, it was gently warmed in increments of 15-30 seconds in a microwave to avoid overboiling until thoroughly melted again. Once melted, it was cooled under cold

running water until comfortable to the touch. Unused agar was kept for up to 3 months at room temperature.

2.2.7.2 LB broth

20 g of LB broth (Sigma-Aldrich L3022) was dissolved in 1 L of Milli-Q water in a 1 L Duran bottle and autoclaved for 15 minutes at 121°C. Unused broth was kept for up to 3 months at room temperature.

2.2.8 Cell-based assay (CBA) reagents

2.2.8.1 CBA media

500 mL of DMEM (Gibco 41965-039) was supplemented with 50 mL of heat-inactivated FBS (Gibco 10082147) and 5 mL of AA (Gibco 15240-062). Media was stored at 4°C and used within three months.

2.2.8.2 Poly-D-lysine (PDL) stock solution

5 mg of poly-D-lysine (PDL) powder (Sigma P6407) was reconstituted by adding 5 mL of sterile distilled water to create a 1 mg/mL solution. This was filtered through a 0.22 µm sterile filter, aliquoted, and stored at -20°C for up to six months. Freeze-thaw cycles were minimised.

2.2.8.3 Homebrew polyethylenimine (PEI)

45 mg polyethylenimine was dissolved in 6.5 ml of distilled water on a rolling mixer in the dark for 1 hour. When fully dissolved, concentrated HCl was used to adjust the pH to 7.2, and the final volume made up to 8 ml with additional distilled water as required. The solution was then filter sterilised, aliquoted and kept in the dark prior to use.

2.2.8.4 Chicken anti-neurofascin secondary antibody

100 µg of chicken anti-neurofascin (anti-NF) antibody (R&D Systems AF3235) was reconstituted at 200 µg/mL in sterile PBS, aliquoted, and stored at -20°C for up to one year. Thawed aliquots were kept at 4°C for up to one month.

2.2.8.5 4% PFA

10 mL of 16% paraformaldehyde (PFA; Thermo Fisher Scientific 28908) was diluted in 30 mL of PBS and kept at 4°C for up to two months.

2.2.8.6 CBA washing media

DMEM (Gibco 41965-039) was supplemented with HEPES (Sigma-Aldrich H3375) at a concentration of 20 mM.

2.2.8.7 Poly-L-lysine (PLL) stock solution

5 mL of poly-L-lysine (PLL; Sigma P2636) was diluted in 500 mL of PBS (Gibco 10010023) to create a 1% solution. This was then filter sterilised and stored at 4°C for up to six months.

2.2.8.8 CBA media (no glucose)

500 mL of DMEM without glucose (Fisher Scientific 11520416) was supplemented with 50 mL of heat-inactivated FBS (Gibco 10082147) and 5 mL of AA (Gibco 15240-062). This was stored at 4°C and used within three months.

2.2.9 Flow cytometry and fluorescence-activated cell sorting (FACS) reagents

2.2.9.1 FACS buffer

25 mL of heat-inactivated FBS was diluted in 500 mL of PBS containing 0.1% sodium azide (Merck S2002) to create a 5% solution. This was filter sterilised and stored at 4°C for up to six months.

2.2.9.2 MACS buffer

MACS buffer was freshly prepared by combining 500 mL of PBS with 15.5 mL of FBS and 2 mL of 0.5 M sterile EDTA, pH 8.0 (Thermo Fisher Scientific 15575020).

2.2.9.3 scBCM + $MgCl_2$

scBCM + $MgCl_2$ was prepared fresh for each cell sort. 1 mL of 1 M $MgCl_2$ (Sigma-Aldrich 208337) was added to 200 mL of scBCM to yield a 5 mM solution and filter sterilised through a 0.22 μm syringe filter. The resulting solution was stored overnight at 4°C the day before use.

2.2.9.4 DNase buffer

0.3 mL of 10,000 U/mL recombinant DNase I (Sigma-Aldrich 04536282001) was combined with 30 mL of scBCM + $MgCl_2$ solution on the day of use.

2.2.10 Sanger and Nanopore sequencing reagents

2.2.10.1 Buffer RPE

Four volumes of 99% ethanol were added to the Buffer RPE from the RNeasy® 96 Kit (Qiagen 74181) with each new kit.

2.2.10.2 Random primer mix

2.5 µL of random hexamer primers (Thermo Fisher Scientific SO142), 0.25 µL of CH5 (#200) universal immunoglobulin reverse primer (Eurofins; appendix 8.1.1), and 1.75 µL of nuclease-free water were mixed per well of reverse transcription polymerase chain reaction (RT-PCR) reaction. All reagents were prepared on a 4°C cool block inside a UV-sterilised hood.

2.2.10.3 25% Igepal solution

275 µL of Igepal CA-630 (MP Biomedicals 0219859680) was added to 1125 µL of nuclease-free water using a cut P1000 micropipette tip for easier dispensing. This was stored at room temperature in an opaque container for up to one year.

2.2.10.4 RT Mastermix

The RT Mastermix was freshly prepared in a UV-sterilised 1.5 mL Eppendorf tube inside the UV hood on a 4°C cool block. Components were added in the following order: 10 µL of Superscript IV (SSIV) 5X RT buffer (contained in Invitrogen 18090050B Superscript IV kit), 2.5 µL of 10 mM deoxyribonucleotide triphosphates (dNTPs; Invitrogen 18427013), 2 µL of 25% Igepal solution, 1 µL of 0.1 M dithiothreitol (DTT; Invitrogen 18090050B), 0.5 µL RNAsin ribonuclease inhibitor (Promega N2518), and SSIV enzyme (contained in Superscript IV kit) per well of RT-PCR reaction. The RNAsin and Superscript IV enzyme were kept at -20°C until just before use, and then thawed on the 4°C cool block inside the UV hood before adding to the RT Mastermix last. The RT Mastermix was then vortexed and centrifuged briefly before use.

2.2.10.5 PCR1 primer mixes

PCR1 primer mixes were prepared separately inside a UV-sterilised hood to avoid cross-contamination. To make the heavy chain PCR1 leader primer mix (PCR1-H), 10 µL of each PCR1-H primer (appendix 8.1.2) was combined with 140 µL of nuclease-free water in a 1.5 mL Eppendorf tube. To make the kappa light chain PCR1 leader primer mix (PCR1-κ), 10 µL of each PCR1-κ primer were combined with 140 µL of nuclease-free water. To make the lambda light chain PCR1 leader primer mix (PCR1-λ), 10 µL of each PCR1-λ primer were combined with 110 µL of nuclease-free water. PCR1 primer mixes were stored at -20°C.

2.2.10.6 PCR1 Mastermix

10 µL of GoTaq G2 polymerase (Promega M7823), 2 µL of PCR1 primer mix, and 6 µL of nuclease-free water per well of PCR1 reaction were combined in a UV-sterilised 1.5 mL Eppendorf on a 4°C cool block.

2.2.10.7 PCR2 primer mixes

The PCR2 primer mixes were prepared inside a UV-sterilised hood similarly to the PCR1 mixes, combining 10 µL of each primer for that specific chain (appendix 8.1.2) with nuclease-free water to a final volume of 200 µL for each primer mix.

2.2.10.8 PCR2 Mastermix

This was prepared like the PCR1 Mastermix but using PCR2 primers.

2.2.10.9 Nanopore RT mixture

To prepare 10 µL of the Nanopore RT mixture, the following components were combined and used immediately: 1 µL of 10 mM dNTP mix (Promega U1511), 2.5 µL of 4x template-switching reaction buffer (New England Biolabs M0466L), 0.3846 µL of template-switching oligo (appendix 7.2.4, Integrated DNA Technologies), 0.25 µL of RNAsin Plus (Promega N2611), 1 µL of template-switch RT mix (New England Biolabs M0466L), and 4.8654 µL of nuclease-free water (QIAGEN 29115).

2.2.10.10 Nanopore RT-PCR mixture

Each primer listed in Appendix 8.1.4 (Integrated DNA Technologies) was diluted 1:10 in nuclease-free water. To prepare 9 µL of the Nanopore RT-PCR mixture, 5 µL of NEBNext Ultra II Q5 Master Mix (New England Biolabs M0544S), 0.5 µL of each diluted primer, and 1.5 µL of nuclease-free water were combined and used immediately.

2.2.11 HisPur cobalt purification

2.2.11.1 MES Buffer

0.5 M MES buffer (pH 5.0; Alfa Aesar J62081.AE) was diluted to a final concentration of 20 mM and sodium chloride (Sigma-Aldrich S9888) was diluted to 0.1 M in 100 mL of Milli-Q water.

2.2.11.2 Equilibration/Wash Buffer

Sodium phosphate (Sigma-Aldrich S8282) and sodium chloride were dissolved in 200 mL of Milli-Q water to concentrations of 50 mM and 300 mM, respectively, and imidazole (Sigma-Aldrich 2399) was added to 10 mM.

2.2.11.3 Elution Buffer

The same sodium phosphate and sodium chloride mixture from the Equilibration/Wash Buffer was used, with imidazole adjusted to a final concentration of 150 mM.

2.2.12 HisPur nickel-nitrilotriacetic acid (Ni-NTA) purification

All reagents used for Ni-NTA purification were adjusted to pH 7.4 using 1 M NaOH and filtered through a 0.22 μm filter before use. Reagents were stored at room temperature for up to three months.

2.2.12.1 Equilibration Buffer

20 mM sodium phosphate, 300 mM sodium chloride, and 10 mM imidazole were combined in Milli-Q water.

2.2.12.2 Wash Buffer

25 mM of imidazole was added to Equilibration Buffer.

2.2.12.3 Elution Buffer

250 mM of imidazole was added to Equilibration Buffer.

2.2.13 Western blotting

All reagents were stored at room temperature for up to three months following preparation.

2.2.13.1 1X MOPS SDS Running Buffer

50 mL of 20X MOPS SDS Running Buffer (Thermo Fisher Scientific NP0001) was diluted in 950 mL of deionised water.

2.2.13.2 1X Bis-Tris Transfer Buffer

50 mL of 20X Bis-Tris Transfer Buffer (Thermo Fisher Scientific BT001) was diluted in 950 mL of deionised water.

2.2.13.3 PBST

PBS was mixed with Tween-20 (Sigma P7949) to create a 0.05% solution.

2.2.14 Borate buffer (0.67 M, pH 8.5)

4.14 g of boric acid (Sigma B7901) was added to 100 mL of deionised water, mixed, and heated on a stir plate until the boric acid fully dissolved. Sodium hydroxide (NaOH) was added dropwise to the solution to raise the pH to approximately 8.5.

2.2.15 PCSK9 protein

25 µg of biotinylated human proprotein convertase subtilisin/kexin type 9 (PCSK9) protein with an Avitag and His tag (Acro Biosystems PC9-H82E7) was reconstituted in 125 µL of sterile water to create a 200 µg/mL stock solution. The solution was mixed gently with a P200 micropipette every 5 minutes for 30 minutes at room temperature to ensure thorough mixing. Aliquots were stored at -20°C for up to three months.

2.3 PBMC processing

PBMCs were isolated from healthy control and patient whole blood using Lympholyte-H media (Cedarlane CL5020) in SepMate tubes (StemCell Technologies 85450). The isolated PBMCs were centrifuged and washed to remove contaminants, then resuspended in a 1:1 mixture of RPMI 1640 cell culture media and freezing media. The cell suspensions were immediately transferred to -80°C in a Corning CoolCell LX Cell

Freezing container (Merck CLS432002) prior to transfer to liquid nitrogen storage after 24 hours.

2.4 PBMC cultures

2.4.1 PBMC thawing and counting

Cell culture media was prepared fresh on the day of thaw, with one 10 mL aliquot per vial warmed to 37°C in a hot water bath. An additional 12 mL vial of cell culture media per vial was brought to room temperature.

Cryopreserved PBMC vials were thawed by swirling in a 37°C water bath until a small ice crystal remained. Thawed cells were transferred to a biosafety cabinet (BSC) where 1 mL of warmed media was added dropwise with a P1000 micropipette and mixed gently. The mixture was then combined with the remaining 10 mL of warmed media and an additional 1 mL used to rinse the original vial.

Cells were left undisturbed for 5 minutes, centrifuged at 400xg for 5 minutes at 21°C, and the supernatant was aspirated using a vacuum. Each cell pellet was resuspended in 1 mL of room temperature media and left for 2 minutes before adding 9 mL more to reach a 10 mL total volume. The cells were then centrifuged, the supernatant removed, and the pellet resuspended in 1 mL of room temperature media. Each cell pellet was allowed to rest for at least 2 minutes in the media before adding 9 additional mL of media to each cell pellet, for a total of 10 mL. The resuspended PBMCs were then centrifuged again and the supernatant removed by vacuum aspirator before resuspending in 1 mL of room temperature cell culture media per cell pellet using a P1000. PBMCs from the same patient were combined and mixed well. Cell concentration was determined by

mixing 5 µL of mixed cells with 485 µL of media and 10 µL of Trypan blue (Invitrogen T10282) in a 1.5 mL Eppendorf tube inside the BSC. A 10 µL aliquot of this mixture was placed on a haemocytometer, counted under 10x magnification on a Leica bright-field microscope, and averaged across four quadrants. The average count was multiplied by 10^6 to calculate the cell concentration in cells/mL.

2.4.2 Bulk unsorted cultures

Protocols for immunoglobulin production in PBMCs were developed according to the flow diagram in Figure 7.

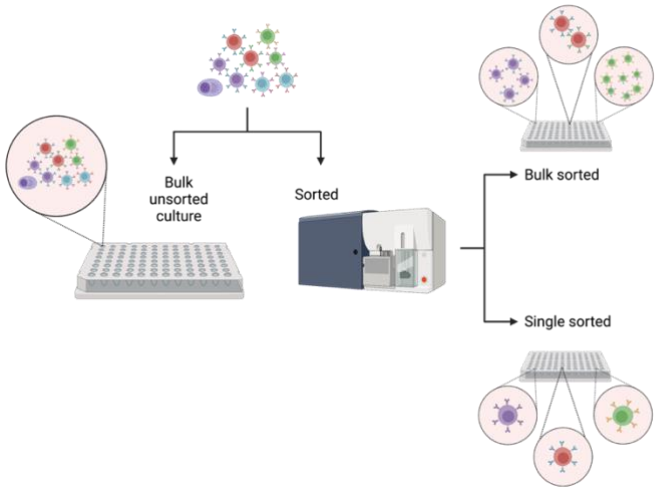

Figure 7: Culture strategy for PBMCs. *Bulk unsorted cells were directly plated in 96-well plates, with all subpopulations of B cells present in each well. Bulk sorted cells were sorted into 15 mL conical tubes and then plated at varying concentrations within subpopulations, so that any given well contained B cells only from one subpopulation.*

For bulk unsorted cultures, after counting, PBMCs were resuspended in RPMI 1640 cell culture media at a concentration of $1x10^5$ or $1x10^6$ cells/mL. 200 µL of this mixture was seeded into each well of a 96-well, flat-bottom, tissue culture (TC)-treated 96-well microplate (Merck CLS3595 or Starlab CC7682-7596). After approximately 10 minutes, when the cells had settled and adhered, 100 µL of media was removed from each well using a 300 µL multichannel pipette and replaced with 100 µL of freshly

prepared, supplemented RPMI 1640 cell culture media containing cytokines at double the desired final concentration to simulate a media change. PBMCs were cultured for five to 14 days at 37°C in an incubator in the presence or absence of various cytokines to stimulate immunoglobulin production (Table 3).

2.4.3 Bulk sorted cultures

After sorting by FACS as detailed in section 2.9.1, bulk sorted PBMCs were seeded into flat-bottom TC-treated 96-well plates (Fisher Scientific 10695951) at the desired concentration. Cells were allowed to settle and adhere to the plate surface for at least 20 minutes. Half of the media in each well was then carefully removed using a multichannel micropipette and replaced with media (if supplemented with cytokines, cytokines were added to the media at double their desired final concentration). The plates were subsequently incubated for 14 days before collection and culture supernatants were immediately frozen at -80°C for downstream analysis.

2.4.4 Single-sorted cultures

2.4.4.1 Day -1

MS40L cells expressing membrane-bound CD40 ligand (mCD40L) were plated the day before single B-cell sorting. Confluent MS40L cells were washed with 10 mL of sterile PBS, then detached using 1 mL of 1X trypsin-EDTA (Thermo Fisher Scientific 25200056) and incubated at 37°C for 1-2 minutes. Trypsin activity was neutralised by adding 10 mL of MS40L media, and the cell suspension was transferred to a 50 mL conical tube.

Cells were counted using a haemocytometer. To maintain the MS40L cell culture, a new T75 flask was seeded with 13 mL of fresh MS40L media and a 1:25 dilution of the trypsinised cells. The remaining cells were centrifuged at 1200 rpm for 5 minutes at room temperature, then washed twice with 10 mL of scBCM.

After the final wash, MS40L cells were resuspended in scBCM and plated at 1000 cells/well in 96-well flat-bottom plates, achieved by dispensing 100 µL of a 10,000 cells/mL suspension into each well. Plates were incubated overnight at 37°C in a humidified incubator with 5% CO_2 to establish a stable feeder layer.

2.4.4.2 Day 0

Single B cells were prepared and sorted from cryopreserved PBMCs directly onto MS40L feeder cells in scBCM by FACS, as detailed in section 2.9.2.

2.4.4.3 Days 1-25

Single B cells were cultured for 25 days post-plating. Media changes were performed on days 0, 4, 8, 11, 14, 18, and 22. Supernatants were collected during media changes on days 14 and 25, then immediately frozen at -80°C for subsequent analysis. On day 25, cells were lysed for RNA preservation and downstream applications.

2.5 ELISAs

2.5.1 Total IgG/IgM ELISAs

Total IgG levels were measured using Bethyl Laboratories (E80-104) and Invitrogen (88-50550) total IgG ELISA kits, while total IgM was quantified using an Invitrogen Total IgM ELISA kit **(**88-50620-88). Absorbance was measured at 450 nm using a

BMG LabTech FLUOstar Omega plate reader. Data were analysed using a four-parameter logistic curve generated with MyAssays.com.

2.5.1.1 Bethyl Total IgG ELISA

Plates were coated with 95 µL of Plate Coating Solution in Nunc Maxisorp 96-well plates (Invitrogen 44-2404-21) and incubated for 1 hour at room temperature on a shaker plate at 600 rpm. Standards were prepared by serially diluting a 4.4 mg/mL IgG stock to generate concentrations ranging from 250 ng/mL to 3.9 ng/mL. The serial dilution was performed in Sample Diluent, and a blank sample was prepared using 500 µL of Sample Diluent. After incubation, plates were washed four times using Wash Solution, blotted dry on a paper towel, and blocked with 200 µL of Blocking Solution per well for 30 minutes at room temperature under foil on a shaker plate at 600 rpm.

After washing plates again four more times, 100 µL of each standard in duplicate, and 50 µL of each sample were added to wells and incubated for 1 hour at room temperature under foil on a shaker plate. Plates were washed four times, incubated with 100 µL/well of HRP Detection Antibody Solution for 1 hour under foil, then washed again four times. 100 µL of room temperature 3,3',5,5'-Tetramethylbenzidine (TMB) Substrate Solution was added to each well, and the plates were incubated for 15–20 minutes at room temperature under foil on a shaker plate. The reaction was stopped by adding 100 µL of Stop Solution to each well, and the absorbance was measured at 450 nm.

2.5.1.2 Invitrogen Total IgG and IgM ELISAs

96-well Nunc Maxisorp plates were coated with 100 µL/well of Capture Antibody Solution, sealed, and incubated overnight at 4°C. On the following day, the Capture Antibody Solution was discarded by flicking the plate into a sink, followed by two

washes with Wash Buffer. Residual buffer was removed by blotting the plate on absorbent paper. To block nonspecific binding, 250 µL/well of 2X Blocking Buffer was added and incubated for 2 hours at room temperature on a shaker plate at 400 rpm. Standards and samples were prepared, with human sera diluted 1:10,000 if necessary inside a BSC. Standards were reconstituted to the concentration specified on the standard vial using distilled water and serially diluted two-fold to generate a standard curve. After blocking and washing twice, 100 µL/well of each standard (tested in duplicate) or (pre-diluted) sample was added to the appropriate wells and incubated for 2 hours at room temperature on a shaker plate at 400 rpm.

Following incubation and four additional washes, the plate was blotted dry and 100 µL/well of Detection Antibody Solution was added. The plate was sealed and incubated again at room temperature for 1 hour on a shaker plate, washed four times, and 100 µL/well of room temperature TMB substrate solution added. The plate was incubated at room temperature for 15 minutes to allow colour development. 100 µL/well of Stop Solution was then added to terminate the reaction and the absorbance was measured at 450 nm.

2.5.2 NF155 and NF186 ELISAs

Nunc MaxiSorp 96-well plates were coated with 100 µL/well of Plate Coating Solution containing 100 ng of commercial NF155 or NF186 protein and incubated overnight at 4°C. The following day, the Plate Coating Solution was discarded by tipping it off into a sink, ensuring the wells did not dry before adding 200 µL/well of Blocking Solution and incubating for 1 hour at room temperature. Following incubation, the Blocking Solution was tipped off, 100 µL of sera diluted in Blocking Solution (1:100 for screening, 1:200

for subclass analysis) was added to the wells, and the plates were incubated for 1 hour at room temperature. Following incubation, plates were washed five times by submersion in a PBS wash bath and incubated with 100 µL/well of Secondary Antibody Solution for 1 hour at room temperature. Following a final four washes, during a fifth wash, wells were left to sit with PBS while the OPD Substrate was prepared. After removing the fifth PBS wash and patting the plates dry, 50 µL of OPD Substrate was added to each well for 20 minutes at room temperature, protected from light. The reaction was stopped with 25 µL/well of 4 M H_2SO_4. Absorbance was read at 492 nm, with OD measurements of PBS-coated wells subtracted from those of NF-coated sample wells to correct for background signal. ODs of at least four standard deviations above negative controls after correction were considered positive.

2.5.3 IgM GM1 ELISA

Nunc MaxiSorp 96-well plates were coated with 100 µL/well of GM1 solution and allowed to air dry overnight in a fume hood. Wells coated with methanol only were included as negative controls. The following day, plates were stored at 4°C for at least 1 hour, and then blocked with 200 µL/well of 2% BSA in PBS for 1 hour at 4°C. Samples were diluted as required in 1% BSA in PBS, and 100 µL of diluted sample was added per well and incubated at 4°C for 2 hours. After the solution was tipped and shaken off, the plates were washed five times by plunging into cold PBS and emptying thoroughly. 100 µL/well of secondary antibody (Table 4) diluted 1:3000 in 1% BSA was then added and incubated for 1 hour at 4°C. Following a final wash, 50 µL of OPD substrate solution was added to each well for 20 minutes, then stopped with 25 µL of 4 M H_2SO_4. Absorbance was read at 492 nm. After background correction, ODs > 0.2 were considered positive.

2.6 Plasmid midi prep

Plasmid DNA was purified using an Invitrogen PureLink Fast Low-Endotoxin Midi Plasmid Purification Kit (Thermo Fisher Scientific A35892). Next to a Bunsen burner, ampicillin (Sigma-Aldrich A5354) was diluted 1:1000 from a 100 mg/mL stock solution and added to autoclaved LB agar. 25 mL of the agar was transferred to a 10 cm petri dish and allowed to cool for 1 minute with the lid slightly ajar, then sealed with parafilm and stored at 4°C.

Next, 15 µL of stable, high-efficiency competent *E. Coli* (New England Biolabs C3040I) was transferred to a 0.5 mL Eppendorf tube, and 2 µL of previously-purified DNA was added next to a Bunsen burner. This mixture was incubated on ice for 30 minutes before undergoing heat shock at 42°C on a heat block for 30 seconds, then returned to ice for 5 minutes. To promote recovery, 250 µL of room temperature Super Optimal broth with Catabolite repression (SOC) outgrowth medium (New England Biolabs B9020S) was added, and the mixture was incubated at 37°C in a shaking incubator at 250 rpm for 1 hour. Following incubation, 50 µL of the transformation mixture was dripped evenly around the prepared LB agar plate and spread in a zigzag pattern using an L-stick. The plate was left with the lid slightly ajar for 3 minutes to allow excess moisture to evaporate. Plates were then inverted and incubated overnight at 37°C in an incubator.

The following day, single colonies were selected based on medium size, uniform circular shape, and lack of isolation from neighbouring colonies using a P200 pipette tip. Each pipette tip containing the selected colony was transferred to a single 15 mL conical tube containing 5 mL of LB broth supplemented with ampicillin (1:1000

dilution). Tubes were incubated at 37°C in a shaking incubator at 250 rpm for 4 hours. Colony density was checked by measuring absorbance using a BMG LabTech FLUOstar Omega microplate reader. Once acceptable density was confirmed, each culture was transferred to 100 mL of LB broth with ampicillin in 1 L Duran bottles. The cultures were incubated overnight at 37°C in a shaking incubator at 250 rpm.

The following day, cultures were transferred to two 50 mL conical tubes per 1 L Duran bottle, centrifuged at 3500xg for 10 minutes at 21°C, and the supernatant was discarded. Bacterial pellets were resuspended in 10 mL of Resuspension Buffer, combining up to two cell pellets from the same originating plasmid in one 50 mL conical tube to improve yield, followed by the addition of 10 mL of Lysis Buffer with six inversions to mix. After a 3-minute incubation, once the solution turned dark purple indicating successful lysis, 10 mL of Precipitation Buffer was added and mixed by inversion until the solution turned yellow.

The lysate was loaded into a syringe filter, incubated for 5 minutes to allow precipitates to float to the top, and then filtered through a syringe filter into a new 50 mL conical tube. Lysates were then mixed with 10 mL of Binding Buffer by inverting the tubes 10 times. The mixture was transferred to spin columns 10 mL at a time and centrifuged at 500xg for 2 minutes, discarding the flow-through until all lysate had been filtered. Each column was washed once with 700 µL of Wash Buffer 1, followed by centrifugation at 17,000xg for 1 minute; this was repeated twice with Wash Buffer 2 (containing ethanol). The columns were centrifuged twice more, the flow-through discarded, and then transferred to clean 1.5 mL Eppendorf tubes. 100 µL of pre-warmed (65°C) Elution Buffer was added to each spin column. After a 10-minute incubation, plasmid

DNA was collected by centrifugation at 17,000xg for 1 minute. The plasmid DNA concentration was measured in triplicate using a Nanodrop spectrophotometer set to "double-stranded DNA" mode. Samples were aliquoted and stored at -20°C.

2.7 Live CBA

Transiently transfected live CBAs using HEK293T cells were employed to detect NF155 and NF186 binding in PBMC culture supernatants and monoclonal antibodies (mAbs).

2.7.1 HEK293T culture

Cryopreserved HEK293T cells were thawed into CBA media as described in section 2.4. A total of $2x10^6$ cells were added to 10 mL of CBA media and seeded into a TC-treated T75 flask. The flask was gently swirled to ensure even cell distribution and incubated undisturbed for three days to reach 70-80% confluency.

Cells were passaged by washing with PBS to remove residual media, followed by incubation with a thin layer of TrypLE (Gibco 12605-028) for 3 minutes at 37°C. The dissociated cells were diluted 1:5 with PBS, centrifuged at 400xg for 5 minutes, and the supernatant removed using a vacuum aspirator. The cell pellet was resuspended in CBA media, and 20-50 µL was transferred to a new T75 flask containing 10 mL of media. Cells were maintained by passaging 1-2 times weekly.

2.7.2 24-well plate CBA

For CBAs performed in 24-well TC plates (Starlab CC7682-7524), HEK293T cells were seeded at $5x10^4$ cells/well on PDL-coated glass coverslips.

2.7.2.1 Day 1

On day 1, acid-treated glass coverslips were dried and prepared. One coverslip was placed in each well. 100 µL of diluted PDL solution was added dropwise to each coverslip to ensure uniform coverage and incubated undisturbed at room temperature for 1 hour. After incubation, excess PDL was removed using a vacuum aspirator inside the BSC, and the coverslips were dried for an additional 30-60 minutes. If HEKs already in culture were used for the CBA, they were dissociated and prepared as a single-cell suspension while the PDL-coated coverslips dried.

Once the coverslips were dry, $5.0x10^4$ cells/well were plated by resuspending/diluting the HEKs in CBA media to a final concentration of $5.0x10^5$ cells/mL. Subsequently, 100 µL of the cell suspension was added dropwise to each coverslip to ensure complete coverage. Cells were allowed to settle undisturbed for 10-15 minutes before the plate was transferred to an incubator. After at least 10-20 minutes in the incubator, when the HEKs had fully attached to the coverslips, 400 µL of additional CBA media was gently added to the side of each well, and the plate was returned to the incubator.

2.7.2.2 Day 2

On day 2, the HEKs were transfected using a PEI-DNA complex. Homebrew PEI (5.625 µg/µL) was diluted to 1 µg/µL in 150 mM sodium chloride, and this solution was added dropwise to 50 µL of plasmid DNA to achieve a final plasmid concentration of 1 µg/µL. NF155 and NF186 plasmids were either co-transfected in the same well or transfected and tested in separate wells. The PEI-plasmid mixture was vortexed, briefly centrifuged, and incubated for 15 minutes at room temperature. After incubation, 100 µL of the PEI-plasmid mixture was added dropwise around each well to ensure even

distribution, resulting in a final volume of 600 µL in each well. The cells were then incubated for at least 7 hours or overnight before the media was aspirated and replaced with 500 µL/well of fresh CBA media. The plate was subsequently returned to the incubator.

2.7.2.3 Day 3

On day 3, the plates were left undisturbed to allow continued cell growth and transgene expression.

2.7.2.4 Day 4

On day 4, CBA media was pre-warmed to room temperature. Reconstituted chicken anti-NF secondary antibody was diluted 1:1000 in DMEM supplemented with 1% BSA and 1% AA, alongside serum controls diluted at 1:100. Samples to be tested for binding were similarly diluted if needed. All samples and controls being tested for neurofascin binding were combined with chicken anti-NF antibody to verify successful transfection.

Inside the BSCs, HEKs were gently washed with 250 µL/well of the room temperature CBA media and replaced with 250 µL of fresh media. The media was carefully aspirated from the edges of the wells and replaced with 250 µL/well of the serum/ or sample/chicken anti-NF mixtures. Plates were incubated for 1 hour at 37°C while 4% PFA was warmed to room temperature. Following incubation, wells were washed three times with 300 µL PBS, taking care not to disturb the cells.

Next, half of the media in each well was removed and replaced with 300 µL of 4% PFA, and the plates were incubated for 20 minutes at room temperature. Wells were then washed five times with 300 µL of CBA washing media. To stain the cells, 300 µL of

goat anti-human IgG Heavy + Light Alexa Fluor (AF)488 (Invitrogen A11013; 1:750 dilution) or goat anti-human IgG F(ab')2 Fc-specific AF488 (Invitrogen H10120; 1:750 dilution), combined with goat anti-chicken IgY AF546 (Invitrogen A11040; 1:1000 dilution), in CBA washing media with 1% BSA were applied to the fixed cells (Table 5). The plates were covered with aluminium foil and incubated on a shaker at 30-40 rpm for 1 hour at room temperature.

After incubation, the wells were washed four times with PBS. Subsequently, 300 µL of PBS containing 0.1% Triton X-100 (Merck X100) and 4',6'-diamidino-2-phenylindole (DAPI; Thermo Fisher Scientific D1306; 1:50,000 dilution) was added to each well to permeabilise the cells. Plates were incubated for 30 minutes on a shaker at 30-40 rpm. The cells were washed twice with 300 µL of PBS before imaging. Coverslips were either immediately mounted on glass slides with Vectashield mounting medium (Vector Laboratories H-1000) and sealed with nail varnish, or stored covered in foil at 4°C on a shaker overnight before mounting and imaging the following day. Positive signal was determined by brightness relative to controls and co-localisation with commercial neurofascin antibody binding.

2.7.3 96-well plate CBA

2.7.3.1 Day 1

On day 1, a glass-bottom 96-well tissue culture plate (Greiner 655090) was coated with 200 µL/well of PLL stock solution and incubated for at least 30 minutes at room temperature. After incubation, the PLL was removed with a vacuum aspirator. Plates were dried if used immediately; otherwise, the edges of the plate cover were sealed with parafilm for storage for up to one month. Once the wells were dry, HEK293T cells were

thawed or dissociated as detailed in section 2.7.1 and added to DMEM (no glucose; Fisher Scientific 11520416) at a concentration of $2.67x10^5$ cells/mL. Subsequently, 150 µL of this cell suspension was added to each well, resulting in $4.0x10^4$ cells/well. The plate was then placed in the incubator overnight.

2.7.3.2 Day 2

On day 2, HEKs were transfected by combining 0.25 µg/well of plasmid DNA with 4.2 µL/well of DMEM without supplements (Thermo Fisher Scientific A1443001) and mixing thoroughly. Next, 0.3 µL/well branched PEI (Sigma-Aldrich 408727) was added and mixed gently by pipetting. The mixture was incubated for 10 minutes at room temperature to allow complex formation. Subsequently, 150 µL/well of CBA media (no glucose) was added to the transfection mixture and mixed thoroughly. The supernatant was carefully removed from the wells using a multichannel micropipette, and 150 µL/well of the transfection mixture was added. The plate was incubated for 7-8 hours. After incubation, the transfection mixture was removed and replaced with 150 µL/well of fresh CBA media (no glucose) and left to incubate overnight.

2.7.3.3 Day 3

On day 3, the CBA was performed as described in section 2.7.2.4, using 50-100 µL of sample per well (depending on sample availability/volume constraints). Plates were incubated for 1 hour at room temperature on a shaker plate. Following incubation, the samples were removed from each well using a multichannel micropipette, and the wells were gently washed twice with 180 µL/well of CBA washing media. Next, 150 µL of room temperature 4% PFA was added to each well and incubated for 10 minutes on a shaker to fix the cells. The PFA was then removed, and the wells were washed twice

with CBA washing media using a 'flick' method to remove residual liquid without disturbing the fixed cells.

Fixed HEKs were subsequently incubated with 50-100 µL/well of secondary antibody for 45 minutes at room temperature on a shaker plate, followed by two washes with CBA washing media. If applicable, a tertiary antibody was applied and incubated for an additional 45 minutes. After incubation, the wells were washed twice with 180 µL of CBA washing media and twice with PBS. Wells were stored in PBS and either imaged immediately or kept at 4°C on a shaker plate in the dark for up to one month. For longer-term storage, plates were sealed with parafilm and kept at 4°C in the dark.

Antibodies used for CBAs can be found in Table 5.

Primary/ secondary/ tertiary	Host	Specificity	Conjugate	Manufacturer	Cat. #
Primary	Chicken	Neurofascin	-	R&D Systems	AF3235
Secondary	Goat anti-human	IgG (Heavy + Light)	Alexa Fluor™ 488	Invitrogen	A11013
	Goat anti-chicken	IgY (Heavy + Light)	Alexa Fluor™ 546	Invitrogen	A11040
	Goat anti-human	IgG (Heavy + Light)	Alexa Fluor™ 568	Life Tech	A21090
	Goat anti-human	IgG (F(ab')2 Fc-specific)	Alexa Fluor™ 488	Invitrogen	H10120
	Mouse anti-human	IgG1	-	Sigma	I2513
	Mouse anti-human	IgG2	-	Sigma	I5635

	Goat anti-human	IgM (Heavy chain)	Alexa Fluor™ 488	Life Tech	A21215
	Goat anti-human	IgM (Heavy chain)	Alexa Fluor™ 594	Invitrogen	A21216
	Goat anti-human	IgM (Fc5µ Heavy chain-specific)	TRITC	Cambridge Bioscience	609-4031
	Goat anti-chicken	IgG (Heavy + Light)	Biotin	Vector Laboratories	BA-9010
Tertiary	Goat anti-mouse	IgG	Alexa Fluor™ 546	Life Tech	A11003
	-	Streptavidin	Pacific Blue	Invitrogen	S11222

Table 5: CBA primary, secondary, and tertiary antibodies, *including host species, antigen specificity, conjugate, manufacturer, and catalogue numbers. The antibodies target various immunoglobulin subclasses (IgG, IgM) and neurofascin, with fluorescent conjugates like Alexa Fluor and TRITC for detection, as well as biotin-streptavidin systems for enhanced signal detection. Cat. #: catalogue number.*

2.8 Flow cytometry

2.8.1 Preparation for flow cytometry

Cultured PBMCs were collected under sterile conditions within a BSC to maintain sterility for subsequent flow cytometric analysis. The culture plate was centrifuged at 400xg for 5 minutes using a plate spinner. Using a multichannel pipette, 120 µL of supernatant (or cell mixture, depending on flow cytometry application) was collected from each well and transferred into two new plates, distributing 60 µL per plate. One plate was sealed and stored at -80°C for subsequent ELISA and CBA.

If performing flow cytometry on cells and not supernatant, 100 µL of pre-warmed RPMI 1640 medium (Gibco 21875-034) was added to each well, and the cells were gently pipetted up and down to dislodge them, taking care to avoid introducing air

bubbles. Cells from wells corresponding to the same experimental condition were pooled into a single 15 mL conical tube. To maximise recovery, each well of the culture plate was washed 1-2 times with 100 µL of RPMI, and the washes were combined into the respective 15 mL conical tube.

Freshly thawed control PBMCs were prepared concurrently following the protocol described in section 2.4.1, stopping at the step where cells were incubated in 10 mL of media for 5 minutes before centrifugation. Both the thawed PBMCs and the culture-derived cells were centrifuged at 400xg for 5 minutes at 21°C with acceleration and deceleration settings of 9. After centrifugation, the cell pellets were resuspended in 100-200 µL of chilled FACS buffer, depending on pellet size. Cells were counted and resuspended at a final concentration of 10^7 cells/mL in sterile, chilled FACS buffer containing 10% (v/v) 0.22 µm filter-sterilised NMS. Samples were maintained on ice until staining.

For fluorophore staining (Table 6), 45 µL (approximately $0.45x10^6$ cells) was aliquoted into individual polypropylene 5 mL FACS tubes. To block Fc receptors, 5 µL of normal mouse serum (NMS) was added to each tube, yielding a final concentration of 10% NMS, and the tubes were incubated on ice at 4°C for 15 minutes. To generate a live/dead control, 10^6 cells were transferred into a separate Eppendorf tube, incubated at 65°C for 5 minutes, and then placed on ice to ensure cell death.

Fluorophore dilutions were prepared in FACS buffer for single stain and fluorescence-minus-one (FMO) controls. Fluorophore cocktails were added to each sample to reach a final volume of 100 µL per tube, and the tubes were incubated on ice at 4°C for 30-45 minutes, protected from light. Following incubation, 1 mL of FACS buffer was added to

each tube to wash the cells. Samples were centrifuged at 400xg for 5 minutes at 4°C, and the supernatant was discarded. This washing step was repeated, and cells were resuspended to a final concentration of 0.5-1x10^7 cells/mL in chilled FACS buffer. Stained cells were kept on ice and protected from light until flow cytometry analysis.

Marker	Clone	Fluorochrome	Cat. #
CD3	OKT3	FITC	eBioscience 11-0037-41
CD14	HCD14	Pacific Blue	Biolegend 325615
CD19	SJ25C1	APC-Cy7	Biolegend 363009
CD19	HIB19	APC-eFluor780	eBioscience 47-0199-41
CD27	O323	BV605	Biolegend 302829
CD38	HB7	PE	Biolegend 356604
CD38	HB7	PE-Cy7	Biolegend 356607
DAPI		Pacific Blue	Invitrogen D1306

Table 6: Flow cytometry fluorophores, *including markers, their corresponding clones, fluorochromes, and manufacturer catalogue numbers. Fluorophores were employed to identify and distinguish specific immune cell populations, including B cells, T cells, and antibody-secreting cells (ASCs). Cat. #: catalogue number.*

2.8.2 Determination of proportion of antibody-secreting cells (ASCs)/plasmablasts

Flow cytometry was used to quantify ASCs in PBMC cultures using a BD LSRII cytometer and a panel including CD19, CD3, CD27, CD38, and DAPI for live/dead discrimination. Single-stained controls and compensation beads were used to correct for spectral overlap, and FMO controls were included for CD27 and CD38 to define high-expression gates. The gating strategy, as outlined in Figure 8, followed established definitions for circulating plasmablasts. Events were first gated on forward scatter (FSC)/side scatter (SSC) to identify lymphocytes, followed by FSC-A versus FSC-H gating to exclude doublets. Live cells were selected by DAPI exclusion. $CD19^+$ B cells were gated next, with concurrent exclusion of $CD3^+$ T cells. Within the $CD19^+CD3^-$ population, ASCs/plasmablasts were defined as $CD27^{++}CD38^{++}$, based on clear separation from background fluorescence using FMOs. These gates were applied

consistently across all samples with thresholds held constant to allow direct comparison between culture conditions and donors. The $CD27^{++}CD38^{++}$ gate distinguishes activated ASCs from memory B cells ($CD27^{+}CD38^{-}$) and new emigrant/transitional B cells ($CD27^{++}CD38^{++}$), ensuring specific enumeration of ASCs.

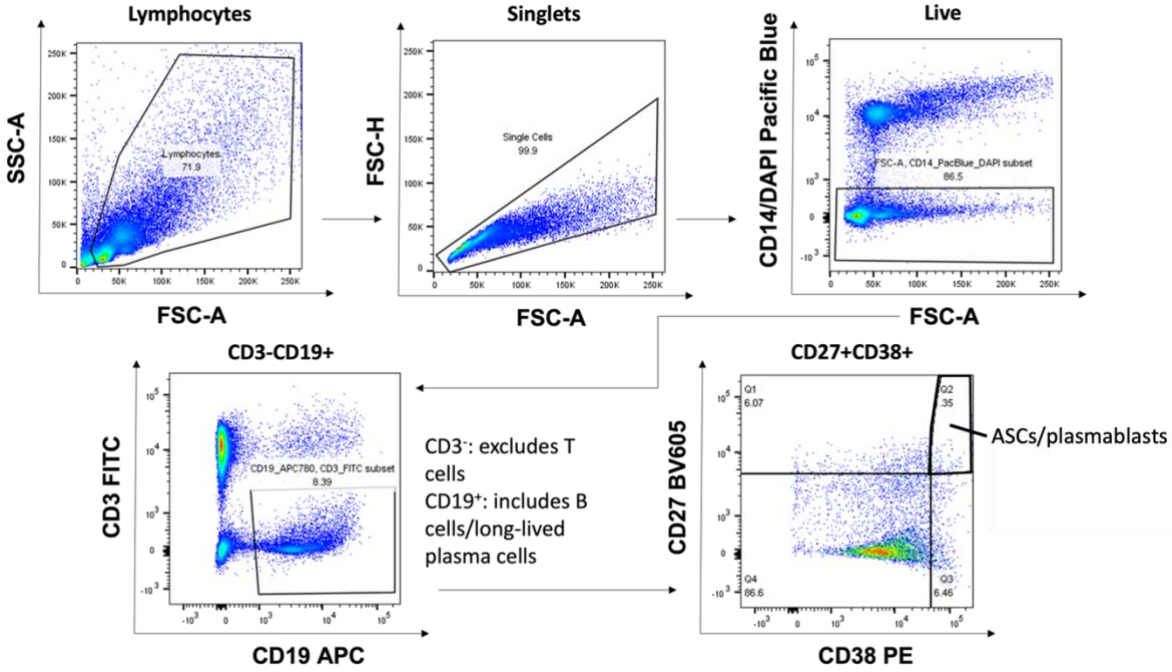

Figure 8: ASC/plasmablast gating strategy. *The sequential gating includes (1) selection of lymphocytes, (2) exclusion of doublets, (3) identification of live cells (DAPI⁻), (4) gating for B cells and long-lived plasma cells ($CD19^{+}$), (5) exclusion of T cells ($CD3^{-}$), and (6) final identification of ASCs/plasmablasts ($CD27^{++}CD38^{++}$).*

2.9 FACS

2.9.1 Bulk sorted cultures

Antibody cocktails (Table 7) were prepared in Eppendorf tubes and kept on ice in the dark prior to thawing PBMCs. PBMCs were thawed following the protocol in section 2.4.1, using 10 mL of chilled, sterile-filtered MACS buffer per vial. The PBMCs were transferred into a 50 mL conical tube and centrifuged at 1300 rpm for 5 minutes at room temperature with acceleration and deceleration settings of 9. The supernatant was aspirated, and PBMCs were resuspended in a reduced volume of chilled, sterile-filtered

MACS buffer for counting. After counting, cells were centrifuged again, the supernatant discarded, and the cells were resuspended to the desired concentration in chilled, sterile-filtered FACS buffer containing 1% NMS (0.22 µm filter-sterilised). Cells were incubated on ice for 10 minutes to block Fc receptors. For live/dead control preparation, an aliquot of PBMCs was transferred into a separate tube, heated at 65°C for 5 minutes, and subsequently placed on ice. These heat-killed cells were later added to the DAPI live/dead control tube.

Marker	Clone	Fluorochrome	Cat. #
Human CD3	OKT3	FITC	11-0037-41 eBioscience
Human CD3	UCHT1	Pacific Blue	300418 Biolegend
Human CD14	HCD14	Pacific Blue	325615 Biolegend
Human CD38	HB-7	PE	356604 Biolegend
Human CD38	HB-7	PE-Cy7	356607 Biolegend
Human CD27	O323	BV605	302829 Biolegend
Human CD19	SJ25C1	APC-Cy7	363009 Biolegend
Human IgD	IA6-2	FITC	555778 BD Pharmingen
Human CD10	HI10a	PE-Dazzle594	312227 Biolegend
Dead cells		DAPI	D1306 Invitrogen

Table 7: Bulk and single sort flow panel fluorophores. *An overview of the fluorophores used in bulk and single-cell FACS including specific markers, antibody clones, fluorochromes, and corresponding manufacturer catalogue numbers. These fluorophores facilitate the identification and isolation of various live immune cell populations, including B cells, T cells, and plasma cells. Cat. #: catalogue number.*

For fluorophore staining, the required volume of PBMCs was transferred into a 15 mL conical tube, and control PBMCs was allocated into tubes designated for FMO, single-stain, and unstained controls. All samples were centrifuged, the supernatants discarded, and the appropriate antibody cocktails were then added. Samples were incubated on ice for 30-45 minutes in the dark.

Following incubation, patient PBMCs were washed twice with chilled, sterile-filtered FACS buffer, while a smaller volume of buffer was used for healthy controls. After the

final wash, single-stain, FMO, and unstained controls were resuspended in chilled FACS buffer, while patient PBMCs were resuspended in DNase buffer.

Before sorting, a sterile 40 μm cell filter was fitted onto a sterile FACS tube, pre-wet with 1 mL of filtered DNase buffer, and the buffer was discarded. The PBMCs were then passed through the pre-wetted filter into a conical tube, followed by an additional 1 mL of DNase buffer to maximise cell recovery. Samples were kept on ice and protected from light until sorting, while appropriate aliquots of scBCM medium were prepared for bulk collection.

A BD FACSAria III was used to bulk sort PBMCs. $CD3^{-}CD14^{-}DAPI^{-}$ cells were sorted into 15 mL conical tubes using the following cell markers and gating strategy (Figure 9):

- Mature naïve: $CD19^{+}CD27^{-}IgD^{+}CD10^{-}$ (P6)
- New emigrant: $CD19^{+}CD27^{-}IgD^{+}CD10^{+}$ (P7)
- Unswitched memory: $CD19^{+}CD27^{+}IgD^{+}$ (P11)
- Switched memory: $CD19^{+}CD27^{+}IgD^{-}$ (P10)
- ASCs/plasmablasts: $CD19^{+}CD27^{++}CD38^{++}$ (P8)

Sorted cells were immediately placed on ice for transport and seeded into 96-well flat-bottom TC plates with stimulatory cytokines, if applicable (Table 3).

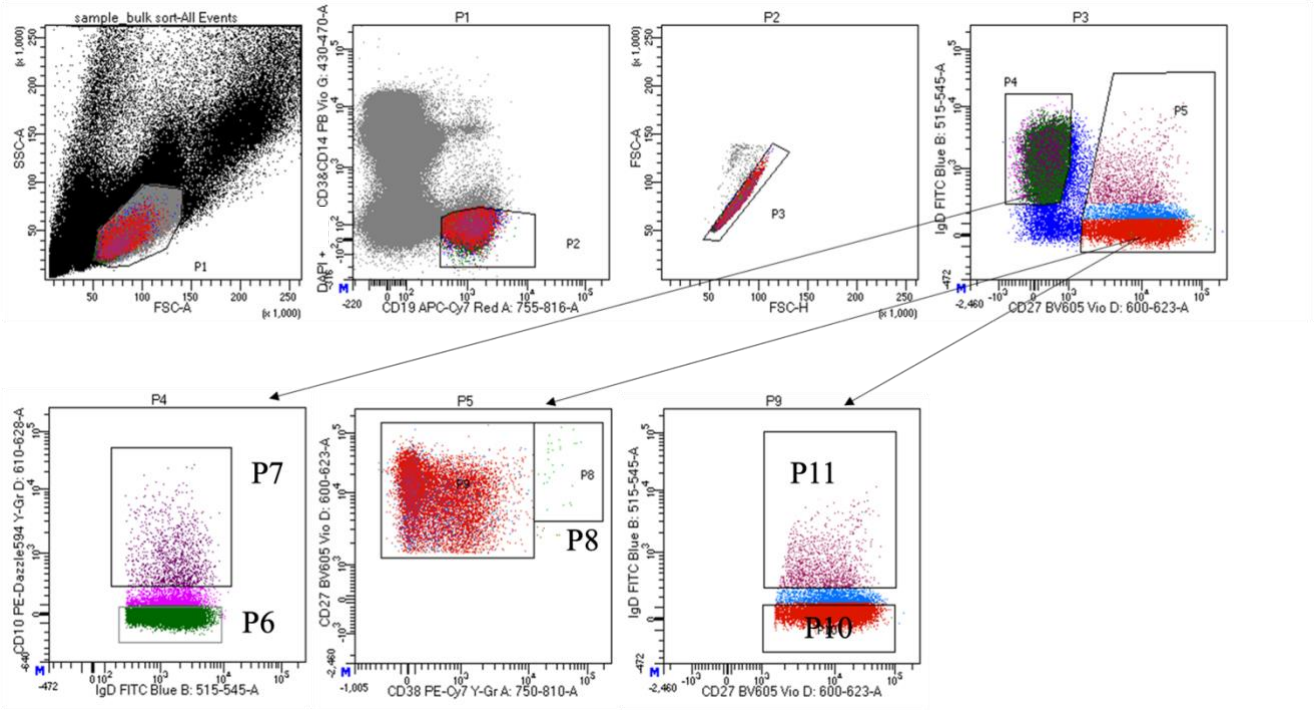

Figure 9: Bulk sort gating strategy used to bulk sort PBMCs. *Cells were first gated to exclude T cells ($CD3^-$), monocytes ($CD14^-$), and dead cells ($DAPI^-$). The remaining $CD3^-CD14^-DAPI^-$ cells were then further sorted into subsets based on surface markers as follows: (P6) mature naïve ($CD19^+CD27^-IgD^+CD10^-$), (P7) new emigrant ($CD19^+CD27^-IgD^+CD10^+$), (P11) unswitched memory ($CD19^+CD27^+IgD^+$), (P10) switched memory ($CD19^+CD27^+IgD^-$), and (P8) ASCs/plasmablasts ($CD19^+CD27^{++}CD38^{++}$).*

2.9.2 Single-sorted cultures

For single-cell sorting, FACS buffer containing 1% NMS was prepared and used to dilute and prepare antibody cocktails (Table 7), which were distributed into polypropylene flow cytometry tubes and kept on ice in the dark until use.

PBMCs were transferred from liquid nitrogen to dry ice and thawed according to the protocol described in section 2.4.1. After thawing, cells were resuspended in chilled FACS buffer containing EDTA (Thermo Fisher Scientific 15575020) and prepared for sorting similarly to the steps outlined for bulk sorting in section 2.9.1. Live, single switched memory B cells were identified and gated as $CD3^-CD14^-DAPI^-$

$CD19^{+}CD27^{+}IgD^{-}$ (Figure 9, gate P10). These cells were sorted individually into 96-well plates pre-seeded with MS40L feeder cells and cultured according to section 2.4.4.

2.10 B-cell receptor complementary DNA synthesis and amplification of variable domain heavy and light chain sequences

B-cell receptors (BCRs) from the supernatants of cultured single B cells were sequenced according to the pipeline depicted in Figure 10.

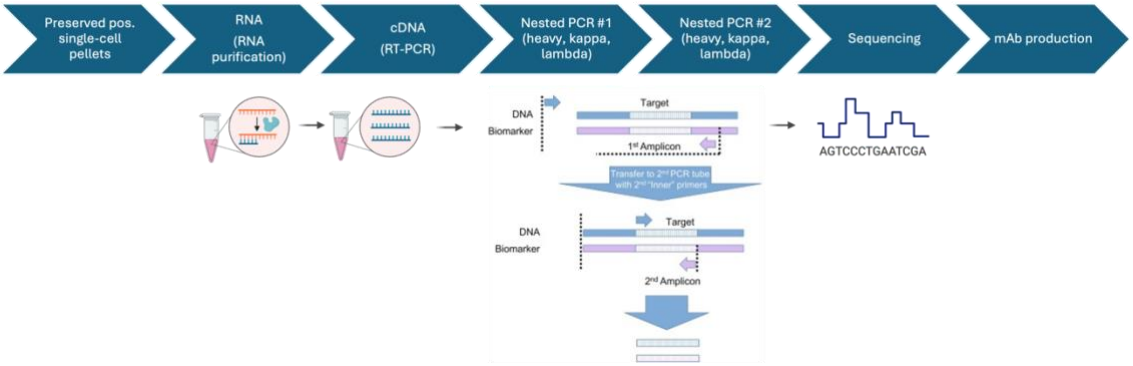

Figure 10: B-cell receptor (BCR) sequencing pipeline for mAb production. *The process began with single-cell pellets, from which RNA is isolated, preserved, and purified. The purified RNA undergoes reverse transcription (RT) to generate complementary DNA (cDNA), followed by nested PCR amplification targeting the Ig heavy, kappa, and lambda chains. Two successive rounds of PCR ensure sufficient amplification and specificity of the target sequences. The resulting amplicons are subjected to sequencing for V(D)J gene analysis and clone identification. Finally, the sequenced BCR genes are used to produce recombinant mAbs for downstream applications, including antigen-binding studies and functional assays. Pos.: positive.*

2.10.1 RNA preservation

Following removal of culture supernatants on day 25, 20 µL of RLT lysis buffer (Qiagen 79216) supplemented with 1% 14.5 M b-ME (Sigma-Aldrich M6250) was added to each well, and the plates were gently agitated. The plates were stored at -80°C.

2.10.2 RNA purification

To purify preserved RNA, an RNeasy® 96 Kit (Qiagen 74181) was used. All working surfaces and materials, including pipettes, pipette tips, and PCR plate seals, were

thoroughly cleaned with RNaseZap (Thermo Fisher Scientific AM9780) to prevent contamination. The plate(s) containing the preserved RNA were then thawed on ice. Once thawed, the plates were centrifuged by pulsing a pre-cooled benchtop centrifuge up to 2500xg at 4°C.

At the bench, 100 µL of Buffer RLT was added to each well of the PCR plate containing 50 µL of preserved RNA, resulting in a final volume of 150 µL per well. The plate was placed flat on the bench and shaken vigorously back and forth for 10 seconds, then rotated 90° and shaken again for an additional 10 seconds to ensure thorough mixing. Next, 150 µL of 70% ethanol was added to each well and mixed by pipetting up and down, resulting in a total volume of 300 µL per well.

Using a multichannel pipette, the entire volume from each well of the PCR plate was transferred to an RNeasy 96 plate mounted on a vacuum manifold connected to a vacuum pump. Autoclave tape was applied over any unused wells to maintain vacuum pressure. The vacuum was then applied until the liquid had completely passed through the membrane into the waste container (approximately 1 minute), after which the vacuum was switched off and the manifold ventilated.

Next, 1 mL of Buffer RW1 was added to each well, and the vacuum was reapplied for approximately 1 minute until the buffer had completely passed through the plate. The manifold was ventilated, and the RNeasy 96 plate was briefly removed so the waste tray could be emptied. After reassembly, 1 mL of Buffer RPE (containing ethanol) was added to each well, followed by vacuum application for approximately 1 minute until the transfer was complete. This step was repeated with a second 1 mL volume of Buffer RPE to ensure thorough washing of the membrane. The RNeasy 96 plate was then

removed from the vacuum manifold and tapped firmly several times on a stack of paper towels to remove any residual liquid. The plate was returned to the manifold, and the vacuum was applied for an additional 10 minutes to remove any remaining ethanol.

Following this, the waste tray was replaced with an elution microtube rack containing 1.2 mL elution microtubes, assembled with the corresponding elution microtube adapter. To elute the RNA, 70 µL of nuclease-free water was added directly onto the membrane of each well, incubated for 1 minute, and the vacuum applied until the water passed completely through the membrane (approximately 1 minute). This elution step was repeated once more with an additional 70 µL of nuclease-free water to maximise RNA yield. Finally, the microtubes were sealed using the caps provided in the kit and stored at -20°C until further use.

2.10.3 Sanger sequencing

2.10.3.1 Complementary DNA (cDNA) preparation (RT-PCR)

To prepare cDNA from the preserved RNA, RT-PCR was performed using a SSIV RT Kit (Invitrogen 18090050B). Preparation was conducted inside a UV-sterilised hood to minimise contamination. The hood was treated with UV light for 20 minutes, followed by thorough cleaning with RNaseZap. All reagents, including those for the Random primer mix and RT Mastermix, were transferred onto a 4°C cool block and sprayed with RNaseZap before moving them into the UV hood.

Isolated and preserved RNA samples were thawed on ice while the Random primer mix was prepared. For each row of wells to be processed, 4.5 µL of the Random primer mix was added to the bottom row of the 96-well PCR plate using a multichannel pipette. The

mix was subsequently distributed across each row so that each well contained 4.5 µL of Random primer mix.

Next, 30 µL of thawed RNA was added to each well containing the Random primer mix, yielding a total volume of 34.5 µL per well. The plate was sealed with a UV-treated aluminium plate seal (Merck Z721530) and centrifuged at 400xg for 1 minute at 4°C. The plate was then transferred to a thermocycler preheated to 65°C (cycler lid set to 105°C) and incubated for 5 minutes. Following incubation, the plate was immediately transferred to a box of ice for 10 minutes, after which it was centrifuged again for 1 minute at 400xg at 4°C.

Inside the UV hood, 15.5 µL of the RT Mastermix was added to each well, bringing the final reaction volume to 50 µL. The plate was sealed with a PCR plate seal (Roche 04729757001), centrifuged at 400xg for 1 minute at 4°C, and transferred to the thermocycler for cDNA synthesis using the programme outlined in Table 8.

Temperature (°C)	Duration (minutes)
25	10
50	60
85	10
10	Infinity

Table 8: Thermocycler conditions for cDNA synthesis during Sanger sequencing.

Upon completion of the thermocycler programme, the PCR plate was returned to the UV hood, and a "working plate" was generated by diluting 1 µL of the resultant cDNA in 99 µL of nuclease-free water in a new UV-treated 96-well PCR plate. The cDNA was either used immediately for subsequent nested PCR reactions, stored at 4°C for use within 24 hours, or stored at -80°C for long-term storage.

2.10.3.2 Nested PCRs

Using the cDNA prepared in the previous step, two rounds of nested PCR were performed to amplify the variable region heavy (VH) and light (VL) chain BCR sequences (PCR1 and PCR2). These two nested PCRs were carried out three times for each sample: once each for the heavy, kappa light, and lambda light chains, resulting in six PCR reactions per sample.

Before beginning, all equipment was placed in the UV-sterilised hood and the UV light was run for 20 minutes to minimise contamination. The cDNA working plate was then placed on ice to thaw. After the hood was decontaminated with RNaseZap, the PCR1 Mastermix was prepared. For each row of wells to be processed, the number of reaction rows was multiplied by 18 to ensure sufficient volume. This volume of PCR1 Mastermix was added to the bottom row of a UV-treated 96-well PCR plate and subsequently distributed evenly across the wells using a multichannel pipette so that each well contained 18 µL of PCR1 Mastermix.

Once the cDNA thawed, it was centrifuged at 400xg for 1 minute at 4°C. Then, 2 µL of cDNA was added to each well containing 18 µL of PCR1 Mastermix. The plate was sealed with a PCR plate seal, centrifuged at 400xg for 1 minute at 4°C, and subjected to the thermocycler programme detailed in Table 9.

Temperature (°C)	Duration
95	3 minutes
95	30 seconds (x45)
55	30 seconds (x45)
72	60 seconds (x45)
72	10 minutes
4	Infinity

Table 9: Sanger sequencing nested PCR1 thermocycler conditions.

Upon completion, the PCR1 product was stored at 4°C if PCR2 was to follow within 24 hours or at -80°C for longer-term storage. This PCR1 process was repeated for the two remaining chains, yielding three distinct PCR1 products per sample.

For the second round of nested PCR (PCR2), a similar protocol was followed. The hood was decontaminated, and the UV light was run for 20 minutes with all necessary materials inside. The PCR1 product plate was thawed on ice while the PCR2 Mastermix was prepared. The number of PCR2 reaction rows was multiplied by 18, and the resulting Mastermix was added to the bottom-most row of a 96-well PCR plate before being evenly distributed across all wells so that each well contained 18 µL of PCR2 Mastermix.

Once thawed, the PCR1 plate was then centrifuged at 400xg, 4°C for 1 minute and transferred to the UV hood. Using a multichannel pipette, 2 µL of PCR1 product was added to each well containing 18 µL of PCR2 Mastermix. The plate was sealed, centrifuged for 1 minute at 400xg, 4°C, and subjected to the thermocycler programme detailed in Table 10.

Temperature (°C)	Time
95	3 minutes
95	30 seconds (x35)
55 (heavy and kappa) or 60 (lambda)	30 seconds (x35)
72	60 seconds (x35)
72	10 minutes
4	Infinity

Table 10: Sanger sequencing nested PCR2 thermocycler conditions.

The resulting PCR2 products were stored at -80°C for long-term use. This process was repeated for each of the three BCR chains to generate the full set of amplicons required for subsequent sequencing and mAb production.

2.10.3.3 Gel electrophoresis

Gel electrophoresis was completed for each PCR2 product to confirm successful amplification before purification, using an E-Gel 96 2% with SYBR Safe (Invitrogen G720802). To minimise the risk of contamination, only one PCR2 product was handled at a time. While the PCR2 product for one chain was thawed on ice, the bench workspace and materials were thoroughly cleaned with RNaseZap.

To prepare for the E-Gel, 18 µL of nuclease-free water was added to each well of a new PCR plate. While keeping the new PCR plate on ice, 2 µL of each PCR2 product was transferred into the corresponding well containing nuclease-free water, resulting in a 1:10 dilution. E-Gel Low Range Quantitative DNA Ladder (Thermo Fisher Scientific 12373031) was diluted 1:1 in nuclease-free water (10 µL each) and added to the last well of each PCR plate row.

The E-Gel was carefully removed from its packaging, the comb was gently removed, and the gel was inserted into the corresponding E-Base. A 20 µL multichannel pipette was then used to transfer the diluted samples from the PCR plate to the E-Gel. The right-most well (column 13) of each row was reserved for 19 µL of the diluted DNA ladder. The E-Gel was run for 12 minutes on the "EG" setting.

While the E-Gel ran, 82 µL of nuclease-free water was added to the PCR2 samples on ice, bringing the total volume in each well to 100 µL. The plate was then sealed and kept on ice until further processing.

Upon completion of the run, the gel was imaged using a Bio-Rad ChemiDoc MP Touch Imaging System with the "SYBR Safe" setting in auto mode. Gel electrophoresis for the

remaining two chains was performed separately following the same protocol to prevent cross-contamination. Clear, distinct bands were verified for each sample before proceeding immediately with PCR2 product purification.

2.10.3.4 PCR purification

The Wizard® SV Gel and PCR Clean-Up System (Promega A9281) was used to purify and elute the PCR2 productions, utilising the same vacuum manifold previously employed for RNA purification (section 2.10.2). While the heavy, kappa light, and lambda light chains were purified on the same binding plate, only one PCR2 plate was opened at a time to minimise the risk of cross-contamination. Each plate was resealed before opening the next.

To initiate purification, 100 µL of membrane binding solution was added to each PCR2 sample while the plate remained on ice. The samples were thoroughly mixed using a multichannel pipette, and the entire 200 µL volume from each well was transferred to the corresponding wells of a binding plate mounted on the vacuum manifold. Unused wells were sealed with autoclave tape to maintain vacuum integrity. The plate was incubated for 1 minute, after which the vacuum was applied for approximately 30 seconds until the samples passed through the membrane.

Next, 200 µL of freshly prepared 80% ethanol was added to each well, followed by a 1-minute incubation. The vacuum was reapplied for approximately 30 seconds until the ethanol passed through the membrane. This ethanol wash was repeated twice more, for a total of three washes. Following the final wash, the vacuum was applied for an additional 4 minutes to ensure the removal of residual ethanol. To further facilitate ethanol evaporation, a paper towel was placed over the wells and the vacuum was

maintained for an additional 4 minutes. The binding plate was then removed from the manifold and tapped firmly on a stack of paper towels to dislodge any remaining ethanol. The plate was subsequently placed on top of an empty 96-well plate and centrifuged at 400xg for 1 minute at 21°C.

Following centrifugation, the waste tray beneath the manifold was replaced with a clean 96-well U-bottom collection plate from the purification kit. The vacuum manifold was reassembled, ensuring the binding plate tips aligned with the wells of the collection plate. Using a multichannel pipette, 100 µL of nuclease-free water was added to each well and incubated for 1 minute. The vacuum was applied again until the water passed through the membrane, collecting the purified product in the underlying collection plate.

After the vacuum was turned off, the binding plate was carefully removed, taking care not to dislodge any droplets that may have adhered to the walls. If droplets were observed, the plate was centrifuged at 400xg for 1 minute at 21°C to transfer them to the collection plate. The final collection plate was sealed with an aluminium plate seal. Samples intended for Sanger sequencing within two weeks were stored at 4°C, while those for longer-term storage were placed at -20°C.

2.10.3.5 Preparing the samples for Sanger sequencing

A Nanodrop spectrophotometer was used to measure the concentration of the purified PCR2 products (heavy, kappa, and lambda light chains) for each sample, with measurements taken in triplicate. The resulting concentrations were averaged to obtain a reliable mean value for each sample. All samples were subsequently diluted in nuclease-free water to a final concentration of 10 ng/µL. The single reverse primers for each chain (Appendix 8.1.3) were similarly diluted to a concentration of 3.2 µM. The diluted

samples and primers were then transferred into a 96-well PCR plate and sent to Source Bioscience for Sanger sequencing.

2.10.4 Nanopore sequencing

2.10.4.1 mRNA and cDNA preparation

Total RNA was purified from lysates using the RNeasy protocol detailed in section 2.10.2, followed by mRNA enrichment. Lysates were thawed on ice, and 25 µL of each sample was set aside for library preparation, with the remainder stored at -80°C for future use. Transfers were conducted within a BSC to prevent contamination.

mRNA was isolated using oligo(dT)25 magnetic beads (New England Biolabs S1419S). Beads were resuspended in Wash Buffer II (WBII) at a 1:1 ratio and vortexed to mix before the beads were separated using a DynaMag-96 side magnetic rack (Invitrogen 10548425) and the supernatant was removed. RNA plates were thawed on ice and 25 µL of WBII was mixed with 25 µL of RNA per well. The plate was sealed and incubated at 70°C for 5 minutes in a thermocycler. Afterward, the RNA plate was cooled on ice and the RNA was added to the beads. The plate was secured onto a HulaMixer (Invitrogen 10548425) and incubated with continuous rotation for 10 minutes. Beads were then allowed to settle by placing the plate back onto a magnetic rack, ensuring complete separation of the buffer from the beads before removal of the buffer using a multichannel pipette. The plate was removed from the rack, and WBII was added in two steps: 50 µL was first added, followed by another 50 µL to ensure thorough washing. The plate was returned to the magnetic rack, and beads were allowed to migrate to one side before the plate was shifted to facilitate movement to the opposite side. This washing step was repeated two to three times.

After allowing the beads to settle for at least 1 minute, excess buffer was removed using a multichannel pipette, positioning the pipette tips against the sidewalls of the wells to avoid disturbing the beads. WBII was added again, and the plate was tapped to dislodge any residual droplets before performing additional washes by alternating plate positions in the rack and finally placing the plate back on ice.

The RT Mastermix was prepared using SSIV Reverse Transcriptase (Invitrogen 18090050B). First, the Mastermix was prepared on ice excluding the RT enzyme. The enzyme was added as the final step to avoid premature reactions. The plate was then taken off ice and placed back in the magnetic rack, where the beads were allowed to fully separate before adding the RT enzyme to the RT Mastermix as the final step. Excess buffer was removed from the wells containing beads, and 10 µL of the complete RT Mastermix was added per well. The plate was sealed, briefly centrifuged, and vortexed gently to ensure complete resuspension of beads. If necessary, manual resuspension using a multichannel pipette was performed. The final bead mixture was incubated at 25°C for 5 minutes, followed by 42°C for 90 minutes in a thermocycler to synthesise cDNA.

The cDNA-bound beads were washed twice with 50 µL of DNase-free Tris-EDTA buffer (Sigma-Aldrich 93283) using the magnetic rack to separate the beads from the supernatant. After the final wash, the beads were resuspended in 10 µL of the same buffer. A 1 µL aliquot of the bead suspension was combined with 9 µL of the Nanopore RT PCR mixture. The PCR protocol included an initial denaturation at 98°C for 45 seconds, followed by 34 cycles of 98°C for 10 seconds, 64°C for 15 seconds, and 72°C

for 5 minutes, concluding with a final incubation at 72°C for 5 minutes in a thermocycler.

The cDNA was purified using ProNex size-selective chemistry beads (Promega NG103A). Beads were added at a 1:1 ratio to cDNA, incubated for 10 minutes, and washed twice with ProNex wash buffer (Promega NG105A). The beads were mixed using the side magnet and incubated for at least 1 minute before the wash buffer was removed. After drying for at least 5 minutes to eliminate residual ethanol, the cDNA was eluted in 20 µL of ProNex elution buffer (Promega NG116A). After a 5-minute incubation at room temperature, the plate was placed back on the side magnet, and the eluted cDNA supernatant was transferred to a new LoBind® 96-well plate. DNA concentration was determined using a Qubit 4 Fluorometer (Invitrogen Q33238).

2.10.4.2 Barcoding and library preparation

For barcoding, 40 ng of each cDNA sample was combined with 1 µL of a unique PCR Barcoding Expansion 1-96 PCR primer mix (Oxford Nanopore Technologies EXP-PBC096) and 25µl of NEBNext Ultra II Q5 master mix (New England Biolabs M0544S) in a new LoBind 96-well plate. The mixture was incubated in a thermocycler at 95°C for 3 minutes, followed by 14 cycles of 95°C for 15 seconds, 62°C for 15 seconds, and 65°C for 1 minute, with a final incubation at 65°C for 3 minutes.

The amplified products were centrifuged at 400xg for 1 minute at maximum acceleration and deceleration and 55 µL of ProNex size-selective chemistry beads were added to each well. The plate was mixed by pipetting before a 10-minute incubation at room temperature. After incubation, the plate was placed on a side magnet for 2 minutes, and the supernatant was removed. Each well was washed twice with 100 µL of

ProNex wash buffer. The beads were dried for 5 minutes to remove residual ethanol before removing the plate from magnetic rack and eluting the barcoded cDNA in 15 µL of ProNex elution buffer. After a 5-minute incubation at room temperature, the plate was placed on the side magnet again, and the eluted cDNA supernatant was transferred to a new LoBind 96-well plate. DNA concentration was measured with a Qubit 4 Fluorometer.

Barcoded cDNA samples were pooled into a single Eppendorf DNA LoBind tube (Invitrogen 003010805) to a total of 1 µg. AMPure XP beads (Beckman Coulter Life Sciences A63880) were added at a 2.5:1 ratio to concentrate the sample, and the mixture was incubated at room temperature for 5 minutes using a HulaMixer. The tube was centrifuged at 400xg for 1 minute at maximum acceleration and deceleration, then placed on the magnetic rack. The supernatant was removed, and the sample underwent two washes with 1 mL of 80% ethanol. After the final wash, the ethanol was removed, and the tube was centrifuged again at 400xg for 1 minute to eliminate any remaining ethanol. The beads were dried for 30 seconds before resuspension in 51 µL of nuclease-free water, followed by a 2-minute incubation at room temperature. The tube was placed on the magnetic rack for at least 1 minute, and the eluate was transferred to a new LoBind DNA tube. DNA concentration was measured using a Qubit 4 Fluorometer.

2.10.4.3 Sequencing run preparation

For end-preparation, 50 µL of the concentrated pooled cDNA was combined with 7 µL of NEBNext Ultra II end-prep buffer and 3 µL of enzyme mix (New England BioLabs E7546S) in a LoBind DNA tube. The reaction was incubated at 20°C for 5 minutes, followed by 65°C for 5 minutes in a thermocycler. The DNA was mixed with an equal

volume of AMPure XP beads, and the resulting mixture was incubated at room temperature for 5 minutes using a HulaMixer. The tube was centrifuged at 400xg for 1 minute before placement on the magnetic rack. The supernatant was removed, and the sample underwent two ethanol washes, first with 500 µL of 80% ethanol and then with 200 µL. Following the final wash, ethanol was removed, and the tube was centrifuged at 400xg for 1 minute to ensure all ethanol was eliminated. The beads were dried for 30 seconds before resuspension in 61 µL of nuclease-free water, followed by a 2-minute incubation at room temperature. The tube was placed on the magnetic rack, and the eluate was transferred to a new LoBind DNA tube. DNA concentration was measured using a Qubit 4 Fluorometer.

Adapter ligation was performed by adding 25 µL of NEBNext® quick ligation reaction buffer, 10 µL of NEBNext Quick T4 DNA Ligase (New England BioLabs E6056S), and 10 µL of Ligation Adapter (Oxford Nanopore Technologies SQK-LSK114) to 60 µL of pooled barcoded cDNA. The mixture was gently pipetted to mix, centrifuged at 400xg for 1 minute, and incubated at room temperature for 10 minutes.

The ligated DNA was combined with 40 µL of AMPure XP beads for purification, and the mixture was incubated at room temperature for 5 minutes using a HulaMixer. After centrifugation at 400xg for 1 minute, the tube was placed on the magnetic rack. The supernatant was removed and the cDNA was washed twice with 250 µL of short fragment buffer (Oxford Nanopore Technologies SQK-LSK114). After removing the final wash buffer, the tube was centrifuged again at 400xg for 1 minute. The beads were dried for 30 seconds before resuspension in 15 µL of elution buffer (Oxford Nanopore

Technologies SQK-LSK114), incubated at room temperature for 10 minutes, and subsequently placed on a magnetic rack to collect the eluted library.

The final DNA library was prepared on ice by diluting 8 ng of DNA to 12 µL in elution buffer. This 12 µL DNA was then combined with 37.5 µL sequencing buffer and 25.5 µL library beads (Oxford Nanopore Technologies SQK-LSK114) for sequencing. The prepared library was loaded onto a MinION flow cell (Oxford Nanopore Technologies FLO-MIN114) inserted into the MinION Mk1B device (Oxford Nanopore Technologies MIN-101B). Flow cell priming and quality checks were performed before starting the sequencing run at 260 base pairs per second.

2.10.5 Immunoglobulin sequence annotation

2.10.5.1 Sanger sequencing

Immunoglobulin sequences were annotated using the US National Library of Medicine's IgBlast tool (https://www.ncbi.nlm.nih.gov/igblast) and the international ImMunoGeneTics information system (IMGT) V-QUEST tool (https://www.imgt.org/IMGT_vquest). These tools were used to identify the V(D)J gene segments with the highest sequence homology. The annotated germline sequences generated from both platforms were compared to assess consistency and reliability. Somatic hypermutations were quantified by determining nucleotide differences between the queried sequences and their closest germline counterparts. The data obtained were subsequently analysed to identify patterns of mutation and gene usage.

2.10.5.2 Nanopore sequencing

Sequencing data from Nanopore runs were basecalled by Dr Mateusz Makuch using Guppy (Oxford Nanopore Technologies) in high-accuracy mode according to published protocols.[89] Reads with a quality score below 10 were filtered out, and index barcodes were trimmed before assigning transcripts to their respective samples. Each transcript was aligned against a reference of human antibody gene sequences derived from the IMGT database using *minimap2* with settings optimised for long-read data. The aligned sequences were annotated using IgBlast to determine V(D)J and constant region family usage. Transcripts with identical V(D)J/C assignments were grouped and polished using *Racon* and *Medaka* to generate an error-corrected consensus sequence for both heavy and light chains. These consensus sequences were then re-analysed using *minimap2* and IgBlast to confirm alignment and V(D)J family assignments. The most abundant sequence for each chain was manually reviewed to infer the most likely heavy-light chain pairing for each single B cell.

2.11 Twist Bioscience cloning and mAb production

2.11.1 IgG

IgG BCR heavy and light chain sequences were cloned into IgG1 expression vectors (Appendix 8.2.1) by Twist Bioscience using their custom cloning services. The resulting constructs were verified via Sanger sequencing prior to antibody production.

2.11.2 IgM

IgM heavy and light chain sequences obtained from the Nanopore sequencing of cultured and expanded single $CD27^{+}IgD^{-}$ B cells from a pan-NF AN patient were used

to design custom IgM mAbs in collaboration with Twist Bioscience. A canonical J chain sequence was retrieved from UniProt/NCBI and inserted into the pTwist CMV BG WPRE Neo vector (Twist Bioscience; Appendix 8.2.2) to create the J chain construct.

The heavy chain sequences were cloned by Twist Bioscience into the OANG custom IgM vector (courtesy of Oxford Autoimmune Neurology Group), while the light chain sequences were inserted into either the pTwist CMV human Ig kappa or lambda vectors (Twist Bioscience), depending on the light chain type. The three plasmids – heavy chain, light chain, and J chain – were co-transfected into HEK293 cells.

Transfected cells were cultured under standard conditions (37°C, 5% CO_2, humidified environment), and the supernatants containing the secreted IgM mAbs were harvested after sufficient incubation. The antibodies were delivered as unpurified HEK293 supernatants for downstream testing and analysis.

2.12 Antigen bait production

2.12.1 Vector sequences, constructs, and plasmid production

The gene sequences encoding the extracellular domains of NF155 and NF186 were retrieved from NCBI (NF155: NM_001160331; NF186: NM_001005388). Functional tags were incorporated into the constructs, including a flexible linker sequence downstream of the extracellular domain to preserve proper protein folding and structural flexibility (Figure 11). The linker was followed with an AviTag sequence to enable site-specific biotinylation via BirA enzyme activity, ensuring consistent and efficient

biotinylation at a single, defined site. A His tag was also added to the constructs to enable purification using affinity chromatography.

Figure 11: NF155 and NF186 antigen bait constructs. *Each bait was constructed with the extracellular domain of each protein plus a flexible linker, an Avitag for efficient enzymatic biotinylation, and a His tag for purification. PAT: proline-alanine-threonine-rich. His: histidine.*

2.12.2 Production and biotinylation *in vivo* in HEK293T cultures

2.12.2.1 Small-scale

For small-scale antigen bait production, HEK293T cells were thawed following the procedure described in section 2.7.1 and seeded into TC-treated T25 flasks (Corning 430639) at a density of 10^6 cells/flask. The cells were incubated overnight at 37°C in an incubator.

The following day, when biotinylation of bait proteins was required, plasmid DNA and BirA enzyme (courtesy of Bo Sun) were combined in a sterile Eppendorf tube within a BSC. In a separate sterile Eppendorf tube, PEI (Sigma-Aldrich 408727) was diluted in PBS. The plasmid DNA (or DNA/BirA mixture) was then added to the diluted PEI, mixed gently by pipetting, and incubated at room temperature for 10-15 minutes to allow complex formation.

While the transfection mixture incubated, 5 mL of fresh cell culture media was added to each flask. After the incubation period, the transfection mixture was added dropwise to the corresponding culture flask while gently rocking the flask in a circular motion to

ensure even distribution across the cell monolayer. The media inside the flask was subsequently supplemented with 50 mM D-Biotin (Life Technologies B20656) to achieve a final concentration of 0.1 mM. The flask was then returned to the incubator and cultured for 3-4 days.

After culturing, the supernatant was carefully poured into a conical tube inside the BSC. The tube was centrifuged at 900xg for 10-15 minutes. The resulting supernatant was transferred to a new conical tube and centrifuged again at 4000xg for an additional 10-15 minutes to remove any remaining cellular debris. The clarified supernatant was then passed through a 0.22 μm sterile filter inside the BSC to ensure sterility and remove residual particulates before proceeding with downstream purification steps.

2.12.2.2 Large-scale

For large-scale production of biotinylated antigen bait proteins, HEK293F cells were cultured and transfected under suspension conditions. On day 1, the cells were seeded at a density of $1x10^6$ cells/mL in 50 mL of Freestyle 293 Expression Medium (Gibco 12338018) within a vented Erlenmeyer flask (Corning 431143). Cultures were maintained under continuous shaking overnight at 130 rpm in a 37°C incubator with 8% CO_2 overnight.

On day 2, 100 μL of 50 mM D-Biotin (Thermo Fisher Scientific B20656) was added directly to the culture medium 1 hour before transfection to facilitate efficient biotinylation of the antigen bait proteins.

For transfection, 50 μg of plasmid DNA encoding the bait protein was diluted in 2.5 mL of Opti-MEM Reduced Serum Medium (Gibco 31985070) in a sterile 15 mL conical

tube. In a separate tube, 150 µg of linear PEI (Thermo Fisher Scientific 047336.03; stock concentration: 1 mg/mL) was diluted in 2.5 mL of Opti-MEM. Both solutions were incubated at room temperature for 5 minutes. The PEI solution was then added dropwise to the DNA solution, followed by a brief 3-second vortex pulse to ensure thorough mixing. The resulting DNA-PEI complex was incubated at room temperature for 10 minutes to allow complex formation.

For biotinylation of the bait proteins, a 4:1 ratio of DNA to BirA plasmid DNA was used. The transfection mixture was added dropwise to the HEK293F culture while gently swirling the flask to evenly distribute the mixture. The culture was then returned to the 37°C incubator with 8% CO_2 for 3 hours.

After 3 hours, 500 µL of 1 M Sodium Butyrate (pH 7.4, sterile-filtered using a 0.2 µm filter; Sigma-Aldrich B5887) was added to the culture medium to enhance recombinant protein expression. At this stage, an additional 100 µL of 50 mM D-Biotin was also supplemented. The culture was maintained under the same shaking and incubation conditions for 3 days, after which the media was harvested and processed for downstream protein purification on day 5.

2.12.3 Lysis

If required, HEK293T cells were lysed to extract intracellular antigen bait proteins for downstream analysis. Prior to lysis, an ice bucket, radioimmunoprecipitation assay (RIPA) buffer (Thermo Fisher Scientific 89900), protease inhibitor cocktail (PIC; Sigma-Aldrich P8340), and PBS were prepared. The lysis buffer was freshly prepared by adding 1 mL of ice-cold RIPA buffer to 10 µL of PIC per T25 flask.

Before initiating lysis, culture supernatants were carefully removed from each flask and stored for downstream analysis, if applicable. Cells were then washed twice with ice-cold PBS to remove any residual culture media and non-adherent proteins, ensuring the complete removal of the final wash by aspiration.

To lyse the cells, 1 mL of the freshly prepared lysis mixture was added directly to each T25 flask. The flasks were placed on ice and incubated for 15 minutes to allow for initial cell membrane disruption. After the incubation period, cells were detached by gentle pipetting to achieve a uniform cell suspension. If cells remained adherent, a sterile cell scraper (Corning 3010) was used to facilitate detachment. The lysates were transferred into sterile 1.5 mL low-bind Eppendorf tubes (Invitrogen 003010805) and kept on ice while subsequent lysates were processed. To ensure complete lysis, the tubes were incubated for 30 minutes at 4°C with continuous gentle mixing on a rotating mixer inside the cold room.

Following incubation, lysates were homogenised by repeated pipetting to disrupt any remaining cellular aggregates. The homogenised samples were centrifuged at 10,000xg for 5 minutes at 4°C. Following centrifugation, the supernatant containing the intracellular protein fraction was carefully transferred to a fresh low-bind tube for subsequent purification. The pellet, consisting of cell debris, was retained if further analysis was required. The lysate was either used immediately for purification or stored at -80°C for later use.

2.12.4 Purification

2.12.4.1 HisPur cobalt purification

The purification of His-tagged NF155 and NF186 antigen bait proteins was first carried out using HisPur Cobalt Resin (Thermo Fisher Scientific 89964) through immobilised metal affinity chromatography (IMAC). The purification process was performed under native conditions, and all steps were executed at room temperature unless otherwise specified.

To initiate the purification process, 1 mL of HisPur Cobalt resin was added to two separate 15 mL conical tubes, one designated for NF155 and the other for NF186. The resin was equilibrated by centrifugation at 700xg for 2 minutes. The supernatant was carefully discarded using a P1000 pipette, and 2 mL of Equilibration/Wash Buffer was added to each tube. The resin was gently resuspended until fully mixed, ensuring optimal conditions for subsequent protein binding. After a second round of centrifugation at 700xg for 2 minutes and removal of the supernatant, the resin was resuspended in an additional 2 mL of Equilibration/Wash Buffer to maintain consistent binding conditions.

Protein extracts of NF155 and NF186 were prepared by mixing 5 mL of each extract with 5 mL of Equilibration/Wash Buffer. This dilution minimised viscosity and facilitated better interaction with the resin. Each protein solution was added to its respective tube containing the equilibrated cobalt resin. To maximise binding efficiency, the tubes were incubated on a HulaMixer for 30 minutes at room temperature, allowing the His-tagged proteins to interact with the cobalt ions on the resin.

Following the binding incubation, the tubes were centrifuged at 700xg for 2 minutes, and the supernatants were saved for downstream analysis to determine unbound protein fractions. To remove non-specifically bound proteins, the resin was washed twice with 2 mL of Equilibration/Wash Buffer. Each washing step included centrifugation at 700xg for 2 minutes, and the supernatants were saved for analysis to monitor protein purity and binding efficiency.

To elute the His-tagged NF155 and NF186 proteins, 1 mL of Elution Buffer was added to each tube. The tubes were gently mixed and centrifuged at 700xg for 2 minutes, and the supernatants containing the eluted proteins were collected in fresh low-bind Eppendorf tubes. The elution step was repeated twice more, and each fraction was collected separately to ensure maximum recovery and efficient separation.

The concentration of the eluted proteins was measured using a Nanodrop spectrophotometer by determining the absorbance at 280 nm. The molar extinction coefficients listed in Table 11 were used to quantify the yields and concentrations of the eluted NF155 and NF186 antigen bait proteins, calculated using the ExPASy Protparam tool based on their amino acid sequences and His tags.

Protein/fluorophore	Molecular weight (kDa)	Molar extinction coefficient (ε/1000) (μM^{-1} cm^{-1})
NF155	123.54	177.34
NF186	127.49	169.89
PCSK9	71.04522	56.515
PE	-	1.96
DL594	-	0.08

Table 11: Molecular weights and inferred molar extinction coefficients of bait proteins, control protein, and fluorophores. *Protparam was used to calculate the extinction coefficients. NF: neurofascin; PCSK9: proprotein convertase subtilisin/kexin type 9; PE: phycoerythrin; DL: DyLight™.*

2.12.4.2 HisPur Ni-NTA purification

The His-tagged antigen bait proteins were also purified from the supernatant of HEKs using IMAC with HisPur Ni-NTA resin (Thermo Fisher Scientific 88222). This method exploits the strong and specific interaction between polyhistidine tags and nickel ions to achieve efficient and selective protein recovery.

To begin, the Ni-NTA resin was gently resuspended to ensure homogeneity. For each bait protein, 5 mL of resin slurry was transferred to a clean 15 mL conical tube. The resin was equilibrated by centrifugation at 700xg for 2 minutes, and the supernatant was carefully decanted. Two resin-bed volumes (5 mL each) of Equilibration Buffer were added, and the resin was gently mixed using a serological pipette. The mixture was centrifuged again under the same conditions to fully equilibrate the resin.

If the culture supernatant containing the secreted His-tagged antigen bait protein had been stored at -80°C, it was first thawed on ice. The supernatant was then mixed with an equal volume of Equilibration Buffer to optimise binding conditions. This mixture was added to the equilibrated Ni-NTA resin and incubated in a HulaMixer for 30 minutes at room temperature to allow binding of the His-tagged proteins.

Following incubation, the tubes were centrifuged at 700xg for 2 minutes, and the supernatant was carefully removed and retained for potential downstream troubleshooting. To remove non-specifically bound proteins, the resin was washed three times with two resin-bed volumes (5 mL) of Wash Buffer. After each wash, the tube was centrifuged at 700xg for 2 minutes, and the supernatants from each wash step were collected and stored for analysis.

Protein elution was achieved by adding one resin-bed volume (2.5 mL) of Elution Buffer directly to the resin. The mixture was centrifuged at 700xg for 2 minutes, and the supernatant containing the eluted protein was collected in a clean low-bind Eppendorf tube. This elution step was repeated twice more, with each fraction collected separately. The absorbance of the eluted fractions was measured at 280 nm using a Nanodrop spectrophotometer to verify protein yield.

The purified proteins were either used immediately for downstream experiments or subjected to buffer exchange. Aliquots were transferred to low-bind tubes and flash-frozen by direct placement on dry ice before long-term storage at -80°C.

2.12.5 Buffer exchange

Immediately following elution, buffer exchange was performed using an Amicon Ultra-15 centrifugal filter unit (UFC905008) with a 50 kDa molecular weight cutoff (MWCO) to replace the elution buffer with Dulbecco's phosphate-buffered saline (DPBS) or PBS. To prepare the filter, the eluate was pipetted directly onto the membrane. The filter unit was then centrifuged at 3000xg for 10 minutes at 4°C, allowing the protein to concentrate above the membrane. The flow-through was collected and retained for potential troubleshooting if necessary.

To ensure complete buffer exchange, the sample was washed three times with PBS. For each wash, an equal volume of PBS was added to the concentrated protein solution, followed by centrifugation at 3000xg for 10 minutes at 4°C. The flow-through from each wash was similarly collected to confirm the removal of any residual elution buffer components.

After the final wash and centrifugation, the remaining protein solution above the membrane was carefully transferred to a sterile, low-bind Eppendorf tube. The final protein concentration was determined using a Nanodrop spectrophotometer and the corresponding molar extinction coefficient (Table 11). The purified proteins were aliquoted into 0.5 mL low-bind Eppendorf tubes and immediately flash-frozen on dry ice. Once fully frozen, the aliquots were transferred to -80°C long-term.

2.12.6 Western blotting

Protein samples for Western blot analysis were prepared by mixing equal volumes of the sample with 4X Bolt lithium dodecyl sulfate (LDS) Sample Buffer (Thermo Fisher Scientific B0007). If needed, deionised water was added to achieve a total volume of 40 µL per sample. Samples were denatured by heating at 70°C for 10 minutes in a heat block to ensure consistent protein denaturation and loading. A Full Range Protein Ladder (Thermo Fisher Scientific 26614) was included in each gel to enable protein size estimation.

Proteins were separated by sodium dodecyl sulfate-polyacrylamide gel electrophoresis (SDS-PAGE) using Bolt 4-12% Bis-Tris Plus Gels (Thermo Fisher Scientific NW04122BOX) in a Mini Gel Tank (Thermo Fisher Scientific A25977). Before loading, the gel wells were prepared by removing the combs and rinsing three times with 1X 3-(N-morpholino)propanesulfonic acid (MOPS) SDS Running Buffer. Each well was loaded with 40 µL of the prepared protein sample or 10 µL of the protein ladder. The gel tank was filled with 1X MOPS SDS Running Buffer, and electrophoresis was conducted at 200 V for 35 minutes to ensure effective sized-based protein separation.

Following electrophoresis, proteins were transferred onto a polyvinylidene fluoride (PVDF) membrane using 1X Bis-Tris Transfer Buffer. The transfer stack was assembled in the Bolt Transfer System by layering sponge pads, filter paper (Thermo Fisher Scientific 1704158), the gel, and the PVDF membrane. Care was taken to avoid air bubbles that could disrupt protein transfer. The transfer was performed at a constant voltage of 20 V for 60 minutes. Transfer efficiency was assessed by briefly staining the membrane with Ponceau S buffer (Sigma-Aldrich P7170) to check for protein bands, followed by a thorough wash with PBST to remove the stain. To reduce nonspecific binding, the membrane was blocked with 5% BSA in PBST for 1 hour at room temperature with gentle agitation on an orbital shaker. The membrane was then incubated overnight at 4°C with the primary antibody (Table 12), diluted in PBST supplemented with 1% BSA.

The next day, the membrane was washed three times for 5 minutes each with PBST to remove unbound primary antibody. The membrane was subsequently incubated with a secondary antibody (Table 12) diluted in PBST + 1% BSA for 1 hour at room temperature. If applicable, a tertiary antibody (Table 12) was applied following three additional PBST washes. After the final antibody incubation, the membrane underwent three washes of 10 minutes each in PBST.

Primary/ secondary/ tertiary	Host	Specificity	Conjugate	Manufacturer	Cat. #
Primary	Chicken	Neurofascin	-	R&D Systems	AF3235
Primary	Rabbit	6×His tag	-	Cell Signaling Technology	2365T

Secondary	Goat anti-chicken	IgG (Heavy + Light)	Biotin	Vector Laboratories	BA-9010
Secondary	Goat anti-chicken	IgY (Heavy + Light)	HRP	Invitrogen	A16054
Secondary	Goat anti-rabbit	IgY (Heavy + Light)	HRP	Dako	P0448
Tertiary	-	Streptavidin	HRP	Biolegend	405210
Tertiary	Goat anti-human	IgG (Fc-specific)	HRP	Sigma	A0170

Table 12: Western blotting antibodies. *Summary of antibodies used for Western blotting, including host species, specificity, conjugation, manufacturer, and catalogue number (Cat. #). Primary antibodies targeted neurofascin and His-tagged proteins, while secondary antibodies were used for signal amplification via biotin or HRP conjugation. In some experiments, a tertiary streptavidin-HRP conjugate was employed.*

Signal detection was achieved via chemiluminescence using ECL Prime Western blotting detection reagent (Merck GERPN2232). The membrane was evenly coated with 5 mL of substrate and imaged using the Bio-Rad ChemiDoc MP Touch Imaging System.

2.12.7 Streptavidin pull-down

To evaluate biotinylation efficiency of antigen bait proteins, streptavidin pull-down assays were performed using streptavidin beads.

2.12.7.1 Small-scale pull-down

For small-scale antigen bait production, streptavidin pull-downs were conducted using Sigma Streptavidin Beads (Sigma-Aldrich S1638). An aliquot of 200 µL of streptavidin beads was transferred into a clean microcentrifuge tube and washed twice with 1 mL of 50 mM Tris-HCl (pH 8.0) containing 150 mM NaCl. The wash steps involved centrifugation at 3000 rpm for 1 minute to pellet the beads, followed by removal of the

supernatant. After the final wash, the beads were resuspended in the same buffer to a final volume of 220 µL, accounting for residual liquid after washing.

Two Eppendorf tubes were prepared for each antigen bait protein: one for incubation with streptavidin beads and one as a control without beads. For each sample, 3 µg (based on Nanodrop readings) of protein was added to each tube, and the total volume was adjusted to 150 µL with 50 mM Tris-HCl (pH 8.0) supplemented with 150 mM NaCl. Subsequently, 100 µL of the resuspended streptavidin beads were added to the designated tubes, while the samples in the control tubes were processed without beads.

Samples were incubated on ice for 1 hour, with gentle mixing by flicking the tubes every 10 minutes to facilitate optimal binding of biotinylated proteins to the streptavidin beads. After incubation, the samples were centrifuged at 3000 rpm for 3 minutes to pellet the beads. Supernatants were carefully removed and reserved for analysis via Western blotting.

2.12.7.2 Large-scale pull-down

To assess the biotinylation efficiency of antigen baits produced at large scale, Dynabead M-270 Streptavidin beads (Thermo Fisher Scientific 65305) were used in conjunction with a magnetic plate-based separation system. Initially, 100 µL of Dynabeads were washed thoroughly with PBS to remove the storage buffer and equilibrate the beads for protein binding. Washing steps were performed using a magnetic 96-well plate separator (Thermo Fisher Scientific 12027) to ensure efficient and rapid bead collection.

For protein binding, 3 µg of human recombinant NF155 or NF186 was prepared in PCR tubes and mixed with 50 µL of streptavidin-coated Dynabeads resuspended in DPBS

(Gibco 14190250). The reaction was incubated at 4°C for 1 hour on a HulaMixer to facilitate optimal binding of biotinylated proteins to the beads. Following incubation, the magnetic plate was used to draw the beads to one side of the wells, allowing the unbound protein to be separated from the streptavidin-bound complex. The cleared supernatant was transferred to a new low-bind Eppendorf tube and brought to a total volume of 150 µL with DPBS.

To prepare samples for electrophoresis, aliquots of 12 µL, 6 µL, and 3 µL of the eluate were transferred to separate tubes. To each sample, 2.5 µL of 4X NuPAGE LDS Sample Buffer (Thermo Fisher Scientific NP0007) was added, and the final volume was adjusted to 20 µL with DPBS. Control samples were prepared by adding 240 ng of commercial NF155 or NF186 protein to 2.5 µL of NuPAGE LDS buffer, and the total volume was brought up to 20 µL.

Samples were denatured by heating at 70°C for 10 minutes on a heat block, then cooled to room temperature before loading onto a 4–12% Bolt Bis-Tris Mini Gel. Electrophoresis was performed using 20X Bolt MOPS SDS Running Buffer, with gels run at 200 V for 55 minutes. A PageRuler Plus Prestained Protein Ladder (Thermo Fisher Scientific 26619) was loaded alongside samples for molecular weight estimation.

Following electrophoresis, gels were washed three times with distilled water to remove residual SDS and staining artifacts. Gels were then incubated overnight at room temperature with Imperial Protein Stain (Thermo Fisher Scientific 24615) to visualise protein bands. The following day, gels were washed five times with distilled water, with each wash lasting 30 minutes to 1 hour. Once thoroughly destained, protein bands were imaged using a Bio-Rad ChemiDoc MP Touch Imaging System.

2.12.8 Coomassie blots

To evaluate the efficiency of streptavidin pull-down and indirectly assess the biotinylation of antigen bait proteins, Imperial Protein Stain (Thermo Fisher Scientific 24615) was used for gel staining. Following electrophoresis under non-reducing conditions (as used for Western blotting), the gels were transferred into clean staining trays and washed four times for 5 minutes each with 50 mL of ultrapure water.

The Imperial Protein Stain was mixed gently by inverting the bottle several times to ensure homogeneity. Then, 25 mL of stain was added to fully cover the gel in the staining tray. The trays were placed on an orbital shaker and incubated for 2 hours at room temperature to facilitate thorough protein staining.

After staining, the dye solution was discarded, and the gels were transferred into fresh trays containing 200 mL of ultrapure water. The gels were incubated overnight at room temperature on an orbital shaker to reduce background staining and enhance contrast. A folded Kimwipe tissue was placed in the water to absorb excess dye, further improving visual clarity. Following destaining, the gels were imaged using a Bio-Rad ChemiDoc MP Touch Imaging System.

2.12.9 Confirmation of biotinylation-to-antigen ratio

To quantify the degree of biotinylation of the NF155 and NF186 antigen baits, a biotin-to-antigen ratio assay was performed using streptavidin-phycoerythrin (SA-PE; eBioscience 12-4317-87) conjugate, followed by serial dilution analysis and Western blot detection (Figure 62, Appendix 8.4).

First, the concentration of each biotinylated antigen bait was determined by measuring absorbance at 280 nm (A_{280}) using a Nanodrop spectrophotometer and the molar extinction coefficients in Table 11. The calculated concentrations were then used to prepare 40 µL of each biotinylated antigen at a final concentration of 2 µM in 1X PBS.

To generate a dilution series, an SA-PE working solution was prepared by diluting SA-PE to 1 µM in 1X PBS. From this stock, a series of two-fold serial dilutions were performed using 1X PBS as the diluent, resulting in final concentrations ranging from 0.5 µM to 0.03125 µM.

Samples were prepared for Western blot analysis under non-reducing conditions using 20 µL of each sample per well in 15-well 4–12% Bis-Tris mini-gels. Following separation by electrophoresis, proteins were transferred onto a nitrocellulose membrane. The transfer was conducted at 10 V for 60 minutes.

Post-transfer, the membrane was blocked according to section 2.12.6 and then incubated overnight at 4°C with an SA-HRP secondary antibody (Perkin Elmer FP1049) at a 1:5000 dilution in PBST supplemented with 5% BSA. After washing with PBST the following day, the membrane was developed using ECL and protein bands were visualised using the Bio-Rad ChemiDoc MP Touch Imaging System.

2.12.10 Tetramerisation

The protocol for tetramerising the antigen baits was adapted from Phelps et al (2024).[90] An overview of these steps is visualised in Figure 62 (Appendix 8.4).

2.12.10.1 Control tetramer

To generate the control tetramer, SA-PE was first purified to remove sodium azide, which can interfere with NHS-ester labelling. A 250 µL volume of 0.2 mg/mL SA-PE was diluted in 15 mL of 0.01 M PBS and loaded into a 100 kDa Amicon Ultra 15 centrifugal filter (Millipore UFC910008). The solution was centrifuged at 2000xg for 7 minutes until the retentate returned to a final volume of approximately 250 µL. The filtrate was collected in a separate 50 mL conical tube for reference. The washing process was repeated twice by topping up the Amicon filter with PBS and centrifuging again at 2000xg for 7 minutes until the filtrate was clear.

Following washing, the retentate containing SA-PE was recovered into a fresh 1.5 mL Eppendorf tube. To adjust the pH, 500 µL of PBS and 40 µL of 0.67 M borate buffer (pH 8.5) were added to the SA-PE solution. The entire volume of the washed SA-PE was then transferred to a 65 µg vial containing DyLight 594-normal human serum (DL594-NHS) ester (Thermo Fisher Scientific 11879370), pre-warmed to room temperature. The vial was capped and inverted multiple times to ensure complete solubilisation of the dye. The reaction was incubated at room temperature for 1 hour in the dark.

Following incubation, the SA-PE-DL594 reaction mix was transferred to a fresh 100 kDa Amicon filter, diluted with 15 mL of PBS, and centrifuged at 2000xg for 15 minutes. The filtrate was collected in a new 50 mL conical tube. Washing and centrifugation steps were repeated until the filtrate appeared clear, indicating the removal of unbound DL594-NHS ester. The retentate containing the SA-PE-DL594 backbone was recovered, and the final volume was recorded.

The concentration of the SA-PE-DL594 backbone was determined using a Nanodrop spectrophotometer in UV-Vis mode. The concentrations of PE and DL594 were calculated using their specific extinction coefficients (Table 11). The concentration of PE was used to calculate the volume of biotinylated control antigen needed to create the complete control backbone, and then the control backbone was stored overnight at 4°C.

The reconstituted biotinylated PCSK9 protein (control antigen) was added to the control backbone the following day to create the complete control antigen. The required volume of PCSK9 was calculated based on the PE concentration, six biotin binding sites, and the measured concentration of the PCSK9 protein. The appropriate volume of PCSK9 protein was added to the SA-PE-DL594 backbone, and the reaction was incubated at room temperature for 1 hour in the dark.

Following incubation, the control tetramer mixture was loaded into a 100 kDa Amicon Ultra 2 centrifugal filter (UFC210024) and centrifuged at 4000xg for 12 minutes to concentrate the tetramer to 2 µM. The concentration of the flow-through was measured via Nanodrop, and the tetramer was diluted in 100% glycerol (Merck G5516) for long-term stability. The final control tetramer was stored at -20°C for up to one year.

2.12.10.2 Bait tetramers

To generate the bait tetramers, the required volume of each biotinylated antigen was calculated based on the biotin-to-streptavidin ratio. The biotinylatNF155 and NF186 baits were retrieved from -80°C storage and thawed on ice. In separate 1.5 mL Eppendorf tubes, the appropriate volume of each biotinylated antigen was combined with 100 µL of SA-PE. The solutions were mixed thoroughly by gentle pipetting and incubated at room temperature for 30 minutes in the dark.

For purification and removal of unincorporated antigen, 300 kDa Microcon centrifugal filters (Biomax MPE300025) were utilised, with a dedicated filter for each antigen bait. The entire volume of each reaction mixture was loaded onto each filter, which was then topped up with 1X PBS to its maximum capacity. Centrifugation was performed at 2000xg for 7 minutes in a fixed rotor microcentrifuge. If necessary, the process was continued in 7-minute increments at 5000xg until the retentate volume was reduced to approximately 200 µL. Filtrates from each wash step were collected in separate tubes for potential downstream troubleshooting.

Following purification, the filters were inverted and centrifuged at 1000xg for 3 minutes to collect the retentates containing the tetramerised antigens. The final volume of each retentate was recorded.

To determine the concentration of the tetramers, absorbance at 566 nm was measured using a Nanodrop in UV-Vis mode. The concentration of PE was calculated using its specific extinction coefficient, providing an estimation of the tetramer concentration. The purified tetramer solutions were then diluted to a final concentration of 2 µM PE using 1X PBS.

For long-term stability, the 2 µM PE solution was further diluted by adding an equal volume of 100% glycerol to create a 50% glycerol solution. The final tetramer preparations were aliquoted into low-bind tubes and stored at -20°C for extended use.

3 Development and Optimisation of PBMC Cultures for *In Vitro* Antibody Production

3.1 Introduction and rationale

The development of a reliable *in vitro* system to stimulate B cells and induce immunoglobulin (Ig) secretion was a foundational step for the downstream characterisation and cloning of pan-neurofascin (pan-NF^{+}) autoantibodies in this body of work. Peripheral blood mononuclear cells (PBMCs) from healthy donors and patients with pan-NF autoantibodies were cultured under a range of stimulatory conditions to optimise both total and antigen-specific IgG production. These cultures aimed to promote differentiation of B cells into antibody-secreting cells (ASCs)/plasmablasts, thereby enabling the detection and analysis of secreted antibodies, including those with specificity for neurofascin isoforms neurofascin-155 (NF155) and NF186.

Protocols developed for other antibody-mediated neurological disorders have successfully demonstrated that PBMCs can be stimulated *in vitro* to secrete antigen-specific IgG. For example, Makuch et al (2018) cultured PBMCs from patients with N-methyl-D-aspartate receptor (NMDAR) antibody encephalitis and recovered NR1-specific antibodies from culture supernatants, confirming ASC generation via $CD27^{++}CD38^{++}$ flow cytometric profiles.[91] Similarly, Wilson et al (2018) stimulated PBMCs from patients with neuromyelitis optica spectrum disorder (NMOSD) and demonstrated aquaporin-4 (AQP4)-specific antibody production *in vitro*, identifying contributions from both naïve and memory B-cell subsets.[92]

These findings provided the rationale for developing a robust PBMC culture system tailored to the investigation of IgG1 pan-NF autoimmune nodopathy (AN). The goal was to establish culture conditions capable of supporting the secretion of pan-NF autoantibodies *in vitro* and ultimately enable the recovery of individual antibody-producing clones for downstream mAb production and repertoire sequencing. In addition, a culture system of this kind allows assessment of the capacity of specific B-cell subpopulations to generate autoantibodies, thereby informing hypotheses about B-cell tolerance failure and the cellular origin of pathogenic clones.

Accordingly, a series of optimisation experiments were undertaken, initially using PBMCs from healthy donors to refine the composition of a stimulatory cytokine cocktail and identify optimal conditions such as cell seeding density and culture duration. These experiments were guided by published protocols[91,92] and further informed by immunopathological features of IgG1 pan-NF AN, including its IgG1 subclass bias and resistance to first-line immunotherapies.

The following sections describe the iterative development of this *in vitro* system. The finalised protocol achieved consistent induction of μg/mL quantities of total IgG and laid the foundation for subsequent experiments aimed at detecting antigen-specific antibodies and isolating autoreactive B-cell clones.

3.2 Initial healthy control PBMC culture trials

Initial experiments focused on developing a PBMC culture system capable of reliably stimulating IgG production *in vitro*. Healthy donor PBMCs were used to optimise stimulation conditions ahead of patient PBMC experiments, enabling systemic evaluation of cytokine cocktails, cell seeding density, and culture duration.

3.2.1 Rationale for cytokine selection

Cytokine combinations were selected based on prior studies in antibody-mediated neurological disease and broader literature on B-cell activation. In particular, protocols for NMDAR antibody encephalitis and NMOSD demonstrated that stimulation with toll-like receptor (TLR) 7/8 agonists (eg, Resiquimod; R848), IL-2, and CD40 ligand (CD40L) induced ASC differentiation and antigen-specific IgG secretion from unfractionated PBMCs.[91,92] Additional studies in GBS and CIDP highlighted elevated levels of pro-inflammatory cytokines such as tumour necrosis factor-alpha (TNFα), interferon-gamma (IFNγ), interleukin (IL)-6, and IL-17, which are associated with enhanced B-cell activation and prolonged immune responses, and contribute to disease pathogenesis.[93,94]

Accordingly, early culture experiments tested combinations of R848, IL-2, soluble CD40L (sCD40L), TNFα, IFNγ, IL-1β, and IL-6 to assess their effects on total IgG output to begin standardising culture conditions in preparation for downstream antigen-specific assays. RPMI was used as the initial culture medium.

3.2.2 Screening of cytokine combinations and cell densities

Healthy control PBMCs from three donors (Con010-012) were plated in bulk at $2x10^4$, $1x10^5$, or $2x10^5$ cells/well in 96-well plates and stimulated for 5 days with one of three cytokine combinations:

- R848 + IL-2
- R848 + IL-2 + TNFα
- R848 + IL-2 + TNFα + IFNγ

Total IgG concentrations in culture supernatants were measured by ELISA. No significant increase in total IgG was observed with the addition of TNFα or IFNγ (two-way ANOVA, p=0.9921). However, IgG concentration rose in proportion to cell density, with a 10-fold increase in seeding density yielding a ~10-fold increase in IgG production (Figure 12).

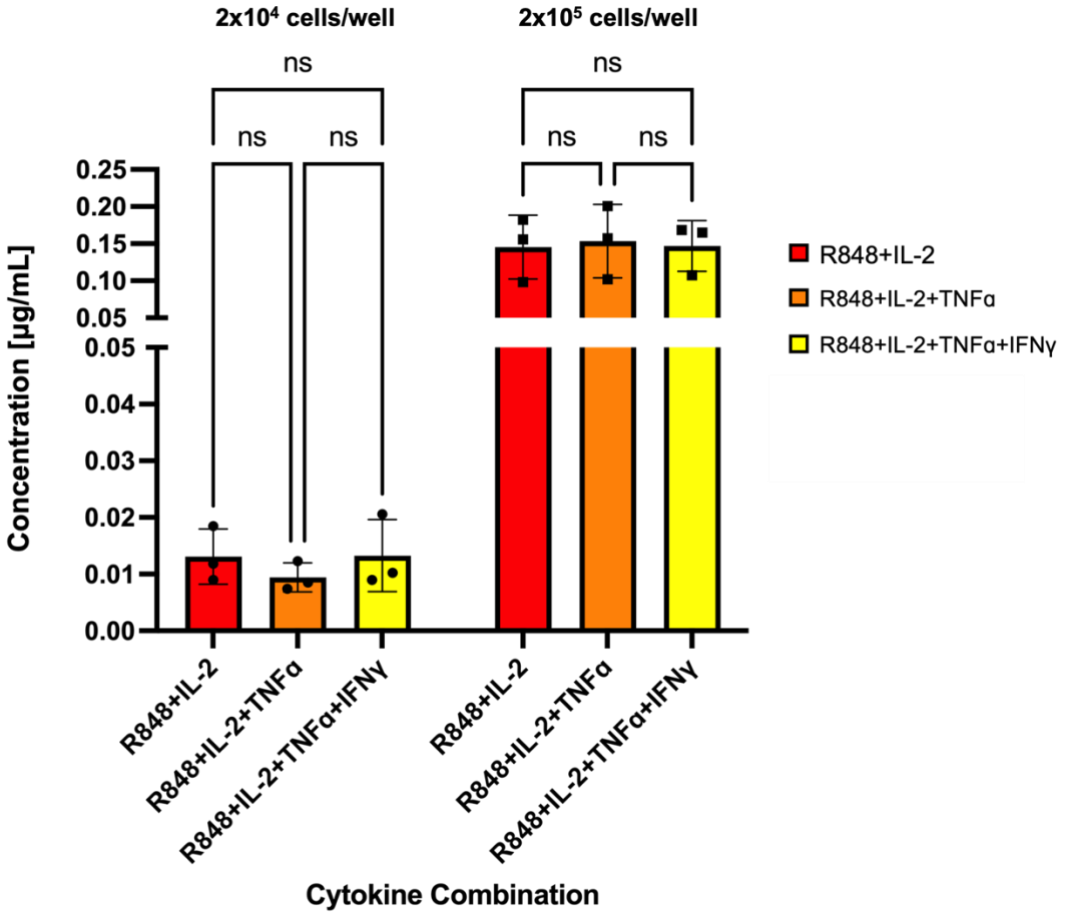

Figure 12: Dose-dependent increase in total IgG production with increasing PBMC seeding density, but no enhancement from additional pro-inflammatory cytokines. *PBMCs from three healthy donors (Con010–012) were cultured for 5 days at two seeding densities (2x10⁴ and 2x10⁵ cells/well) and stimulated with one of three cytokine combinations: (1) R848 + IL-2, (2) R848 + IL-2 + TNFα, or (3) R848 + IL-2 + TNFα + IFNγ. Culture supernatants were harvested and analysed for total IgG concentration by ELISA. IgG concentrations scaled proportionally with cell input, but no significant increase in IgG production was observed with the addition of TNFα or IFNγ (two-way ANOVA, p = 0.9921). Each point represents a technical replicate; bars show the mean ± SD across triplicate wells.*

Based on these findings, a seeding density of $2x10^5$ PBMCs/well was adopted for all subsequent bulk unsorted cultures to maximise total, and therefore antigen-specific, IgG production.

3.2.3 Evaluation of sCD40L addition and culture duration

At this stage in culture development, total Ig production in 5-day cultures remained suboptimal for downstream detection of antigen-specific clones. To address this, the effect of sCD40L and extension of culture duration on IgG yield was tested, as previous reports suggested that sCD40L may enhance ASC differentiation and Ig secretion *in vitro*.[91,92]

PBMCs from three healthy donors (Con010-12) were cultured at $2x10^5$ cells/well with R848 + IL-2 + sCD40L for either 6 or 14 days. Total IgG concentrations were measured by ELISA and compared across timepoints. In line with the 6- vs 14-day comparison done by Makuch et al (2018), this experiment was designed to determine whether extended culture duration allowed for increased cumulative IgG secretion.[91]

As shown in Figure 13, IgG concentrations were significantly higher in 14-day compared to 6-day conditions (Kruskal-Wallis, $p < 0.0001$), confirming the benefit of extended culture duration. Figure 14 demonstrates that stimulation markedly increased IgG output compared to unstimulated controls. Although adding sCD40L to R848 and IL-2 did not significantly enhance IgG production (Kruskal-Wallis, $p > 0.9999$), it was included in the final protocol based on its proven effectiveness in promoting strong IgG responses in downstream single-cell culture systems.[91,92]

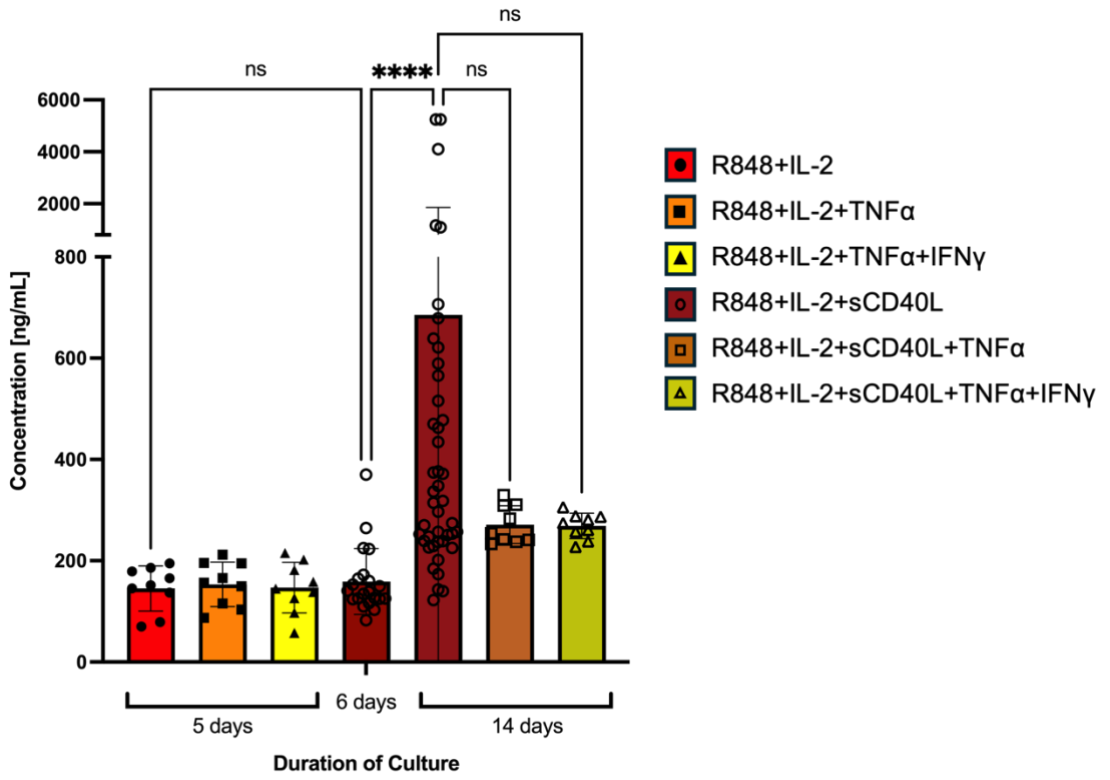

Figure 13: Effect of sCD40L addition and extended culture duration on total IgG production in healthy control PBMCs. *PBMCs from three healthy donors (Con010-012) were cultured at 2x10^5 cells/well for either 6 or 14 days under various cytokine stimulation conditions: R848 + IL-2 alone, R848 + IL-2 + sCD40L, and the same with or without TNFα and IFNγ. The left three 5-day culture bars are the same data as shown in Figure 12. Darker-coloured bars to the right indicate the addition of sCD40L. Total IgG concentrations in supernatants were measured by ELISA. Each bar represents a distinct experiment using a unique donor and condition, except for the red 14-day bar, which combines data from two experiments; individual dots correspond to technical replicates. While sCD40L inclusion did not significantly alter IgG production at day 6 (Kruskal-Wallis, $p > 0.9999$), a significant increase in IgG production was observed in 14-day cultures stimulated with R848 + IL-2 + sCD40L compared to their 6-day counterparts (Kruskal-Wallis, $p < 0.0001$). These results, along with the successful induction of IgG production utilising CD40L in downstream single-cell culture protocols, supported the extension of culture duration in the finalised protocol as well as inclusion of sCD40L without TNFα or IFNγ. Bars represent mean ± SD.*

3.2.4 Re-evaluating cytokine synergy in 14-day cultures

Previous short-term experiments revealed no consistent benefit of adding pro-inflammatory cytokines such as TNFα or IFNγ to the core stimulation cocktail of R848 or IL-2 (Figure 12). However, as these cultures were limited to ≤6 days, it remained unclear whether cytokine synergy might emerge in longer-duration assays.[93,94]

To re-assess potential combinatorial effects under extended conditions, PBMCs from the same three healthy donors (Con010-12) were cultured for 6 or 14 days using four cytokine combinations:

- R848 + IL-2
- R848 + IL-2 + sCD40L
- R848 + IL-2 + sCD40L + TNFα
- R848 + IL-2 + sCD40L + TNFα + IFNγ

Cultures were seeded at $2x10^5$ cells/well and total IgG concentrations were measured at each timepoint using ELISA.

As shown in Figure 13 & Figure 14, inclusion of TNFα or IFNγ did not yield significant increases in total IgG production over the core R848 + IL-2 + sCD40L combination after 14 days (Kruskal-Wallis test; $p > 0.9999$). While modest donor-specific variation was observed (Figure 27), no consistent benefit of TNFα or IFNγ addition was detected across replicates or experiments. Furthermore, there was no significant difference in IgG production was found between 6 days of culture with R848 + IL-2 + sCD40L and 14 days of culture with TNFα (Kruskal-Wallis test; $p = 0.5612$) or TNFα + IFNγ (Kruskal-Wallis test; $p = 0.5460$).

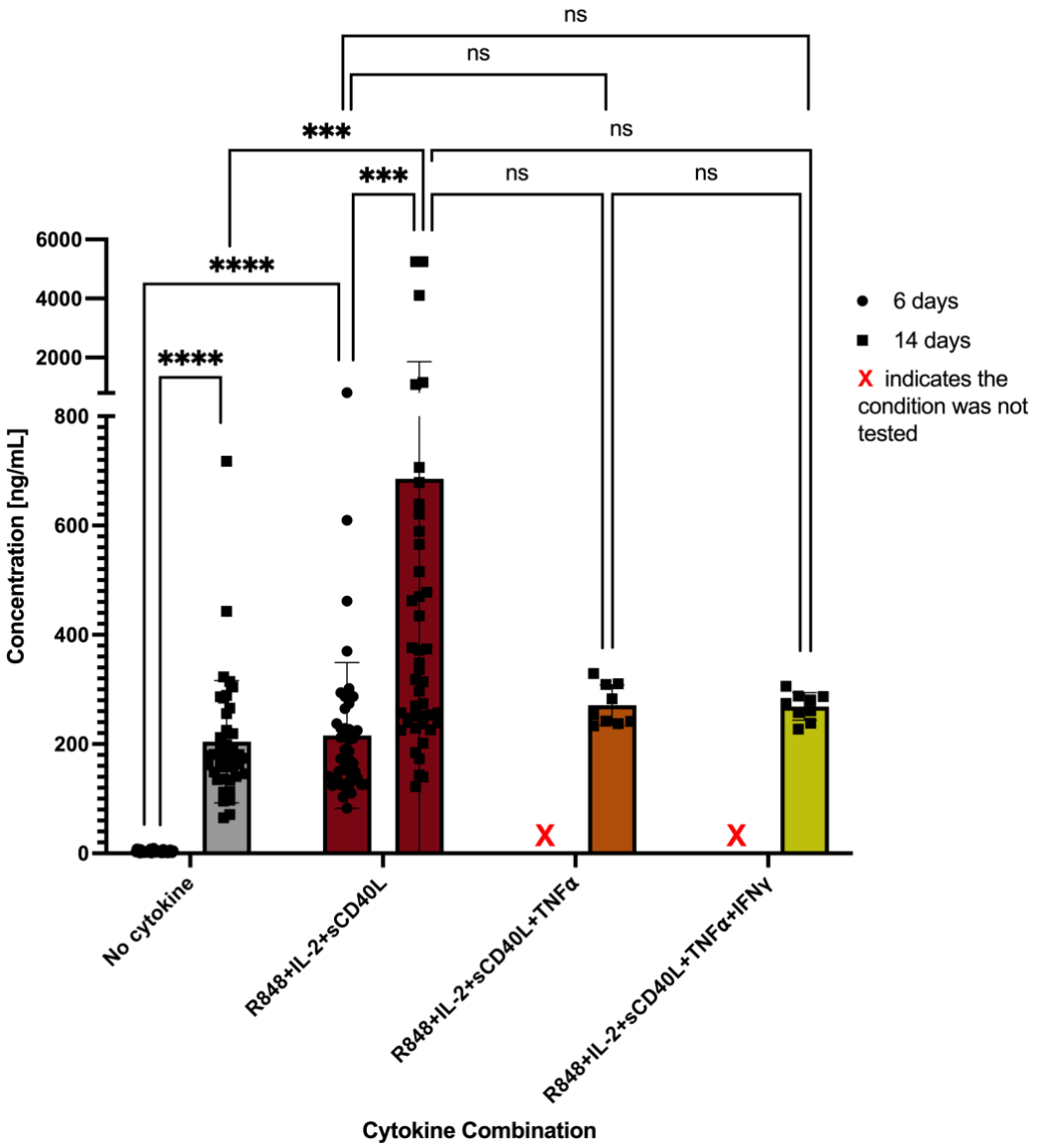

Figure 14: Addition of TNFα and IFNγ does not enhance total IgG production in PBMC cultures, but extension of culture duration from 6 to 14 days does. *PBMCs from three healthy donors (Con010-012) were cultured at $2x10^5$ cells/well with various cytokine combinations for either 6 or 14 days. Stimulatory conditions included R848 and IL-2 alone, or in combination with sCD40L, TNFα, and IFNγ. Total IgG concentrations in supernatants were measured by ELISA. Cultures extended from 6 to 14 days in the presence of R848, IL-2, and sCD40L produced a significantly higher concentration of IgG (red bars; Kruskal-Wallis, $p = 0.0003$). However, after 14 days of culture, the inclusion of TNFα (orange bar) or TNFα + IFNγ (yellow bar) failed to increase IgG production beyond that achieved with R848, IL-2, and sCD40L alone (Kruskal-Wallis; $p > 0.9999$). There was no significant difference in IgG production between 6 days of culture with R848 + IL-2 + sCD40L and 14 days of culture with TNFα (Kruskal-Wallis; $p = 0.5612$) or TNFα + IFNγ (Kruskal-Wallis; $p = 0.5460$). These results support the exclusion of TNFα and IFNγ from the final stimulation cocktail and the extension of culture duration to 14 days. Bars represent mean ± SD of technical replicates. Data points represent technical replicates.*

These findings supported the retention of R848 + IL-2 + sCD40L as the core stimulation cocktail for all subsequent 14-day PBMC cultures. TNFα and IFNγ were

excluded from further healthy donor experiments but remained candidates for future patient-specific investigations, particularly in settings where ASC formation or antigen-specific Ig secretion proved limited.

3.2.5 Transition to single-cell B-cell media

To align with protocols that were to be used in future single-cell workflows – where recovery of rare, antigen-specific IgG-secreting cells would be critical – the culture medium was switched at this stage from standard RPMI 1640 to a *single-cell B-cell media* (scBCM) for all subsequent PBMC stimulation experiments. This change was prompted by ongoing difficulties in eliciting robust total IgG production and the established success of scBCM in CNS autoantibody discovery using low-frequency autoreactive B-cell populations (unpublished data).

A preliminary investigation was conducted across PBMCs from three healthy donors (Con013-015) with R848, IL-2, and sCD40L in scBCM to assess total IgG output. As shown in Figure 15, scBCM not only supported robust IgG production, but also generated as high, if not higher, average concentrations across replicate wells compared to historical RPMI 1640 results. This suggested that scBCM at least maintained, and in some cases enhanced, overall antibody yield.

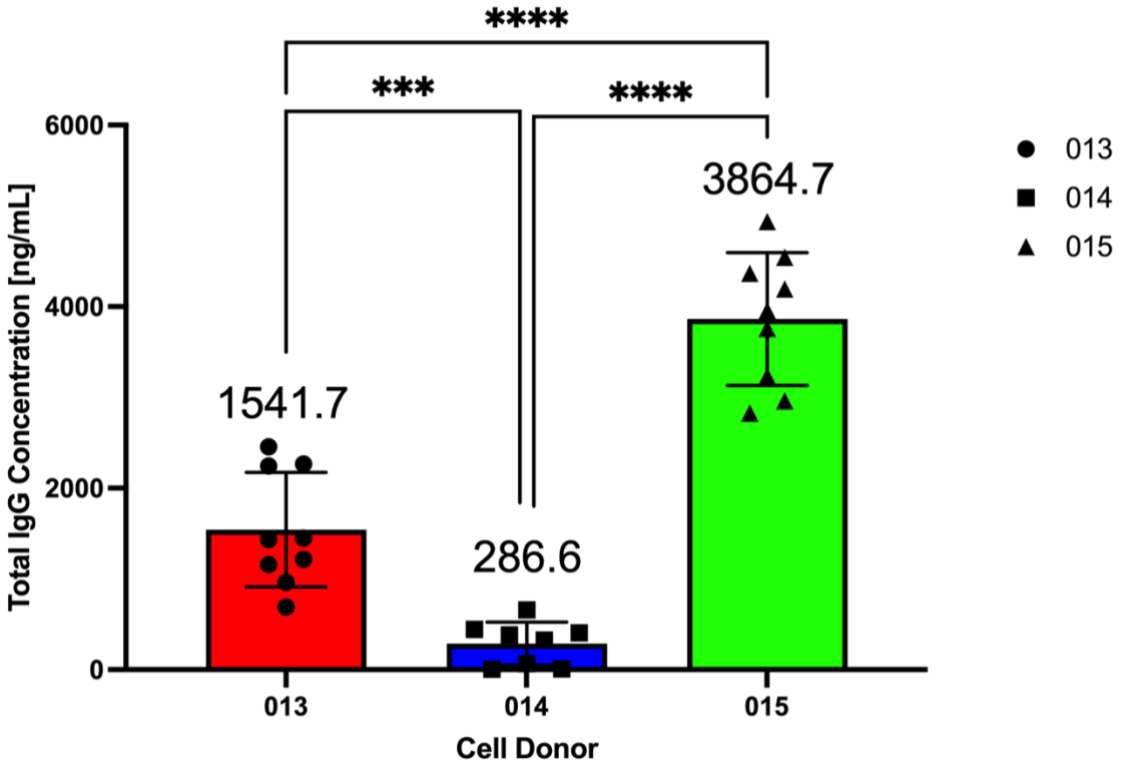

Figure 15: Total IgG production across three healthy donors after 14 days of culture with R848, IL-2, and sCD40L in scBCM. *PBMCs from healthy donors Con013, 014, and 015 were cultured in scBCM with R848, IL-2, and sCD40L for 14 days at a seeding density of $2x10^5$ cells/well. Total IgG concentrations were assessed by ELISA. Bars represent mean ± SD of technical replicates within each donor. Technical replicates are represented by individual points. Values above bars indicate mean IgG production across replicate wells within that donor. Total IgG production differed significantly between donors (one-way ANOVA, $p < 0.0001$). Overall results across these donors indicated that scBCM was comparable, if not more effective, in inducing robust total IgG production compared to RPMI 1640 without the supplements included in scBCM.*

Importantly, scBCM had been optimised for subset-isolated and single-cell cultures. In fractionated cultures, where specific B-cell subsets are grown without the possible buffering effect of the full PBMC pool, both media composition and individual supplement choices were suspected to potentially affect differentiation. Thus, while a direct statistical comparison was not possible between the RPMI-based media and the scBCM, as different healthy control samples were tested with the scBCM, the strong (and possibly superior) performance of scBCM in this early assessment provided confidence that it would support downstream bulk-sorted and single-cell workflows without compromising yield or sensitivity.

Based on these findings, scBCM was adopted for all subsequent bulk, fractionated, and single-cell B-cell culture experiments.

3.2.6 Summary comparison of all tested conditions

Figure 13 summarises total IgG production across all conditions trialled in RPMI 1640, with cultures seeded at a density of $2x10^5$ PBMCs/well. Stimulation conditions included R848 and IL-2 alone or in combination with TNFα, IFNγ, and sCD40L. Media formulations tested up to this point were RPMI 1640 and scBCM, and culture durations ranged from 6 to 14 days.

Across all experiments, the highest IgG concentrations were consistently observed in 14-day cultures stimulated with R848, IL-2, and sCD40L. The addition of TNFα or TNFα + IFNγ did not reproducibly enhance IgG production at any time point. While sCD40L did not yield a statistically significantly increase in IgG compared directly to R848 and IL-2 alone, its inclusion was retained due to prior use in related B-cell culture systems and its compatibility with single-cell culture.[92] While statistical comparison of total IgG production in RPMI 1640 versus scBCM was not possible, preliminary evidence indicated strong performance of scBCM, whose formulation would be aligned with future single-cell experiments.

Based on these findings, the combination of R848, IL-2, and sCD40L in scBCM over 14 days was selected as the standard protocol for all subsequent experiments.

3.2.7 Application of final protocol to patient PBMCs

Following optimisation in healthy donor PBMCs, the finalised culture protocol was next applied to PBMCs from two patients with AN: one with $NF155^+$ antibodies (Bio-081)

and one with pan-NF^+ antibodies (Bio-099). PBMCs from a healthy donor (Con015) were included for comparison and processed in parallel.

Each sample was cultured in triplicate at $2x10^5$ cells/well across two conditions: (1) stimulated cultures (R848, IL-2, and sCD40L in scBCM), and (2) unstimulated cultures (RPMI 1640 media without cytokines, used as the base for scBCM). To control for background signal, three wells containing media only were included per condition. Cultures were maintained for 14 days, after which total IgG concentrations in the supernatants were measured by ELISA.

As shown in Figure 16, IgG production varied markedly across donors/patient groups. The $NF155^+$ patient produced the highest concentrations (~15-35 μg/mL), followed by the healthy control (~6 μg/mL). The pan-NF^+ patient produced the lowest total IgG levels (~2 μg/mL) under stimulated conditions. A two-way ANOVA confirmed significant differences in IgG output between donors ($p < 0.0001$). Unstimulated wells from all three donors showed minimal or undetectable IgG.

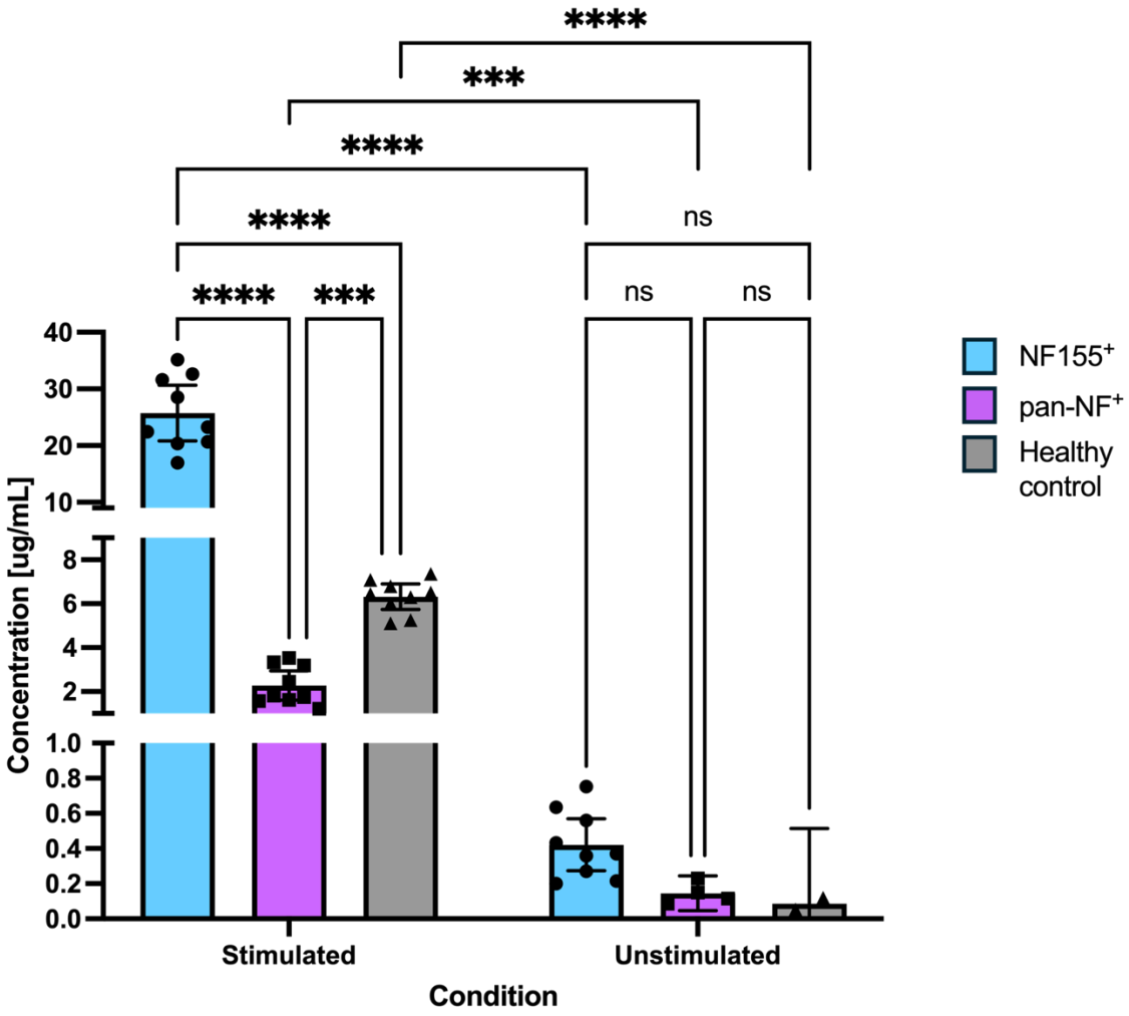

Figure 16: Total IgG production from stimulated and unstimulated 14-day PBMC cultures in patients with autoimmune nodopathy and a healthy control. *PBMCs from one NF155⁺ patient (Bio-081; blue), one pan-NF⁺ patient (Bio-099; pink), and one healthy control (Con015; grey) were cultured at 2x10⁵ cells/well for 14 days in either stimulated conditions (R848, IL-2, sCD40L in scBCM) or unstimulated conditions (RPMI media without phenol red or cytokines). Each condition was tested in nine replicate wells per donor. Bars represent the mean ± SD of total IgG concentrations (µg/mL) across replicate wells as measured by ELISA. A two-way ANOVA was conducted for all statistical analyses. While all donors exhibited low or undetectable IgG in unstimulated wells, substantial donor-to-donor variability in IgG production was observed under stimulated conditions, with the NF155⁺ patient showing the highest concentrations and the pan-NF⁺ patient the lowest.*

Despite measurable total IgG secretion in the stimulated conditions, no antigen-specific IgG reactivity against NF155 or NF186 was detected in any supernatant by CBA (data not shown). These results prompted further investigation into whether this reflected an absence of autoreactive B cells or insufficient differentiation into ASCs under the tested conditions.

3.3 ASC generation in culture and its relationship to IgG output

To assess whether the limited antigen-specific IgG detected in patient cultures reflected impaired induction of autoreactive ASCs from less mature B-cell subsets *in vitro* (rather than IgG secretion from pre-existing, non-autoreactive ASCs), flow cytometry was used to evaluate the generation of ASCs over time in healthy control cultures as a baseline.

3.3.1 Initial optimisation of flow cytometry panel for ASC detection

To quantify ASC generation in healthy control cultures under optimised stimulation conditions, a flow cytometry panel was developed to identify $CD19^{+}CD27^{++}CD38^{++}$ ASCs within PBMCs, based on gating strategies used in autoimmune encephalitis and NMOSD studies.[91,92]

Initial testing was performed on unstimulated day 0 PBMCs from healthy donors to define baseline gating. The panel included six fluorophore-conjugated antibodies and a viability dye (Table 13).

Marker	Fluorophore	Dilution	Purpose
CD3	FITC	1:200	T-cell exclusion
CD14	PB (Pacific Blue)	1:100	Monocyte exclusion
CD19	APC-eFluor780	1:100	Pan-B-cell identification
CD27	BV605	1:100	Memory and ASC marker
CD38	PE	1:50 initially, later titrated to 1:200	Activation/ASC marker
DAPI		1:5000	Live/dead discrimination

Table 13: Fluorophores and dilutions used for initial ASC panel development. *Antibodies and viability dye included in the six-colour flow cytometry panel designed to identify ASCs within PBMCs. The panel was optimised to detect $CD19^{+}CD27^{++}CD38^{++}$ ASCs while excluding T cells, monocytes, and dead cells. Fluorophores were selected for minimal spectral overlap and clear resolution of key populations, with dilutions titrated based on initial pilot testing in healthy donor samples.*

This panel enabled separation of B-cell subsets at baseline (Figure 17) and formed the foundation for subsequent ASC gating.

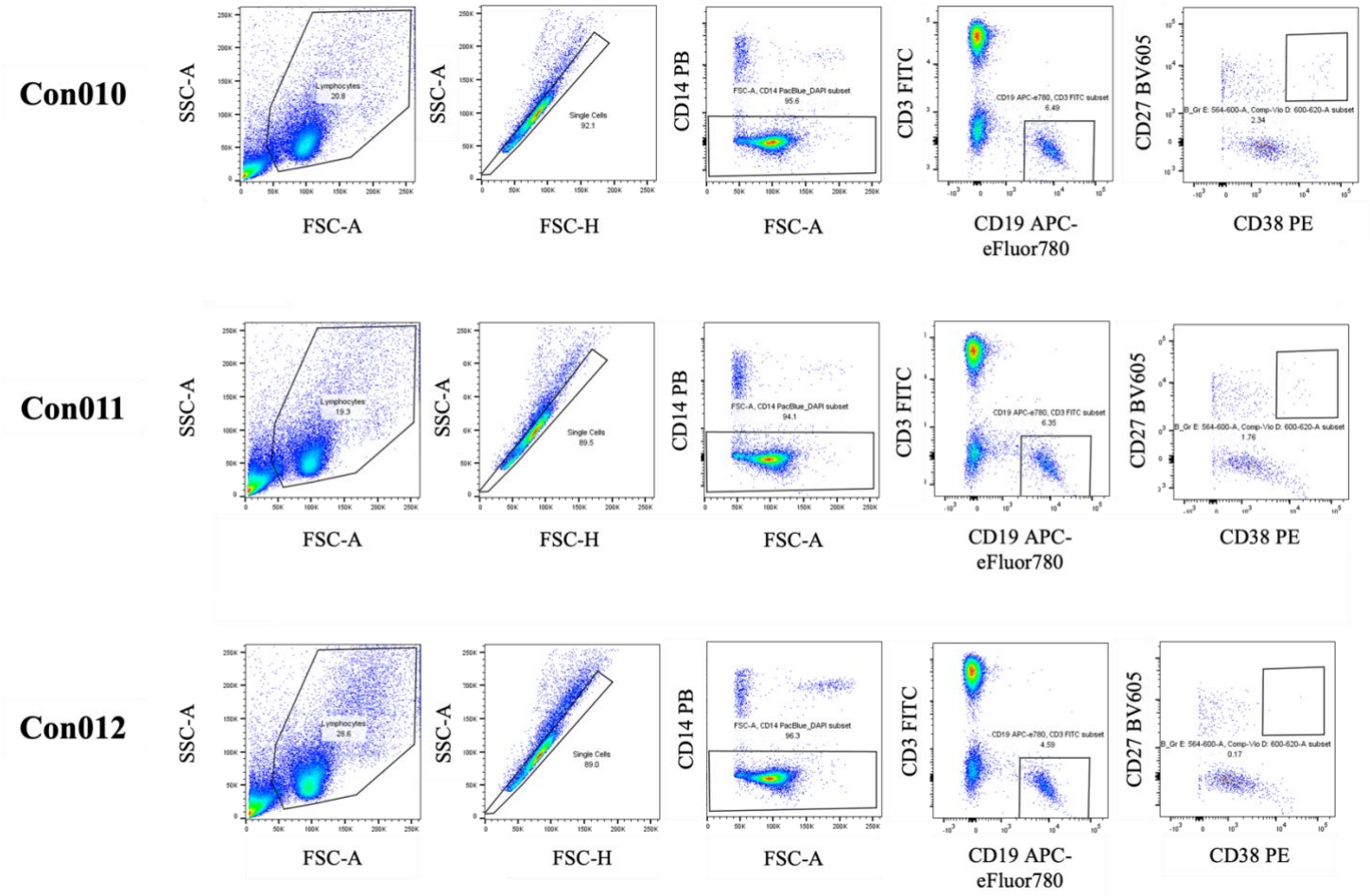

Figure 17: Initial testing of fluorophore panel for ASC identification at baseline. *Representative flow cytometry plots showing unstimulated, freshly thawed PBMCs from a healthy donor stained with the preliminary six-colour antibody panel designed to detect antibody-secreting cells (ASCs). $CD19^{+}$ B cells were gated from live $CD3^{-}CD14^{-}DAPI^{-}$ lymphocytes, and ASC populations were identified based on high expression of CD27 and CD38. This pilot gating at day 0 provided baseline reference values and confirmed the panel's capacity to resolve $CD27^{++}CD38^{++}$ ASCs in healthy donor samples prior to stimulation.*

3.3.2 Confirmation of ASC differentiation using flow cytometry

To validate the induction of ASC differentiation under optimised stimulation conditions, flow cytometric analysis of $CD19^{+}CD27^{++}CD38^{++}$ ASCs was performed at three time points: day 0 (immediately post-thaw), day 6, and day 14. PBMCs from three healthy donors (Con010-012) were cultured with R848, IL-2, and sCD40L in scBCM, and nine replicate wells were analysed per time point.

As shown in Figure 18, ASC frequencies were low at baseline (~2%), peaked at day 6 (~14%) after stimulation, and declined to near-baseline levels by day 14 (<0.1%). In contrast, total IgG concentrations in culture supernatants rose steadily throughout the culture period.

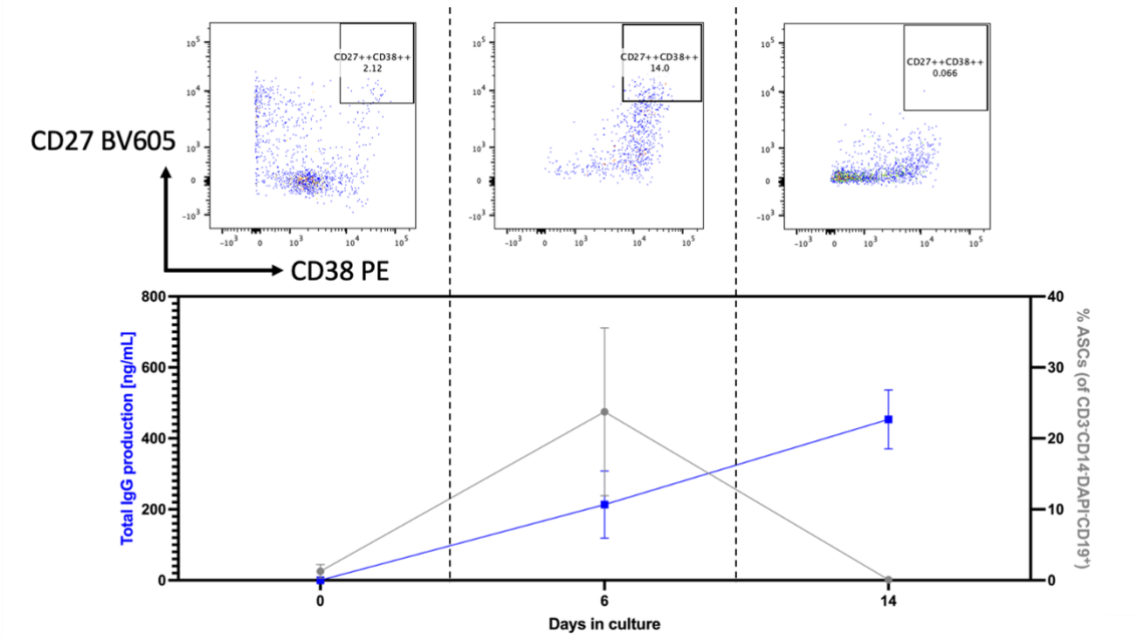

Figure 18: In vitro ASC generation and cumulative IgG secretion in healthy donor PBMC cultures. *PBMCs from three healthy donors were stimulated with R848, IL-2, and sCD40L in scBCM and analysed at days 0, 6, and 14 of culture.* ***Top:*** *Representative flow cytometry plots showing $CD19^{+}CD27^{++}CD38^{++}$ ASCs (gated on live $CD3^{-}CD14^{-}DAPI^{-}CD19^{+}$ lymphocytes) at each timepoint from healthy donor Con011. ASC frequency peaked at day 6 and declined by day 14.* ***Bottom:*** *Quantification of total IgG concentration (blue line, left axis) and ASC frequency (grey line, right axis) over time. Data points represent mean ± SD across nine replicate wells per timepoint. These results highlight a temporal dissociation between ASC frequency and antibody accumulation, with sustained IgG secretion continuing after the peak of ASC expansion.*

This kinetic dissociation – ASC frequency peaking early, followed by continued antibody accumulation – is consistent with prior studies in autoimmune encephalitis and supported the use of extended culture durations to maximise IgG yield.[91]

Furthermore, stimulation of PBMCs appeared to have a significant effect on ASC frequency over 6 days compared to unstimulated PBMCs from the same healthy control (Figure 19).

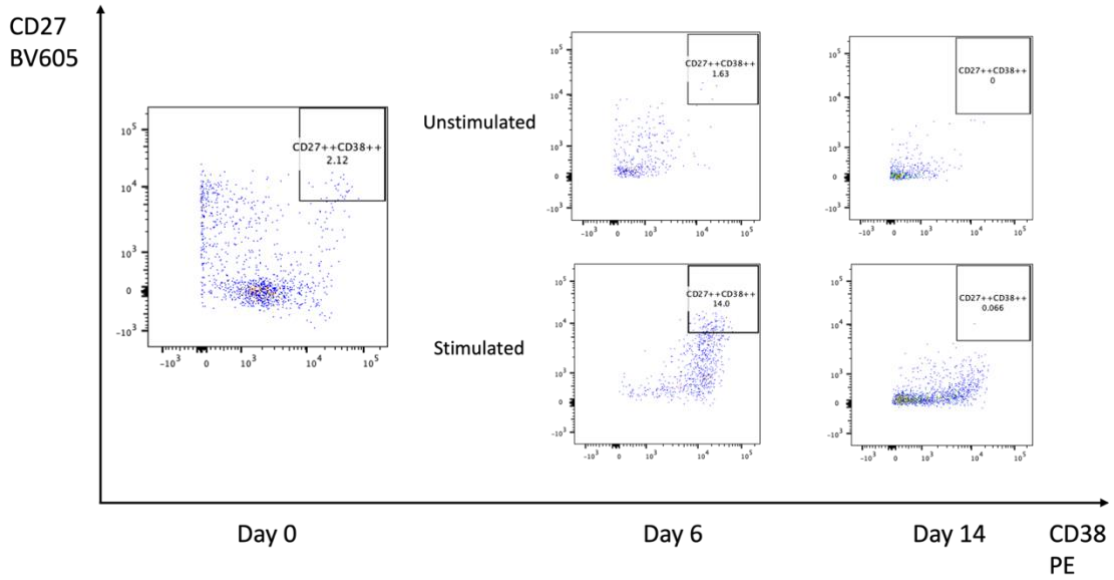

Figure 19: Stimulation-dependent ASC differentiation in healthy control PBMC cultures over time. *Flow cytometry plots showing $CD19^{+}CD27^{++}CD38^{++}$ ASCs gated on live $CD3^{-}CD14^{-}DAPI^{-}CD19^{+}$ lymphocytes at days 0, 6, and 14 in unstimulated (top; RPMI + 10% FBS) and stimulated (bottom; R848, IL-2, and sCD40L in scBCM) PBMC cultures. ASC frequencies increased markedly by day 6 in the stimulated condition (14.0%) and declined to below-baseline levels by day 14, consistent with expected ASC kinetics. In contrast, ASC generation decreased over time in unstimulated cultures. These data demonstrate that ASC expansion is stimulation-dependent under this culture protocol, and IgG output in vitro is likely not attributable to passive persistence of pre-existing ASCs alone.*

Together, these results confirmed that the stimulation protocol reliably induces ASC differentiation of earlier B cells *in vitro* compared to unstimulated conditions, and that IgG secretion persists beyond the transient peak of ASC frequency.

3.3.3 Association between ASC frequency and total IgG levels

To evaluate the relationship between ASC differentiation and Ig secretion, $CD19^{+}CD27^{++}CD38^{++}$ ASC frequencies were quantified by flow cytometry at day 6 and day 14, and corresponding total IgG concentrations were measured in matched culture supernatants by ELISA. PBMCs from three healthy donors (Con010-012) were stimulated with R848, IL-2, and sCD40L and cultured in triplicate.

As shown in Figure 20, ASC frequency at day 6 was moderate-to-strongly associated with total IgG concentration at the same time point (Pearson $r = 0.72$, $p < 0.01$). This association remained positive at day 14 ($r = 0.59$, $p < 0.01$), despite a decline in ASC frequency. These results confirmed that ASC generation contributed to total IgG output and that IgG continued to accumulate beyond the peak of ASC expansion.

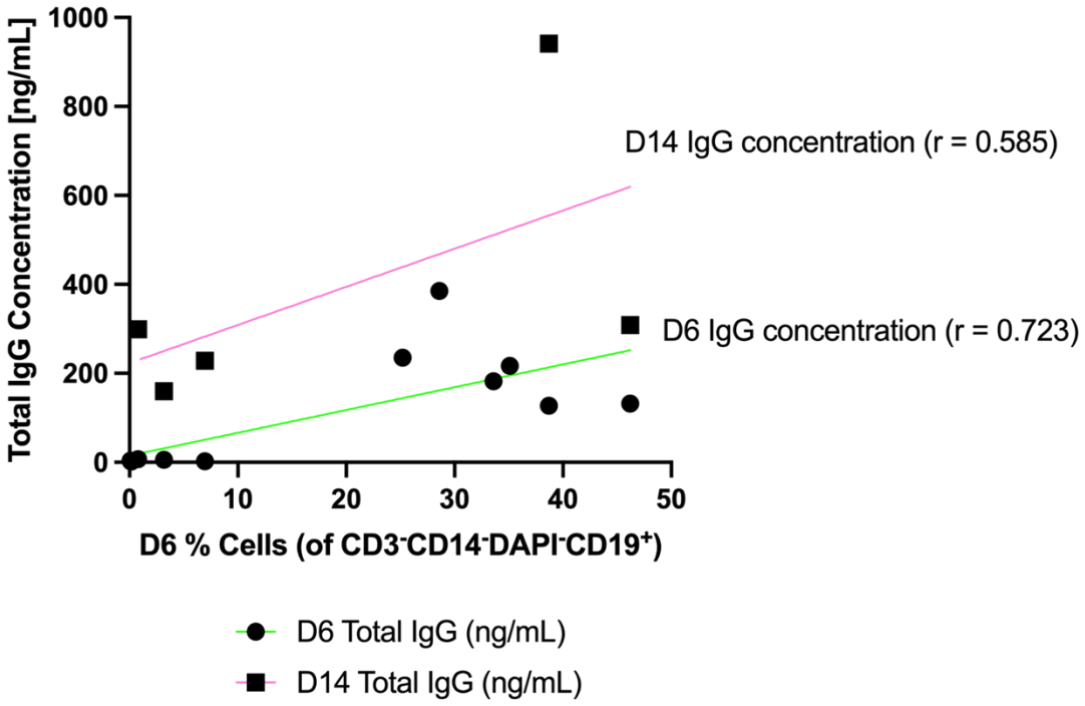

Figure 20: Correlation between ASC frequency and total IgG production in vitro in healthy donor PBMC cultures. *$CD19^{+}CD27^{++}CD38^{++}$ antibody-secreting cell (ASC) frequencies and matched total IgG concentrations were measured in stimulated PBMC cultures from three healthy donors (Con010-012). Cultures were maintained for 14 days under standard stimulation conditions (R848, IL-2, sCD40L). ASC proportions were quantified by flow cytometry at day 6 (circles and green line) and day 14 (squares and pink line), and corresponding supernatants were analysed by ELISA. A strong positive correlation was observed between ASC frequency and IgG titre at day 6 ($r = 0.72$, $p < 0.01$), and a moderate positive correlation persisted at day 14 ($r = 0.59$, $p < 0.01$), despite a decline in ASC numbers. Each point represents a replicate culture well.*

Collectively, these findings indicated that the stimulation protocol was sufficient to drive both differentiation and sustained secretion of antibody-producing cells *in vitro*.

3.3.4 Resolving $CD38^{++}$ ASCs from $CD38^{intermediate}$ memory B cells

Once the above flow cytometry panel was applied to stimulated PBMCs in these experiments, however, the panel revealed increased CD38 expression in activated B cells. To determine the optimal fluorophore for resolving this upregulated marker, CD38 PE and CD38 PE-Cy7 (both at a 1:200 dilution) were directly compared. CD38 PE-Cy7 yielded improved separation of $CD27^{++}CD38^{++}$ AS from $CD38^{intermediate}$ memory B cells, with reduced spectral spillover (Figure 21 &

Figure 22). CD38 PE-Cy7 was therefore selected for all subsequent bulk and single-cell sort experiments.

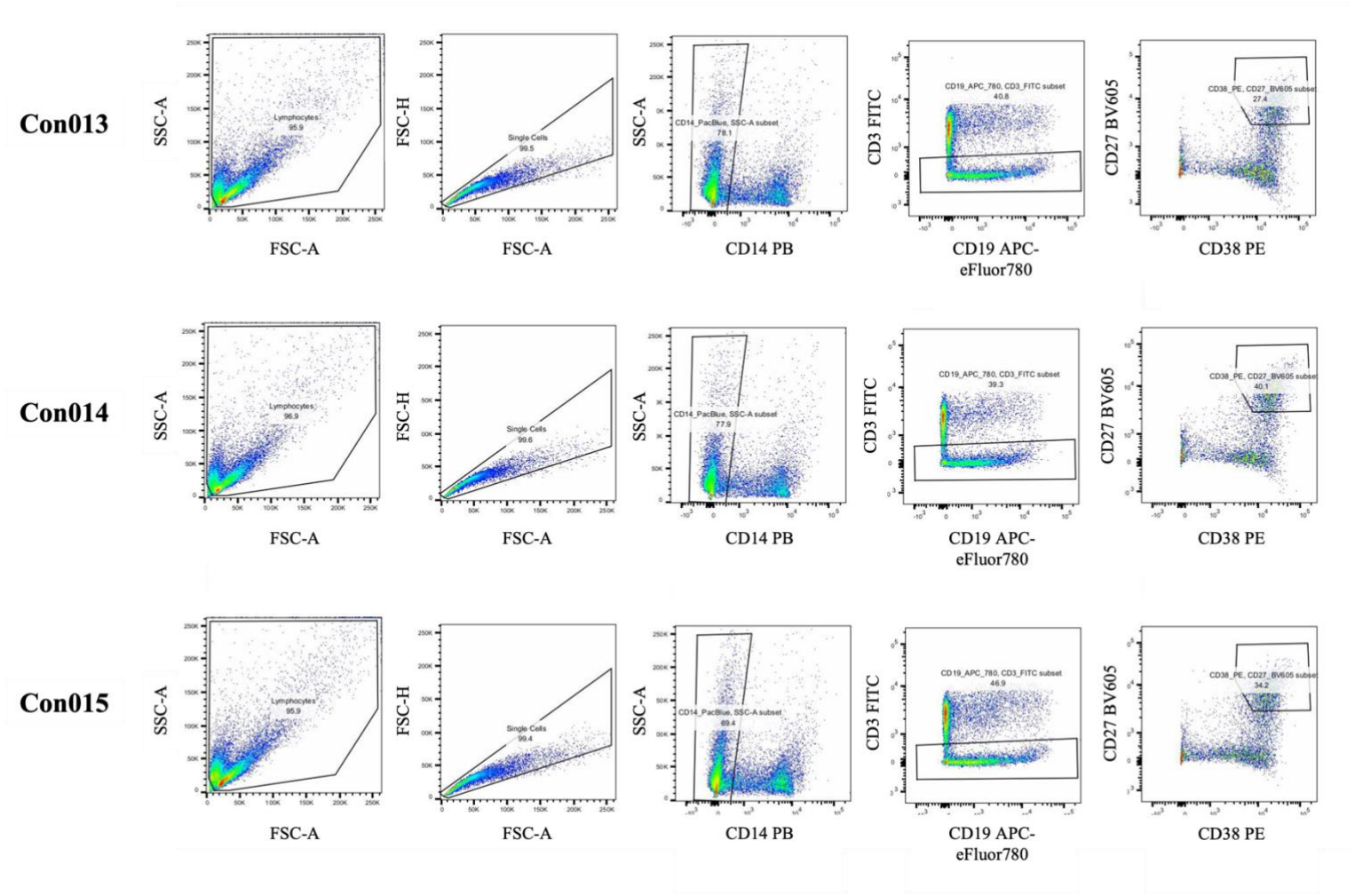

Figure 21: CD38 PE fails to fully resolve CD27^{++}CD38^{++} ASCs from CD38^{intermediate} B cells after stimulation. *Representative flow cytometry plots from healthy donor PBMCs cultured for 6 days with R848, IL-2, and sCD40L, stained using the initial antibody panel with CD38 PE. Although ASC populations were visible, signal spread and overlap with CD38^{intermediate} B cells limited resolution. This prompted evaluation of alternative fluorophores for improved ASC discrimination.*

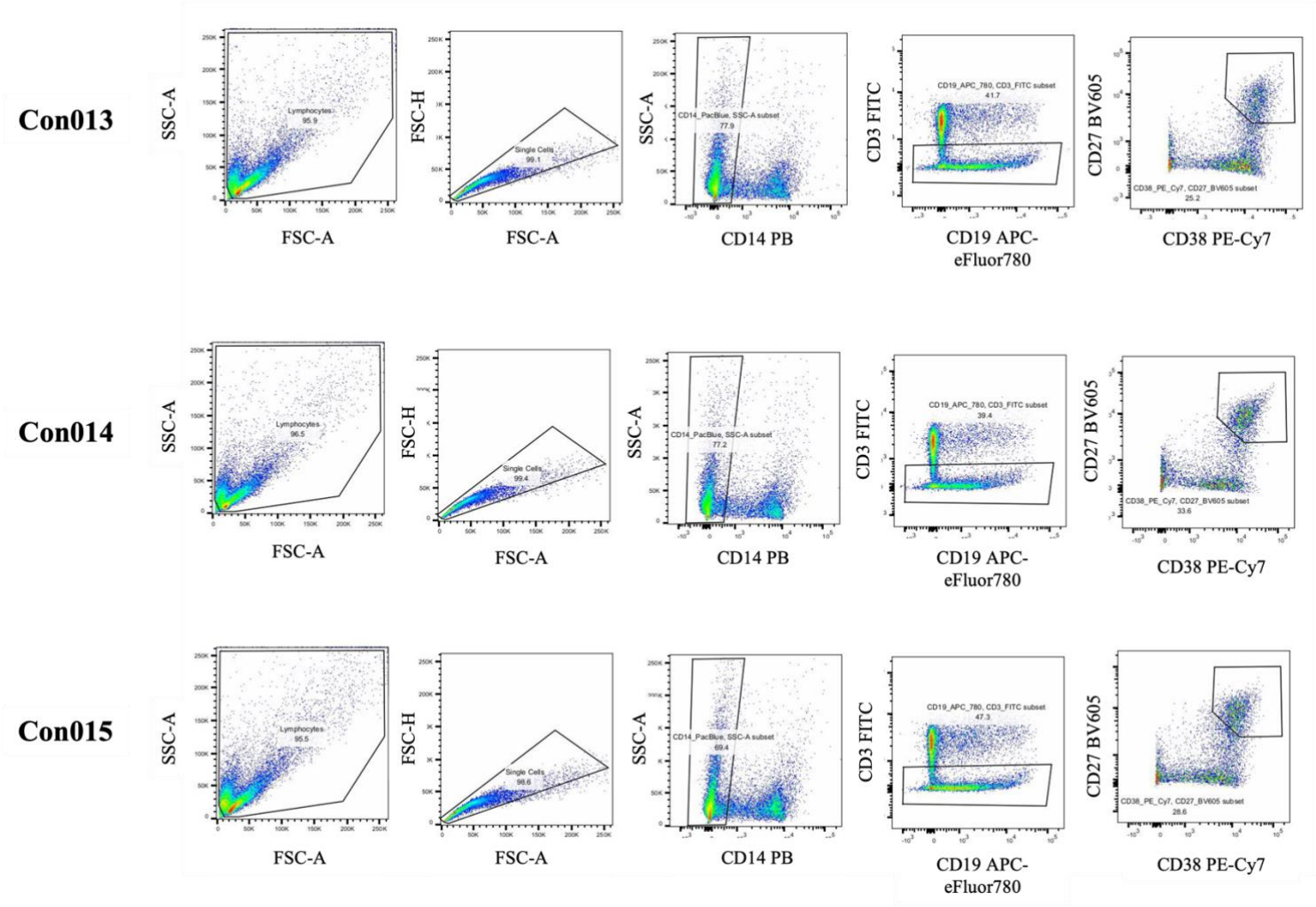

Figure 22: CD38 PE-Cy7 enables clearer separation of CD27^{++}CD38^{++} ASCs following stimulation. *Representative plots from the same stimulated PBMC cultures as in Figure 21, stained using the modified panel with CD38 PE-Cy7 at the same dilution (1:200). Compared to CD38 PE, PE-Cy7 provided sharper distinction between ASCs and surrounding B-cell subsets, with reduced spectral spillover and improved signal-to-noise ratio. This fluorophore was selected for all subsequent ASC and sort panel applications.*

Gating followed a standard sequential approach: exclusion of doublets and dead cells (FSC-H/FSC-A and $DAPI^-$), followed by lineage exclusion ($CD3^-CD14^-$), identification of $CD19^+$ B cells, and finally gating on $CD27^{++}CD38^{++}$ ASCs. Gates were validated using fluorescence-minus-one (FMO) and single-stain controls.

This refined panel was used to assess ASC frequencies in healthy donor PBMC cultures and provided the foundation for the expanded sorting panel described in section 3.4.

3.3.5 Summary of optimised conditions for total IgG and ASC yield

These optimisation experiments established a reproducible *in vitro* stimulation system for inducing IgG secretion from healthy control PBMCs. The following parameters were established as optimal for maximising both total IgG production and ASC generation:

- **Seeding density**: $2x10^5$ PBMCs/well
- **Culture duration**: 14 days
- **Stimulation cocktail**: R848 (2.5 µg/mL), IL-2 (50 ng/mL), sCD40L (50 ng/mL)
- **Media**: scBCM

These conditions consistently yielded µg/mL levels of IgG in supernatants and supported the differentiation of $CD19^+CD27^{++}CD38^{++}$ ASCs, as confirmed by flow cytometry. ASC frequencies peaked around day 6 and declined thereafter, while IgG continued to accumulate through day 14. This temporal dissociation between peak ASC frequency and total IgG concentration was further supported by a moderate-to-strong correlation between ASC proportion and IgG output across timepoints.

This protocol was subsequently applied to patient-derived PBMCs, where total IgG secretion was observed in some cases. However, no antigen-specific IgG against NF155 or NF186 was detected, prompting the development of additional strategies to enrich for autoreactive clones.

This baseline stimulation framework formed the experimental foundation for the next phase: implementing flow cytometry-based B-cell sorting to functionally assess individual subpopulations and enable downstream mAb generation and functional characterisation.

3.4 Flow cytometry development and bulk sorting experiments

Following the establishment of a robust and reproducible PBMC bulk culture protocol capable of inducing ASC differentiation and IgG secretion, the next phase involved developing preparative flow cytometry methods to enable functional characterisation of defined B-cell subsets. While bulk unsorted cultures were suitable for optimisation of stimulation conditions and measurement of total IgG output, they lacked the resolution necessary for isolating individual antibody-producing cells for downstream sequencing and mAb generation.

To overcome this limitation, multicolour flow cytometry was employed to enable the phenotypic identification and bulk sorting of specific B-cell subpopulations. The ultimate objective was to isolate viable populations containing pan-NF-specific cells and functionally interrogate their antibody secretion potential *in vitro*. This section details the development and validation of a flow cytometry-based sorting strategy designed to support this goal.

3.4.1 FACS bulk sort panel testing and quality control

3.4.1.1 Transition from ASC profiling to subset sorting

Following the development of a reproducible *in vitro* stimulation protocol for ASC induction and IgG secretion (section 3.3), flow cytometry was next adapted to support preparative B-cell subset sorting. While the initial panel was optimised for identifying $CD19^{+}CD27^{++}CD38^{++}$ ASCs, this minimal configuration lacked the granularity required for downstream sorting of phenotypically distinct populations, particularly when aiming to isolate cells representative of each major stage of B-cell development.

The ASC panel consisted of CD3 and CD14 for lineage exclusion, DAPI for viability, and CD19, CD27, and CD38 for ASC identification. This approach sufficed for quantifying ASCs and correlating ASC frequency with IgG output. However, to enable bulk sorting of biologically distinct subpopulations – including new emigrant, naïve, and memory B cells – two additional markers were incorporated. CD10 was added to identify transitional/new emigrant cells and exclude bone marrow emigrants, while IgD enabled resolution of unswitched versus switched memory compartments.

This expanded panel was designed based on previously published protocols in CNS autoimmunity and adapted for compatibility with both bulk and single-cell workflows.[91,92] It was optimised for clean separation of B-cell subsets prior to functional culture and mAb production.

3.4.1.2 Finalisation of panel and pre-sorting validation

To refine the expanded B-cell panel, titration of each fluorophore-conjugated antibody was performed using three dilutions: a starting dilution informed by prior ASC and

Oxford Autoimmune Neurology Group (OANG) single-cell sorting protocols, plus one dilution above and below (or two above/below, in the case that dilution set 1 started at 1:20 or 1:200, respectively). This allowed optimisation for signal resolution and minimal spectral overlap in multicolour panels (Table 14).

Fluorophore	Dilution set 1	Dilution set 2	Dilution set 3
CD3 PB	1:100	1:50	1:200
CD14 PB	1:100	1:50	1:200
CD27 BV605	1:20	1:50	1:100
CD38 PE-Cy7	1:200	1:50	1:100
IgD FITC	1:50	1:20	1:100
CD10 PE-Dazzle594	1:100	1:50	1:200
CD19 APC-eFluor780	1:100	1:50	1:200
DAPI	1:5000	1:5000	1:5000

Table 14: Fluorophore-conjugated antibodies and titration dilutions used for the finalised B-cell bulk sorting panel. *Each antibody was titrated across three dilutions to optimise resolution and minimise spectral overlap in multicolour flow cytometry. The final panel incorporated lineage exclusion (CD3, CD14), viability (DAPI), B-cell identification (CD19), memory and activation profiling (CD27, CD38), and discrimination of transitional and unswitched memory subsets (CD10, IgD). Dilution set 1 was selected for all downstream experiments based on optimal staining performance. This configuration was used for preparative bulk sorting of healthy and patient-derived B-cell subsets for functional culture and monoclonal antibody production.*

Markers such as CD20, IgA, IgM, and IgG were considered but ultimately excluded; their inclusion would have required additional fluor channels, increased panel complexity, and potentially compromised resolution of core gating populations. Given that the aim at this stage was not to characterise isotype diversity but to isolate broad B-cell subsets for downstream culture and functional assessment, a leaner panel was favoured.

Dilution set 1 (Table 14) was selected for optimal separation of the subsets of interest and subsequently validated for consistent staining and reproducible separation of all

target populations. This final configuration was adopted for all downstream healthy donor and patient sorting experiments.

3.4.2 Bulk sorting of B-cell subsets from a patient and healthy donors

Following optimisation of the B-cell FACS panel and titration of fluorophore dilutions in healthy control samples, the workflow was applied to PBMCs from an $NF155^+$ AN patient (Bio-081). This sample was selected as an initial test case to trial the full sort-to-culture pipeline on a clinically relevant, but less limited, specimen compared to pan-NF^+ AN cases.

3.4.2.1 Sorting strategy and culture layout

PBMCs were stained with the final eight-colour panel and gated for live $CD3^-CD14^-DAPI^-CD19^+$ lymphocytes. Within this population, the following B-cell subsets were defined and sorted out of $CD3^-CD14^-DAPI^-CD19^+$ singlets (Figure 23):

- **P7: New emigrant** ($CD27^-IgD^+CD10^+$): 3.57%
- **P6: Mature naïve** ($CD27^-IgD^+CD10^-$): 43.37%
- **P11: Unswitched memory** ($CD27^+IgD^+$): 3.38%
- **P10: Switched memory** ($CD27^+IgD^-$): 26.40%
- **P8: ASCs/plasmablasts** ($CD27^{++}CD38^{++}$): 0.08%

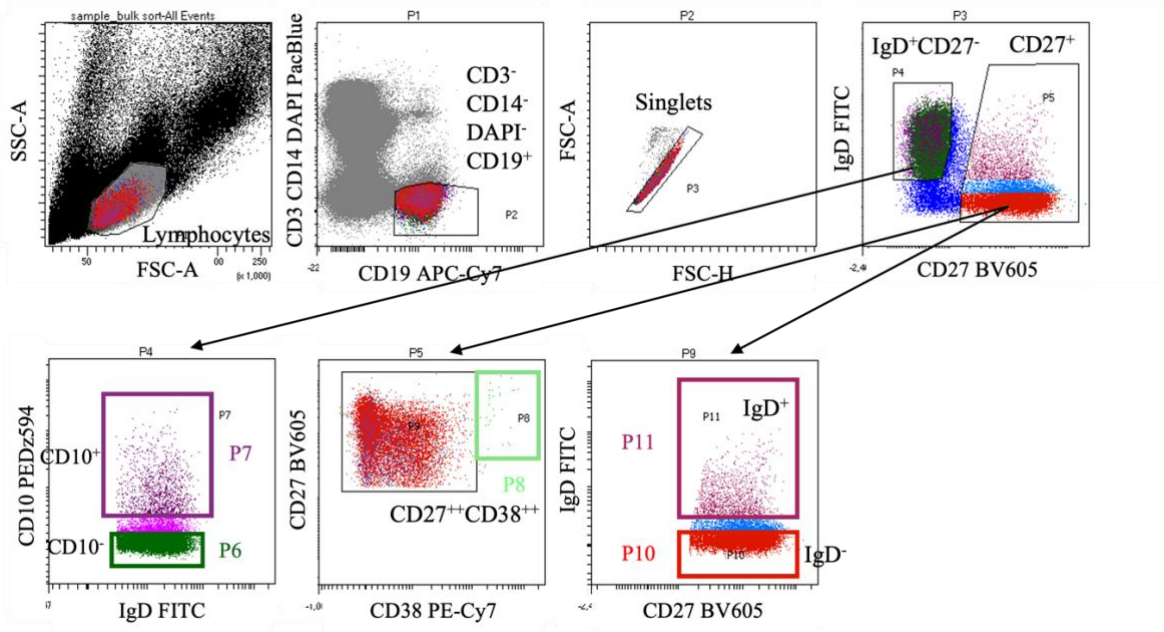

Figure 23: Flow cytometry gating strategy for subset sorting of PBMCs from an NF155⁺ AN patient.
Representative gating from a bulk-sort experiment on thawed PBMCs from Bio-081. Initial gates identified live singlet CD3⁻CD14⁻DAPI⁻CD19⁺ B cells (P2-P3). Within this population, four major subsets were defined: mature naïve (P6: CD27⁻IgD⁺CD10⁻, dark green), new emigrant (P7: CD27⁻IgD⁺CD10⁺, purple), unswitched memory (P11: CD27⁺IgD⁺, magenta), and switched memory (P10: CD27⁺IgD⁻, red). CD27⁺⁺CD38⁺⁺ ASCs (P8, light green) were detected but excluded from sorting due to low post-thaw frequency. Gating was informed by previously validated single-cell sorting protocols and optimised for downstream subset-specific culture.

Due to low ASC/plasmablast frequency post-thaw (0.08%), CD27⁺⁺CD38⁺⁺ ASCs were not included in the sort to prioritise memory subsets.

Sorted cells were plated in 96-well flat-bottom plates at variable densities (500-10,000 cells/well) in scBCM supplemented with R848, IL-2, and sCD40L. This design enabled testing of Ig secretion across subsets and evaluated whether higher seeding densities might suppress output due to intraclonal competition, as reported in unpublished work from OANG. Negative controls included media-only wells and unstimulated PBMC cultures.

3.4.2.2 Immunoglobulin secretion profiles: IgG and IgM

Culture supernatants were harvested on day 14 and assessed for total IgG by ELISA. Switched memory B cells showed the highest levels of IgG secretion per cell, whereas

unswitched memory, new emigrant, and mature naïve populations produced undetectable IgG across all input densities tested (Figure 24). IgG output was calculated per cell to assess whether higher cell numbers suppressed per-cell productivity, as has been observed in some B-cell culture systems. No such suppression was observed; rather, per-cell IgG levels remained stable or increased across seeding densities. No significant main effect of input cell seeding density was observed on mean total IgG output per cell (two-way ANOVA, $P = 0.2618$).

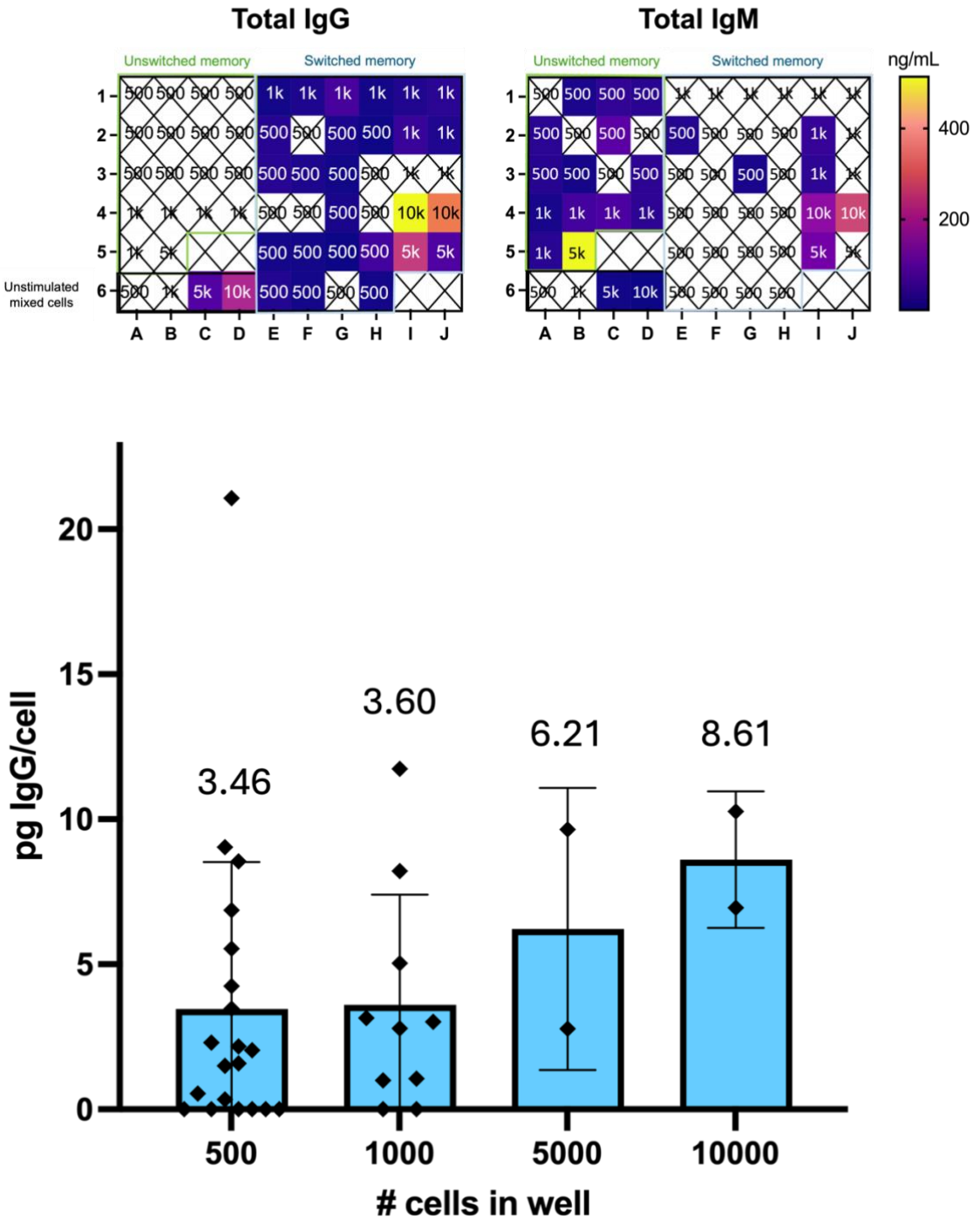

Figure 24: Immunoglobulin secretion from FACS-isolated memory B-cell subsets cultured at varying input densities. Top panel: *Heat maps showing total IgG (left) and total IgM (right) concentrations from 14-day cultures of FACS-isolated unswitched and switched memory B cells from an NF155⁺ AN patient (Bio-081). Cultures were stimulated with R848, IL-2, and sCD40L in scBCM, and seeded at input densities of 500, 1000, 5000, or 10,000 cells/well, as indicated by numbers over each well. Concentrations were derived from ELISAs performed at a 1:10 dilution. IgM and IgG were undetectable in mature naïve and new emigrant subsets (not shown). Unstimulated control wells containing unsorted PBMCs are shown bottom left of each heat map and labelled as "Unstimulated mixed cells". Wells with an "X" over them and no colour indicate wells with undetectable levels of Ig.* ***Bottom panel:*** *IgG output per cell (pg/cell) from the switched memory population, calculated by dividing total IgG per well by input*

cell number. Each point represents a single well; bars indicate mean ± SD across replicates. Mean pg/cell values are annotated above each bar. No significant effect of seeding density on IgG output per cell was observed (two-way ANOVA, P = 0.2618). 1k = 1000; 5k = 5000; 10k = 10,000.

To further probe isotype output, all wells were additionally tested for total IgM (Figure 24). No IgM was detected in the mature naïve or new emigrant populations (not shown). Among memory B-cell subsets, unswitched memory wells predominantly secreted IgM (14/18 wells; 77.77%), with no detectable IgG production; conversely, switched memory wells predominantly secreted IgG (20/34 wells IgG only [58.82%], and 6/34 wells contained both IgG and IgM [17.65%]). A minority of switched memory wells (1/34; 2.94%) produced IgM only, and 7/34 (20.59%) wells produced neither isotype. Additionally, 2/4 (50%) unstimulated wells of unsorted cells produced low levels of both IgG and IgM.

These findings highlighted a divergence in isotype secretion between switched and unswitched memory B-cell subsets *in vitro*. They suggested successful recovery of functionally switched memory cells and may reflect ongoing isotype switching or plasticity under stimulation conditions, although the possibility of mixed populations in the sorted subsets cannot be excluded, as switched memory cells were sorted as $CD27^{+}IgD^{-}$ (rather than $CD27^{+}IgG^{+}$) and unswitched memory cells as $CD27^{+}IgD^{+}$.

3.4.2.3 Lack of detectable antigen-specific antibody

Despite detectable total Ig secretion from this $NF155^{+}$ AN patient's B cells, no NF155-specific IgG or IgM was detected by ELISA (data not shown). An IgM class GM1 monoclonal antibody was used as a positive control in total IgM ELISAs, though no validated NF155-specific IgM control was available at the time.

To further probe for antigen-specific IgG, memory subset supernatants were also tested using CBA for reactivity against NF155 and NF186. No antigen-specific signal was detected in any condition (data not shown).

These results demonstrated that memory B-cell subsets from an NF155^{+} AN patient could be successfully sorted and stimulated to secrete both IgG and IgM. However, the absence of detectable antigen-specific reactivity suggested either insufficient culture conditions to induce autoreactive clone differentiation, or a frequency of pan-NF-specific precursors too low to detect in this format.

3.4.3 Enhanced cytokine testing in bulk-sorted healthy B-cell subsets

Given the absence of antigen-specific IgG in bulk-sorted patient B-cell cultures, it remained unclear whether this was due to a true lack autoreactive clones or suboptimal stimulation. To explore whether additional stimulation could enhance Ig production, a follow-up experiment was conducted using healthy donor PBMCs and an expanded cytokine cocktail.

This experiment aimed to: (1) evaluate whether stronger stimulation could enhance IgG output across all B-cell subsets; and (2) assess the capacity of each subset to secrete antigen-specific IgG due to this augmented IgG output.

3.4.3.1 Rationale for enhanced cytokine cocktail

Building on the standard R848 + IL-2 + sCD40L combination, three additional cytokines were added based on prior evidence of their roles in ASC differentiation and Ig secretion: TNFα, IL-1β, and IL-21.[92] TNFα and IL-1β are pro-inflammatory cytokines elevated in autoimmune and neuroinflammatory conditions, with known roles

in B-cell activation and plasma cell survival,[95–97] while IL-21 is a key driver of ASC differentiation and class switching.[98,99]

The resulting six-cytokine cocktail (R848 + IL-2 + sCD40L + TNFα + IL-1β + IL-21) was tested against the standard cocktail in bulk-sorted B-cell subsets from a healthy donor.

3.4.3.2 Experimental design

B cells were sorted as described in section 3.4.2.1 into mature naïve, new emigrant, unswitched memory, and switched memory subsets from healthy donor Con020. The maximum number of cells that could be sorted from each subpopulation was divided so that both the standard and enhanced cytokine cocktail conditions had at least two replicate wells within each subset. The number of cells in each well between subsets ranged from approximately 4500-8300 cells/well to balance the need for at least two replicate wells for each condition with enough cells in each well to produce detectable levels of IgG, based on the previous experiment:

- New emigrant: 5919 cells/well
- Mature naïve: 8285 cells/well
- Unswitched memory: 4558 cells/well
- Switched memory: 6416 cells/well

Each population was then cultured for 14 days in scBCM with either the standard or enhanced cytokine cocktail. Supernatants were collected at the end of 14 days and assessed for total IgG and total IgM by ELISA.

3.4.3.3 Total IgG and IgM production under enhanced stimulation

As shown in Figure 25, the addition of TNFα, IL-1β, and IL-21 markedly increased total IgG production across all B-cell subsets. While the highest IgG concentrations (>1 μg/mL) were observed in unswitched and switched memory cells, the new emigrant population also produced substantial quantities of IgG – unlike under the standard cocktail, where output was negligible.

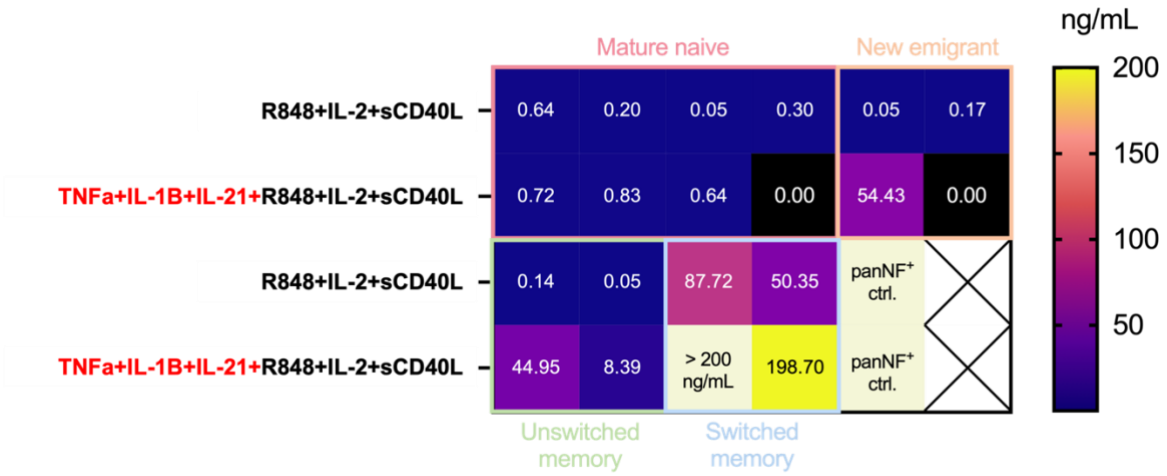

Figure 25: Impact of enhanced cytokine stimulation on total IgG production by sorted B-cell subsets from a healthy donor. *Heat map showing total IgG concentrations (ng/mL) measured by ELISA (supernatants tested at a 1:2 dilution) after 14-day cultures of FACS-isolated B-cell subsets from a healthy donor. The mature naïve subset had 8285 cells/well; new emigrant: 5919 cells/well; unswitched memory: 4558 cells/well; switched memory: 6416 cells/well. Cells were stimulated with either the standard cocktail (R848, IL-2, and sCD40L) or an enhanced cocktail (R848, IL-2, sCD40L, TNFa, IL-1β, and IL-21). Addition of TNFa, IL-1β, and IL-21 substantially increased IgG production across all subsets compared to the standard stimulation, with the greatest titres observed in memory populations but notable gains also detected in early-stage (mature naïve and new emigrant) subsets. IgG concentrations exceeding 200 ng/mL are shown in light tan and fell above the upper limit of quantification for the assay's standard curve. Serum from pan-NF⁺ patient Bio-007 was used as a positive control ("panNF⁺ ctrl.").*

IgM secretion followed a distinct pattern to IgG (Figure 26). Under the standard stimulation cocktail (R848, IL-2, and sCD40L), IgM secretion was detectable only in unswitched and switched memory B-cell subsets, with negligible output from mature naïve and new emigrant populations. Upon addition of TNFα, IL-1β, and IL-21, IgM concentrations increased markedly across all subsets. Unswitched and switched memory B cells showed the highest IgM production, with multiple wells exceeding the upper

limit of assay quantification (>1000 ng/mL). Mature naïve and new emigrant subsets also demonstrated induced IgM secretion under enhanced conditions, albeit at lower levels, on average.

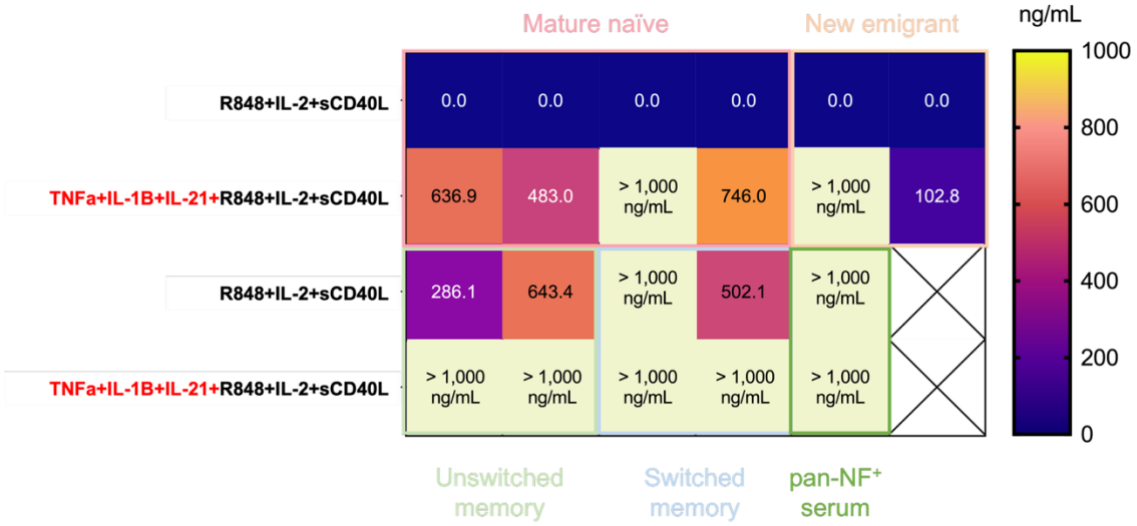

***Figure** 26: **Total IgM production by sorted B-cell subsets from a healthy donor cultured under standard versus enhanced stimulation conditions.** Heat map showing concentrations from ELISA quantification of total IgM in 14-day cultures of FACS-isolated mature naïve, new emigrant, unswitched memory, and switched memory B-cell subsets (same experiment as shown in Figure 25). Cultures were stimulated either with the standard cocktail (R848, IL-2, and sCD40L) or the enhanced cocktail (R848, IL-2, sCD40L, TNFa, IL-1β, and IL-21). Cells were bulk sorted from PBMCs of a healthy donor (Con020) and cultured in scBCM. Unstimulated PBMCs from a pan-NF+ patient (Bio-007) were included as a control ("pan-NF+ serum"). IgM concentrations exceeding 1000 ng/mL are shown in light tan and fell above the upper limit of quantification for the assay's standard curve. Enhanced stimulation increased IgM secretion across all subsets, with particularly robust responses in unswitched and switched memory B cells.*

These findings confirmed that both early-stage and memory B-cell compartments retain the capacity for IgM secretion and that cytokine-driven stimulation can significantly augment output even in populations not typically associated with high IgM production.

3.4.3.4 Implications of enhanced stimulation for antibody discovery

These results demonstrated that all tested B-cell subsets are capable of secreting immunoglobulin under appropriate stimulatory conditions in a healthy control, affirming the general responsiveness of sorted populations in this culture system. The robust IgM output from early B-cell subsets reinforced the importance of including IgM

screening in future assays, particularly when investigating autoreactive clones that may not have undergone class switching.

The results of this experiment also had important implications for patient experiments, suggesting the absence of antigen-specific IgG in patient cultures was unlikely to stem from limitations in culture protocol alone. While memory compartments in healthy donors reliably produced IgG, earlier populations only did so with the addition of IL-21 and inflammatory cytokines. This raised the possibility that patient-derived B cells – particularly those that are antigen-experienced but dysfunctional – may require tailored cytokine support to unmask autoreactivity.

Finally, the divergence in IgG and IgM production across subsets highlighted a methodological consideration for discovery workflows: reliance on IgG detection alone may miss relevant autoreactive clones, particularly those that are IgM^+ or fail to class switch *in vitro*. Parallel IgG and IgM screening would therefore be essential for comprehensive detection.

3.5 Discussion and limitations

This chapter described the systematic development of an *in vitro* stimulation system for human PBMCs, aimed at supporting antibody production for downstream detection of pan-NF^+ autoantibodies. The finalised culture protocol – comprising R848, IL-2, and sCD40L in scBCM over 14 days – was reproducible and robust across multiple healthy donors and some patient samples. However, despite reliable IgG secretion, antigen-specific responses to NF155 or NF186 remained elusive. The following sections interpret key findings from the optimisation pipeline and highlight remaining challenges and considerations for future refinement.

3.5.1 Extending culture duration

A critical turning point in the development of the *in vitro* stimulation protocol was the decision to extend the culture duration to 14 days. Initial experiments revealed that although ASC generation peaked around day 6, total IgG concentrations continued to rise thereafter, consistent with continued secretion by short-lived plasmablasts and transitional plasma cells. This observation aligned with prior studies in autoimmune encephalitis, where ASC frequencies declined after day 7 despite ongoing IgG accumulation in culture supernatants.[91]

In this context, prolonging the culture period allowed for a linear or near-linear accumulation of IgG, reaching titres in the low μg/mL range by day 14 – a critical threshold for downstream detection of low-frequency antigen-specific antibodies. Given that autoreactive clones often comprise a minority of the total B-cell repertoire, the increased assay sensitivity afforded by longer culture durations was essential for the objectives of this study.

Although the most rigorous approach would have involved a head-to-head comparison of 5-, 6-, and 14-day cultures both with and without sCD40L, this was precluded by sample limitations. Instead, comparisons were made between 6- and 14-day cultures, which demonstrated a clear and statistically significant increase in total IgG over time. Notably, this accumulation occurred irrespective of further increases or decreases in ASC frequency, reinforcing the importance of extended survival and sustained secretory function rather than additional differentiation.

The inclusion of sCD40L in the stimulation cocktail was hypothesised to support the persistence of ASCs during this extended culture period. Although sCD40L alone did

not significantly enhance IgG production in shorter cultures, its retention was justified by its compatibility with established ASC-supportive conditions and its anticipated role in downstream single-cell culture workflows. Together, these refinements enabled a more consistent and reproducible detection of secreted immunoglobulin and formed the basis for all subsequent patient and sorting experiments.

3.5.2 Cytokine synergy

An additional avenue explored during protocol development was the potential for cytokine synergy to augment ASC differentiation and immunoglobulin secretion. Several cytokines – including TNFα, IFNγ, IL-1β, and IL-21 – have been implicated in promoting B-cell activation, class-switch recombination (CSR), and plasma cell survival, particularly in inflammatory and autoimmune contexts such as CIDP and systemic lupus erythematosus (SLE).[93,94] Their inclusion was therefore hypothesised to potentiate IgG production when added to the core stimulation cocktail of R848, IL-2, and sCD40L.

Initial experiments focused on TNFα and IFNγ, two pro-inflammatory cytokines that are elevated in serum and CSF in subsets of patients with inflammatory neuropathies.[93,94] Previous studies had suggested that TNFα may enhance antigen-specific IgG production in PBMC cultures from patients with NMOSD, particularly when combined with CD40L signalling.[92] However, in the present work, the addition of TNFα or IFNγ, individually or in combination, in both 6- and 14-day PBMC cultures, did not produce a consistent increase in total IgG production beyond that achieved with the core cocktail alone. These findings were consistent across donors and time points,

and statistical analyses revealed no significant interaction effects (two-way ANOVA, $p > 0.9999$).

While these results argued against a synergistic role for TNFα or IFNγ in the bulk PBMC system, this did not exclude the possibility that these cytokines may exert subset-specific effects, particularly in contexts of immunosenescence, pre-existing immune activation, or chronic inflammation. Importantly, their omission from the final stimulation protocol allowed for a leaner and more standardised culture system, which improved reproducibility across healthy and patient-derived samples. However, moving to a bulk sorted format would be anticipated to remove the paracrine effects and interactions between different cell types likely to be present in the unsorted cultures.

As such, subsequent experiments involved additional cytokines, including IL-21 and IL-1β, tested in a bulk-sorted context (section 3.4.3), where their inclusion produced clear enhancements in both IgG and IgM secretion from early-stage and memory B-cell subsets. These findings support the notion that cytokine responsiveness is highly context-dependent, varying by both cell subset and culture configuration. In particular, the absence of effect observed in bulk unsorted cultures may reflect endogenous cytokine production by non-B cells (eg, monocytes or T cells), which could saturate relevant signalling pathways and obscure the impact of exogenous cytokine supplementation. Accordingly, future iterations of this culture system may benefit from tailored cytokine supplementation based on donor characteristics or specific experimental goals, particularly in the setting of rare or functionally impaired autoreactive clones.

3.5.3 Donor-to-donor variability in IgG production and technical considerations

Across the healthy donor optimisation experiments, substantial donor-to-donor variability in total IgG production was observed, even under standardised stimulation conditions. PBMCs from six different healthy individuals were stimulated with the core R848 + IL-2 + sCD40L cocktail and cultured at a uniform seeding density of $2x10^5$ cells/well. As shown in Figure 27, IgG secretion varied considerably between donors, particularly by day 14.

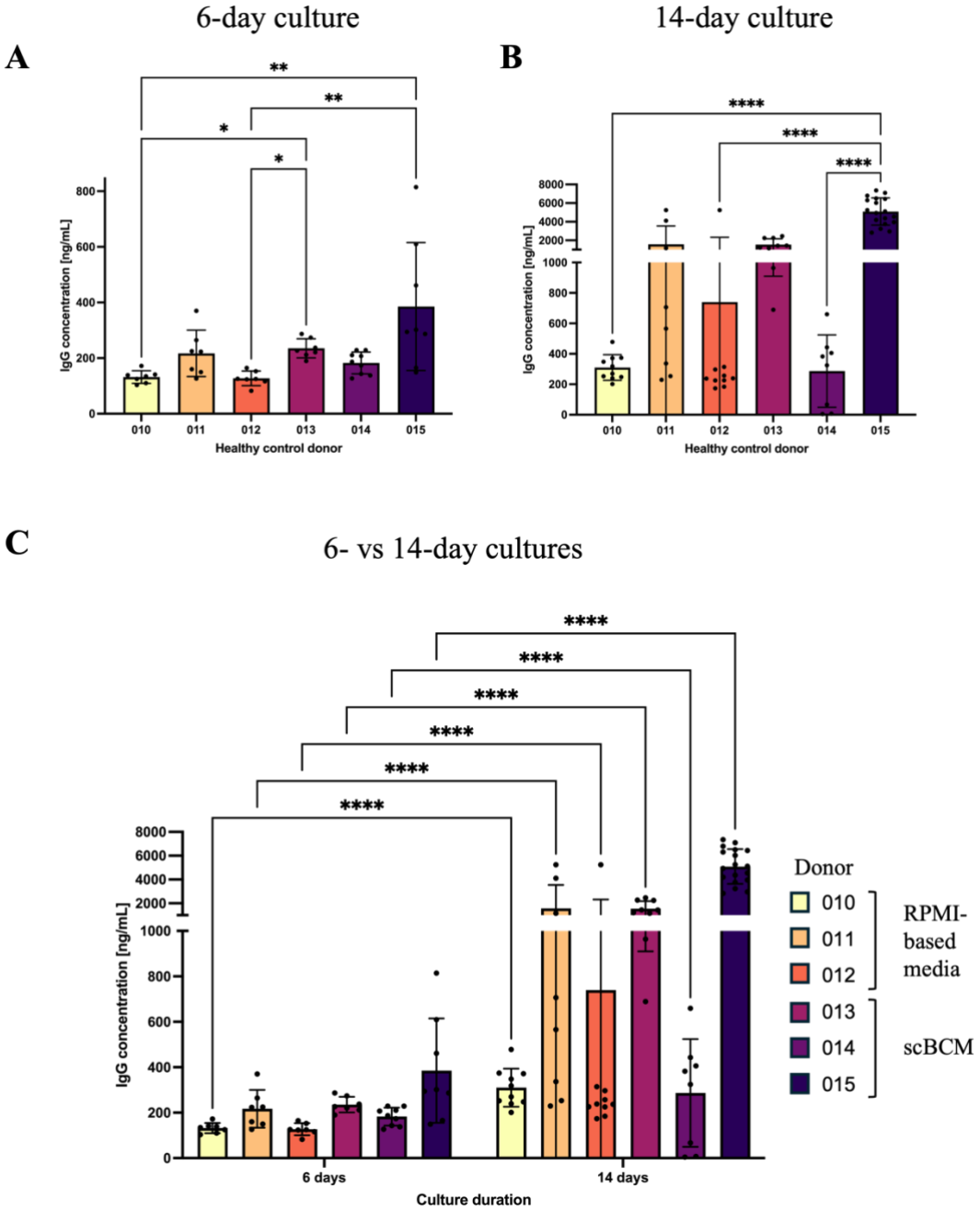

Figure 27: Donor-to-donor variability in total IgG production from stimulated PBMC cultures. *PBMCs from six healthy donors were stimulated with R848, IL-2, and sCD40L and cultured at $2x10^5$ cells/well under otherwise standard conditions. Donors Con010-012 (left bars) were cultured in RPMI 1640, while donors Con013-015 (right bars) were cultured in single-cell B-cell media (scBCM).* ***(A)*** *Total IgG titres at day 6 across donors.* ***(B)*** *Total IgG titres at day 14 across donors.* ***(C)*** *Paired comparison of IgG titres for each donor at day 6 and day 14. Each bar represents an individual donor. Individual points represent technical replicates within each donor. Bars represent the mean ± SD of technical replicates for each donor. Statistical testing (Kruskal-Wallis ANOVA) revealed significant inter-donor differences in IgG output at both time points (day 6: $0.0010<p<0.0268$; day 14: $p<0.0001$), and a consistent increase in IgG secretion with extended culture. These results highlight inter-individual variability in B-cell responsiveness and underscore the importance of biological replicates in culture optimisation studies.*

At day 6, total IgG concentrations remained uniformly low across all samples (<200 ng/mL), and although statistical differences were detectable between some donors (Kruskal-Wallis ANOVA, $0.0010 < p < 0.0268$), the magnitude of variation was modest. By day 14, however, these differences became more pronounced: some donors secreted <500 ng/mL, while others exceeded 3 µg/mL. All donors exhibited a significant increase in IgG production with prolonged culture (Kruskal-Wallis ANOVA, $p < 0.0001$), yet the absolute concentrations and response kinetics diverged considerably between individuals (Figure 27B).

Importantly, these results must be interpreted in light of a technical caveat: the day 6 and day 14 comparisons across the six donors combined PBMCs cultured in two different media formulations. Donors Con010-012 were cultured in RPMI 1640, whereas Con013-015 were cultured in the scBCM. Although stimulation conditions were otherwise identical, the potential for subtle media-related effects cannot be excluded.

Such heterogeneity is consistent with previous reports in PBMC cultures from individuals with neuroimmune diseases and may reflect intrinsic differences in B-cell subset composition, immune history, or activation thresholds.[100,101] While all donors ultimately produced detectable IgG, the marked inter-individual differences in titre underscore the necessity of including biological replicates in optimisation studies and interpreting pooled data with appropriate caution.

This variability also had important implications for patient experiments. In particular, it cautioned against over-interpreting apparent differences in IgG output between patient and control PBMCs without accounting for the extent of inter-individual spread.

Notably, the pan-NF^{+} AN patient failed to mount a strong IgG response under conditions that elicited robust secretion in both healthy controls and the NF155^{+} patient (Figure 16). These findings raised the possibility that individual differences in B-cell responsiveness, rather than intrinsic protocol insufficiencies, may underlie some observed failures to detect antigen-specific IgG, and emphasised the need for strategies that can enrich for low-frequency autoreactive clones within a heterogeneous background. In parallel, the observation of well-to-well variation in IgG titres within donors highlighted the necessity of including internal technical controls in all culture assays. Unstimulated and media-only wells, along with replicate conditions, were essential not only for distinguishing biological signal from assay artefact, but also for ensuring interpretive confidence in cases of marginal or null antigen-specific responses.

3.5.4 Switch to scBCM

A further refinement to the culture protocol involved transitioning from standard RPMI 1640 to a modified scBCM, previously developed for low-frequency antigen-specific IgG detection in CNS autoantibody workflows (unpublished data). This formulation contains tailored nutrients, growth factors, and supplements that support plasmablast survival and Ig secretion, especially when clonal expansion is limited.

Although a formal head-to-head comparison between RPMI- and scBCM-cultured PBMCs was not possible, since RPMI cultures used donors Con010-12 and scBCM used Con013-015, the scBCM cultures yielded robust total IgG levels, as illustrated in Figure 15. Variation in donor response notwithstanding, scBCM did not impair IgG output and in two of three donors produced notably higher concentration than observed with RPMI.

The decision to adopt scBCM across all subsequent bulk and single-cell B-cell culture was therefore supported by: (1) evidence of efficacy in CNS autoreactive B-cell workflows where rare ASC recovery is critical;[91] (2) design compatibility with downstream workflows, maximising assay consistency; and (3) demonstrated performance, with no reduction – and in some cases, enhancement – in total IgG secretion.

Thus, even in the absence of a direct statistical comparison, the adoption of scBCM aligned with methodological precedent and supported the experimental objective of enhancing antigen-specific IgG detection without compromising overall yield.

3.5.5 ASC generation as a prerequisite for antigen-specific IgG

The generation of $CD19^{+}CD27^{++}CD38^{++}$ ASCs was a critical functional readout for culture productivity and served as a proxy for B-cell differentiation under *in vitro* stimulation. Across multiple healthy donor PBMC cultures, ASC frequencies consistently peaked around day 6 and declined thereafter, while total IgG levels continued to rise through day 14 (Figure 18). This temporal dissociation between peak ASC frequency and IgG accumulation highlighted a key kinetic feature of the assay system: even as ASC numbers waned, previously differentiated plasmablasts and transitional plasma cells continued to secrete immunoglobulin. This was further supported by an increase in ASC levels after 6 days of culture with stimulation versus unstimulated conditions. Overall, these findings supported both the mechanistic plausibility of the culture protocol and the rationale for extended culture duration to capture cumulative IgG output.

Quantitative analysis confirmed a moderate-to-strong correlation between ASC frequency and IgG titre at day 6 ($r = 0.72$), and a persistent, albeit attenuated, association at day 14 ($r = 0.59$). While this trend was expected, it nevertheless provided important validation that $CD27^{++}CD38^{++}$ ASC emergence is a biologically meaningful marker of culture responsiveness. The continued accumulation of IgG beyond day 6, despite a decline in ASC frequencies, suggests that much of the antibody production during the latter half of the culture period likely originated from B cells that had already undergone differentiation by day 6. However, as no intermediate timepoints were analysed between days 6 and 14, the possibility cannot be excluded that additional differentiation events occurred during this interval. Nonetheless, the data remain consistent with early differentiation, rather than sustained generation of new ASCs, as the principal driver of IgG secretion at later timepoints.

In the $NF155^{+}$ AN patient sample, ASCs were detected by flow cytometry but were of insufficient abundance to warrant preparative sorting. This observation reinforced the view that while ASC generation can be achieved in some patient samples, the frequency of these cells post-thaw may be prohibitively low, either due to disease-related intrinsic B-cell dysfunction or technical limitations in sample viability and recovery. By contrast, no ASC profiling was performed with pan-NF^{+} AN patient PBMCs at this juncture due to cell constraints and prioritisation of culture-based antigen-specific assays.

Together, these data emphasised the importance of ASC differentiation as a prerequisite for successful antibody secretion *in vitro*. They also underscored the potential value of incorporating ASC detection into routine quality control for PBMC-based assays, particularly in settings where antigen-specific readouts are negative. In such cases, the

absence of antigen-specific Ig may reflect a technical failure of stimulation, rather than true biological absence of autoreactive clones. Conversely, no detectable antigen-specific IgG despite the presence and differentiation of ASCs with cytokine stimulation would argue for low precursor frequency, the need for more specific stimuli to differentiate autoreactive clones into Ig-producing ASCs, or even loss of autoreactive clones entirely during culture, thus informing the selection of more targeted enrichment strategies in future work.

3.5.6 Isotype heterogeneity in bulk sorted memory B-cell cultures

In addition to assessing total IgG output, all culture supernatants from memory B-cell subset wells were evaluated for IgM secretion to probe for evidence of isotype heterogeneity and potential CSR *in vitro*. IgG secretion was restricted to the switched memory subset, while IgM was produced predominantly by unswitched memory B cells. However, several switched memory wells also secreted both IgG and IgM, and a minority secreted IgM alone. No IgG production was detected from unswitched memory wells.

This clear segregation of isotype output broadly aligned with phenotypic expectations based on surface IgD and CD27 expression. However, the presence of a small number of wells co-secreting IgG and IgM within the switched memory gate raised interpretive considerations. These may reflect ongoing CSR *in vitro*, re-expression of IgM in class-switched cells under TLR and CD40L stimulation, or minor misclassification during gating. The possibility of rare double-positive or transitional memory states cannot be excluded, particularly in the context of B-cell plasticity.

Notably, total IgM and IgG output per well generally increased with higher input cell number, but within-well comparisons revealed that high IgM did not predict high IgG levels, and vice versa. This suggests that isotype secretion was regulated independently in many wells, and that antibody output was likely dominated by clonal contributions rather than bulk population effects.

These findings underscore the need for future multiplex isotype screening across B-cell subsets and input densities and support the integration of paired phenotypic and molecular characterisation (eg, intracellular staining, RNA-seq) to definitively resolve clonal relationships between IgM- and IgG-secreting cells within memory subsets.

3.5.7 Implications for detecting rare autoreactive clones

One of the key challenges encountered throughout this work was the absence of detectable antigen-specific IgG against NF155 or NF186 in bulk, unsorted PBMC cultures from patients with pan-NF^+ and $NF155^+$ AN. While robust total IgG secretion was achieved in several donors, including both healthy controls and the $NF155^+$ patient, no supernatants yielded neurofascin-reactive signal on CBA or ELISA. These findings prompted a careful reassessment of the likely abundance and detectability of autoreactive clones under the employed culture conditions.

A central explanation considered was the low precursor frequency of NF155-/NF186-specific B cells within the unfractionated PBMC pool. As has been shown in other autoimmune contexts – including NMDAR antibody encephalitis and SLE – autoreactive B cells may circulate at very low frequencies, often <1 in 10^4 to 10^5 total B cells.[102–105] Given that the culture system used a maximum of $2x10^5$ PBMCs per well, and only a fraction of those are $CD19^+$ B cells, the effective sampling of the

autoreactive repertoire in bulk cultures was likely insufficient to reliably capture pan-NF-specific clones in retrospect.

Moreover, even when present, autoreactive B cells may exhibit impaired differentiation into ASCs due to intrinsic functional defects or regulatory constraints.[106–108] In the NF155^{+} patient sample, for instance, flow cytometry confirmed ASC generation, but no NF155-specific IgG was detected in culture supernatants. This dissociation could reflect a failure of autoreactive cells to respond to polyclonal stimulation and differentiate into ASCs in culture. In the pan-NF^{+} patient, by contrast, total IgG output was lower and ASC profiling was not performed, raising the possibility that global B-cell dysfunction or low cell viability further compounded detection challenges.

These findings highlighted a fundamental limitation of bulk PBMC culture for rare antigen-specific B-cell detection: the technique is reliant not only on sufficient precursor frequency, but also on functional responsiveness and survival over the 14-day stimulation period. In such a context, the absence of signal cannot be interpreted as definitive evidence of clonal absence.

Accordingly, these results strongly supported the implementation of enrichment strategies to improve the probability of detecting rare autoreactive clones. Targeted approaches such as preparative sorting of memory or ASC-enriched subsets, antigen baiting, and/or single-cell culture formats that allow clonal expansion and tracking were likely to be more effective. These methods also enable the interrogation of individual cell outputs and pairing with sequencing pipelines, which are essential for downstream mAb generation.

Thus, while the optimised PBMC culture system proved robust for inducing total IgG secretion and ASC differentiation, it was hypothesised that its capacity to elicit NF155- and NF186-specific antibodies was ultimately limited by the rarity of the target clones. Future efforts to identify and characterise these pathogenic antibodies would therefore prioritise strategies that enrich for rare specificities and accommodate the biological heterogeneity observed in patient samples.

3.5.8 Methodological limitations

While the finalised PBMC stimulation protocol yielded reproducible induction of total IgG across multiple healthy donors and selected patient samples, several limitations emerged during its development and application that constrain interpretation and guided future optimisation.

A primary limitation was the sensitivity of the antigen-specific detection assays employed. Both ELISA and CBA were initially optimised for serum-based readouts and may lack the analytical sensitivity required to detect low-abundance IgG in *in vitro* culture supernatants. In several instances, supernatant concentrations fell within or just above the lower limit of quantification, raising the possibility that antigen-specific reactivity could have been present but undetectable. This was particularly relevant in bulk cultures where total IgG levels, although measurable, remained modest compared to serum-derived values.

A second constraint was the narrow scope of cytokine combinations trialled in most experiments. While the core cocktail of R848, IL-2, and sCD40L supported robust ASC differentiation and IgG secretion in healthy donor PBMCs, it may not have been sufficient to fully activate autoreactive or functionally impaired B-cell subsets in patient

material. Additional cytokines with known roles in B-cell activation – including IL-21, TNFα, and IL-1β – were tested only in a limited subset of sorted B-cell experiments from a healthy donor, precluding broader conclusions about their utility across donor types. Moreover, mCD40L co-culture or direct B-cell receptor (BCR) stimulation, which may more closely approximate physiological activation, were not assessed within this chapter's experiments.

Sample availability was also a key limitation. Several optimisation experiments could not be performed using matched donor material due to the exhaustion of PBMC stocks, limiting the ability to perform rigorous head-to-head comparisons across variables such as media formulation or culture duration. This affected, for example, the evaluation of scBCM versus RPMI 1640, where different healthy donors were used. Although the results suggested equivalent performance, the confounding influence of donor-to-donor variability could not be fully excluded.

Another interpretive consideration arose in the analysis of isotype secretion across sorted memory B-cell cultures. Although IgG was the primary focus, IgM was also assessed in all subpopulations. IgG was restricted to the switched memory subset, while IgM was produced primarily by unswitched memory B cells, although a proportion of switched memory wells also secreted IgM, either alone or alongside IgG. A small number of switched memory wells secreted both isotypes. This result may reflect true heterogeneity within the switched gate, including ongoing or incomplete class switching, or alternatively, gating imprecision, plasticity, or limitations in surface marker resolution. The observed distribution of isotype secretion (Figure 24) highlights the functional complexity of memory B-cell populations *in vitro*. Refinements such as

intracellular Ig staining or single-cell sequencing may help resolve ambiguous populations in future work.

The lack of antigen-specific IgM screening via CBA in addition to ELISA in these early bulk sorting experiments was another limitation. In bulk-sorted cultures from the $NF155^+$ AN patient, supernatants were assessed for total IgG, total IgM, NF155-specific IgG, and NF155-specific IgM via ELISA. However, no NF155-specific Ig of either isotype was detected. While supernatants were subsequently tested for antigen-specific IgG binding by CBA as well, antigen-specific IgM was not evaluated in this way. In retrospect, this omission may have missed relevant neurofascin-reactive clones secreting IgM rather than IgG, particularly given the later identification of neurofascin-specific IgM in single-cell culture experiments (Chapter 4). At the time, the decision not to perform antigen-specific IgM testing via CBA was primarily driven by the limited supernatant volumes and prioritisation of IgG-based assays, which are conventionally considered the predominant pathogenic isotype across AN.[2,3,57,80] Future experiments would benefit from systematic screening for antigen-specific IgM alongside IgG by CBA, especially in contexts where class switching may be incomplete or atypical.

Lastly, the use of cryopreserved rather than fresh PBMCs throughout all experiments may have introduced artefactual variability. Post-thaw viability was acceptable in most cases, but subtle effects on B-cell function, particularly in fragile or antigen-experienced subsets, could not be ruled out. The absence of detectable ASCs in some patient samples may therefore reflect not only biological differences, but also the impact of cryopreservation on subset recovery and activation potential.

These limitations do not undermine the validity of the established stimulation system but highlight key areas for methodological refinement. Incorporating more sensitive detection platforms, expanding cytokine screening in patient-derived samples, and ensuring better-matched experimental controls will strengthen the interpretability of future culture-based studies.

3.6 Summary and future directions

3.6.1 Finalised bulk unsorted culture protocol and key outcomes

The optimisation pipeline described in this chapter culminated in the development of a reproducible PBMC stimulation protocol capable of inducing robust total IgG secretion across both healthy control and patient-derived samples. Through iterative experimentation, a series of critical parameters were identified that shaped the finalised protocol. The key experimental factors assessed at each stage of this process and the main findings are summarised in Figure 28 below.

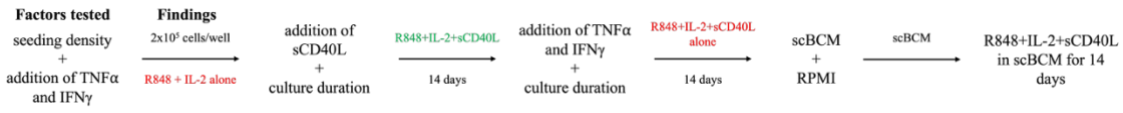

Figure 28: Summary of factors tested and the main findings at each stage of the iterative PBMC bulk unsorted culture refinement process. *R848: Resiquimod; scBCM: single-cell B-cell media.*

A key outcome was the establishment of a strong, dose-dependent relationship between PBMC seeding density and total IgG output. Increasing the number of input cells per well yielded proportionate increases in IgG concentration, highlighting the importance of adequate precursor availability for culture responsiveness. A seeding density of $2x10^5$ B cells per well emerged as the optimal condition, balancing assay sensitivity with practical constraints on cell availability.

Extension of culture duration to 14 days was another pivotal refinement. While ASC frequencies peaked at day 6, total IgG titres continued to accumulate through day 14, underscoring the sustained secretory activity of differentiated B cells. This finding supported the inclusion of longer time points in downstream assays aimed at detecting low-frequency antigen-specific clones, which may otherwise have fallen below detection thresholds in shorter cultures.

Concerning stimulatory conditions, the combination of R848, IL-2, and sCD40L consistently supported ASC generation and IgG production across multiple donors. While the inclusion of sCD40L did not produce a statistically significant enhancement in total IgG titres relative to R848 and IL-2 alone, it was retained due to its compatibility with plasma cell-supportive pathways and downstream single-cell cultures. By contrast, the addition of pro-inflammatory cytokines TNFα and IFNγ provided no consistent benefit in unsorted cultures, and their exclusion improved assay simplicity and reproducibility.

The finalised protocol in bulk unsorted cultures therefore comprised:

- **Cell input**: $2x10^5$ PBMCs/well
- **Culture medium**: RPMI-based scBCM
- **Stimulation cocktail**: R848 (2.5 μg/mL), IL-2 (50 ng/mL), sCD40L (50 ng/mL)
- **Culture duration**: 14 days

Under these conditions, μg/mL levels of total IgG were reliably achieved, and $CD27^{++}CD38^{++}$ ASC differentiation was confirmed by flow cytometry.

3.6.2 Pivot to cell sorting strategies as a stepping stone toward single-cell analysis

Despite the successful induction of total IgG secretion in bulk PBMC cultures, the absence of detectable antigen-specific IgG to NF155 or NF186 prompted a strategic pivot toward FACS. The goal of this shift was to enhance the resolution and sensitivity of the antibody detection pipeline, enabling isolation of autoreactive B-cell subsets that may have been diluted or functionally suppressed in unfractionated cultures and begin to narrow down which B-cell subset(s) may harbour autoreactivity against neurofascin.

A dedicated multicolour flow cytometry panel was developed and validated to permit high-resolution sorting of key B-cell subsets, including mature naïve, new emigrant, unswitched memory, switched memory, and ASC populations. Panel optimisation included titration of all fluorophore-conjugated antibodies and refinement of gating strategies to maximise separation of phenotypically distinct populations while ensuring compatibility with downstream functional culture.

Bulk-sorting experiments were initially conducted on sorted PBMCs from an $NF155^{+}$ AN patient under optimised stimulation conditions (R848, IL-2, and sCD40L in scBCM) for 14 days. IgG secretion was confined to switched memory B cells, while IgM production was predominantly observed in unswitched memory B cells, although switched memory wells also secreted IgM in a subset of cases. A proportion of switched memory wells secreted both isotypes, highlighting functional heterogeneity within phenotypically switched subsets. However, no antigen-specific reactivity to NF155 was detected, suggesting that further stimulation or enrichment was required.

To address this, an enhanced cytokine cocktail was explored in a subsequent healthy donor sort culture. Supplementation with TNFα, IL-1β, and IL-21 led to marked

increases in total IgG production across all B-cell subsets and induced IgG and IgM secretion even from early-stage cells that had previously been non-productive. These results demonstrated that cytokine responsiveness was highly context-dependent and reinforced the need to tailor stimulation conditions to both cell type and disease context.

Collectively, these findings laid the groundwork for more refined strategies such as single-cell sorting and mAb production, establishing a functional bridge between B-cell phenotyping and downstream antibody characterisation.

3.6.3 Moving toward identification and characterisation of individual autoreactive B cells

The culmination of the PBMC culture optimisation and subset-sorting experiments made clear that bulk approaches, while informative for optimising total IgG output, were unlikely to resolve the central challenge of identifying rare antigen-specific B-cell clones. Despite robust total IgG secretion from both healthy donor and some patient cultures, and confirmed ASC generation under stimulation, attempts to recover neurofascin-specific antibodies from bulk conditions remained unsuccessful. This highlighted the need for higher-resolution methods capable of isolating individual autoreactive B cells for downstream interrogation.

Single-cell sorting was therefore adopted as the next strategic pivot. By enabling the culture and analysis of individual B cells in isolation, this approach provided a means to directly assess clonal specificity for sequencing, functional characterisation, and downstream mAb development. Crucially, it also offered the potential to disentangle biological variability in B-cell responsiveness from technical limitations in culture conditions or detection sensitivity.

To contextualise and evaluate this next phase, a head-to-head comparison was designed between two patient samples: one with pan-NF^+ antibodies and one with a well-characterised $CASPR2^+$ response previously shown to yield antigen-specific IgG in culture. This comparison would serve not only to benchmark the performance of the optimised assay pipeline but also to clarify whether the absence of pan-NF reactivity reflected a true biological feature or a limitation of prior methodologies.

The following chapter details the execution and findings of this experiment, marking a key transition from culture system development to the targeted identification of autoreactive clones.

4 Single-Cell Sorting and Sequencing to Isolate Rare Pan-Neurofascin-Reactive Clones

4.1 Introduction

The successful optimisation of *in vitro* stimulation protocols and implementation of bulk B-cell sorting strategies laid the groundwork for transitioning to single-cell resolution approaches. While reproducible induction of total immunoglobulin G (IgG) secretion was achieved across B-cell subsets in healthy donor peripheral blood mononuclear cell (PBMC) cultures, consistent detection of antigen-specific IgG in patient-derived cultures remained elusive. This suggested that autoreactive clones may be present at low frequencies, necessitating higher-resolution methods for their detection and isolation.

Single-cell sorting offers key advantages over bulk methods. It enables the direct interrogation of individual B cells, allowing recovery of clonally distinct antibody sequences and the functional screening of monoclonal specificities without confounding from intraclonal competition or polyclonal dilution. Furthermore, it permits direct comparison between disease samples, distinguishing technical failure from true biological absence of autoreactivity. Given that a central aim of this project was to generate and functionally characterise recombinant monoclonal antibodies (mAbs) from single-cell sequences, single-cell workflows were adopted to enable this outcome.

Due to the substantial resource demands of single-cell approaches, early experimental efforts focused on refining the bulk culture system to confirm its suitability for detecting antigen-specific responses prior to scaling up. Despite optimised conditions, recovery of

antigen-specific IgG could not be achieved in bulk patient cultures, prompting the initiation of single-cell experiments. As an additional measure to validate system sensitivity, cytokines known to enhance B-cell activation (TNFα, IL-1β, IL-21) were incorporated into healthy donor cultures, resulting in significantly increased IgG secretion.

Accordingly, bulk unsorted, bulk sorted, and single-cell sorted cultures were established in parallel from a pan-neurofascin-positive (pan-NF$^+$) patient and a CASPR2-positive (CASPR2$^+$) comparator with previously validated antigen-specific responses using the same culture protocol. This design allowed benchmarking across responder and non-responder contexts to distinguish technical from biological explanations for the lack of antigen-specific Ig in pan-NF/neurofascin-155 (NF155) autoimmune nodopathy (AN) patient cultures. The following sections present the results of these experiments, culminating in the identification and characterisation of autoreactive B-cell clones in pan-NF AN.

4.2 Experimental overview

To directly compare antibody production outcomes between responder and non-responder states, parallel culture experiments were established using PBMCs from two patients: one with pan-NF AN (Bio-099) and one with confirmed CASPR2$^+$ reactivity (JR624794). For each patient, three culture formats were performed in parallel: one bulk unsorted, one bulk sorted, and one single-cell sorted culture. This comprehensive approach enabled validation of the culture protocol as well as broad profiling and high-resolution interrogation of B-cell responses and single autoreactive B-cell clones.

For bulk unsorted cultures, 30 replicate wells of PBMCs from each patient were cultured for 14 days in single-cell B-cell medium (scBCM) supplemented with an enhanced cytokine combination comprising Resiquimod (R848), interleukin (IL)-2, soluble CD40L (sCD40L), tumour necrosis factor-alpha (TNFα), IL-1β, and IL-21. Bulk-sorted cultures were established using four canonical B-cell subpopulations: new emigrant, mature naïve, unswitched memory, and switched memory cells. Subsets were sorted by fluorescence-activated cell sorting (FACS) and plated at 5000 cells/well in scBCM under identical cytokine conditions. This seeding density represented an experimentally defined balance between optimising total IgG production and maintaining sufficient replicate numbers to account for intra-subset variability (Chapter 3).

From the pan-NF^+ patient, a total of 165,428 B cells were sorted and distributed as follows: mature naïve (n=53,673; 10 wells plated), new emigrant (n=44,630; 8 wells), unswitched memory (n=27,437; 5 wells), and switched memory (n=39,688; 7 wells). Sorting of the $CASPR2^+$ patient cells yielded: mature naïve (n=138,923; 3 wells plated), new emigrant (n=13,056; 2 wells), unswitched memory (n=13,779; 2 wells), and switched memory (n=35,056; 4 wells). The ultimate number of CASPR2 patient cells plated was lower due to sample limitations.[1] All conditions were tested in a single experimental run.

To provide immunophenotypic context, relative frequencies of B-cell subpopulations were assessed from this experiment and two prior bulk-sort experiments, representing

[1] A different experiment (not conducted by the author) was intended to utilise these cells, and the single-cell sort was a priority within this experiment; thus, only a minimal number of wells were plated for bulk cultures.

one NF155^{+} patient (Bio-081), one pan-NF^{+} patient (Bio-099), one CASPR2^{+} patient (JR624794), and one healthy control (Con-017). Figure 29 shows subpopulation frequencies based on the proportion of total CD19^{+} B cells sorted.

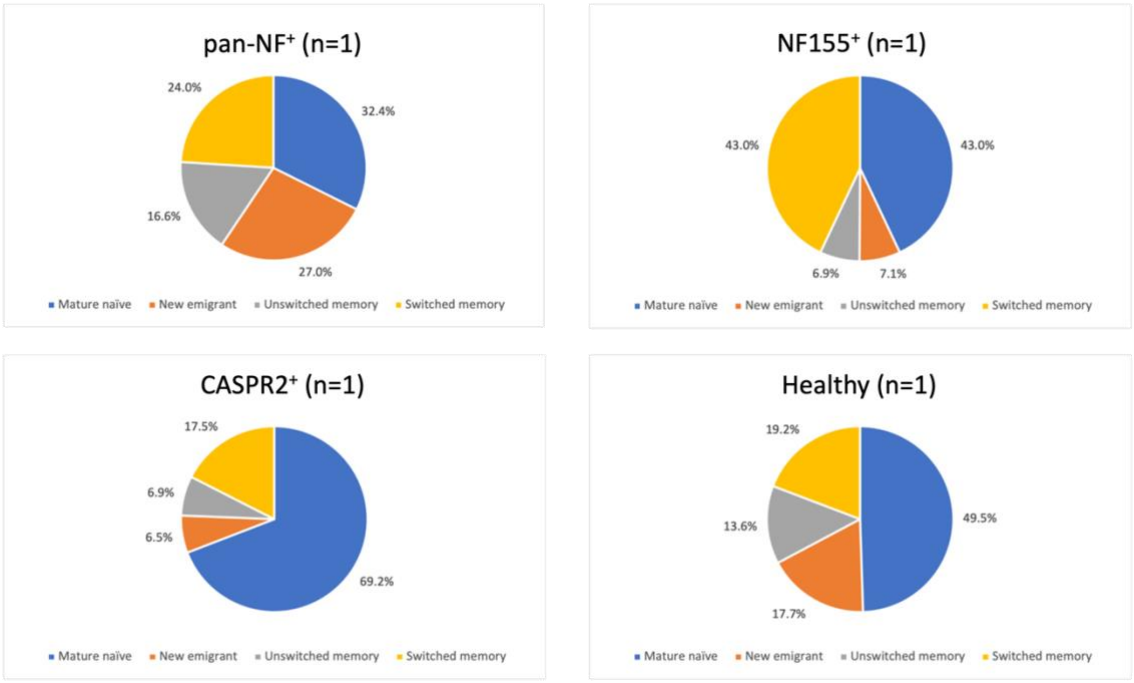

Figure 29: Relative frequencies of canonical B-cell subpopulations among CD19^{+} B cells sorted from peripheral blood of individual donors. *Pie charts show the proportion of mature naïve, new emigrant, unswitched memory, and switched memory B-cell subsets within the total CD19^{+} B-cell compartment of each patient, as determined by FACS. Data are presented for one representative donor per group: pan-NF^{+} (Bio-099), NF155^{+} (Bio-081), CASPR2^{+} (JR624794), and healthy control (Con-017). Percentages reflect [subpopulation cell count] ÷ [total CD19^{+} cells sorted per donor].*

For single-cell cultures, five 96-well plates (480 wells) were seeded per patient. Each well contained a single CD27^{+}IgD^{-} memory B cell (defined as “switched” memory), deposited onto a feeder layer of 1000 irradiated MS40L cells expressing membrane-bound CD40L (mCD40L). Cultures were maintained in scBCM with B-cell activating factor (BAFF), IL-2, IL-4, and IL-21 for 25 days, and supernatants were harvested at days 14 and day 25 for downstream analysis of total and antigen-specific Ig secretion.

This design enabled systematic evaluation of total and antigen-specific Ig production across multiple formats, providing both a technical benchmark for culture responsiveness and a framework for recovering rare autoreactive clones.

4.3 Antibody production in bulk cultures

4.3.1 Bulk unsorted cultures

4.3.1.1 Total IgG production

To evaluate the performance of the enhanced stimulation protocol, bulk cultures of unsorted PBMCs from the pan-NF^{+} and CASPR2^{+} patients were established in parallel first. These cultures served as a baseline reference for downstream comparison with bulk sorted and single-cell culture formats.

Total IgG was detectable in the majority of culture supernatants, though concentrations remained low overall (Figure 30). Median concentrations in both donors were below 50 ng/mL, with no statistically significant difference observed between groups (unpaired t-test, P = 0.7260). While CASPR2^{+} wells showed slightly higher average levels of IgG, the difference was not marked. Post-hoc review of the ELISA standard curve indicated that many samples fell near or below the lower limit of quantification, limiting precision in absolute measurements.

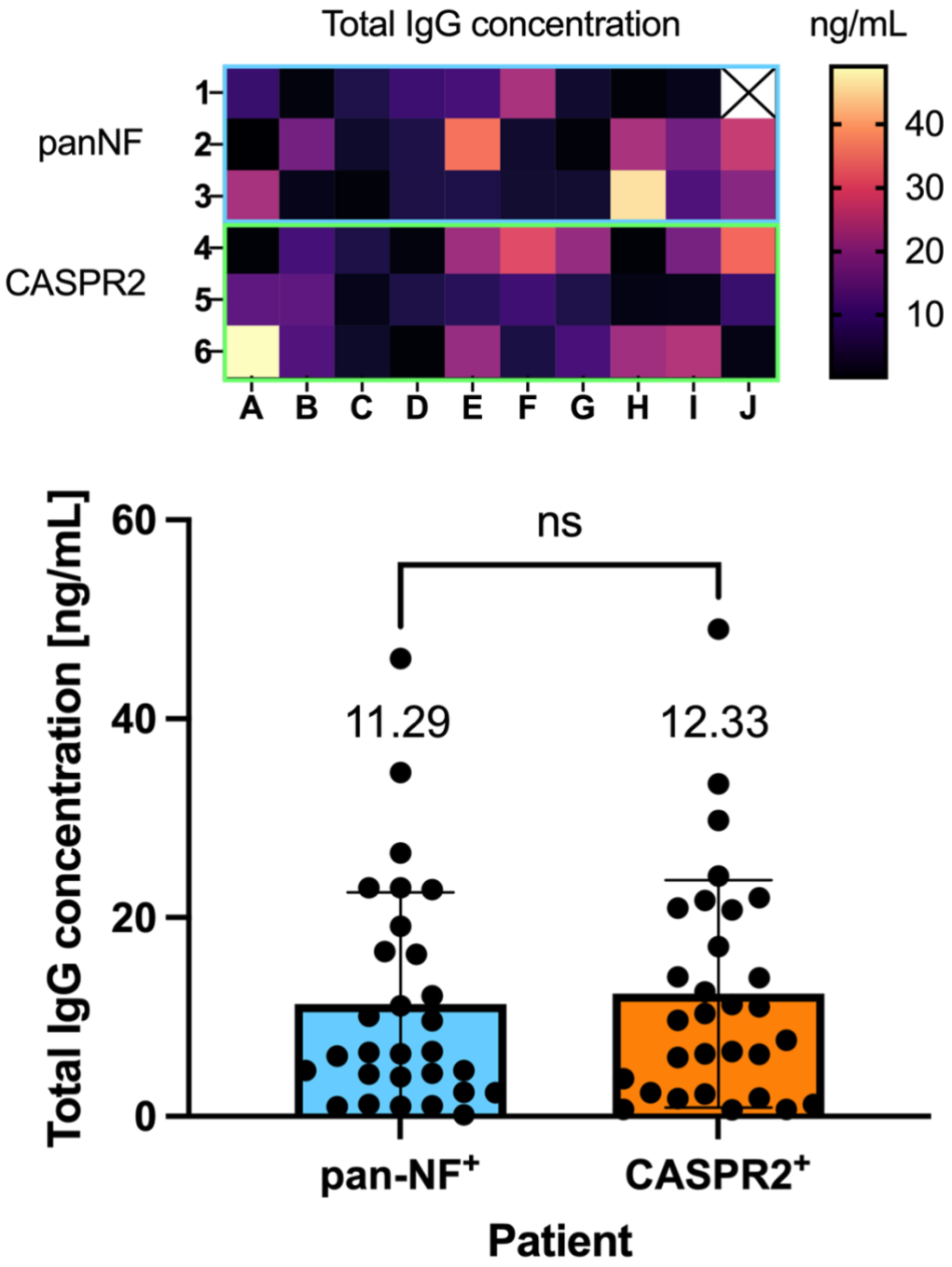

Figure 30: Total IgG production in 14-day cultures of bulk unsorted PBMCs from a pan-NF⁺ and CASPR2⁺ patient. *Wells were seeded with 5000 cells each and stimulated with R848, IL-2, CD40L, TNFα, IL-1β, and IL-21.* ***Top panel:*** *heatmap showing relative IgG concentrations (ng/mL) per well, assessed via ELISA. Each square represents a single culture well; colour intensity reflects relative IgG concentration.* ***Bottom panel:*** *distribution of concentrations from the same dataset, shown as mean ± SD across replicate wells (n = 29 for pan-NF⁺; one well excluded due to experimental error; n = 30 for CASPR2⁺). Most values fell below 50 ng/mL, and no significant difference was observed between donors (unpaired t-test, P = 0.726). However, interpretation should be made with caution due to assay limitations at low concentrations.*

Despite these limitations, the results confirmed that the cytokine-enhanced protocol was sufficient to stimulate polyclonal IgG production in both donor samples. This outcome validated the responsiveness of the stimulation system and supported its continued use in bulk- and single-cell sorted experimental formats.

4.3.1.2 Antigen-specific antibody detection

Antigen-specific IgG screening was not performed on the bulk unsorted cultures in this experiment, as subsequent analyses focused on sorted and single-cell culture formats.

4.3.2 Bulk-sorted cultures

4.3.2.1 Total IgG production

To evaluate the secretory potential of distinct B-cell subpopulations under optimised stimulation conditions, bulk-sorted cultures were established from four canonical subsets: new emigrant, mature naïve, unswitched memory, and switched memory B cells. 5000 cells were plated per well and stimulated with a cytokine cocktail comprising R848, IL-2, CD40L, TNFα, IL-1β, and IL-21.

In the pan-NF^+ patient, IgG production was primarily restricted to the switched memory subset, with consistently higher concentrations of IgG observed across replicate wells compared to low or negligible IgG in mature naïve, new emigrant, and unswitched memory subset wells (Figure 31). This pattern suggested that, in this patient, the

switched memory compartment was selectively responsive to stimulation under these conditions.

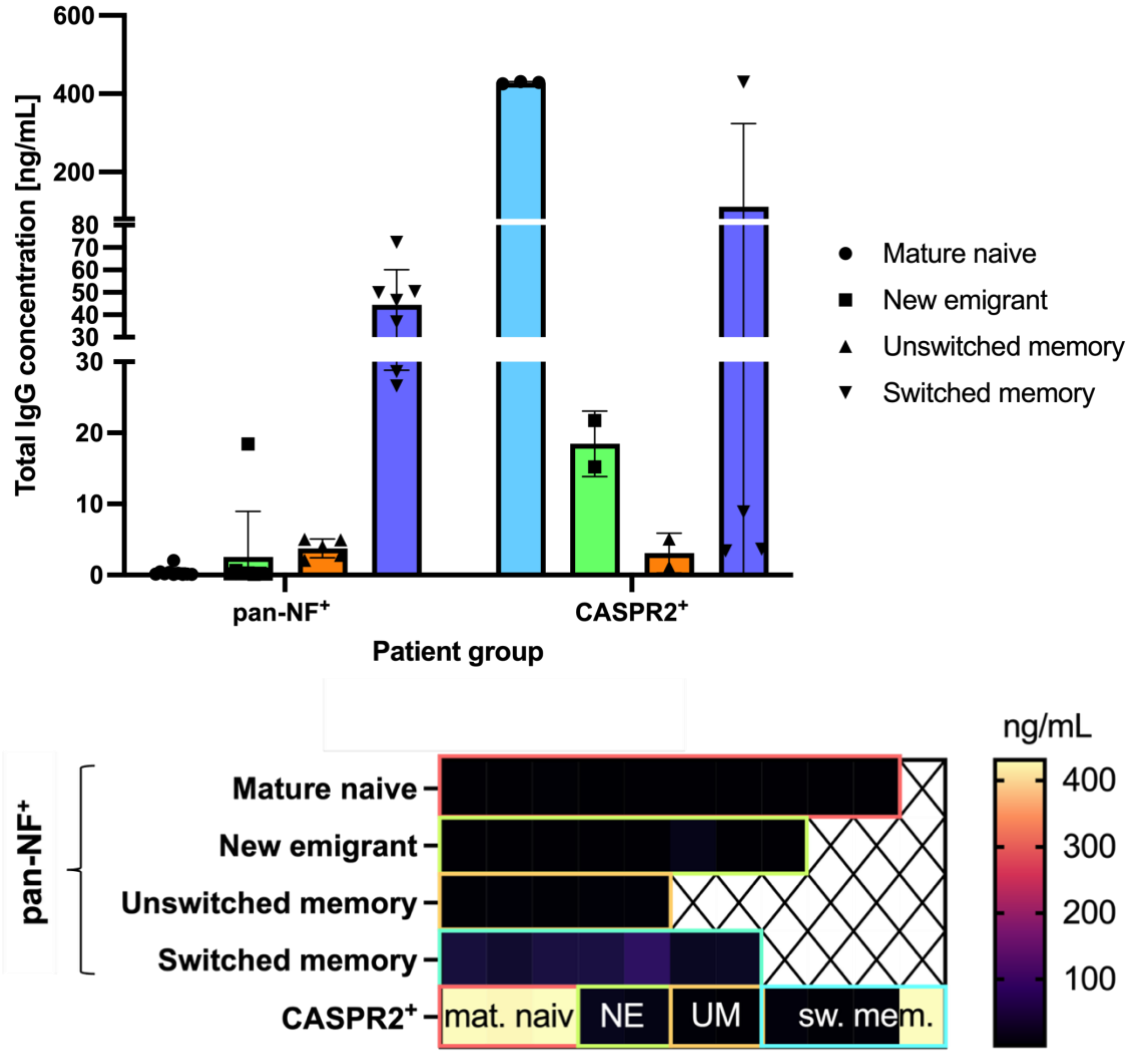

Figure 31: Total IgG production in 14-day bulk sorted PBMC cultures from pan-NF⁺ and CASPR2⁺ patients, *seeded at 5000 cells/well and stimulated with R848, IL-2, CD40L, TNFα, IL-1β, and IL-21.* ***Top panel:*** *bar plot displaying mean ± SD of IgG concentrations for each subset. In the pan-NF⁺ patient, IgG secretion was largely restricted to the switched memory population, whereas in the CASPR2⁺ patient, production was detectable across all subpopulations, with highest levels in switched memory and mature naïve compartments. Supernatants from the pan-NF⁺ sample were tested neat and supernatants from the CASPR2⁺ sample were tested at a 1:5 dilution.* ***Bottom panel:*** *ELISA heatmap showing IgG concentrations (ng/mL) per well for each subpopulation: mature naïve (mat. naïv), new emigrant (NE), unswitched memory (UM), and switched memory (sw. mem.). Statistical significance was not evaluated due to the low number of biological replicates (n ≤ 10 per subset), and observed trends should be interpreted with caution.*

In the CASPR2⁺ patient, IgG was detected across all four subpopulations, with the highest concentrations observed in the mature naïve and switched memory subsets

(Figure 31). This broader distribution of IgG production contrasted with the restricted response observed in the pan-NF$^+$ donor.

No statistical comparisons were performed due to the low number of biological replicates per subset ($n \leq 10$), and these observations should be interpreted descriptively.

4.3.2.2 Antigen-specific antibody detection

To determine whether any of the sorted B-cell subpopulations generated antigen-specific IgG, culture supernatants were screened for reactivity against both targets by live cell-based assay (CBA). Due to limited supernatant volume, ELISA screening was not performed, as CBAs offered greater sensitivity for low-concentration antigen-specific detection.

In the pan-NF$^+$ patient, a single well from the switched memory subset demonstrated NF155-specific IgG reactivity. No wells showed reactivity against NF186 (Figure 32). In the CASPR2$^+$ patient cultures, no antigen-specific reactivity was detected against CASPR2 (data not shown).

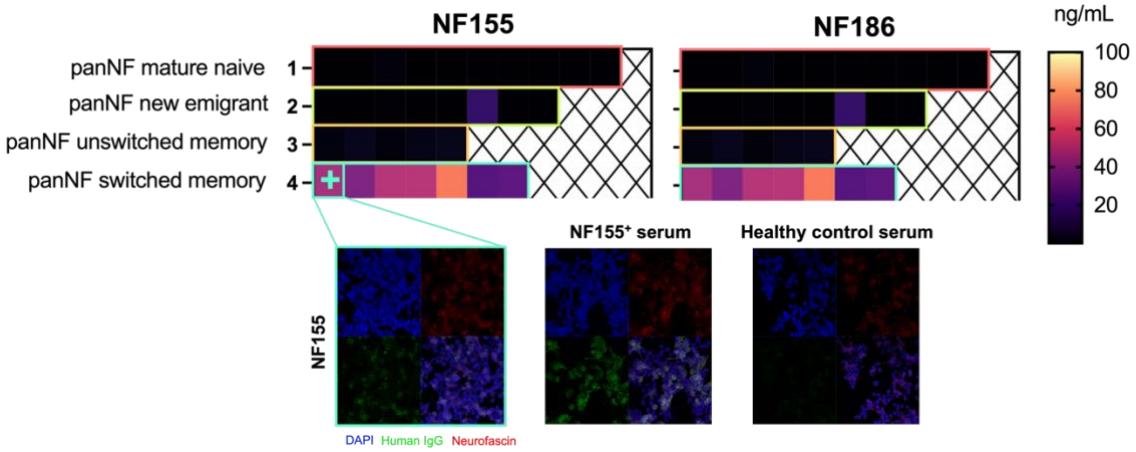

Figure 32: Total IgG production and antigen-specific IgG detection in bulk-sorted B-cell subpopulations from a pan-NF⁺ patient following 14-day stimulation. Top panel: *ELISA heatmaps displaying total IgG production (ng/mL) per well across four B-cell subsets: mature naïve, new emigrant, unswitched memory, and switched memory. These heatmaps serve as a reference for IgG secretion across subpopulations.* ***Bottom panel:*** *Representative CBA images from the switched memory subset of the pan-NF⁺ patient, showing specific binding of IgG to NF155-expressing HEK293T cells (green: human IgG, red: neurofascin, blue: DAPI nuclear stain). The sole antigen-specific signal was observed in one switched memory well against NF155; no reactivity was detected against NF186 in any of the pan-NF⁺ cultures.*

4.4 Single-cell cultures and antibody production

4.4.1 CASPR2⁺ single-cell cultures

To complement bulk-sorted analyses and facilitate mAb generation, single $CD27^{+}IgD^{-}$ memory B cells from a $CASPR2^{+}$ patient were sorted and cultured individually in five 96-well plates (480 wells total). Total IgG production was detected in a substantial proportion of wells across all five plates (Figure 33). Concentrations varied between wells, with some exceeding 80 ng/mL and others falling below the assay detection limit, confirming stimulation of IgG secretion under these conditions.

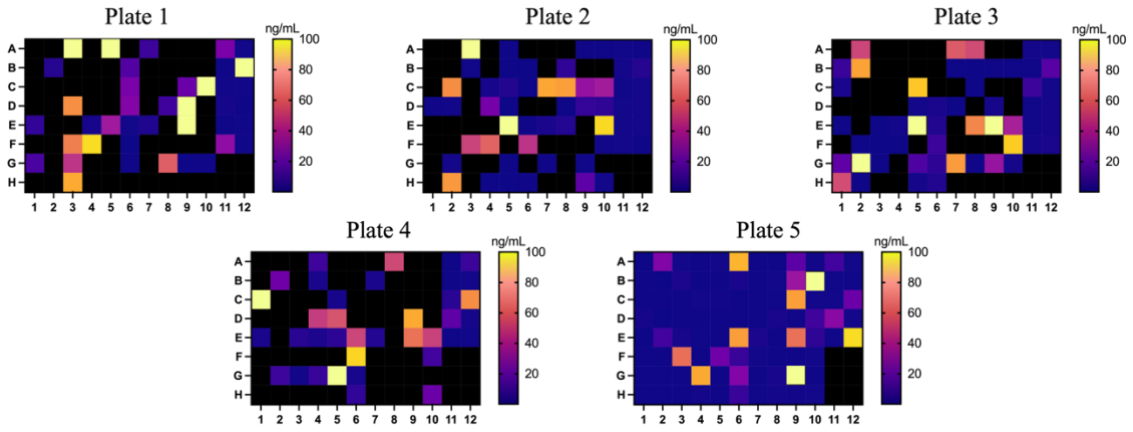

Figure 33: Total IgG production in CASPR2⁺ single-cell cultures. *Total IgG production from five 96-well plates, as measured by ELISA. Each heatmap shows IgG concentration (ng/mL) per well. Concentrations exceeding the assay's upper limit of detection (100 ng/mL) were detected in multiple wells across all plates.*

Despite robust total IgG secretion, no CASPR2-specific IgG was detected in any individual well by CBA. Pooled supernatants from corresponding rows across the five plates were re-screened using a pan-isotype (IgA/IgM/IgG) secondary antibody to increase detection sensitivity. A weak signal was observed in one pool (C6), but this did not meet pre-defined positivity criteria and was not investigated further (Figure 34).

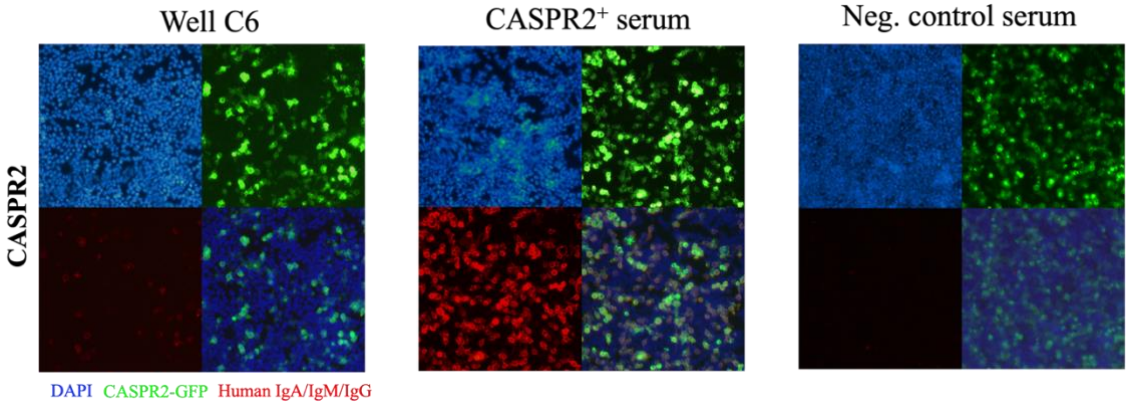

Figure 34: CBA screening for antigen-specific IgG in CASPR2⁺ single-cell cultures. *No CASPR2-specific IgG was detected in pooled supernatants using standard anti-human IgG secondary antibodies. To enhance detection sensitivity, pooled supernatants from row-matched wells across 5 plates (eg, all wells in row A) were re-screened using an anti-human IgA/IgM/IgG pan-isotype secondary antibody (Jackson ImmunoResearch, 109-006-064; 1:500 dilution). A weak signal was observed in one pooled well (C6), but this did not meet standard criteria for positivity. Images show staining with DAPI (blue), CASPR2-GFP (green), and human Ig (red). CASPR2⁺ serum and healthy control serum are shown for comparison.*

4.4.2 Pan-NF$^+$ single-cell cultures

Parallel single-cell cultures were established from the pan-NF$^+$ patient (Bio-099) using the same approach.

Detectable IgG was observed in 323/480 wells (67.3%) above the ELISA lower limit of detection (1.6 ng/mL), with several wells exceeding the assay's upper quantification limit (100 ng/mL) (Figure 35). These results indicated that the stimulation protocol reliably induced antibody secretion across a majority of single-sorted CD27$^+$IgD$^-$ memory B cells.

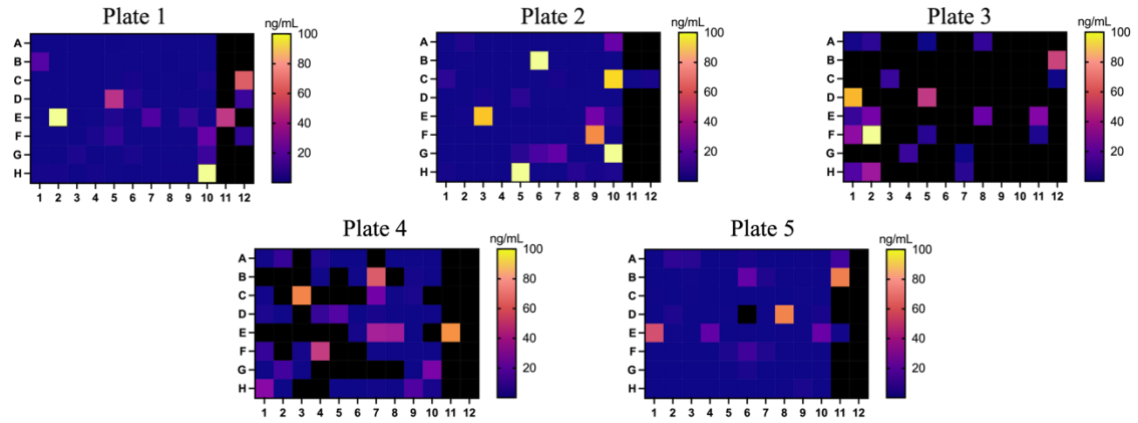

Figure 35: Heat maps showing total IgG production from five 96-well plates of CD27$^+$IgD$^-$ memory B cells single-sorted from a pan-NF$^+$ patient. *Cells were cultured for 25 days on MS40L feeder cells with R848, IL-2, IL-21, TNFα, and IL-1β. Supernatants were tested neat via ELISA. IgG concentrations are shown in ng/mL; colour intensity reflects absolute concentration. A total of 323/480 wells (67.3%) produced IgG above the ELISA lower limit of detection (1.6 ng/mL). Several wells exceeded the assay's upper quantification range (100 ng/mL), indicated by saturated yellow signal.*

CBAs performed on neat supernatants (first pooled; then unpooled from wells with positive signal) identified three wells with neurofascin-specific IgG reactivity (Figure 36). Clone 5A6 showed moderate reactivity to NF155 only; clone 3G2 showed weak binding to NF186 only; and clone 4G2 bound strongly to NF186, with weak fluorescence for NF155 below positivity thresholds. In total, NF155-specific reactivity

was detected in 1/480 wells (0.21%), and NF186-specific reactivity in 2/480 wells (0.42%).

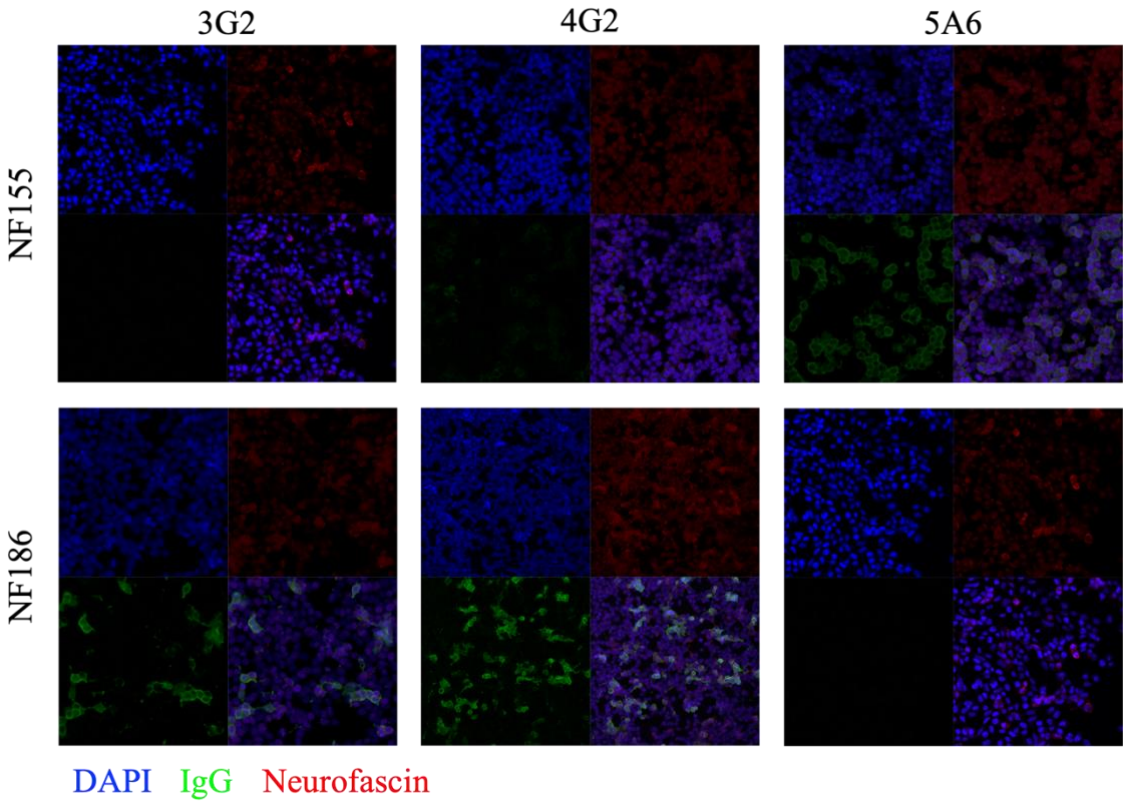

Figure 36: CBA images of three CD27⁺IgD⁻ single memory B-cell clones from a pan-NF AN patient showing antigen-specific IgG reactivity to neurofascin isoforms. *Supernatants were tested neat. Sample 5A6 showed moderate IgG reactivity to NF155 only; sample 3G2 showed weak reactivity to NF186 only; sample 4G2 showed strong NF186 and very weak NF155 reactivity that was not considered positive. Images show DAPI (blue), human IgG (green), and neurofascin (red). Co-localisation indicates specific binding. These represent 2/480 (0.42%) NF186⁺ wells and 1/480 (0.21%) NF155⁺ wells.*

These results provide the first direct evidence of neurofascin-reactive memory B cells at single-cell resolution from a pan-NF AN patient, demonstrating the feasibility of capturing these rare clones for downstream sequencing and mAb generation.

4.5 Single-cell sequencing and monoclonal antibody production

4.5.1 Sanger and Nanopore sequencing of autoreactive clones

To define the clonal identities of neurofascin-reactive B cells identified in section 4.4, supernatants from three CBA-positive single clones (3G2, 4G2, and 5A6) were selected for Ig gene sequencing. Each well had shown clear, spatially discrete IgG reactivity to NF155 or NF186. The corresponding cells were retrieved from index-sorted plates, RNA was extracted, and cDNA was generated. Nested PCR amplification of heavy chain (IGH) and kappa/lambda light chain (IGK/IGL) variable regions was performed using protocols optimised for single-cell input (section 2.10). Three non-autoreactive single $CD27^{+}IgD^{-}$ memory B-cell clones from the same patient and cell sort were also sequenced as controls.

Productive in-frame VH and VL sequences were obtained for clones 5A6 and 4G2 (Table 15). Clone 3G2 yielded a productive light chain but no recoverable heavy chain sequence despite repeated PCR and Nanopore sequencing attempts. Of the three negative control clones that were sequenced, two yielded complete VH and VL sequences, and one (D6_1) yielded only a productive light chain.

Reactivity	Clone ID	Reactivity	Chain	Isotype	Variable (V) region family	Joining (J) region family	Diversity (D) region family	Amino acid replacements in V region gene segment	Amino acid replacements in CDR3
Autoreactive	3G2	NF186	L	κ	IGKV3-15*01	IGKJ2*01	-	0	0
	4G2	NF186	H	IgG	IGHV2-5*02	IGHJ6*02	IGHD3-10*03	0	0
			L	κ	IGKV1-17*03	IGKJ2*01	-	1	0
	5A6	NF155	H	IgG	IGHV3-9*01	IGHJ3*02	IGHD3-22*01	0	0
			H	IgM	IGHV3-9*01	IGHJ3*02	IGHD3-22*01	0	0
			L	κ	IGKV1-12	IGKJ4*01	-	0	0
			L	λ	IGLV3-1*01	IGLJ2*01	-	0	0
Negative controls	D6_1	-	L	λ	IGLV2-14*03	IGLJ1*01	-	11	4
	D6_2	-	H	IgG	IGHV3-30*18	IGHJ3*02	IGHD3-16*02	4	0
			L	λ	IGLV2-23*02	IGLJ3*02	-	0	0
	D6_3	-	H	IgG	IGHV3-30-3*01	IGHJ6*02	IGHD3-10*01	16	0
			L	λ	IGLV1-44*01	IGLJ7*01 or *02	-	10	3

Table 15: Immunogenetic characteristics of antigen-reactive and non-reactive B-cell clones. *V(D)J gene usage and mutation analysis from single-cell cultures of three neurofascin-reactive (3G2, 4G2, 5A6) and three non-reactive (D6_1–3) clones, sequenced via nested PCR and Sanger sequencing. Productive, in-frame VH and VL sequences were obtained except for 3G2 and D6_1, which yielded only a light chain. All NF-reactive clones expressed κ light chains, while all negative controls expressed λ. Clone 5A6 yielded transcripts for both κ and λ light chains, as well as both IgG and IgM heavy chains (the latter detected via Nanopore only), indicating possible dual expression. Somatic mutation patterns were minimal or absent in all neurofascin-reactive sequences, contrasting with the high mutation burden in non-reactive clones. These results suggest a phenotypically memory-like but genetically unmutated profile for neurofascin-reactive B cells, and potential bypassing of canonical germinal centre maturation pathways. NF: neurofascin; L: light chain; H: heavy chain; κ: kappa; λ: lambda; IGH: heavy chain; IGL: lambda light chain; IGK: kappa light chain; CDR3: complementarity-determining region 3.*

Sequencing revealed that all neurofascin-reactive clones expressed kappa light chains. Clone 5A6 yielded transcripts for both kappa and lambda light chains and both IgG and IgM heavy chains. All negative control clones expressed lambda light chains, and all negative controls with productive heavy chain sequences expressed IgG heavy chains. VH gene usage among reactive clones spanned IGHV2 and IGHV3 families, with IGKV1 and IGKV3 observed among kappa clones, and IGLV1 and IGLV2 usage in lambda clones. Somatic hypermutation (SHM) was minimal or absent in all neurofascin-reactive clones; no complementarity-determining region 3 (CDR3) amino acid replacements were detected. By contrast, all non-reactive control clones harboured multiple framework and CDR3 region mutations, consistent with the phenotype of their sorted parent population ($CD19^{+}CD27^{+}IgD^{-}$ switched memory B cells).

As Sanger sequencing was performed with IgG-specific primers, and Nanopore sequencing (with both IgG and IgM primers) was only applied to 3G2, 4G2, and 5A6, potential IgM transcripts in control clones were not assessed. Clone 3G2 was not re-sequenced with alternative primers due to prioritisation of successfully amplified clones for downstream work.

4.5.2 IgG1 mAb production and testing

Recombinant IgG1 mAbs were generated from the productive VH and VL sequences of clones 4G2 and 5A6. Both kappa and lambda light chain constructs were expressed for 5A6. Constructs were synthesised, expressed, and purified in collaboration with Twist Bioscience. mAbs were tested for antigen binding against NF155 and NF186 using ELISA and live CBA.

In serial dilution CBAs (10 to 0.02 μg/mL)[109] separately transfected for NF155 or NF186, none of the IgG1 mAbs showed binding to either NF155 or NF186. These results were consistent across two independent experiments. Positive and negative control sera and mAbs yielded expected staining patterns, confirming assay validity.

ELISAs were also performed using commercial recombinant NF155 and NF186, as well as NF155 and NF186 antigen bait constructs produced in-house (Chapter 5), as capture antigens. The mAbs were tested across a dilution series from 10 μg/mL to 0.02 μg/mL, as well as $NF155^+$ (Bio-007) and pan-NF^+ (SR863) patient sera as positive controls and a healthy donor as a negative control, with PBS-coated wells used for background subtraction. As with the CBAs, mAb optical density (OD) readings remained at background levels (data not shown).

To confirm successful expression and structural integrity of the IgG1 mAbs, ELISAs were next conducted using the mAbs themselves as the capture antigens. Each well was coated at 5 μg/mL or 10 μg/mL and probed with horseradish peroxidase (HRP)-conjugated secondary antibodies targeting the IgG Fc region of the heavy chain, or kappa or lambda light chains. Strong signal was observed in all mAb preparations and positive controls with their respective heavy or light chain-specific secondary antibodies (Figure 37), confirming coating and functional expression. These results demonstrated that the lack of antigen-specific signal in the preceding ELISAs was likely not due to failed mAb expression.

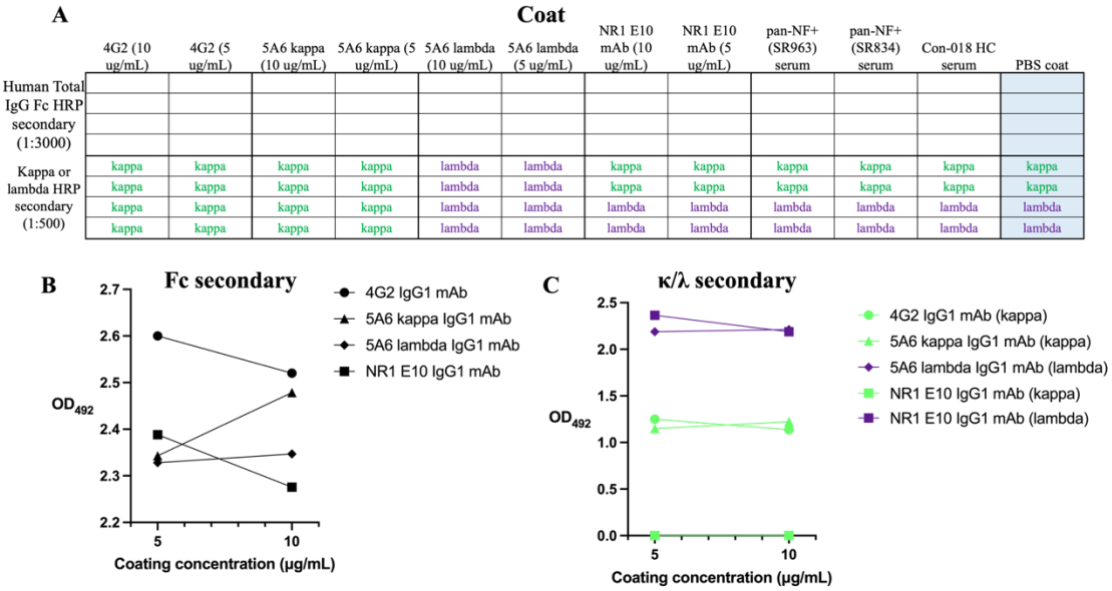

Figure 37: Total IgG ELISA confirming functional IgG mAbs. (A) *ELISA plate layout used to test expression of IgG1 mAbs derived from NF155/NF186⁺ clones. Each well was coated at 10 µg/mL or 5 µg/mL with each mAb and detected using HRP-conjugated secondary antibodies specific for total IgG Fc (1:3000) and light chain isotypes (kappa or lambda, 1:500). A control mAb (NR1 E10, known λ light chain; courtesy of Dr Bo Sun) and patient sera (two pan-NF⁺ and one healthy donor; each diluted 1:100 in PBS before coating) were included for reference. Pan-NF⁺ control sera displayed a mean corrected OD of 0.804 using the Fc-specific secondary, 0.1655 for the kappa light chain secondary, and 2.39525 for the lambda light chain secondary, all considered above the positivity threshold (data not shown). The healthy control serum had a mean corrected OD of 0.6405 using the Fc-specific secondary, 0.135 for the kappa light chain secondary, and 2.2605 for the lambda light chain secondary, also all considered above the positivity threshold (data not shown).* ***(B-C)*** *Background-corrected optical density (OD) values from ELISA after subtracting the mean OD of PBS-coated negative control wells using an Fc-specific secondary antibody (B) or kappa or lambda light chain secondary antibody (C), based on the known/presumed light chain of the mAb being tested. Each point represents a mean of experimental duplicates or quadruplicates. All mAb preparations showed strong signal with their cognate heavy and light chain detection reagents, confirming successful IgG production and coating. HC: healthy control; pan-NF: pan-neurofascin; Fc: fragment crystallisable region.*

4.6 Discovery of predominant IgM reactivity

The failure of recombinant IgG1 mAbs derived from autoreactive clones to bind their target antigens prompted a re-evaluation of isotype as a determinant of antigen specificity. Despite robust neurofascin reactivity observed in single-cell culture supernatants for clones 4G2 and 5A6, neither IgG1 mAb exhibited measurable binding at this stage when expressed in an IgG1 backbone and tested by ELISA or CBA. This discrepancy, combined with confirmation of successful IgG1 mAb production and coating (Figure 37), raised the possibility that native antigen binding may be isotype-

dependent. Furthermore, earlier CBAs to screen supernatants had employed secondary antibodies targeting both the Ig heavy and light chains for IgG detection, rather than Fc-specific reagents, introducing the possibility that some antigen reactivity attributed to IgG may in fact have originated from secreted IgM. This consideration prompted a systematic investigation of isotype-specific binding properties.

Retrospective analysis of the Nanopore sequencing data also revealed that clone 5A6 expressed both IgG and IgM heavy chain transcripts (Table 15), suggesting co-expression or a recent isotype switching event. To investigate this, the original single-cell supernatants for clones 3G2, 4G2, and 5A6 were re-screened using an anti-human IgM secondary antibody (μ-chain specific) on live CBA. This re-screening identified strong NF186-specific IgM reactivity for 4G2 and moderate NF155-specific IgM reactivity for 5A6, consistent with earlier antigen-specific IgG results and confirming the presence of antigen-specific IgM (Figure 38). Conversely, 3G2 did not display IgM-specific NF155 or NF186 reactivity.

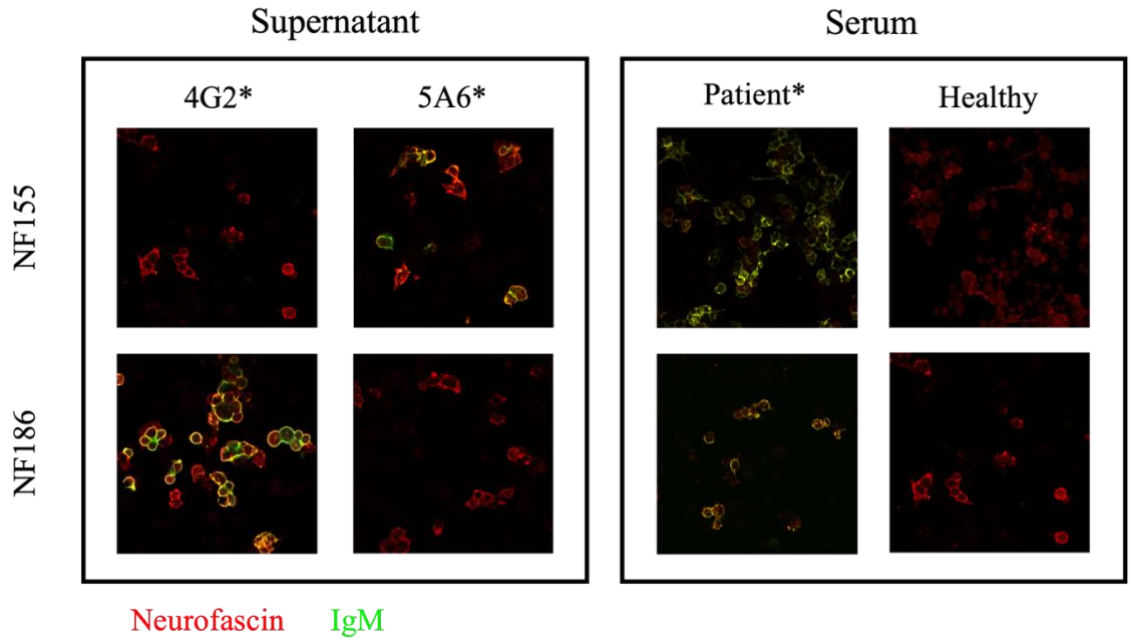

Figure 38: Detection of IgM reactivity to neurofascin in vitro by CBA from single CD27^{+}IgD^{-} memory B cells from a pan-NF AN patient. *Neurofascin reactivity was assessed using live CBA with an anti-human IgM (μ-chain specific) secondary antibody (green) and commercial neurofascin staining (red). Two single-cell culture supernatants demonstrated strong and specific NF155 or NF186 binding in the IgM isotype. The patient's own serum (Bio-099; marked with *) exhibited pan-neurofascin IgM binding consistent with the supernatant results, whereas serum from a healthy control showed no reactivity. DAPI nuclear stain was not performed due to reagent limitations.*

Further testing for IgG subclass reactivity revealed that the 4G2 supernatant exhibited both IgM and IgG1 reactivity against NF186, while no IgG2 was detected (Figure 39). In contrast, the 5A6 supernatant was negative for both IgG1 and IgG2 reactivity to either antigen (data not shown), despite evidence of NF155-specific IgG in earlier assays. IgG3 and IgG4 were not tested due to limited supernatant volume.

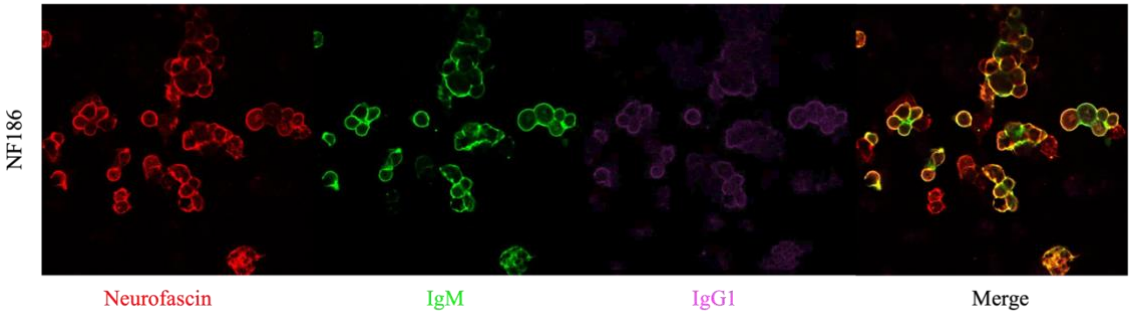

Figure 39: Detection of IgG1 and IgM subclass reactivity against NF186 in clone 4G2 by live CBA. *Live CBA was performed on clone 4G2 supernatant using subclass-specific secondary antibodies to detect IgM (green) and IgG1*

(magenta). Neurofascin staining (commercial protein) is shown in red. Co-localisation of IgM and IgG1 with neurofascin was evident in the merged panels, consistent with dual isotype production from this single-cell clone.

Encouraged by these findings, a comprehensive IgM-specific screen was performed across all 480 single CD27^{+}IgD^{-} memory B-cell clones sorted and cultured from the pan-NF^{+} patient. Unlike previous pooled IgG screens, this approach tested each supernatant individually to avoid potential masking of low-level signals. Limited supernatant volume precluded re-screening for IgG in these wells.

In total, 14 out of 480 (2.92%) single-cell culture supernatants from patient Bio-099 exhibited evidence of neurofascin-specific reactivity, as summarised in Table 16 & Table 17. Of these, 13 wells were definitively positive for IgM, including 7 NF155^{+} only wells (1.46%, including clone 5A6), 1 NF186^{+} only well (0.21%, clone 4G2), and 2 pan-NF^{+} wells (0.42%). 3 additional supernatants displayed clear IgM reactivity to one neurofascin isoform with possible cross-reactivity to the other. In stark contrast, only 3 wells demonstrated clear IgG reactivity: one NF155^{+} only well and two NF186^{+} only wells (0.21% and 0.42%, respectively). Notably, no IgG pan-NF^{+} reactivity was observed, and only one clone (3G2) with IgG binding did not display corresponding IgM reactivity. Supernatants from 2/3 single-cell wells that were screened for both isotypes (4G2 and 5A6) demonstrated dual IgM and IgG reactivity to neurofascin. Overall, neurofascin-reactive IgM clones (13/480; 2.71%) were over four times more prevalent than their IgG counterparts (3/480; 0.63%).

	Frequency of antigen-specific reactivities (n=480)					Total
Isotype	**NF155^{+} only**	**NF186^{+} only**	**NF155^{+} (w/ possible NF186^{+} cross-reactivity)**	**NF186^{+} (w/ possible NF155^{+} cross-reactivity)**	**pan-NF^{+}**	
IgM	7 (1.46%)	1 (0.21%)	1 (0.21%)	2 (0.42%)	2 (0.42%)	13
IgG	1 (0.21%)	2 (0.42%)	0 (0.00%)	0 (0.00%)	0 (0.00%)	3

Table 16: Frequency of neurofascin-reactive clones by isotype and antigen specificity among supernatants of 480 single CD27^{+}IgD^{-} memory B-cell clones from a pan-NF AN patient. *Confirmed IgM and IgG neurofascin-reactive*

clones are categorised by their apparent specificity for NF155, NF186, or both (pan-NF⁺). Additional subcategories indicate possible cross-reactivity to the alternate isoform. Only confirmed positive signals are included; clones with inconclusive or non-reproducible staining are excluded. Counts are reported as absolute numbers with percentages relative to the total number of clones screened (n = 480). Note that two clones (4G2 and 5A6) exhibited dual IgM and IgG reactivity and are represented in both isotype rows. Total column indicates the sum of clones per isotype with confirmed reactivity to at least one of the targets for at least one isotype.

Representative CBA images from these screens illustrated strong and specific binding, with clear co-localisation of human IgM and neurofascin signal (Figure 40).

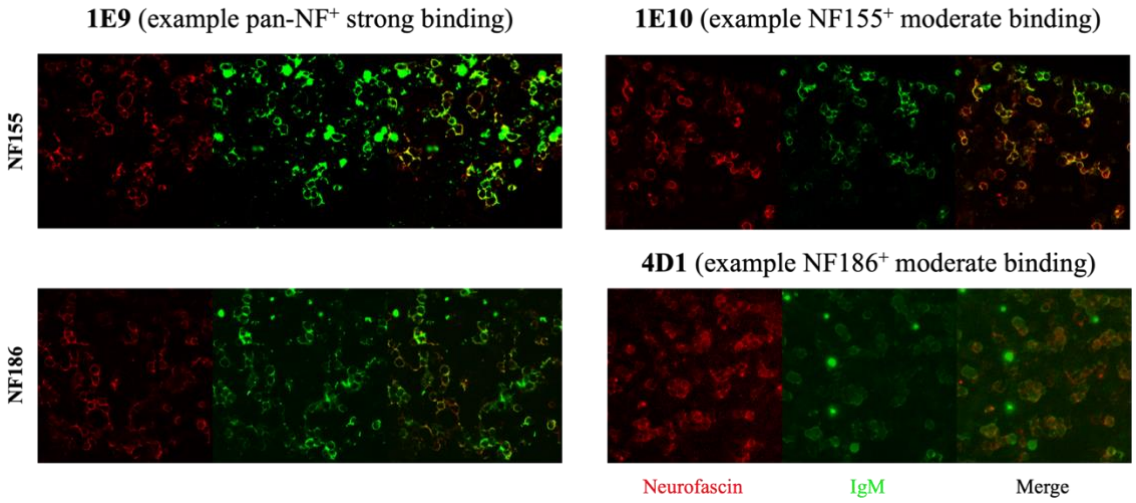

Figure 40: Representative images from re-screening of 480 single-cell culture supernatants for IgM reactivity to NF155 and NF186. *Live CBAs were performed on unpooled, undiluted supernatants from single CD27⁺IgD⁻ memory B-cell cultures of a pan-NF⁺ patient. Human IgM (green) binding was detected using an AlexaFluor 594-conjugated secondary antibody. Successful transfection and expression of neurofascin was visualised using streptavidin-Pacific Blue conjugate, as the red (594) channel was required to optimise IgM detection. For visual clarity and consistency with other figures, colours were digitally reassigned in post-processing to display neurofascin in red and IgM in green. Co-localisation (yellow/orange) indicates positive reactivity. Shown are examples of strong pan-NF⁺ reactivity (left panels), moderate NF155-specific reactivity (top right), and moderate NF186-specific reactivity (bottom right). DAPI staining was not used in this assay due to usage of the blue channel for neurofascin visualisation.*

These findings confirmed that neurofascin-specific IgM was not only present but predominant among reactive single CD27⁺IgD⁻ memory B-cell clones from the pan-NF⁺ patient. The detection of pan-NF⁺ IgM clones, which had been absent in IgG screens, suggested that the initial focus on IgG reactivity and mAb generation may have overlooked a broader spectrum of antigen-specific reactivity and motivated production and further functional characterisation of IgM-format mAbs in the following experiments.

4.7 Functional characterisation of IgM monoclonal antibodies

4.7.1 Experimental IgM mAbs

To directly assess whether antibody isotype influences neurofascin binding, mAbs were recombinantly expressed in an IgM format using variable regions cloned from antigen-specific single-cell supernatants previously constructed in IgG1 backbones. This approach aimed to test whether the loss of neurofascin binding observed for IgG1 mAbs could be restored by reconstituting the IgM isotype.

IgM expression constructs were generated in collaboration with Twist Bioscience, utilising canonical IgM constant region sequences. The variable heavy chains of clone 4G2 and both light chain variants of clone 5A6 (kappa and lambda) were cloned into these vectors. The light chain variable regions were identical to those used in the original IgG1 constructs. Recombinant expression was performed in HEK293 cells, and unpurified supernatants were provided for functional testing.

Total IgM production was confirmed by ELISA, with serial dilution testing (1:10 to 1:1280) yielding functional concentrations: 294.3 µg/mL for 4G2 IgM, 352.1 µg/mL for 5A6 kappa IgM, and 165.1 µg/mL for 5A6 lambda IgM. Functional analysis via live CBAs assessed NF155 and NF186 reactivity across serial dilutions from neat to 1:64.

The 4G2 IgM mAb demonstrated strong, specific binding to NF186, mirroring the original supernatant results (Figure 41). Binding remained detectable down to 4.6 µg/mL. In contrast, the 5A6 lambda IgM mAb showed binding to both NF155 and NF186, with NF186 reactivity detectable down to a concentration of 20.6 µg/mL, suggesting broader reactivity than observed in its corresponding supernatant. The 5A6

kappa IgM mAb, however, did not show detectable binding to either antigen, reflecting its weaker binding capacity observed in prior analyses.

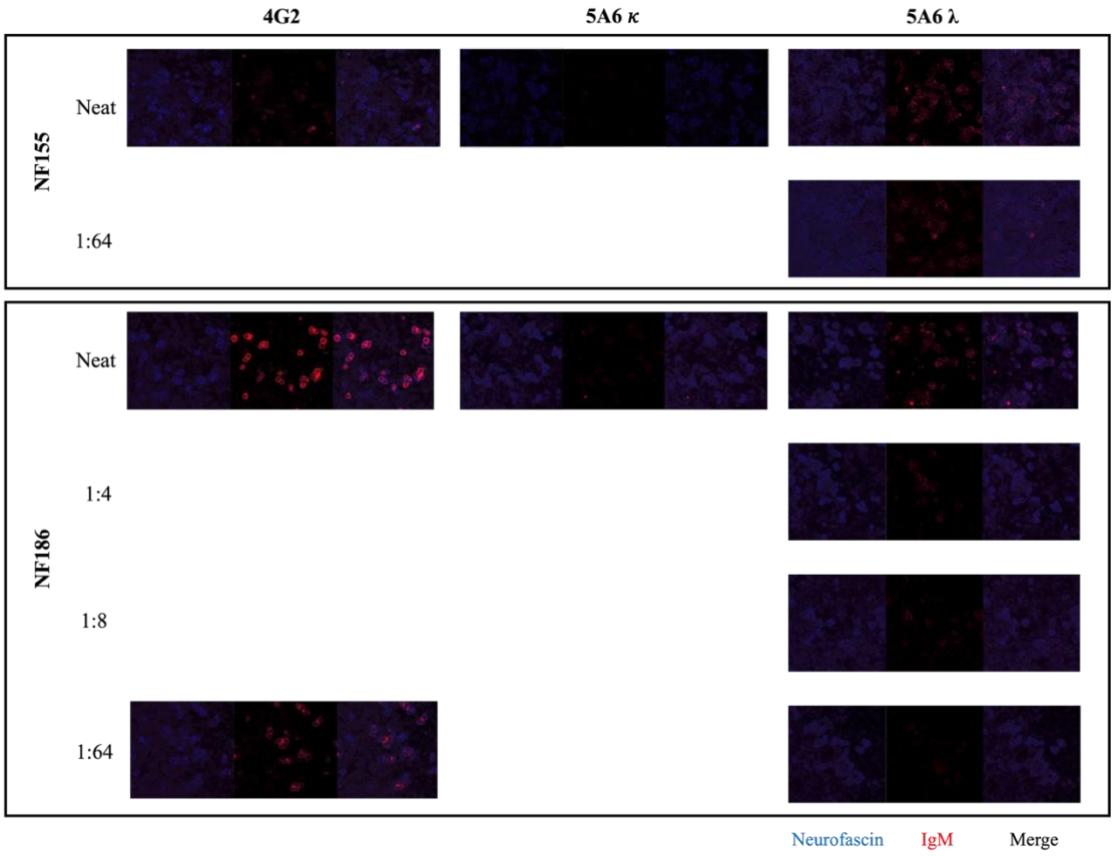

Figure 41: Live CBA testing of recombinant IgM mAbs derived from pan-NF$^+$ clones. *Images of HEK293T cells transfected with either NF155 or NF186, incubated with serial dilutions of supernatants of recombinant IgM mAbs (4G2, 5A6-kappa light chain, 5A6-lambda light chain) and stained with anti-human IgM (red) and commercial anti-neurofascin (red). The 4G2 IgM mAb (left panel) exhibited strong, specific NF186 binding detectable through a 1:64 dilution, with potential cross-reactivity to NF155 when tested neat that did not meet positivity thresholds. The 5A6 lambda IgM mAb (right panel) demonstrated reactivity to both NF155 and NF186, while the 5A6 kappa IgM mAb (middle panel) showed no binding to either isoform. Positive co-localisation of IgM and neurofascin is visualised by magenta signal.*

4.7.2 IgG1 vs IgM mAb binding comparisons

To rigorously compare binding between IgM and IgG1 formats under equivalent conditions, head-to-head CBAs were performed using matched serial dilutions for each mAb (4G2, 5A6 kappa, and 5A6 lambda), from neat to 1:64, against NF155 and NF186. Visual assessment of fluorescence intensity determined the lowest and highest

concentrations at which clear binding was detectable (Figure 42). These ranges were then summarised in a binding comparison plot (Figure 43).

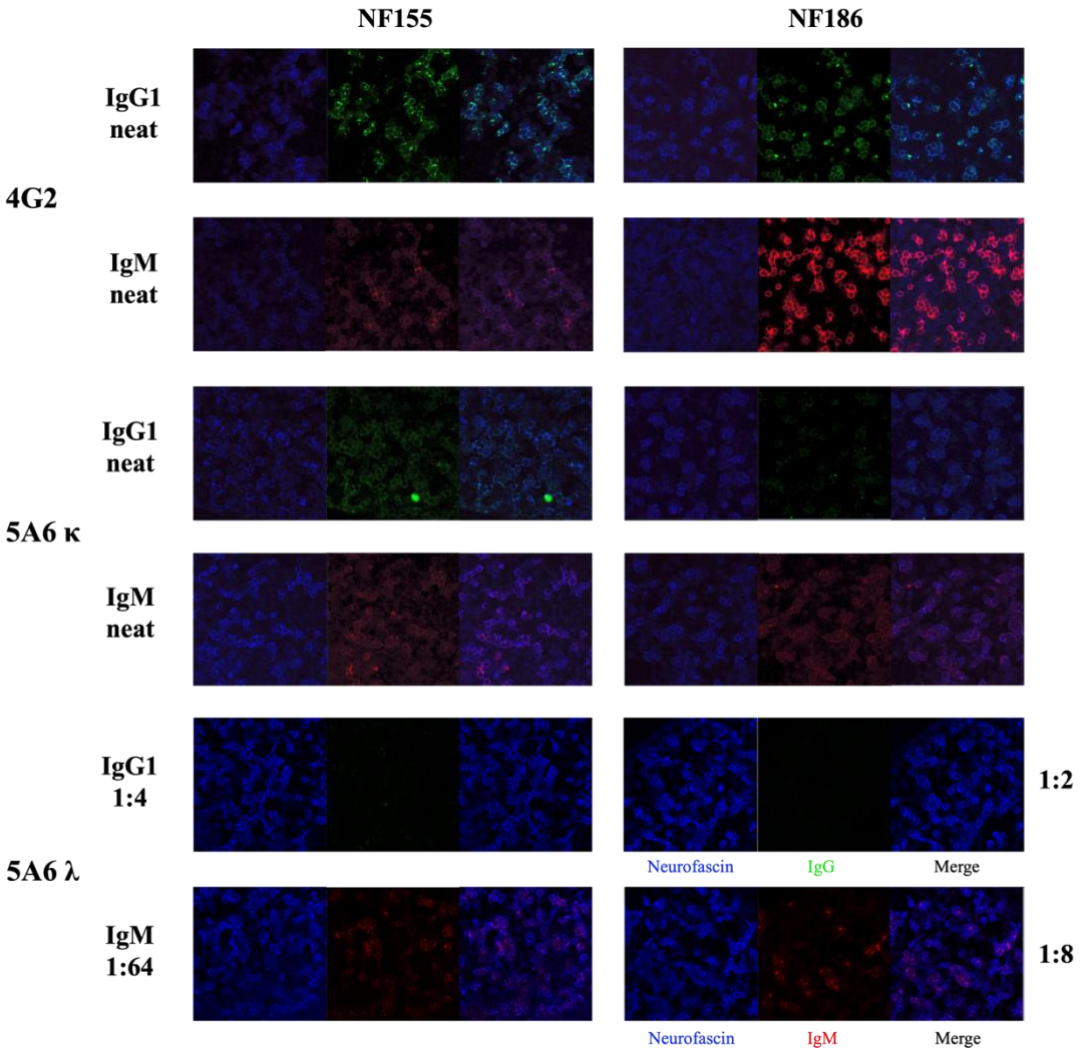

Figure 42: Head-to-head comparison of three IgG1 and IgM mAbs on live CBA. *Representative images of CBAs testing the 4G2, 5A6 kappa (κ), and 5A6 lambda (λ) mAbs in both IgG1 and IgM formats against NF155 (left panels) and NF186 (right panels). IgG1 staining is visualised with anti-human Fc-specific IgG secondary (green), IgM with anti-human μ-chain-specific IgM secondary (red), and commercial neurofascin with streptavidin-conjugated detection (blue).* ***4G2:*** *IgG1 reactivity to both isoforms was detectable undiluted (1400 μg/mL) but dropped below positivity thresholds by 1:32 (43.75 μg/mL) for NF155 and 1:16 (87.5 μg/mL) for NF186 (not shown). In contrast, the IgM version was strongly reactive against NF186 and weakly reactive against NF155 undiluted (294.3 μg/mL), and retained clear NF186 reactivity at 1:64 (4.6 μg/mL; not shown). NF155 reactivity remained until 1:32 (9.2 μg/mL; not shown).* ***5A6 κ:*** *Weak reactivity to NF155 was observed for both isotypes undiluted (IgG1: 640 μg/mL; IgM: 352.1 μg/mL) but was lost by 1:2 dilution (not shown).* ***5A6 λ:*** *IgM mAb binding was stronger and more sustained across dilutions compared to the IgG1 format. IgG1 binding to NF155 was lost by 1:4 dilution (392.5 μg/mL), while IgM reactivity persisted through 1:64 (2.6 μg/mL). Similarly, IgM binding to NF186 remained detectable at 1:8 until 1:16 (20.6-10.3 μg/mL), in contrast to IgG1 which dropped out by 1:2 (785 μg/mL).*

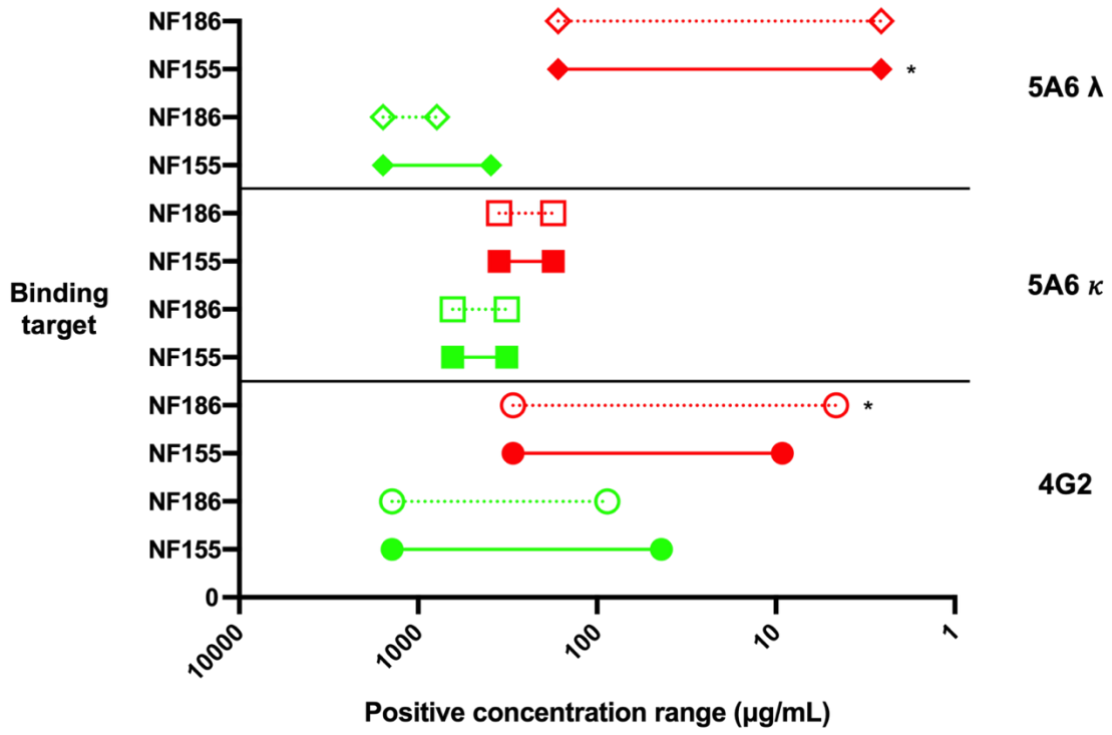

Figure 43: Comparison of positive binding concentration ranges for IgG1 and IgM recombinant mAbs against NF155 and NF186. *Serial dilution CBAs were performed to define the concentration range over which binding to NF155 or NF186 could be observed for each mAb. Each horizontal line represents the lowest and highest tested concentrations at which clear binding was detected for a given mAb-target pair. Red lines indicate IgM mAbs, and green lines indicate IgG1 mAbs. Solid lines and filled shapes correspond to binding against NF155, while dotted lines and unfilled shapes correspond to NF186 binding. Each shape designates a unique mAb: circles = 4G2, squares = 5A6 with κ light chain, diamonds = 5A6 with λ light chain. Asterisks (*) denote mAbs that remained clearly positive at the lowest tested concentration, indicating that the true lower limit of detection lies below the tested range. Concentrations for the IgG1 mAbs were taken from those provided by Twist Bioscience upon production; concentrations for the IgM mAbs were extrapolated based on the total IgM ELISA findings of the unpurified HEK supernatants provided by Twist Bioscience containing the IgM mAbs (section 4.7.1).*

The 4G2 IgM mAb retained strong NF186 binding even at 1:64 dilution (4.6 µg/mL), whereas its IgG1 counterpart's reactivity to both NF155 and NF186 was lost by 1:32 (43.8 µg/mL) and 1:16 (87.5 µg/mL), respectively. The 5A6 lambda IgM mAb exhibited stronger, broader reactivity than its IgG1 counterpart, maintaining NF155 and NF186 binding at the lowest tested concentrations (2.6-5.2 µg/mL), while the IgG1 format's reactivity dropped out by 392.5 µg/mL (NF155) and 785 µg/mL (NF186). The 5A6 kappa IgM mAb displayed weak NF155 binding at neat concentration but no reactivity at higher dilutions, with minimal or absent NF186 signal.

A comprehensive summary of antigen-specific reactivities observed in supernatants and their corresponding mAbs is presented in Table 17. Notably, both the 4G2 and 5A6 clones demonstrated broader reactivity profiles in their mAb formats than in their original supernatants. For example, the 4G2 IgG1 and IgM mAbs both reacted to NF155 and NF186, whereas the original supernatant displayed strong NF186 and barely detectable NF155 binding (not considered positive at the time compared to controls). Similarly, the 5A6 mAbs (particularly the lambda variant) bound both NF155 and NF186, contrasting with the supernatant, which bound NF155 only. However, the 5A6 kappa IgG1 mAb maintained consistency with the supernatant, showing only weak NF155 reactivity and no detectable NF186 binding.

	Sample supernatants				**mAbs**			
	IgM		**IgG**		**IgM**		**IgG**	
	NF155	**NF186**	**NF155**	**NF186**	**NF155**	**NF186**	**NF155**	**NF186**
1H1	+	-	-	-				
1B1	?	+	-	-				
1E10	+	-	-	-				
1E9	+	+	-	-				
1F10	-	?	?					
1F12	-	-	?	-				
2B2	+	-	-	-				
3F11	+	-	-	-				
4D1	?	+	-	-				
4H7	+	-	-	-				
4H9	+	?	-	-				
5E1	+	-	-	-				
5E10	+	+	-	?				
3G2	-	-	-	+ (weak)	Could not recover productive heavy chain sequence			
4G2	-	+ (very strong)	-	+ (very strong)	+ (very weak)	+ (very strong)	+ (moderate)	+ (moderate)
5A6 κ	+	-	+ (moderate)	-	+ (weak)	+ (very weak)	+ (very weak)	-

5A6 λ					+ (very strong)	+ (very strong)	+ (strong)	+ (very weak)

Table 17: Summary of neurofascin-specific IgM and IgG reactivity across single-cell supernatants and corresponding mAbs. *Supernatants from 480 single-cell wells were screened by live CBA for reactivity to NF155 and NF186 using isotype-specific secondary antibodies. IgM and IgG reactivity are listed separately for each antigen. Wells that yielded productive VH and VL sequences were reconstructed as IgM and IgG1 mAbs and retested for antigen binding. Reactivity is denoted as positive (+), negative (−), or ambiguous (?), with semi-quantitative strength assessments (e.g. "very strong", "strong", "moderate", "weak", "very weak") based on relative fluorescence intensity and pattern.*

4.8 IgM screen of pan-NF$^+$ and CNTN1$^+$ AN patients

To assess whether the IgM autoantibodies identified in the pan-NF$^+$ patient represented a broader trend within this disease subtype, 13 serum samples from 8 patients in the pan-NF$^+$ cohort (SR1053, SR1077, SR1091, SR1092, SR1114, SR2348, SR3148, SR3161, SR2416, SR2167, SR2432, SR2988, SR3001) were screened for IgM reactivity to NF155 and NF186. All 13 samples from all 8 patients (100%) tested positive for IgM-class autoantibodies against both antigens (a score of >0.5 was considered positive). In contrast, screening of 19 serum samples from 6 patients with confirmed CNTN1$^+$ AN (SR259, SR366, SR835, SR974, SR2996, SR3212, SR3340, SR211, SR323, SR443, SR251, SR408, SR765, SR3108, SR056, SR3337, SR2273, SR2647, SR2732) detected IgM-class reactivity against CNTN1 in only 3 samples (15.8%). These results suggest a higher prevalence of IgM-class autoreactivity in pan-NF$^+$ patients compared to CNTN1$^+$ patients ($p < 0.001$, Fisher's exact test). All screening was conducted by Emma Tan. Additional patient details are included in Table 1.

4.9 Summary and interpretation of findings

4.9.1 Key experimental findings

The work presented in this chapter successfully employed single-cell sorting and culture approaches to isolate rare autoreactive B-cell clones from a pan-NF^+ patient, contrasting with the low recovery of antigen-specific clones observed in bulk cultures.

A central finding was the predominance of IgM-class autoreactive clones. Out of 480 single $CD27^+IgD^-$ memory B-cell cultures screened from the pan-NF^+ patient, 13 (2.71%) demonstrated clear antigen-specific IgM reactivity, while only 3 (0.63%) exhibited detectable IgG reactivity. The presence of pan-NF-reactive supernatants was exclusively confined to the IgM isotype (2 wells, 0.42%), whereas no IgG pan-NF^+ clones were identified. This predominance of IgM-class reactivity among antigen-specific clones suggests that autoreactivity to neurofascin in this patient may be preferentially mediated by unswitched or minimally mutated B-cell compartments. However, it remains unclear whether these cells represent natural IgM producers (eg, B-1 cells), precursors to class-switched IgG autoreactive B cells, or are themselves pathogenic effectors. Additionally, the finding that the majority of recovered antigen-specific antibody-secreting cells (ASCs) secreted IgM rather than IgG, despite a $CD27^+IgD^-$ "switched" memory phenotype, highlights the importance of functional readouts, as phenotype markers alone may not reliably predict class-switch status or effector potential, particularly in autoimmune contexts.

Recombinant mAbs derived from antigen-specific clones further corroborated these findings. While IgG1 mAbs generated from the sequences of clones 4G2 and 5A6 (including both kappa and lambda light chain constructs) initially failed to demonstrate

detectable neurofascin binding via CBA or ELISA at standard testing concentrations (10-0.02 µg/mL), later testing undiluted (1570-640 µg/mL) revealed measurable reactivity. However, these signals were markedly weaker and less sustained than those observed for the corresponding IgM mAbs at much lower concentrations.

The IgM mAbs exhibited clear and robust binding: the 4G2 IgM mAb bound strongly and specifically to NF186, maintaining detectable signal down to a concentration of 4.6 µg/mL. The 5A6 lambda IgM mAb demonstrated dual reactivity to both NF155 and NF186, with NF186 binding detectable at 20.6 µg/mL, suggesting an expansion of antigen reactivity beyond what was evident in the supernatant. In contrast, the 5A6 kappa light chain IgM variant exhibited minimal or absent reactivity, consistent with weak performance in prior supernatant screens.[2]

Nonetheless, these head-to-head comparisons between IgG1 and IgM mAbs under matched testing conditions provided critical insights. While the IgG1 mAbs retained some detectable binding unconcentrated, their reactivity dropped off rapidly upon dilution, losing signal at much higher concentrations compared to the sustained and stronger binding of the IgM mAbs (Figure 43). This suggests that the IgM format offers enhanced avidity or accessibility for neurofascin epitopes, potentially due to multivalency or conformational effects, and highlights isotype as a key determinant of antigen binding.

[2] While concentrations are expressed in mass/volume terms, it is important to note that IgM has a substantially higher molecular weight than IgG1. Thus, molar concentrations – and therefore the number of antigen-binding sites – differ between isotypes at equivalent µg/mL concentrations. Direct molar comparisons would be necessary to precisely quantify differences in binding efficiency or avidity.

Importantly, these findings represent the first documented evidence of pan-NF-specific autoreactive B-cell clones producing functional IgM autoantibodies. While prior studies have focused predominantly on IgG isotypes in autoimmune nodopathies, this work demonstrates that rare autoreactive B cells can retain IgM isotype expression, expanding the spectrum of potential humoral contributors to disease beyond the IgG subclasses historically associated with nodopathies. This novel observation broadens the current understanding of humoral autoimmunity in AN and highlights the need for further research into the contribution of IgM to disease pathogenesis.

These results were complemented by serological screening, in which sera from all 8 pan-NF$^+$ patients/13 serum samples demonstrated universal IgM-class reactivity to NF155 and NF186, in stark contrast to the limited IgM reactivity (3/19; 15.8%) observed in serum samples from 6 CNTN1$^+$ AN patients. This supports the presence of circulating IgM anti-neurofascin antibodies as a consistent feature of pan-NF AN. Together with the culture data, which showed IgM secretion from memory B cells, these findings imply the coexistence of both unswitched neurofascin-reactive B cells and active IgM$^+$ neurofascin-secreting ASCs in pan-NF$^+$ patients. While class-switch recombination (CSR) often precedes differentiation to ASCs, the detection of circulating IgM suggests that either IgM$^+$ LLPCs or recurrent bursts of short-lived plasmablasts contribute to ongoing IgM autoantibody production. Clarifying the origin, longevity, and functional role of these IgM-producing cells will be critical for understanding their place in disease pathogenesis.

Taken together, these findings provide compelling evidence that autoreactive B-cell clones specific to neurofascin are rare and predominantly unswitched in pan-NF$^+$ AN.

The combination of single-cell culture, immunogenetic sequencing, and functional mAb generation was essential for revealing this pattern, highlighting the critical role of high-resolution approaches in uncovering rare autoreactive populations that may otherwise be masked in bulk cultures.

4.9.2 Interpretation of experimental outcomes

The findings presented in this chapter highlight the critical role of isotype and high-resolution single-cell approaches in uncovering the nature of neurofascin autoreactivity in pan-NF^{+} AN. The predominance of IgM-reactive clones among neurofascin-specific B cells, combined with the limited IgG reactivity observed in both bulk and single-cell formats, raises the possibility that IgM autoantibodies contribute to humoral autoreactivity in this disease subtype. However, it remains unclear whether these antibodies represent pathogenic effectors, natural polyreactive clones, or biomarkers of broader immunological defects. Given the limited screening of healthy controls, it is also possible that low-affinity neurofascin-reactive IgM is present in the general population, but lacks disease relevance, as observed in other autoimmune contexts such as CASPR2 autoimmunity, where healthy individuals may harbour autoreactive B cells without exhibiting high-affinity, memory-derived specificities.[110]

In bulk cultures, total IgG production was low and antigen-specific responses were minimal. The detection of a single NF155-specific well from the switched memory subset of the pan-NF^{+} patient (absent in CASPR2^{+} cultures) suggests that while the stimulation protocol could induce polyclonal IgG secretion, it was insufficient for robust expansion or detection of autoreactive clones in bulk formats. This discrepancy

underscores the need for single-cell resolution approaches to identify rare, antigen-specific cells that may be obscured in polyclonal settings.

The transition to single-cell culture enabled the isolation of rare autoreactive clones, providing clear evidence that neurofascin-specific reactivity in this pan-NF^+ patient appears to arise predominantly from B cells that secrete IgM *in vitro*. Although these cells were sorted as $CD27^+IgD^-$ memory B cells, typically associated with prior class switching, the presence of IgM secretion suggests either incomplete switching, misclassification at the gating stage, or the existence of rare IgD^-IgM^+ populations that may contribute to autoreactivity. Since no surface IgM staining was performed at the time of sort, the true isotype profile of the starting cells remains unresolved, and this limits definitive conclusions about their maturation state. However, negative (non-autoreactive) single $CD27^+IgD^-$ memory B cells from the same sort displayed expected levels of somatic hypermutation based on their surface phenotype, reducing the likelihood the observed effects in culture were due to complete misclassification during sorting, although the possibility that some cells within this gate were truly IgD^+ remains. Incorporating additional markers such as CD11c, FCRL5, or T-bet in future sorts could additionally reveal a more comprehensive view of the autoreactive repertoire.

Notably, the identification of dual-reactive (pan-NF^+) clones exclusively among IgM-secreting clones, and the absence of such reactivity in the IgG format, points to potential isotype-specific differences in binding. This pattern is consistent with the retrospective discovery of IgM transcripts in clone 5A6 and the failure of corresponding IgG1 mAbs to bind antigen, despite confirmed protein expression. These observations suggest that CSR does not necessarily preserve antigen-binding function, and that the IgM isotype

may confer structural or avidity-related advantages, such as multivalency or conformational plasticity, that facilitate recognition of NF155 and NF186 epitopes.

A notable observation from the head-to-head comparison of IgG1 and IgM mAbs was the emergence of antigen reactivities that had not been previously detected in the initial round of testing (Figure 41). For example, the 4G2 IgG1 mAb demonstrated weak NF155 binding that was absent before, and the 5A6 kappa IgM mAb revealed reactivity to both NF155 and NF186. These differences likely reflected improved assay sensitivity in the matched head-to-head format, where consistent serial dilutions, standardised plate conditions, and careful minimisation of dilution artefacts (eg, from residual wash media) reduced variability. Changes in cell density or antigen expression between experiments may also have contributed to signal enhancement.

More broadly, these experiments demonstrated that IgM versions of each mAb consistently displayed stronger and more sustained neurofascin binding than their IgG1 counterparts. This phenomenon is likely attributable to differences in antibody structure and valency: IgM is secreted as a pentamer, conferring ten potential antigen-binding sites, whereas IgG1 is a monomer with only two binding sites, limiting its capacity for stable engagement with multivalent targets. The higher valency of IgM enhances overall avidity, enabling multiple low-affinity interactions to combine into a functionally high-avidity profile. Importantly, as the variable regions (which determine affinity) of each mAb remained identical across isotypes, these effects are unlikely to reflect affinity changes due to class switching. Rather, differences in constant region architecture, glycosylation, or conformational plasticity may influence antigen presentation and paratope orientation. Collectively, these data support a model in which the structural

features of IgM enhance apparent reactivity and allow for more sensitive detection of weak autoreactive clones.

A further technical consideration is that IgG subclass identity was not determined prior to cloning the individual IgG^+ autoreactive clones into IgG1 backbones. This approach was selected based on the pan-NF AN patient's serological profile, which was dominated by IgG1-class autoantibodies. However, neither IgG1 nor IgG2 was detected in the culture supernatant of clone 5A6 when re-screened for IgM and IgG subclasses later, raising the possibility that its native subclass may have differed. Although the reconstructed mAbs shared identical variable regions, mismatching subclass usage – such as forcing expression in an IgG1 format when the native clone may have used IgG3 or IgG4 – could influence binding behaviour. Differences between IgG subclasses, including hinge length, flexibility, and Fc conformation may affect the spatial orientation of antigen-binding domains and thus impact epitope accessibility, especially for conformational targets like NF155 and NF186. Accordingly, failure to preserve native subclass could have contributed to the reduced or only weak binding observed for 5A6 in the IgG1 format.

The serological screen of pan-NF^+ and $CNTN1^+$ patient sera adds contextual support to the observed IgM findings, demonstrating universal IgM-class reactivity in pan-NF^+ patients but minimal IgM in $CNTN1^+$ cases. While this cannot confirm cellular origin or pathogenic relevance, it aligns with the notion that IgM reactivity may be a consistent serological feature in pan-NF^+ AN.

Additionally, the presence of kappa light chains in all neurofascin-reactive clones, the absence of somatic hypermutation in these autoreactive cells, and the detection of dual

light (kappa and lambda) and heavy (IgG and IgM) chain transcripts in clone 5A6 provide important clues about the developmental origin of these clones. The co-expression of IgG and IgM transcripts in this context also offers supporting evidence for active or recent CSR occurring *in vitro* under the stimulation conditions used. The low or absent SHM suggests that autoreactive B cells in pan-NF^+ AN may emerge through non-canonical, extrafollicular pathways, bypassing germinal centre (GC) selection and affinity maturation. This is consistent with models of autoimmunity where early tolerance defects permit the survival of self-reactive clones, particularly in chronic, relapsing disease contexts.[41,111–114]

The failure to detect CASPR2-specific B cells in this patient's single-cell culture, despite confirmed prior detection using similar culture protocols, may reflect stochastic sampling limitations rather than true absence. Previous work indicated a frequency of CASPR2-reactive clones between 1 in 500 and 1 in 1000; thus, the number of single cells tested here may have been insufficient to capture them reliably. This highlights the need for higher-throughput screens or enrichment strategies when investigating low-frequency autoreactive clones.

In summary, the experimental data from this chapter indicate that neurofascin-specific autoreactive B-cell clones in pan-NF^+ AN are rare, predominantly IgM-expressing, and likely emerge through non-classical developmental pathways. The reduced binding of IgG1 mAbs compared to their IgM counterparts highlights the need to consider isotype when investigating autoreactive clones, as isotype switching may compromise antigen binding properties. This likely reflects the enhanced avidity conferred by the pentameric structure of IgM, which allows stronger binding to multivalent antigens, whereas the

monomeric IgG1 format may be insufficient to replicate native autoreactivity *in vitro*. The absence of CASPR2-specific clones in single-cell culture may reflect differences in the predominant B-cell subsets responsible for IgG secretion in each disease, as well as differences in detectable frequencies. These findings underscore the importance of optimising recovery strategies tailored to each target and reinforce the value of high-resolution functional readouts across distinct B-cell compartments.

4.9.3 Limitations and future directions

While the experiments presented in this chapter have provided important insights into neurofascin autoreactivity in pan-NF^+ AN, several limitations remain, offering clear directions for future investigation.

A central limitation of the sequencing strategy was the use of Sanger sequencing alone for the negative control clones using IgG-specific primers, which likely biased recovery towards IgG transcripts and may have underestimated the prevalence of native IgM expression in the negative controls. Nanopore sequencing was applied only to initially identified IgG antigen-reactive clones, leaving the possibility that dual isotype expression, such as that observed for 5A6, might be more widespread. Future work should employ isotype-agnostic, unbiased sequencing methods to capture the full breadth of autoreactive B-cell repertoires.

The failure to recover a productive heavy chain sequence from clone 3G2, combined with the absence of an IgM version of this clone, limited conclusions regarding its full reactivity potential. It remains an open question whether generating an IgM recombinant version of 3G2 might reveal hidden antigen binding capacity. While the work presented here prioritised focusing on clones from which productive sequences and mAbs could

be generated, future efforts should aim to recover complete VDJ sequences from such incomplete clones and systematically test their functionality in multiple isotype contexts.

The functional mAb analyses revealed that IgG1 versions of autoreactive clones consistently displayed lower apparent binding strength than their IgM counterparts, detectable only when tested undiluted and dropping out rapidly upon dilution. This observation raises the possibility that isotype switching may influence apparent avidity or affinity, potentially due to the monomeric versus pentameric antibody architecture or to isotype-specific conformational constraints. Generating monomeric IgM versions of these mAbs would provide a direct test of whether the higher binding strength observed for IgM reflects structural valency or other factors.

Another limitation was the absence of specificity testing of the recombinant mAbs against alternative targets. Without such controls, it remains possible that some observed binding may reflect polyreactivity and/or low-affinity interactions, rather than restricted neurofascin specificity. Future experiments should incorporate both testing against mock- or irrelevant-transfected HEK293T cells to confirm target specificity and use epitope mapping strategies (eg, domain deletion constructs or peptide-based approaches) to define the precise binding sites of neurofascin-reactive mAbs.

Moreover, the pooled supernatant screening strategy likely masked low-abundance antigen-specific reactivity. Employing unpooled or more sensitive detection methods, such as bead-based multiplexed assays, in the future will enhance the likelihood of detecting rare autoreactive clones.

In vitro culture conditions may also fail to fully replicate the *in vivo* environment of autoreactive B-cell development and activation. Factors such as post-translational modifications, multivalent antigen presentation, and local cytokine context might all influence binding outcomes. Direct *ex vivo* analyses of B-cell receptor (BCR) repertoires from relevant tissues, such as nerve biopsies or lymph nodes, and exploration of patient human leukocyte antigen (HLA) characteristics could yield complementary insights.

Finally, while the detection of pan-NF-specific IgM clones and corresponding serum reactivity in pan-NF$^+$ patients represents a key advance, these findings were based on CD27$^+$IgD$^-$ memory B-cell cultures from a single patient. Expanding these approaches to additional B-cell subsets, as well as additional patients with pan-NF$^+$ and other nodopathy subtypes, will be essential to determine the generalisability of these results. Furthermore, assessing whether patients with more severe disease exhibit stronger autoreactive clone binding or distinct B-cell profiles could provide clinically relevant correlations.

4.9.4 Summary

This chapter has provided a detailed examination of autoreactive B-cell populations in pan-NF$^+$ AN, leveraging single-cell sorting, culture, and functional characterisation to dissect isotype-dependent neurofascin reactivity. Neurofascin-specific clones exhibited a striking predominance of IgM secretion, with pan-NF-reactive clones identified exclusively within this isotype and absent in IgG screens. Furthermore, IgM mAbs derived from these clones showed robust and sustained binding to both NF155 and NF186. In contrast, matched IgG1 mAbs derived from the same VH/VL sequences

exhibited only weak or transient reactivity, detectable only at high concentrations and lost rapidly upon dilution. These findings highlight the critical influence of isotype on functional antibody behaviour, with structural features of IgM, particularly multivalency, likely enhancing avidity and enabling detectable autoreactivity. This underscores the importance of reconstructing antibodies in their native isotype when assessing autoreactive function. Moreover, the limited detection of antigen-specific clones in bulk cultures may reflect not only their potential intrinsic rarity, but also the potential masking effects of polyclonal stimulation, suboptimal differentiation, or lower per-cell antibody output. This emphasises the unique resolution afforded by single-cell approaches.

The comprehensive serological analysis, revealing universal IgM-class reactivity among pan-NF^+ patients but minimal reactivity in $CNTN1^+$ cases, strengthens the hypothesis that IgM autoreactivity is a defining feature of this disease subtype. These observations provide a mechanistic framework to inform future research, suggesting that autoreactive clones may arise through non-canonical pathways and that IgM-dominated responses may represent an important immunological feature of this inflammatory neuropathy subtype, though their pathogenic role remains to be determined.

These findings underscore the rarity and isotype-dependent nature of autoreactive clones, highlighting the necessity of innovative enrichment approaches agnostic to isotype or originating subpopulation. To this end, the following chapter details the development and application of custom antigen baits to selectively capture and characterise these elusive clones.

5 Development of NF155 and NF186 Antigen Baits for Enrichment of Pan-Neurofascin-Reactive B Cells

5.1 Introduction

The isolation and characterisation of autoreactive B cells represents a critical challenge in understanding the immunopathology of autoimmune nodopathy (AN) associated with pan-neurofascin-positive (pan-NF^+) autoantibodies. Despite the development of optimised culture conditions capable of supporting total IgG production, antigen-specific responses against NF155 and NF186 remained exceedingly rare, with only 1 bulk-sorted culture well producing detectable NF155-specific IgG and none for NF186. Further highlighting the limitations of conventional sorting methods, single-cell sorting experiments identified NF186-reactive IgG^+ B cells in only 0.4% (2/480 wells) of single $CD27^+IgD^-$ memory B cells from a pan-NF AN patient and NF155-reactive IgG^+ B cells in only 0.2% (1/480 wells). This rarity and the low sensitivity of standard techniques for detecting rare B-cell populations has limited opportunities for detailed analysis of antigen-specific B cells *in vitro* and necessitated the development of an alternative method to improve the efficiency of autoreactive B-cell isolation and subsequent ability to assess IgG autoantibodies. To address this, a method was developed to enrich for pan-NF-reactive B cells using biotinylated antigen bait tetramers, assembled around a streptavidin-fluorophore backbone to enhance binding avidity and improve sensitivity for rare cell detection.[90]

Antigen-specific B-cell enrichment techniques, including fluorescently labelled antigen probes, have been instrumental in studying rare B-cell populations by increasing

binding avidity and enabling high-resolution analyses of antigen-specific B-cell repertoires. The use of antigen tetramers specifically enhances the detection of B cells with low-affinity antigen receptors by presenting multivalent binding opportunities and reducing non-specific interactions.[31,57,86,111,112] This approach allows for the enrichment of antigen-specific B cells that might otherwise remain undetectable by standard monomeric antigen-based strategies.

The antigen baits described herein were designed to include the extracellular domains of NF155 and NF186, with a flexible linker and Avitag to enable enzymatic biotinylation. Control "dummy bait" tetramers were produced in parallel to exclude non-specific binding, allowing for improved discrimination of antigen-specific B cells. Initial experiments focused on establishing a culture protocol suitable for high yield and validation of neurofascin expression, followed by the development of biotinylation and purification protocols suitable for tetramer construction. Early trials using cobalt-based purification resulted in inconsistent yields and incomplete purification of the target proteins, leading to the adoption of a nickel-nitrilotriacetic acid (Ni-NTA) purification approach to improve protein recovery and quality.

Optimisation of the biotinylation reaction was required to achieve a precise 1:1 biotin-to-bait ratio, preventing bait protein aggregation and ensuring efficient incorporation into tetramer complexes. Subsequent large-scale production and functional validation demonstrated that the NF155 and NF186 baits bound patient autoantibodies more effectively than commercially available neurofascin proteins in ELISA assays. Although the antigen baits were not used in live B-cell sorting within this thesis, these findings supported their feasibility for future applications in isolating pan-NF-reactive B cells.

The following experiments assessed each stage of the antigen bait development process, including bait protein expression, purification, biotinylation efficiency, tetramer assembly, and functional validation.

5.2 Antigen bait approach, design, and plasmid production

5.2.1 Antigen baiting strategy

To enable enrichment of pan-NF-reactive B cells, a targeted antigen baiting approach was developed, incorporating site-specifically biotinylated NF155 and NF186 ectodomains for subsequent tetramerisation. The bait constructs included a C-terminal Avitag for BirA-mediated biotinylation, a His tag for affinity purification, and a flexible linker to preserve structural integrity (Figure 11). Following expression and biotinylation, baits were tetramerised on streptavidin-fluorophore backbones to generate fluorescent probes suitable for flow cytometry-based detection and isolation.

Control measures to ensure specificity included a dual-fluorophore labelling strategy (using PE and DyLight(DL)594) to restrict gating to true positive events and a “dummy bait” negative control to exclude B cells binding non-specifically to the streptavidin backbone. These design choices were implemented to minimise background noise and enhance the fidelity of B-cell identification.

Optimisation of bait production proceeded through eight iterative, small-scale trials, each refining expression, purification, or validation parameters (summarised in Table 18). These methodological adaptations aimed to generate reliable and specific antigen baits suitable for subsequent experiments, including their potential application in future B-cell sorting studies.

Trial #	Constructs tested	Purpose of trial	BirA co-transfection?	Biotin supplementation?	Purification resin used	Yield	Biotinylation result	NF expression on WB	Notes
1	NF155 only	Proof-of-concept expression of NF155	No	No	Cobalt	Low	Not applicable	Not tested	Proof-of-concept only
2	NF155 & NF186	Initial detection by Western blot	No	No	Cobalt	Low	Not applicable	Yes (NF155, faint)	Initial protein visualisation by WB
3	NF155 & NF186	Higher seeding density	No	No	Cobalt	Low	Not applicable	Yes (NF155, faint)	Confirmed bait present by WB, but not biotinylated
4	NF155 & NF186	Test co-transfection with BirA + cobalt purification	Yes	Yes	Cobalt	Moderate	Undetectable on pull-down; possible faint signal NF155 WB	NF155 faint; NF186 absent	Trialled co-transfection with BirA
5	NF155 & NF186	Switch to Ni-NTA purification; improve recovery	Yes	Yes	Ni-NTA	Moderate	Faint NF155 WB; NF186 absent	NF155 faint; NF186 absent	Switched to Ni-NTA resin; better Coomassie results
6	NF155 & NF186	Improve biotinylation with refined transfection	Yes	Yes	Ni-NTA	High	No signal (unpurified BirA)	No signal	Used unpurified BirA; high yield but no biotinylation
7	NF155 & NF186	Investigate intracellular retention of bait proteins	Yes	Yes	Ni-NTA	Low (esp. NF186)	No signal (likely due to low yield)	NF155 weak; NF186 absent	Tested lysates vs supernatants; NF155 detected only in supernatant
8	NF155 & NF186	Finalise protocol with fresh BirA and HEKs	Yes (fresh midi-prep)	Yes	Ni-NTA	High for both	Confirmed for both baits	Strong signal both	Fresh HEKs, fresh BirA, best yield and validation

Table 18: Summary of small-scale NF155 and NF186 antigen bait production trials. *Overview of eight iterative trials conducted to optimise the expression, purification, and biotinylation of recombinant NF155 and NF186 antigen bait proteins in HEK293T cells. Each row summarises key experimental variables and outcomes, including the constructs tested, co-transfection with BirA plasmid, biotin supplementation, purification resin choice, protein yield, biotinylation status, and Western blot validation of neurofascin expression. Early trials (1-3) used cobalt resin without biotinylation components and yielded faint or undetectable expression. Trials 4-7 introduced biotinylation reagents and transitioned to Ni-NTA purification, revealing key issues related to resin performance, transfection efficiency, and protein recovery. Trial 8 incorporated fresh low-passage HEK cells and freshly midi-prepped BirA plasmid, resulting in high yield, strong Western blot signal, and confirmed biotinylation for both constructs. These trials established the final optimised protocol used for large-scale bait production and tetramerisation. NF: neurofascin; E1: elution fraction 1; WB: Western blot; Ni-NTA: nickel-nitrilotriacetic acid.*

5.2.2 Plasmid synthesis and quality control

5.2.2.1 Synthesis and delivery

Antigen bait coding sequences for NF155 and NF186 were codon-optimised and synthesised by Twist Bioscience, then cloned into pTwist CMV WPRE Neo expression vectors. These vectors included ampicillin resistance for bacterial selection and a ColE1/pMB1/pBR322/pUC replication origin to ensure high plasmid yield. Detailed information regarding the nucleotide sequences of the antigen bait inserts and vector designs is available in Appendix 8.3. Constructs were delivered lyophilised in 2 µg quantities (NF155: Lot Number S_641b2b65d40deb5d492b148f; NF186: Lot Number S_641b2b65d40deb5d492b1490) and resuspended in nuclease-free Tris-EDTA (TE) buffer. No handling issues were encountered during solubilisation.

5.2.2.2 Sequence verification

Sequence fidelity was confirmed by Twist using next-generation sequencing (NGS), showing 100% concordance with design. Cloning junctions were verified as intact. Subsequent Sanger sequencing across coding regions, also performed by Twist, corroborated sequence accuracy and confirmed correct reading frame and absence of point mutations.

5.2.3 Plasmid amplification and purification

To support repeated transfections, plasmids were amplified via midi prep. Initial yields were suboptimal, particularly for NF186, necessitating protocol refinement.

5.2.3.1 Initial yields and limitations

In early attempts using standard lysis conditions and 100 mL culture volumes, NF155 yields were modest (~380 ng/µL), while NF186 consistently underperformed (~150-190 ng/µL). Variable lysis quality and growth inconsistency were suspected contributors. One NF186 culture yielded a cloudy yellow lysate, suggesting incomplete lysis.

5.2.3.2 Optimisation and improved recovery

Improved yields were achieved by scaling up overnight cultures to 1 L Duran bottles, consolidating bacterial pellets prior to lysis (for NF186), and pooling lysates before filtration. These adjustments enhanced consistency and reduced sample loss. Final concentrations reached 7552.65 ng/µL for NF155 and 2174.4 ng/µL for NF186, both suitable for downstream applications. Aliquots of the prepped plasmids were stored at -20°C long-term.

5.2.4 BirA plasmid preparation

For co-transfection, the BirA plasmid (courtesy of Dr Bo Sun) was amplified via midi prep following the same optimised approach. Due to equipment availability, starter cultures were split across two 500 mL Duran bottles. Combined pellets yielded a final concentration of 3414.6 ng/µL, providing sufficient material for all subsequent bait production experiments. Aliquots were stored at -20°C long-term.

5.3 Proof-of-concept small-scale production of antigen baits

To establish a robust and reproducible workflow for producing biotinylated antigen baits, initial experiments focused on optimising transfection, expression, and purification under small-scale adherent conditions in HEK293T cells. These trials aimed

to confirm that bait proteins were (1) expressed and secreted; (2) properly folded and detectable; and (3) biotinylated in a manner compatible with streptavidin-based downstream applications. Refinement of transfection parameters, purification strategies, and buffer exchange methods was necessary to minimise protein loss and maximise yield prior to proceeding to large-scale production.

5.3.1 Optimisation of bait protein expression and purification

5.3.1.1 Initial expression attempts without biotinylation

Early expression trials omitted BirA co-transfection and biotin supplementation in order to test whether the NF155 and NF186 constructs were intrinsically capable of secretion and detectable expression, without introducing the added variables of *in vivo* biotinylation. These trials also allowed preliminary optimisation of seeding densities and transfection timing.

In the first trial, HEK293T cells were seeded at 3.125×10^5 cells per T25 flask, a scaled-up approximation from a 24-well protocol. This density was selected to reach optimal transfection confluency (~70%) by day 2, but cells were still under-confluent and were left to grow over the weekend. By day 5, cultures were severely overgrown, with widespread cell death likely due to nutrient depletion, necessitating termination of the trial.

To address this, a second trial tested higher seeding densities (6.58×10^5 and 1×10^6 cells/flask) to better approximate confluency by day 2. These flasks remained sub-confluent through day 7, but transfections were performed using DNA and PEI mixed in culture media (rather than PBS or OptiMEM), due to time constraints. This mixing

method possibly impaired PEI-DNA complexation. Supernatants were harvested on day 9 and frozen for later analysis without immediate validation.

A third trial used a substantially higher seeding density ($3x10^6$ cells/flask) to reliably achieve ~80–90% confluency by day 3. Transfections were performed using standard PEI-DNA protocols, and supernatants were harvested on day 6. These were processed with those from Trial 2 and clarified by two-step centrifugation and filtration (as described in section 2.12.2.1).

Western blotting using an anti-neurofascin antibody followed by streptavidin-horseradish peroxidase (HRP) detection revealed bands corresponding to NF155 and NF186 (Figure 44). This confirmed that the constructs could be secreted and partially detected, despite the absence of affinity purification. However, the blots also highlighted several limitations: weak signal intensity and occasional bleed-through from positive control lanes complicated interpretation, and NF186 detection was inconsistent. These results indicated low yield and raised concerns regarding protein concentration, folding, and stability. Importantly, the absence of biotinylation or affinity purification limited sensitivity and precluded any quantitative assessment.

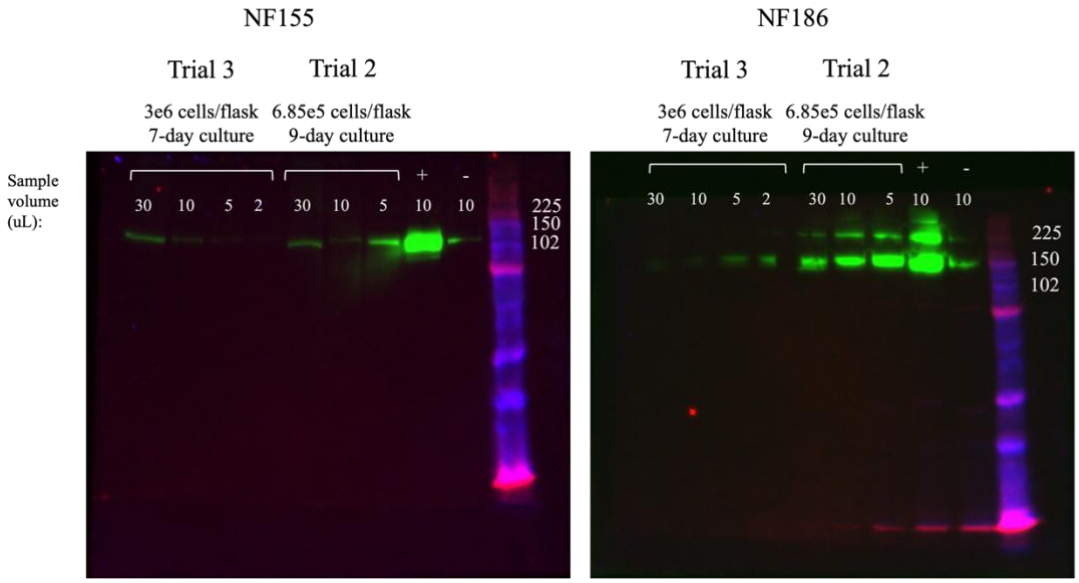

Figure 44: Detection of neurofascin expression in small-scale bait supernatants by Western blotting (Trials 2 and 3). *Western blot analysis of HEK293T supernatants from small-scale bait production trials using chicken anti-neurofascin primary antibody (1:3000), biotinylated goat anti-chicken secondary antibody (1:10,000), and streptavidin-HRP tertiary antibody (1:5000) detection with 10-well Bolt Bis-Tris Plus Mini Protein Gels, 4-12%. Protein harvested from Trials 2 and 3 was concentrated and sterile-filtered before gel loading. 1 µg of commercial NF155 and NF186 proteins were used as positive controls (denoted by "+") and untransfected HEK supernatant was used as a negative control (denoted by "-") to rule out detection of endogenous neurofascin produced by HEKs. Ladder is present in the right-most lane of each blot, with molecular weights marked. Bands corresponding to NF155 and NF186 extracellular domains were faint but present, particularly from Trial 2, confirming secretion of both bait proteins in the absence of biotinylation. Bands decreased in intensity as expected based on decreased sample loading volume. Blot artefacts included control lane signal bleed and unexpected variability in some band intensity at low concentrations, likely due to that bleed-over of control lanes. These results confirmed proof-of-concept expression but suggested low yield and inconsistent NF186 detection.*

These findings informed several refinements for subsequent trials: (1) standardised transfection timing at defined confluency; (2) incorporation of BirA and biotin to enable affinity purification and streptavidin-based quality control; and (3) improved blotting technique and control placement to avoid interpretative artefacts.

5.3.1.2 Co-transfection with BirA and biotin supplementation

Trial 4 was the first to introduce co-transfection with BirA plasmid and supplementation with exogenous biotin to facilitate *in vivo* enzymatic biotinylation of the antigen baits at the AviTag sequence. This was a critical step for enabling streptavidin-based tetramer formation in downstream applications.

Flasks were seeded with $0.8x10^6$ cells, aligning with recommended densities for JetPEI transfection. This adjustment was made in an attempt to align transfection conditions with those previously used for BirA co-transfection, given uncertainties surrounding the optimal conditions for simultaneous antigen bait expression and biotinylation. However, only ~45% confluency was reached by day 2, leading to a delay in transfection until day 4. By then, cells were over-confluent (>98%), which likely reduced transfection efficiency due to decreased proliferation and cell surface accessibility, but transfection was proceeded with anyway.

The transfection protocol involved co-delivery of antigen plasmid and 1.95 µg of BirA plasmid per flask, a quantity scaled up from an earlier 6-well protocol (Dr Bo Sun). Media was supplemented with 0.1 mM D-biotin to provide sufficient substrate for BirA-mediated post-translational biotinylation. This dual strategy was intended to allow for *in situ* generation of biotin-tagged bait proteins in the secretory pathway.

Supernatants were harvested on day 7, clarified, and filtered prior to purification with cobalt-based immobilised metal affinity chromatography (IMAC) resin. This resin was chosen based on prior in-lab experience and was evaluated as a possible alternative to Ni-NTA, with the aim of reducing background binding. Three elution fractions were collected: E1, E2, and E3. Duplicate Nanodrop readings of the E3 fraction revealed modest protein concentrations (average NF155: 193.2 µg/mL; average NF186: 329.5 µg/mL). Due to scheduling constraints, eluates were subsequently stored at -80°C without immediate buffer exchange.

Approximately one month later, buffer exchange and analysis was performed only on the frozen, purified E3 elution fraction due to a shortage of centrifugal filters – a

decision later identified as suboptimal, as His-tagged proteins typically elute in E1 or E2, so it was likely that the bulk of the bait protein had been missed. When additional Amicon filters became available, the cobalt-purified E1 and E2 fractions were buffer exchanged for downstream analysis. Triplicate Nanodrop readings confirmed the majority of each protein was contained in the E1 fraction (average values provided here):

- **NF155 E1:** 315 µg/mL
- **NF155 E2:** 142 µg/mL
- **NF186 E1:** 362 µg/mL
- **NF186 E2:** 246 µg/mL

5.3.1.3 Evaluation of cobalt resin purification

To assess biotinylation, a streptavidin pull-down assay was performed on the E1 and E2 fractions combined. However, pull-down efficiency appeared poor based on the subsequent Coomassie results, which showed no visible bait bands in the pulled-down samples (Figure 45). The lack of band for the positive control suggested technical challenges with the streptavidin pull-down itself.

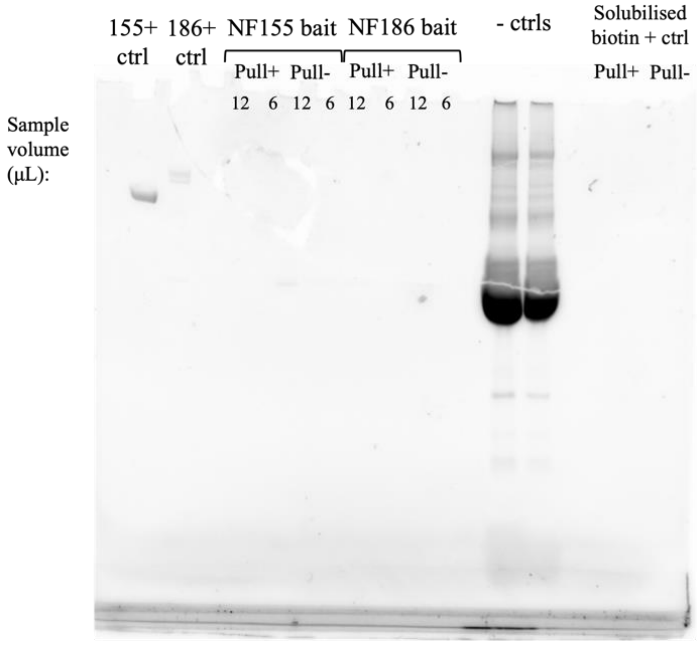

Figure 45: Coomassie-stained gel following streptavidin pull-down of Trial 4 cobalt-purified eluates. *SDS-PAGE gel stained with Imperial Protein Stain following streptavidin bead pull-down of cobalt-purified fractions E1 and E2 combined from Trial 4. 1 µg each of commercial proteins was used in the two left-most wells as positive controls. Samples subjected to streptavidin pull-down ("Pull+") were compared to samples that were not subjected to streptavidin pull-down ("Pull-") as internal controls for both baits. Untransfected HEK supernatant (unpurified) was also tested in duplicate as an additional negative control ("- ctrls"). Finally, 12 mg of solubilised EZ-Link Sulfo-NHS-SS-Biotin in 5 mL of PBS was used as an additional positive control in the right-most two lanes ("Solubilised biotin + ctrl"); one sample was subjected to streptavidin pull-down, the other was not. Despite co-transfection with BirA and biotin supplementation, no visible bands were observed in lanes corresponding to streptavidin-captured bait proteins.*

In parallel, an ELISA using sera from pan-NF and NF155^{+} patients was performed on wells coated with 1 µg/mL of commercial neurofascin protein or antigen bait. Binding signals were low and variable, in contrast to commercial neurofascin proteins, indicating poor bait folding, insufficient coating concentration, or low bait protein yield (Figure 46).[3]

[3] Positivity thresholds in this ELISA were not calculated relative to coat-specific healthy control distributions, but rather relative to an average (and the standard deviation) of healthy control serum across all well coat types. A more rigorous approach, used in Trial 8, defined seropositivity separately for each coating condition as values exceeding 4 standard deviations above the mean OD of healthy controls tested on the same protein coat.

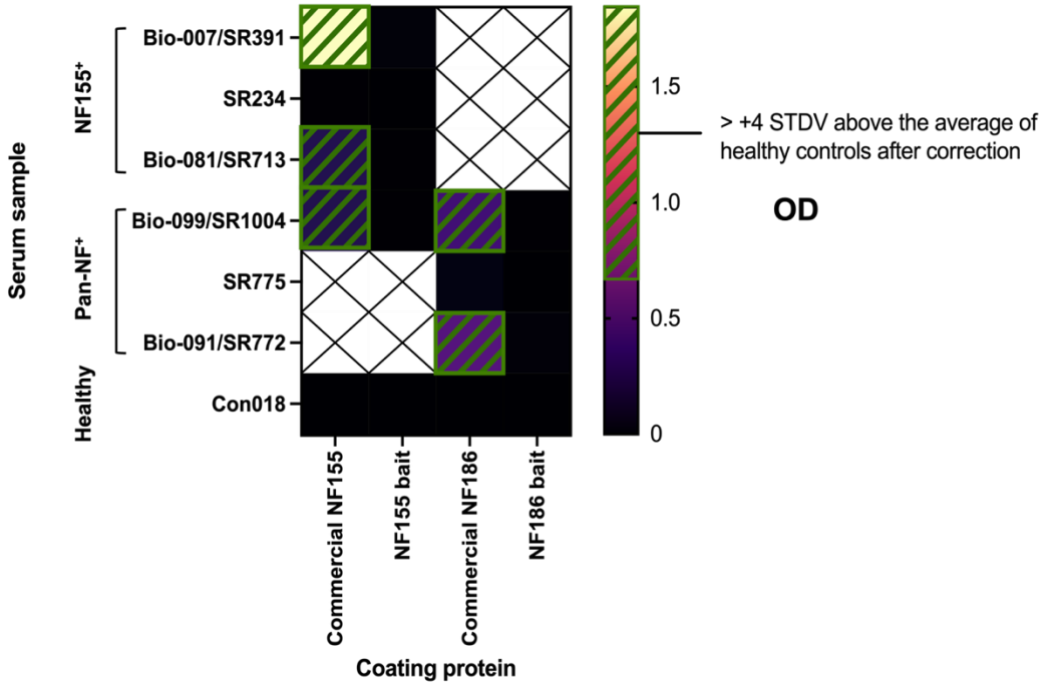

Figure 46: ELISA comparison of in-house antigen baits versus commercial proteins for NF155 and NF186 autoantibody detection. *ELISA assessing autoantibody binding to in-house produced NF155 and NF186 baits (Trial 4) versus commercial equivalents. Plates were coated with bait proteins or commercial proteins and incubated with sera from three NF155⁺ and three pan-NF⁺ patients, alongside one healthy control. To account for non-specific binding, the mean OD from PBS-coated wells testing each serum (not shown) was subtracted from each condition testing that same serum in triplicate. For each antigen coat, a positivity threshold was defined as ≥ 4 standard deviations (STDV) above the mean OD of the healthy control serum following background subtraction, indicated by a green hashed box. Each square represents the mean corrected OD of one sample tested in duplicate. Wells with an "X" indicate conditions that were not tested. While commercial antigens demonstrated robust discrimination between patients and controls, the in-house baits yielded minimal or inconsistent signals, failing to identify any samples as positive.*

A follow-up Coomassie gel was run to compare the purification wash fraction, buffer exchange flow-through fraction, final bait protein from the E1 purification fraction, and final bait protein from the E3 purification fraction to assess whether purification had been effective. Stronger bands were observed in E1 than E3, confirming that the bulk of the protein had eluted earlier (Figure 47). However, smearing and particulates in flow-through fractions and elution fractions around where bands would be expected raised concerns about insufficient purification.

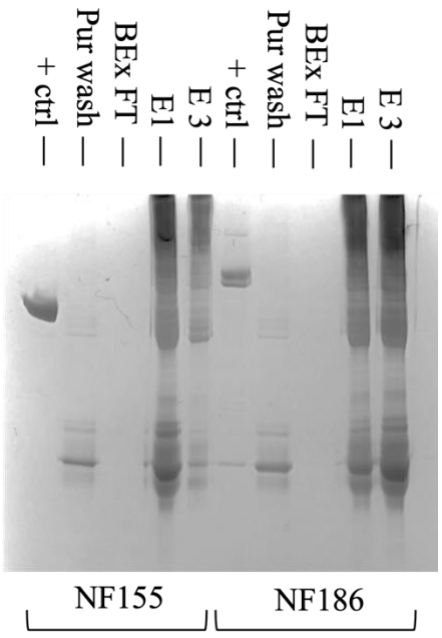

Figure 47: SDS-PAGE analysis of Trial 4 cobalt resin purification and buffer exchange fractions and antigen baits. *Coomassie-stained SDS-PAGE gel showing eluates and flow-through fractions from Trial 4. Commercial proteins were tested as positive controls for each bait ("+ ctrl"). 500 ng of each commercial protein and 15 µL (maximum volume possible) of each bait fraction was tested. The total volume in each well was 20 µL. Visible bands were most intense in baits buffer exchanged from the E1 purification fractions. Bait proteins buffer exchanged from purification fractions E1 and E3 exhibited smearing and variable protein content, indicating inconsistent recovery and potential protein aggregation or degradation. Pur wash: wash fraction before eluting the purified proteins. BEx FT: E1 buffer exchange flow-through fraction before isolating protein above the membrane. E1: final purified and buffer exchanged bait from the first purification elution fraction, where most, if not all, of the protein should be. E3: final purified and buffer exchanged bait from elution fraction 3, the last purification eluate where little to no protein should remain.*

These observations suggested that cobalt resin was suboptimal for purification under the conditions used. Poor bait recovery, low reproducibility, and weak ELISA performance justified a transition to Ni-NTA purification in the subsequent trial.

5.3.1.4 Transition to Ni-NTA purification and improved expression

In Trial 5, the workflow was revised to address the shortcomings of Trial 4. Ni-NTA resin was adopted for purification due to its broader compatibility with His-tagged proteins and higher binding capacity. Buffer exchange was performed immediately after elution to minimise protein degradation and avoid losses during storage.

Flasks were seeded at 1.2×10^6 cells to ensure optimal confluency for PEI transfection. As in Trial 4, transfection included co-delivery of the antigen construct and BirA plasmid, with 0.1 mM D-biotin added to the culture media to support enzymatic biotinylation. To improve transfection uniformity and reduce toxicity, PEI-DNA complexes were mixed in fresh media before being added to the flasks, rather than being added dropwise directly to the adherent culture inside the flask.

Cells remained healthy throughout, and supernatants were harvested and processed on day 5. Ni-NTA resin was incubated with bait-containing supernatants in batches, and three elution fractions were collected (E1-E3). E1 fractions were immediately buffer-exchanged, quantified by Nanodrop, and stored at -80°C for downstream analysis. While the NF155 bait had a moderate yield of 442 μg/mL, the yield of the NF186 bait was more modest at 183 μg/mL.

Trial 5 marked a key turning point in the optimisation pipeline, with improved expression, successful affinity purification, and increased consistency. These results enabled confident progression to further validation.

5.3.2 Validation of bait protein integrity and function

5.3.2.1 Streptavidin pull-down and Coomassie staining

To assess the success of the Ni-NTA purification protocol and evaluate whether bait proteins were biotinylated, a streptavidin pull-down followed by Coomassie staining was performed on buffer-exchanged E1 fractions from Trial 5. NF155 and NF186 baits (3 μg each in 150 μL buffer) were incubated on ice for 1 hour with or without streptavidin-coated magnetic beads. Sham samples (no beads) served as depletion controls. After incubation, 20 μL of each sample was resolved via SDS-PAGE and visualised using Coomassie stain.

Discrete bands at the expected molecular weights for both NF155 and NF186 were observed in all conditions (Figure 48), confirming the presence of properly purified, structurally intact bait proteins. This represented a marked improvement from the cobalt resin-purified baits in Trial 4. Bands were notably more prominent in E1 than previously seen in E3 fractions, validating the revised purification strategy. However,

no consistent depletion was observed in bead-incubated samples, suggesting incomplete biotinylation, suboptimal streptavidin interaction, or limited assay sensitivity.

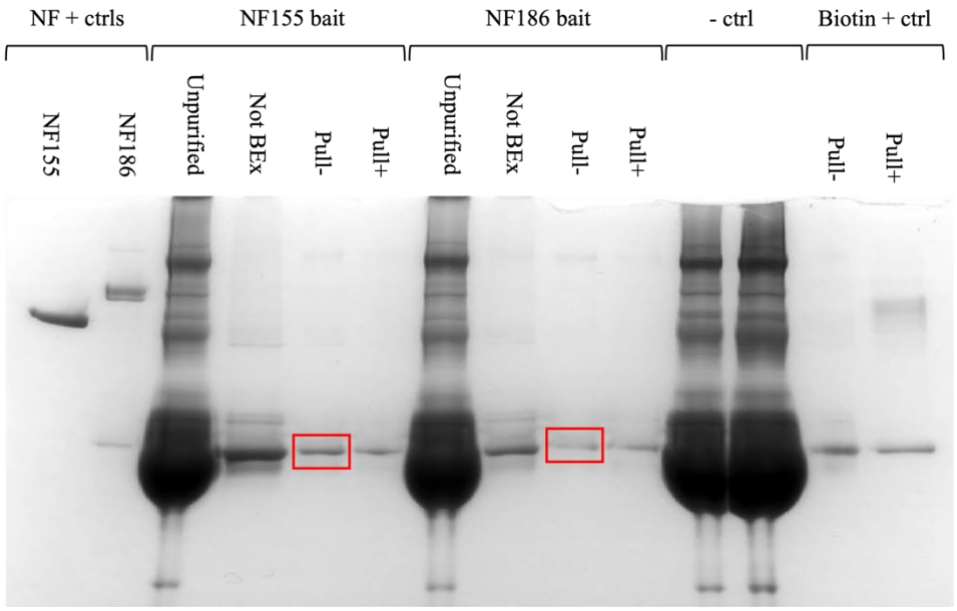

Figure 48: Coomassie-stained SDS-PAGE gel of Trial 5 E1 fractions of NF155 and NF186 bait proteins following Ni-NTA purification. *Bait samples from the first purification eluate fraction (E1) were incubated with (Pull+) and without (Pull-) streptavidin-coated beads to assess depletion as a proxy for biotinylation. Commercial NF155 and NF186 were tested in the left-most two lanes as positive controls for neurofascin (NF + ctrls), and a biotinylated goat anti-chicken antibody was subjected to streptavidin pull-down (Pull+) or not (Pull-) along with the baits and ran in the right-most two lanes as a positive control to assess effectiveness of the streptavidin pull-down (Biotin + ctrl). Furthermore, unpurified, untransfected HEK supernatant was run in duplicate as a negative control for the purification protocol (- ctrl). Overall, 800 ng of each commercial neurofascin protein and 12 µL of each bait protein (NF155: 5.3 µg, NF186: 2.2 µg), negative control, and biotin positive control was tested. Prominent bands at the approximate expected molecular weights for both baits confirmed successful expression and purification (outlined in red). No consistent decrease in band intensity was observed following streptavidin incubation, suggesting low biotinylation efficiency, incomplete pull-down by streptavidin, or assay insensitivity.*

5.3.2.2 Western blot validation of neurofascin expression and biotinylation

To validate antigen identity and biotinylation, parallel Western blots were performed using aliquots of Trial 5 bait proteins. Blots were probed with either chicken anti-neurofascin or streptavidin-HRP antibodies. A faint, but clear NF155 band was detectable on both (Figure 49A-B), confirming successful expression and biotin incorporation. In contrast, NF186 was not visible on either blot despite being detected (faintly) by Coomassie, suggesting poor biotinylation, instability, or quantification error. This discrepancy prompted further troubleshooting to determine whether NF186

was inherently more difficult to express or detect, or whether technical factors such as underloading were responsible.

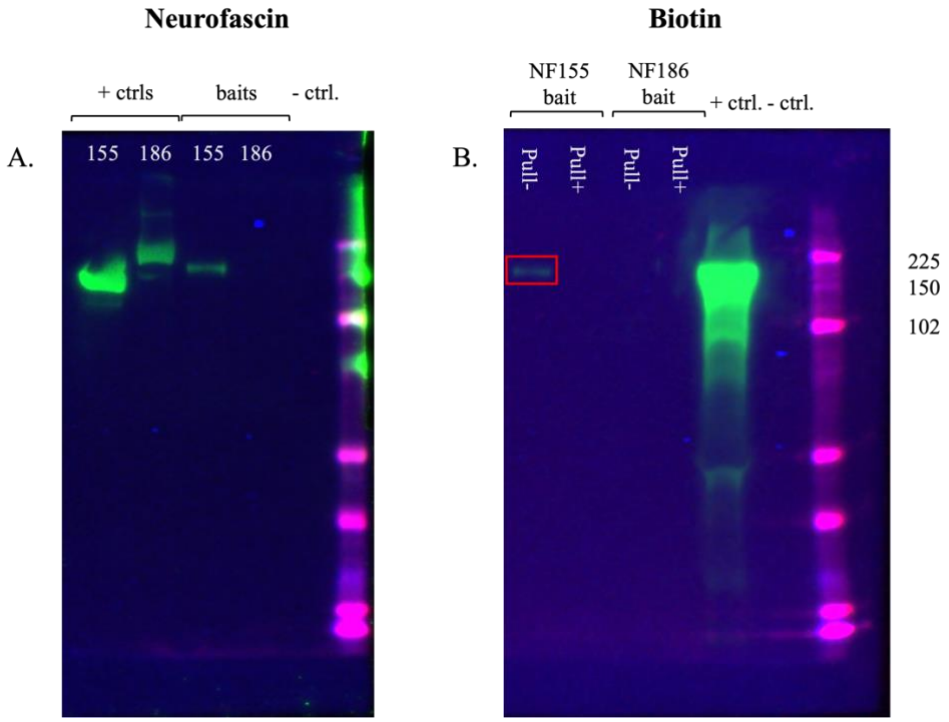

Figure 49: Western blots probing for neurofascin expression and biotinylation in Trial 5 bait proteins. *200 ng of each commercial protein and 250 ng of each bait were tested. Molecular weight markers are indicated on the right of the blots.* ***A:*** *Buffer-exchanged baits from E1 purification fractions and commercial neurofascin proteins as positive controls were separated by SDS-PAGE and blotted with chicken anti-neurofascin (1:3000), followed by goat anti-chicken HRP (1:4000). Untransfected HEK supernatant that had been purified and buffer exchanged using the same protocol as the baits was used as a negative control. A faint band was observed for NF155 at the expected molecular weight, confirming antigen expression. No band was detected for NF186.* ***B:*** *Identical samples as (A) were loaded – pulled down with streptavidin (Pull+) or not pulled down (Pull-) – and probed with streptavidin-HRP (1:5000) to detect biotinylated bait. A biotinylated goat anti-chicken antibody was used as a positive control, and the same purified and buffer exchanged, untransfected HEK supernatant was used as a negative control. A faint band was detected for NF155, confirming partial biotinylation; NF186 showed no detectable signal.*

5.3.2.3 ELISA assessment of bait function

To evaluate antigenicity and functionality, an ELISA was performed using Trial 5 baits as plate-coating antigens, alongside commercial NF155 and NF186 proteins. Patient sera ($NF155^+$ and pan-NF^+) were tested in parallel, as for the Trial 4 bait proteins described in section 5.3.1.3.

The Trial 5 baits yielded weak and inconsistent reactivity compared to commercial proteins (Figure 50), indicating limited antigen binding, possibly due to bait misfolding or low concentration.

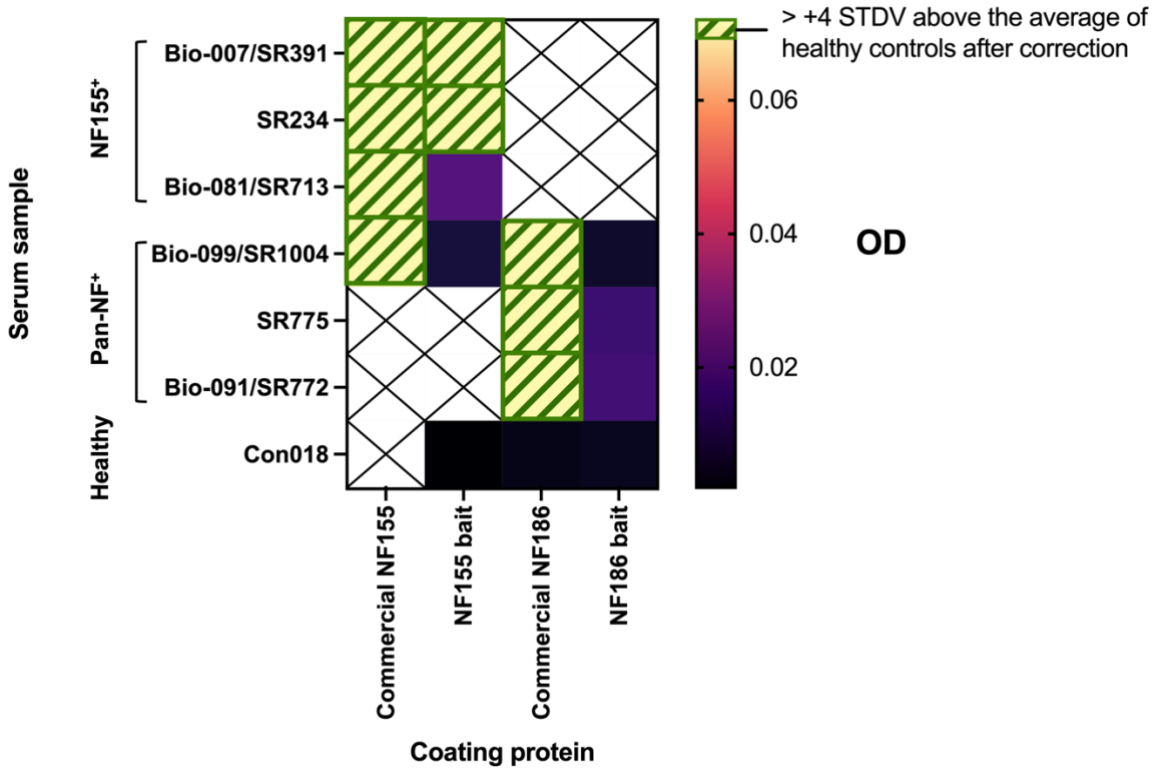

Figure 50: ELISA using Trial 5 NF155 and NF186 baits coated onto ELISA plates to assess autoantibody binding from pan-NF⁺ and NF155⁺ patient sera. *Plates were coated with baits buffer exchanged from E1 purification fractions and probed with sera from three NF155⁺ and three pan-NF⁺ patients; one of the pan-NF⁺ sera was tested for both NF155 and NF186 binding. Similarly to Figure 46, to account for non-specific binding, the mean OD from PBS-coated wells testing each serum (not shown) was subtracted from each condition testing that same serum in triplicate. For each antigen coat, a positivity threshold was defined as ≥ 4 standard deviations (STDV) above the mean OD of the healthy control serum following background subtraction, indicated by a green hashed box. Each square represents the mean corrected OD of one sample tested in duplicate. Weak and inconsistent signal was observed for both baits compared to commercial proteins. A healthy control value was unavailable from the well coated with commercial NF155 protein due to experimental error.*

5.3.2.4 Protocol troubleshooting and limitations

To address the limitations of Trial 5, Trial 6 introduced several refinements. First, this trial was seeded at 1.0×10^6 cells per T25 flask with the intent of conducting a clean replicate using refined transfection parameters. Additionally, rather than scaling DNA amounts based on surface area, DNA dosage was adjusted based on cell number

following Dr Bo Sun's recommendation: 10 µg of total DNA per flask, with a 4:1 expression plasmid-to-BirA plasmid ratio (10 µg bait plasmid, 2.5 µg BirA). PEI was added at a 2:1 ratio relative to total DNA, using commercial PEI at stock concentration. The goal of these changes was to increase transfection efficiency and ensure sufficient expression of both bait and biotin ligase, while minimising PEI toxicity.

Transfection was performed on day 2, despite cells being only 40-50% confluent – a compromise driven by time constraints. Cells were harvested and purified on day 6 following the optimised Ni-NTA protocol. Buffer exchange was completed on the same day, and Nanodrop measurements showed high protein concentrations for both baits: NF155 averaged 494 µg/mL, and NF186 502 µg/mL, with 200 µL of total volume retained for both baits after completing buffer exchange.

Despite these high Nanodrop-measured protein concentrations post-purification, Western blotting showed no detectable biotinylation or neurofascin signal (Figure 51). Retrospective analysis revealed the BirA plasmid used had not been midi-prepped, explaining the failure of biotinylation.

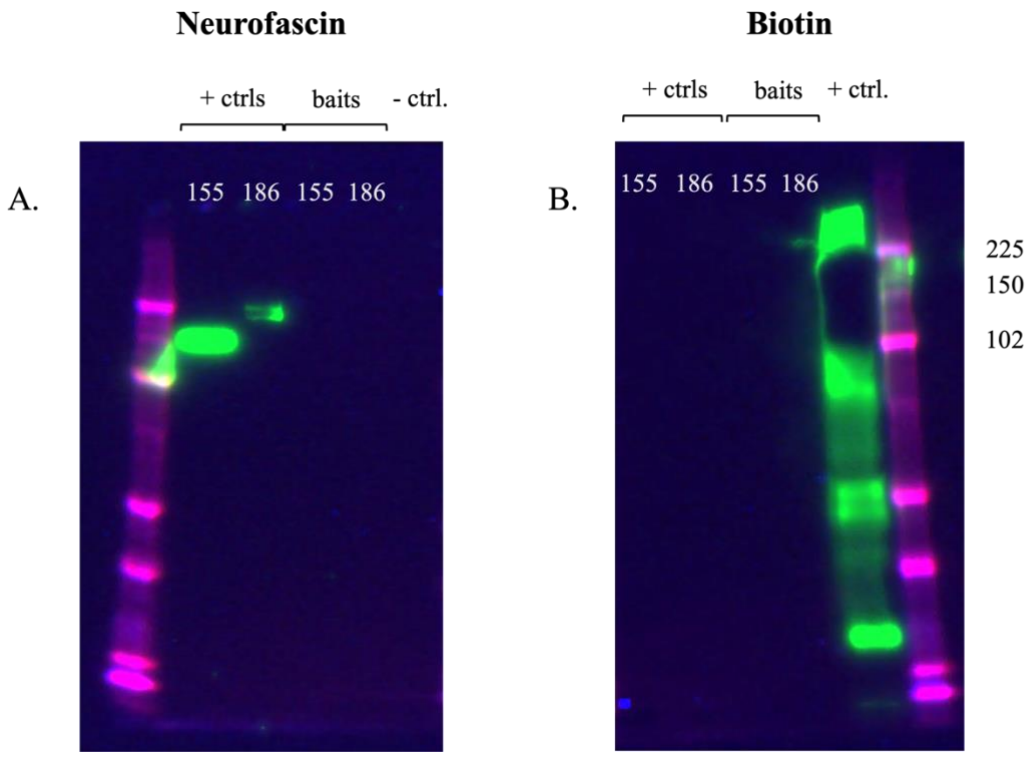

Figure 51: Neurofascin and biotin Western blots for Trial 6 bait proteins (produced using unpurified BirA). *200 ng of each commercial protein and bait were tested. Molecular weight markers are indicated on the right of the blots.* ***A:*** *Similarly to Figure 49, baits buffer exchanged from E1 purification fractions and commercial neurofascin proteins as positive controls were separated by SDS-PAGE and blotted with chicken anti-neurofascin (1:3000), followed by goat anti-chicken HRP (1:4000). 2 µL of untransfected HEK supernatant that had been purified and buffer exchanged using the same protocol as the baits was used as a negative control.* ***B:*** *Identical samples were loaded and probed with streptavidin-HRP (1:5000) to detect biotinylated bait. A biotinylated goat anti-chicken antibody was used as a positive control. Despite high Nanodrop protein concentrations (494 and 502 µg/mL), neither NF155 nor NF186 (respectively) produced bands on either neurofascin or biotin Western blots. Retrospective review confirmed that unpurified BirA was used for co-transfection, likely resulting in failed biotinylation.*

Trial 7 thereafter was designed to investigate whether bait proteins were being secreted into supernatant as expected or retained within the HEK cell membrane due to the consistent lack of bands that would have indicated neurofascin expression on Western blots up to this point. Two flasks were transfected with antigen bait constructs (which include secretion signals), and two flasks with CBA plasmids (known to be retained in the membrane) to serve as controls. No biotinylation was carried out at this stage in order to isolate the source of the potential problem. It is worth noting that for the CBA flasks, however, the transfection media was not replaced with fresh media post-

transfection, a deviation from standard protocol that likely contributed to significant cell death which was observed at harvest.

On day 5, supernatants were harvested and adherent cells were lysed according to section 2.12.3. Ni-NTA purification was performed on both supernatants and lysates. Due to a limited number of Amicon filters, only the E1 purification fractions from the bait plasmid flasks were buffer exchanged on this occasion.

Nanodrop readings showed NF155 was more abundant in supernatants than lysates (432-491 μg/mL vs <20 μg/mL), consistent with expected secretion. However, NF186 concentrations were low across both compartments (<100 μg/mL in all fractions). On Western blots with a total well volume of 22 μL, a weak NF155 band was detected in supernatants only, and only at a higher loading volume relative to the total well volume (3:4) (Figure 52A). No signal was observed for NF186 in any fraction (Figure 52B), despite re-running the blot using a 4-12% Bis-Tris gel that allowed for a larger maximum load volume of 35 μL to better account for the extremely low yield of the NF186 bait in this trial (Figure 53), as well as the lack of a band for the positive control in the previous blot (Figure 52B). This suggested either true absence of NF186 or extremely low detection efficiency.

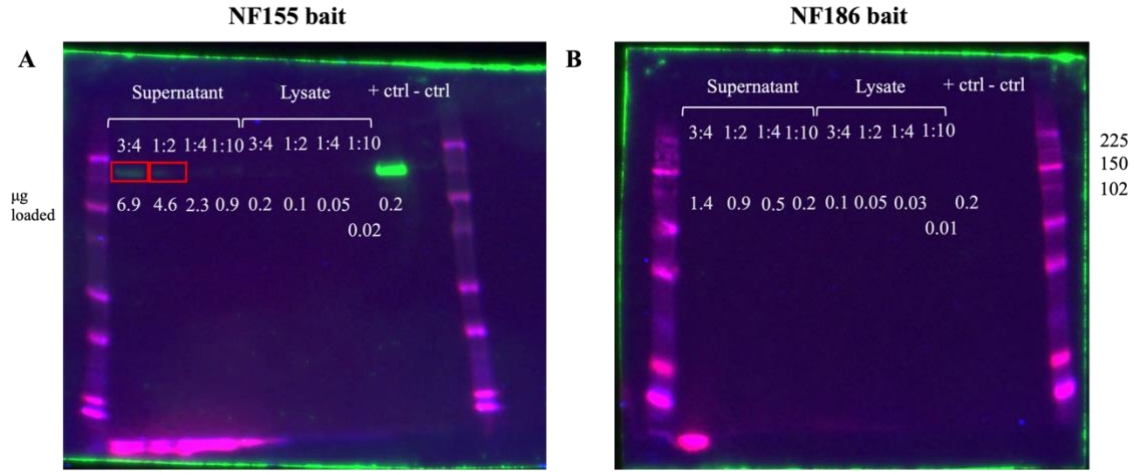

Figure 52: Western blot assessing neurofascin expression in supernatant and lysate fractions from the antigen baits of Trial 7. (A) *NF155 and* ***(B)*** *NF186 bait supernatants and lysates from Trial 7 were tested at varying concentrations and probed with chicken anti-neurofascin antibody to detect neurofascin expression. Ratios indicated above each lane (eg, 3:4) indicate the ratio of supernatant/lysate to the total well volume of that lane (22 µL). Amounts of protein in each lane are indicated below each lane. Positive controls were commercial neurofascin proteins (200 ng). Negative controls were purified and buffer exchanged, untransfected HEK supernatant (2 µL). NF155 was weakly detectable in the supernatant at high concentrations (outlined in red) but not the lysate at any concentration. NF186 was undetectable in both. These results suggested NF155 is secreted, while NF186 may be poorly expressed or unstable.*

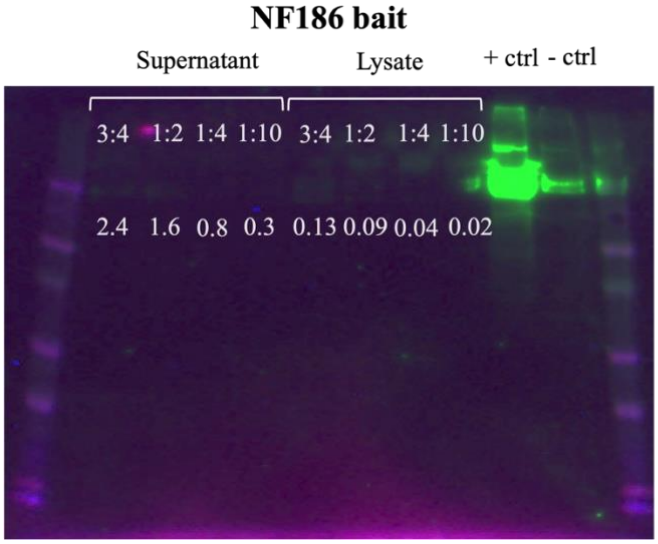

Figure 53: Repeat Western blot on Trial 7 NF186 bait supernatant and lysate samples using maximal volume loading. *Similarly to Figure 52, NF158 bait supernatants and lysates from Trial 7 were tested at varying concentrations, indicated by the ratios above each lane. Each ratio indicates the ratio of supernatant/lysate to the total well volume of that lane (35 µL). The amount of protein loaded into each lane is indicated below each lane (µg). The positive control ("+ ctrl") was 1 µg of commercial NF186 protein due to the lack of positive signal in the previous blot with 200 ng. The negative control ("- ctrl") was purified and buffer exchanged, untransfected HEK supernatant (2 µL). No NF186 bands were detected in any condition, suggesting either low expression or poor detection sensitivity. While the positive control worked in this blot compared to the previous blot in Figure 52, leakage from this positive control lane into the negative control lane still made a lack of signal for the negative control inconclusive.*

A neurofascin Western blot was also carried out for the CBA-transfected flask supernatants and lysates; however, there was no detectable signal, which was likely due to the cell death which occurred as mentioned previously (data not shown).

To rule out endogenous neurofascin reactivity or false positives in the absence of biotinylation of these baits, His tag blots were also performed using a monoclonal 6×His antibody. A clear band was visible for the sample with the highest load of NF155 bait supernatant (3:4; ~6.9 µg), but for no other concentrations of the supernatant or lysate (Figure 54). No bands appeared for the NF186 bait supernatant or lysate. Commercial NF155 protein with a His tag appeared as expected on both blots as a positive control. The absence of signal for the NF186 bait, however, even with high load volumes, raised concerns about bait degradation during storage or transfer, or low expression altogether.

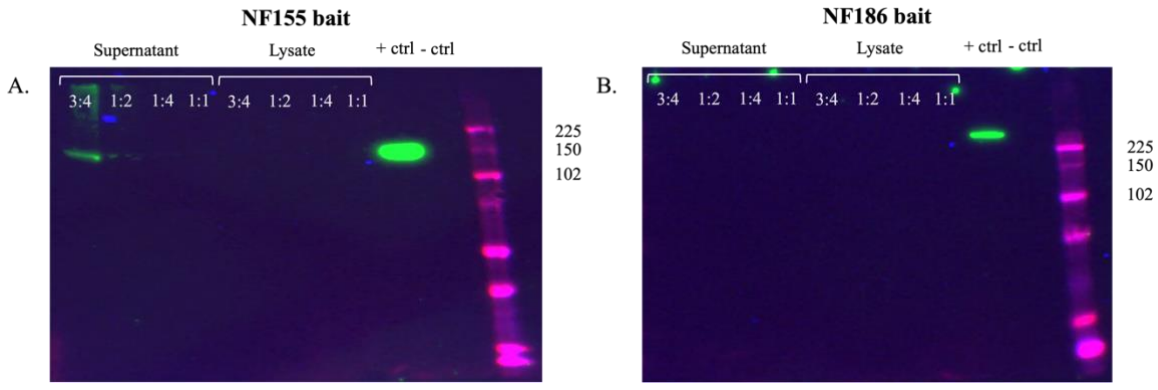

Figure 54: 6×His tag Western blot on Trial 7 baits to confirm neurofascin expression. *Varying amounts of bait along with 200 ng of commercial protein (+ ctrl) or 2 µL of untransfected, purified, and buffer-exchanged HEK supernatant (- ctrl) was loaded in each well, with a total volume of 22 µL in each well. A clear His-tag band was detected in the NF155 supernatant (3:4 dilution; ~6.9 µg), confirming expression. No signal was observed for NF186, likely due to low yield.*

Subsequent re-analysis of Trials 5 and 6 via Western blot with increased loading to the maximum volume of bait possible in each well (26.25 µL; Trial 5 NF155: 11.6 µg,

NF186: 4.8 µg; Trial 6 NF155: 13.0 µg, NF186: 13.2 µg) and a maximum capacity volume of 35 µL total in each well clarified that NF186 had, in fact, been present at low levels (Figure 55 & Figure 56). NF155 from both trials yielded strong signal on neurofascin and streptavidin-HRP blots, and NF186 was faintly but distinctly detected in Trial 6, confirming suspicions of previous underloading potentially due to overestimated concentrations.

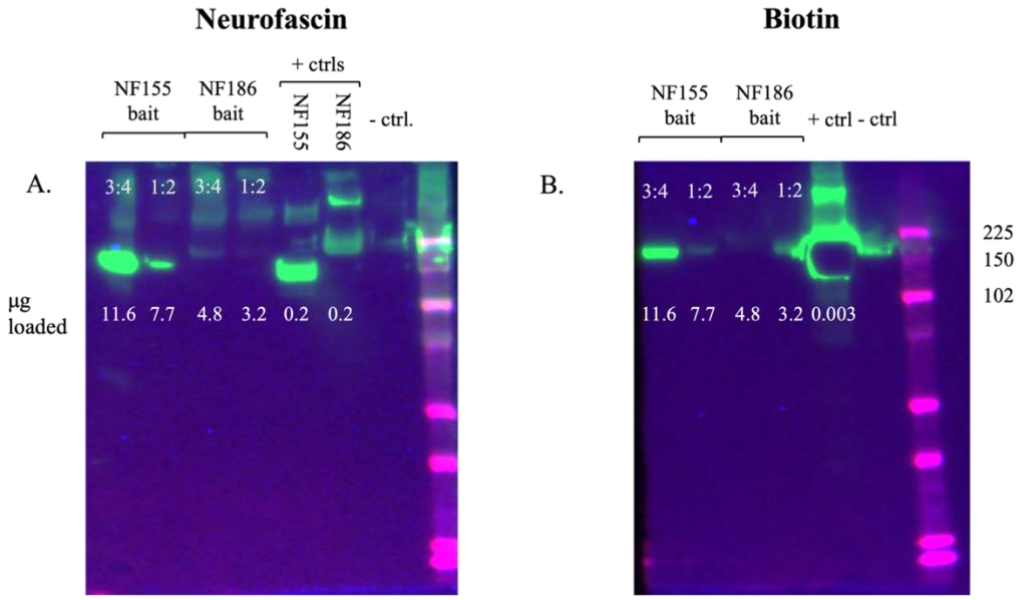

Figure 55: Re-analysis of Trial 5 bait proteins with increased loading volumes on Western blot. *Bait proteins were re-tested at two different concentrations with every well filled to its maximum capacity of 35 µL. Protein amounts are indicated below each lane.* ***(A)*** *200 ng of commercial neurofascin protein or* ***(B)*** *3.65 ng of biotinylated CASPR2 protein (5 µL of 735 ng/mL protein; courtesy of Dr Mateusz Makuch) were used as positive controls. 5 µL of untransfected HEK supernatant that had been purified and buffer exchanged was used as a negative control. NF155 was detectable on both (A) neurofascin and (B) streptavidin-HRP blots, validating that previous underloading contributed to missed detection, and that the NF155 bait had indeed already been successfully expressed and biotinylated. NF186 remained undetectable, once again likely due to low yield. However, apparent over-loading of the biotinylated CASPR2 protein led to bleed-over into the negative control well, once again slightly impairing interpretation of the results.*

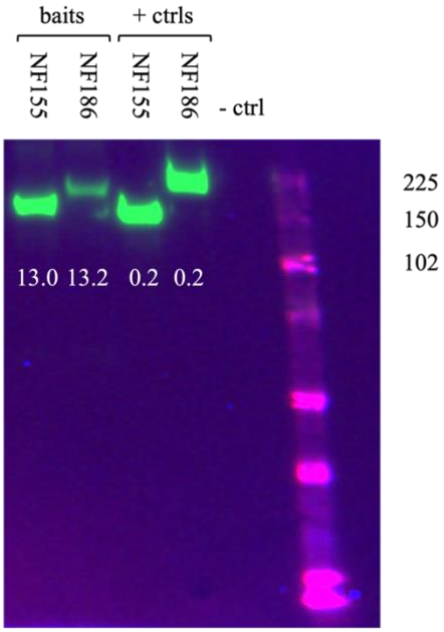

Figure 56: Re-analysis of Trial 6 bait proteins (non-biotinylated) using increased loading volume on neurofascin Western blot probed with chicken anti-neurofascin antibody. *The maximum load volume (26.25 µL) of each bait was loaded to maximise the chances of detection. Protein amounts are indicated in µg below each lane. 200 ng of each commercial protein was loaded as positive controls. 2 µL of purified and buffer exchanged untransfected HEK supernatant was utilised as a negative control. Both NF155 and NF186 were detectable at the expected molecular weights, confirming that expression had occurred but may have been missed in prior experiments due to underloading or degradation.*

5.3.2.5 Final optimisation and successful validation

Trial 8 incorporated all prior insights. Fresh, low-passage HEK293T cells and midi-prepped BirA plasmid were used, and transfection was performed at $1x10^6$ cells/flask with a 4:1 bait-to-BirA ratio. Post-purification, both NF155 and NF186 baits achieved high yields (~760-790 µg/mL) and were clearly detectable on neurofascin and streptavidin-HRP (biotin) Western blots (Figure 57).

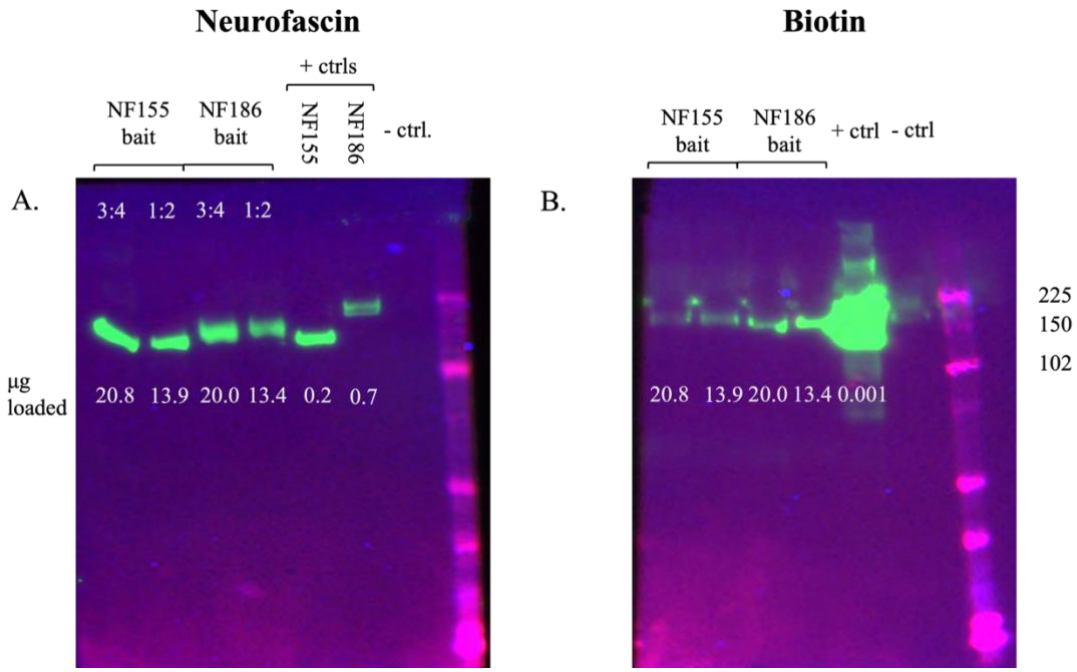

Figure 57: Western blots showing successful expression and biotinylation of NF155 and NF186 baits using freshly midi-prepped BirA and low-passage HEK293T cells as the final validation of Trial 8 baits. *Two different amounts of bait protein were tested (indicated below each lane) with every well filled to its maximum capacity of 35 µL.* ***(A)*** *200 ng of commercial NF155 protein and 700 ng of commercial NF186 protein or* ***(B)*** *1.47 ng of biotinylated CASPR2 protein (2 µL of 735 ng/mL protein) were used as positive controls. The amount of NF186 positive control was increased due to a weak signal at 200 ng on previous blots. 10 µL of untransfected, purified, and buffer exchanged HEK supernatant was used as a negative control. Both constructs produced strong bands on neurofascin and streptavidin-HRP blots, confirming expression and biotinylation. Bleed-over of signal from the CASPR2 control protein remained.*

ELISA plates coated with Trial 8 baits showed weak but specific reactivity in several pan-NF^{+} patient samples (Figure 58), exceeding the 4 standard deviations positivity threshold after background correction. However, signal strength was still reduced

compared to commercial controls, suggesting residual issues with bait folding, stability, or functional concentration.

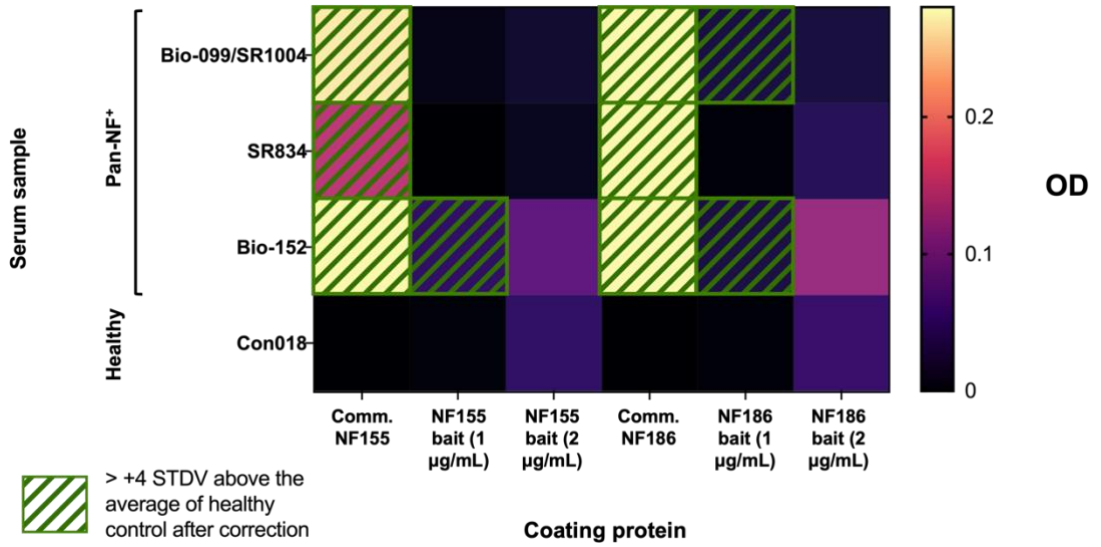

Figure 58: ELISA comparing Trial 8 small-scale antigen baits to commercial NF155 and NF186 protein coats for detection of pan-NF⁺ autoantibodies. *Plates were coated with 100 µL of 1 µg/mL commercial NF155 or NF186 protein or with varying concentrations of Trial 8 antigen baits and then probed with sera from three pan-NF⁺ patients. To control for non-specific binding, the mean OD from PBS-coated wells for each serum (not shown) was subtracted from all corresponding conditions. Each protein coat was also tested in triplicate using a healthy control serum (Con-018); the average OD and standard deviation were used to define a positivity threshold specific at ≥ 4 standard deviations above the control mean for that condition (denoted by a hashed green box). Multiple pan-NF⁺ sera exceeded this threshold for the Trial 8 baits, although with lower absolute signal than the commercial proteins. Comm: commercial. OD: optical density.*

5.3.2.6 Summary of bait production troubleshooting and lessons learned

Across eight trials, bait production was optimised through iterative refinement of transfection conditions, resin choice, BirA plasmid preparation, and loading protocols. Ni-NTA purification substantially improved yield and purity. Crucially, accurate quantification, biotinylation efficiency, and bait stability were identified as key determinants of success. Trial 8 demonstrated robust, reproducible production of both NF155 and NF186 baits, validated by multiple assays. The lessons learned here underpinned the design of large-scale bait production, where protein integrity and functional binding would continue to be closely monitored.

5.4 Large-scale production of antigen baits

In parallel with the final small-scale optimisation trial (Trial 8), large-scale production of biotinylated NF155 and NF186 baits was initiated (courtesy of Dr Bo Sun and Mr Andrew Fower) to enable downstream applications requiring higher protein yield. Although the optimised small-scale protocol yielded validated constructs, variability in bait concentration and coating efficiency, particularly for NF186, as well as the need for higher amounts of protein for downstream fluorescence-activated cell sorting (FACS) applications prompted the need for upscaling.

Production was performed in suspension culture using HEK293F cells, leveraging their scalability, transfection efficiency, and compatibility with serum-free media. While Dr Sun/Mr Fower carried out the large-scale transfections and purifications, all subsequent validation – including Coomassie, Western blotting, ELISA, and biotin:protein quantification – was independently conducted by the author. The following sections detail the scaling process, including adaptations from the small-scale protocol and outcomes at each stage.

5.4.1 Scaling up from optimised small-scale protocol

5.4.1.1 Seeding density and use of suspension culture

Large-scale bait production was initiated using HEK293F cells in 50 mL suspension cultures, seeded at $1x10^6$ cells/mL in vented Erlenmeyer flasks and agitated at 130 rpm. This cell line was selected for its high transfection efficiency, rapid growth kinetics, and adaptability to serum-free conditions. Freestyle 293 medium supported consistent growth and allowed for chemically defined conditions compatible with protein production.

The choice to begin with a single 50 mL flask per construct was based on previously validated parameters within the Irani group for secreted recombinant proteins. This volume allowed for efficient handling and purification while providing sufficient protein for initial ELISA and validation experiments. The use of nonadherent suspension culture streamlined scalability and removed the need for extensive passaging or surface area expansion, supporting reproducibility and throughput in subsequent batches.

5.4.1.2 Transfection conditions and media additives to enhance yield

Transfection was carried out 24 hours post-seeding using the PEI protocol established during small-scale optimisation, with minor adaptations for suspension conditions. Each 50 mL culture received 50 µg of bait plasmid DNA and 150 µg of PEI (1:3 ratio), with DNA:BirA maintained at a 4:1 molar ratio to support efficient co-translational biotinylation. DNA and PEI were diluted separately in Opti-MEM, incubated for 5 minutes, then complexed for 10 minutes before addition to the flasks. Cultures were gently swirled during addition to ensure homogeneous distribution.

D-biotin (0.1 mM) was added to cultures both one hour prior to and again after transfection to saturate the biotinylation system and support efficient substrate availability. To further boost expression, 500 µL of 1 M sodium butyrate was added 3 hours post-transfection. This histone deacetylase inhibitor is known to enhance transcriptional activity by relaxing chromatin structure and is commonly used in HEK293 systems to increase recombinant protein yield. Although not used in small-scale trials, sodium butyrate was incorporated here as a yield-enhancing refinement specific to the large-scale context.

Cells were cultured post-transfection for 3-4 days at 37°C and 130 rpm before harvesting. This interval was chosen to maximise protein expression while minimising cell death or loss of viability. The final culture volume and conditions were fully compatible with the existing Ni-NTA purification pipeline established during small-scale production.

5.4.2 Purification and downstream handling

5.4.2.1 Batch processing and Ni-NTA-based resin purification

Purification of the large-scale NF155 and NF186 bait proteins was performed by Dr Bo Sun using the Ni-NTA resin-based IMAC protocol, previously optimised during small-scale production. The established batch method (detailed in section 2.12.4.2) was followed without modification.

The decision to retain Ni-NTA resin was based on its superior yield and reliability compared to cobalt resin in earlier trials. Notably, the resin exhibited consistent binding affinity and recovery across multiple elution fractions during small-scale validation, with minimal background. As no technical issues were encountered during the large-scale purifications, no additional optimisation steps were required at this stage.

5.4.2.2 Buffer exchange, formulation, and storage strategy

After purification, eluates were buffer exchanged into DPBS using 30 kDa Amicon Ultra-15 centrifugal filter units, as per the protocol in section 2.12.5. This step was also performed by Dr Bo Sun and followed standard parameters used in the small-scale trials, ensuring continuity across experimental batches.

DPBS was selected as the final formulation buffer due to its compatibility with downstream ELISA and flow cytometry applications, and to allow direct comparison of large- and small-scale bait performance. Although buffers such as HEPES-NaCl are known to enhance long-term protein stability in other recombinant systems, DPBS was retained here due to its satisfactory performance in validation assays and widespread compatibility.

Aliquots of the buffer-exchanged baits were dispensed into low-bind Eppendorf tubes, flash-frozen on dry ice, and stored at -80°C. This mirrored the storage conditions used in small-scale production and enabled equivalent handling for downstream quality control and functional testing.

5.4.3 Protein quantification and recovery outcomes

Following buffer exchange, protein concentrations of the large-scale NF155 and NF186 baits were quantified using Nanodrop spectrophotometry at 280 nm. Extinction coefficients and molecular weights, calculated based on amino acid sequences and summarised in Table 11 (section 2.12.4.1), were used to convert absorbance values to molar concentrations.

Triplicate measurements yielded high and consistent protein concentrations: 791.9 µg/mL for NF155 and 763.6 µg/mL for NF186. These values represented the highest yields obtained at any stage of the antigen bait production pipeline and confirmed the scalability and efficiency of the optimised workflow.

5.4.4 Validation and quality control of large-scale baits

5.4.4.1 Streptavidin pull-down and Coomassie to assess biotinylation efficiency

To assess the biotinylation status of large-scale baits, a streptavidin pull-down assay was performed by Dr Sun, followed by Coomassie staining to detect depletion of unbound bait protein from the supernatant (Figure 59). This indirect approach provided a qualitative measure of biotin incorporation.

Each bait (3 µg) was incubated with 50 µL of pre-washed Dynabeads M-270 Streptavidin in DPBS for 1 hour at 4°C with rotation. Beads were magnetically separated, and the unbound supernatant was diluted to 150 µL. Aliquots of 12, 6, and 3 µL (240, 120, and 60 µg, respectively) were analysed by SDS-PAGE alongside baits that were not subjected to pull-down (240 µg in LDS buffer). Gels were stained with Imperial Protein Stain as per section 2.12.8.

For NF155, a noticeable reduction in band intensity was observed in the bead-incubated samples compared to controls, suggesting successful biotinylation and capture by streptavidin beads (Figure 59). For NF186, intensity reduction was more subtle, consistent with previously observed differences in biotinylation efficiency. Nonetheless, discrete bands were visible at expected molecular weights for both baits, confirming successful biotinylation.

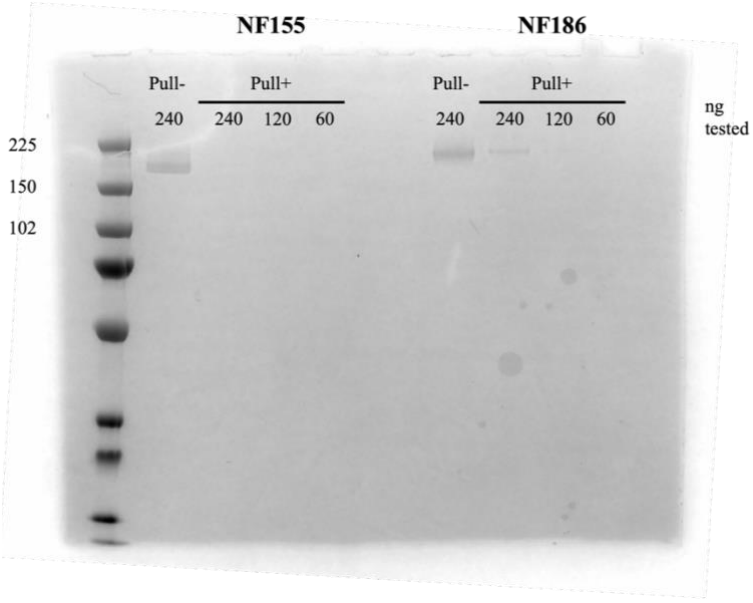

Figure 59: Streptavidin pull-down assay to assess biotinylation of large-scale antigen baits. *Varying concentrations of NF155 and NF186 antigen bait produced large-scale and incubated (Pull+) or not incubated (Pull-) with streptavidin beads were assessed via SDS-PAGE as an indirect test of biotinylation efficiency. Coomassie staining revealed complete depletion of the NF155 band, while NF186 depletion was less pronounced.*

5.4.4.2 ELISA-based assessment of antigen recognition by patient autoantibodies using large-scale baits

To evaluate antigenicity, ELISAs coated with baits or commercial neurofascin protein were performed using sera from pan-NF^+ patients, alongside healthy controls. Assays compared the large-scale baits with Trial 8 small-scale baits and commercial neurofascin proteins under matched assay conditions.

In this experiment, antigen coating concentrations were increased (5-10 µg/mL) to assess whether prior weak signals were due to sub-saturating bait concentrations. OD values were background-corrected by subtracting the mean signal of PBS-coated wells and compared to the distribution of healthy control responses, as per typical protocols. A +4 standard deviation threshold was used to define seropositivity.

Both the Trial 8 and large-scale baits elicited strong, specific responses in several pan-NF^+ patient samples, with signal magnitude comparable to, and in some cases exceeding, those obtained with commercial antigens (Figure 60).

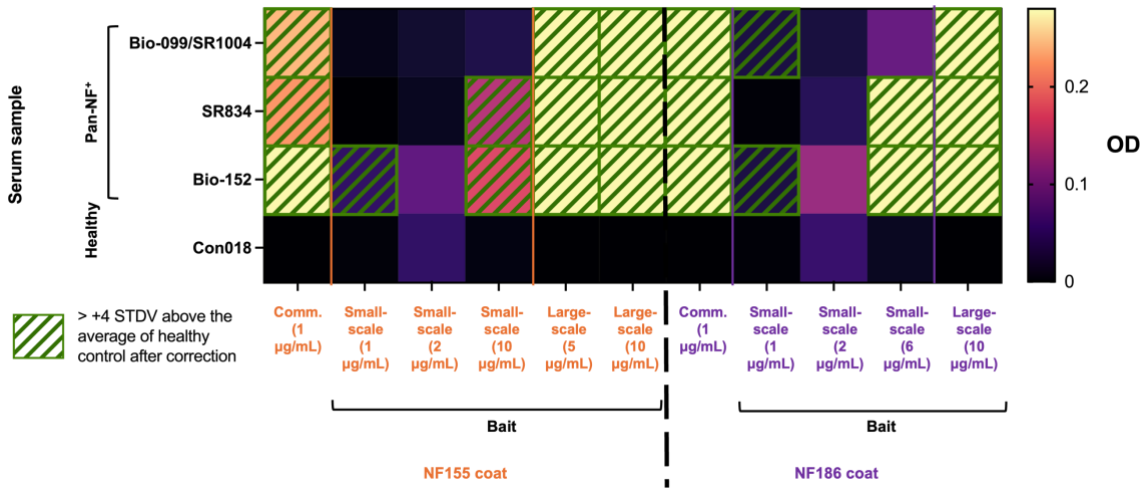

Figure 60: ELISA comparing autoantibody binding to Trial 8 small-scale and large-scale baits. *Plates were coated with large-scale and Trial 8 small-scale NF155 (orange) or NF186 (purple) baits at varying concentrations, alongside commercial neurofascin proteins and PBS controls (not shown). Three pan-NF^{+} patient sera were tested, and OD readings were background-subtracted using PBS-coated well signals, as done previously. Positives (denoted by a hashed green box) were defined as values exceeding +4 standard deviations above the mean of the healthy control serum tested in triplicate for each coating condition. Large-scale and Trial 8 small-scale baits exhibited comparable or stronger reactivity than commercial baits. Comm: commercial. OD: optical density.*

These results confirmed that bait integrity was preserved during large-scale production and that sufficient antigenicity was retained for robust ELISA-based detection.

5.4.4.3 Final confirmation of 1:1 biotin-to-antigen ratio

To confirm successful biotinylation of the large-scale NF155 and NF186 baits, a streptavidin (SA)-PE competition Western blot was performed following the titration-based protocol adapted from Phelps et al (2024), as described in section 2.12.9.[90] This assay evaluates the molar relationship between bait and biotin, a key parameter for tetramerisation.

Serial dilutions of SA-PE (0.5-0.0156 µM) were incubated with 2 µM of each large-scale bait protein (final bait concentration in each well: 1 µM), using dilution volumes calculated from Nanodrop-derived concentrations:

- **NF155**: 15.38 µM → 7.69-fold dilution

- **NF186**: 20.95 µM → 10.475-fold dilution

Following SDS-PAGE and blotting, streptavidin-HRP was used to detect unbound bait. For both NF155 and NF186, bait bands reappeared with 0.25 µM SA-PE, with disappearance observed at higher concentrations, and persistence at lower ones (Figure 61), indicating each bait had no more than one biotin per antigen molecule.

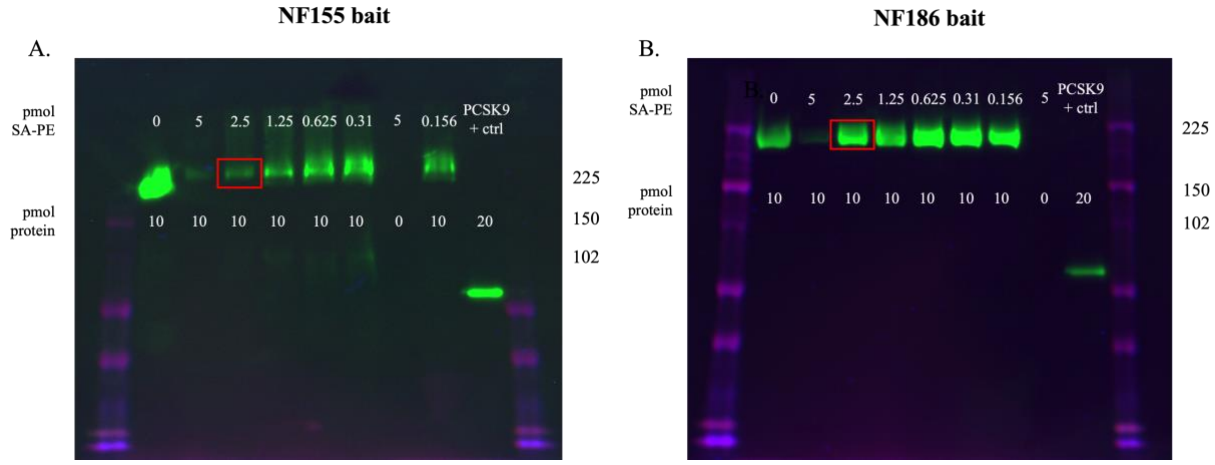

Figure 61: Streptavidin-PE competition Western blot to assess biotin-to-antigen ratio in large-scale NF155 and NF186 antigen baits. *Titrated SA-PE (0.5 µM to 0.0156 µM) was incubated 1:1 with 2 µM of each antigen bait and stained with SA-HRP at a 1:5000 dilution to test for saturation and reappearance of unbound antigen on Western blot. A biotinylated PCSK9 commercial protein was used as a positive control (+ ctrl). The concentration of SA-PE and antigen bait in each lane is indicated above and below each lane, respectively. For both NF155 and NF186, bands reappeared at 0.25 µM SA-PE (indicated by red boxes). SA: streptavidin. Pmol: picomoles.*

5.5 Tetramerisation of large-scale antigen baits

Following successful validation of large-scale NF155 and NF186 bait production and confirmation of 1:1 biotin-to-antigen stoichiometry, the next step was to assemble fluorescent tetramers suitable for FACS. These tetramers were designed for the detection and potential isolation of antigen-specific B cells using SA-PE backbones. This section outlines the preparation and characterisation of both control and neurofascin-specific tetramers using the SA-PE tetramerisation method described in

section 2.12.10 (Appendix 8.4), incorporating both control and neurofascin antigen-specific tetramers.

5.5.1 Control tetramer production

A conjugated control tetramer was first generated using a biotinylated proprotein convertase subtilisin/kexin type 9 (PCSK9) protein and an SA-PE backbone labelled with DL594 NHS ester. This non-specific control was developed to distinguish true antigen-specific B-cell staining from background reactivity due to fluorophore or streptavidin backbone recognition. The PCSK9 protein was selected for its unrelated domains to the NF155 and NF186 baits, except for the same AviTags, His tags, and biotinylation.

5.5.1.1 Preparation of the SA-PE-DL594 backbone

Commercial SA-PE stocks contain sodium azide, which can interfere with NHS ester conjugation chemistry. To remove azide and ensure compatibility with subsequent labelling, three sequential buffer exchanges into PBS were performed using a 100 kDa centrifugal filter. The purified SA-PE was then diluted into borate buffer (pH 8.5), with pH adjusted via careful titration of NaOH. A room-temperature incubation with DL594 NHS ester for 1 hour in the dark enabled conjugation to amine residues on the SA-PE. Post-labelling, the reaction mixture underwent further centrifugal filtration to remove unbound dye. Filtrate clarity confirmed dye removal, and the final labelled backbone (SA-PE-DL594) was concentrated to 150.9 µL. UV-Vis spectrophotometry confirmed successful dual-labelling, with OD_{566} = 1.781 (0.909 µM PE) and OD_{546} = 0.406 (5.075 µM DL594).

At this stage, insufficient PCSK9 was available to fully saturate all biotin binding sites on the SA-PE-DL594 complex. Therefore, the backbone was aliquoted and stored at 4°C in light-protective conditions pending final assembly.

5.5.1.2 Conjugation of PCSK9 and tetramer formation

The biotinylated PCSK9 antigen was thawed the following day, and concentration was confirmed by Nanodrop (average = 367.67 µg/mL; MW = 71.05 kDa), yielding a calculated molarity of 4.33 µM. Based on a PE concentration of 0.909 µM and six biotin-binding sites per SA-PE tetramer, 63 µL of PCSK9 protein was added to 50 µL of backbone. The mixture was incubated at room temperature for 30 minutes.

5.5.1.3 Purification and quality assessment

The tetramer solution was purified using a 100 kDa centrifugal filter to remove unbound PCSK9. The first spin yielded low volume, so extended centrifugation was performed until the retentate reached 83.8 µL. UV-Vis spectrophotometry post-purification showed OD_{566} = 1.048 (1.048 µM PE) and OD_{546} = 0.225 (0.524 µM DL594), confirming retention of both fluorophores and suggesting successful tetramerisation.

5.5.1.4 Stabilisation and storage

An equal volume of 100% glycerol was added to the purified tetramer to generate a 50% glycerol stock at a 0.524 µM final concentration (PE basis). The conjugated control tetramer was aliquoted into low-bind tubes and stored at -20°C. Stability for up to one year was assumed based on standard fluorophore-streptavidin conjugate guidelines.

This workflow validated the efficacy of the SA-PE-DL594 conjugation process and established a robust fluorophore-matched negative control for downstream flow cytometry. The control tetramer would also serve as a technical reference for optimising fluorophore brightness and background signal suppression in dual-labelled antigen-specific tetramers.

5.5.2 Antigen bait tetramer production

Following successful biotinylation and quality control of the large-scale NF155 and NF186 antigen baits, tetramerisation was performed using SA-PE to generate multimeric fluorescent probes for downstream B-cell detection. This procedure followed the established stoichiometric workflow optimised during control tetramer production (section 5.5.1), involving precise antigen-to-streptavidin ratio calculation, centrifugal filtration, and fluorometric quantification.

5.5.2.1 Tetramer assembly

Volumes of NF155 and NF186 baits were calculated using previously determined molarities (15.38 µM for NF155 and 20.95 µM for NF186), along with the molar concentration of SA in the SA-PE stock used (3.77 µM). Based on the stoichiometry of four biotin-binding sites per SA-PE molecule, bait volumes were calculated as:

- **NF155:** $\frac{3.77\ \mu M \times 100\ \mu L \times 4}{15.38\ \mu M} = 98\ \mu L$
- **NF186:** $\frac{3.77\ \mu M \times 100\ \mu L \times 4}{20.95\ \mu M} = 72\ \mu L$

These volumes were added to 100 µL of SA-PE in separate tubes and incubated at room temperature for 30 minutes in the dark to allow tetramer formation.

5.5.2.2 Purification by centrifugal filtration

Immediately after incubation, the reaction mixtures were transferred to 300 kDa centrifugal filters. Initially, PBS was omitted during this transfer, and the spin was paused upon realisation. The volumes were then topped up with ~400 µL PBS and spun at 5000xg for 7 minutes. This improved filtration but did not sufficiently reduce volume. Additional PBS top-ups and two further 10-minute spins at 5000xg were performed, with filtrates collected between each step.

Minor troubleshooting was required during this phase: overfilling of filters initially prevented lid closure, prompting cautious topping up only to the internal filter ring. Despite these early issues, the final PBS washes yielded filtrates that were substantially cleared, indicating successful removal of unbound antigen and fluorophore. The final retentates were recovered by inverting the filter units and centrifuging at 1000xg for 3 minutes into fresh tubes.

5.5.2.3 Quantification and storage

Final retentate volumes were 343 µL for NF155 and 330 µL for NF186. Nanodrop spectrophotometry at 566 nm yielded OD values of 1.045 (NF155) and 1.264 (NF186), corresponding to calculated PE concentrations of:

- **NF155:** $\frac{1.045}{1.96} = 0.533\ \mu M$
- **NF186:** $\frac{1.264}{1.96} = 0.645\ \mu M$

To standardise for long-term storage and experimental use, each sample was diluted 1:1 with 100% glycerol, yielding 50% glycerol stocks at final PE concentrations of 0.2665

μM and 0.3225 μM, respectively. Samples were aliquoted into low-bind tubes and stored at -20°C.

5.5.2.4 Summary

This workflow confirmed successful tetramerisation of both NF155 and NF186 antigen baits. Despite minor procedural deviations during PBS dilution and filter handling, PE retention and fluorophore brightness were preserved, and final yields were sufficient for downstream flow cytometric applications. These tetramers, now validated for stability and fluorophore content, were deemed ready for use in downstream B-cell sorting applications.

5.6 Discussion and limitations

5.6.1 Summary of optimisation outcomes

This chapter described the iterative development, validation, and scale-up of NF155 and NF186 antigen bait proteins and their successful tetramerisation for use in downstream B-cell FACS applications. Across eight sequential small-scale trials, the bait production pipeline was systematically optimised – resolving early issues with protein expression, biotinylation, and purification – culminating in the successful generation of biotinylated NF155 and NF186 constructs that exhibited appropriate structural integrity and functional antigenicity. These reagents were then scaled using HEK293F suspension cultures, purified, validated, and tetramerised with SA-PE backbones. Final constructs were stored in 50% glycerol.

5.6.2 Technical and practical challenges

Several technical challenges were encountered throughout optimisation. Initial expression attempts failed to achieve adequate protein yield or biotinylation, in part likely due to the use of cobalt resin, low transfection efficiency, and degradation or underloading artefacts. Misestimations of bait concentration using Nanodrop also confounded early validation experiments. NF186 posed persistent challenges, exhibiting lower yield, inconsistent biotinylation, and fainter signals across validation assays relative to NF155. Switching to Ni-NTA resin and implementing key procedural changes – including immediate buffer exchange, the use of low-passage HEK293T cells, and midi-prepped BirA plasmids – substantially improved performance.

Misestimations of bait concentration using Nanodrop confounded early validation experiments, leading to inconsistent Western blot and ELISA outcomes. ELISA assessments in Trials 4 and 5 revealed low and inconsistent patient autoantibody binding to the in-house baits, despite strong reactivity to commercial proteins, likely reflecting insufficient bait concentration, poor folding, or low yield. Subsequent Western blot troubleshooting in Trials 6 and 7 reinforced this issue: although Nanodrop measurements suggested high concentrations, detectable signal for both NF155 and NF186 required substantially increased loading volumes, indicating probable overestimation. These highlighted the limitations of Nanodrop-based quantification for large, glycosylated proteins. Further bait localisation studies in Trial 7 confirmed NF155 secretion, while NF186 remained undetectable in both lysates and supernatants by His-tag and neurofascin blots. This implicated low expression or poor stability rather than mislocalisation as the primary issue.

Notably, early ELISA analysis of baits from Trials 4 and 5 used a pooled healthy control standard across all conditions, which may have obscured low-level antigen-specific signals. In retrospect, testing replicate healthy controls per coat and defining +4 standard deviation thresholds for each specific coating condition would have improved interpretability – an approach adopted in subsequent ELISAs.

Similarly, one streptavidin pull-down assay failed to recover detectable bait despite confirmed BirA co-transfection and biotin supplementation. This may have reflected low biotinylation efficiency, bait instability, or technical issues with the pull-down workflow itself, indicated by no positive control signal. Together, these challenges highlighted the need for improved protein integrity validation and quality control at each step prior to functional assay deployment.

Troubleshooting extended to the tetramerisation stage. Initially, filtration-based purification steps suffered from overfilled membranes and insufficient PBS dilution, impeding recovery. These errors were resolved through adjusted loading volumes and increased centrifugation times.

Additionally, certain positive controls (eg, biotinylated CASPR2) showed unexpectedly high signal intensity relative to equivalent quantities of commercial neurofascin proteins. This may reflect higher biotin loading per molecule or more accessible epitopes for streptavidin-HRP binding, reinforcing the need to interpret positive control comparisons with caution.

When testing the biotin-to-antigen ratio of the large-scale baits, both NF155 and NF186 bands reappeared in the lane containing 0.5 μM SA-PE with 2 μM of bait. Because each SA-PE molecule has four biotin-binding sites, the total binding capacity of this

condition should match the final bait concentration if every molecule has a single biotin. In a perfectly stoichiometric system, all bait should be bound at this condition, and no free bait band should be visible on Western blot. However, the clear bands observed at this concentration of SA-PE on both blots indicated that not all bait was bound – suggesting a slight excess of bait relative to binding capacity.

This result likely does not imply over-biotinylation, which is biologically implausible given the use of site-specific enzymatic biotinylation via BirA at a single AviTag. Rather, the most likely explanation is a modest overestimation of bait concentration by Nanodrop, especially since this became a clear problem when it proved difficult to detect bands indicating neurofascin expression or biotinylation on previous Western blots performed on the small-scale baits (section 5.3.2.4). As a result, the apparent reappearance of unbound bait at the 1:1 theoretical binding point likely reflects a true biotin-to-antigen ratio slightly below 1:1, rather than excess biotin. These findings therefore supported the conclusion that the large-scale baits were appropriately biotinylated and structurally intact, confirming their suitability for streptavidin-based multimerisation.

5.6.3 Reflections on scope and experimental decisions

Several decisions were pivotal to the eventual successful development of these antigen bait reagents. The choice to employ site-specific biotinylation using AviTags and BirA, rather than chemical NHS-biotinylation, ensured predictable, single-site biotin incorporation and minimised the risk of epitope masking or bait multimerisation. Adapting the workflow of Phelps et al (2024) to incorporate DL594-labelled SA-PE backbones also enabled the generation of dual-fluorophore “decoy” tetramers, which

will facilitate stringent exclusion of fluorophore- and streptavidin-specific B cells in future assays.[85] Using sodium butyrate post-transfection was a further refinement, introduced during scale-up, which boosted expression in HEK293F cultures.

At the same time, some constraints shaped the scope and interpretation of this work. A key limitation was the absence of a more quantitative method for determining biotinylation efficiency (eg, HABA assay); confirmation instead relied on indirect readouts including streptavidin depletion and Western blotting. Similarly, while the use of a single AviTag per protein likely reduced the risk of streptavidin-mediated lattice formation, this was not directly tested. The large-scale baits were validated for biotinylation by Western blot and demonstrated consistent binding to pan-NF^+ sera by ELISA, yet one important gap remained: neurofascin expression on the final tetramerised baits was not directly confirmed by Western blot. While prior validation steps had supported epitope preservation, direct protein-level confirmation at this final stage would have strengthened the quality control pipeline. In addition, the functionality of the final tetramers was not tested in ELISA using patient sera – a step that would have confirmed antigenicity.

Other technical limitations included use of a biotinylated goat anti-chicken antibody as a surrogate "biotinylated protein" control in early biotin blots. This was supoptimal due to differences in size, folding, and biotin density compared to the bait constructs. No molecular weight ladder was loaded on the Coomassie gel of Trial 5, complicating interpretation of band size. In the same trial, testing pulled-down bait (rather than direct input) on the biotin Western blot likely depleted the bait below detection threshold when yields already proved low, resulting in a false-negative outcome. Moreover, while

the large-scale baits were compared to commercial neurofascin proteins on ELISA, differing coating concentrations (5-10 μg/mL vs 1 μg/mL, respectively) and limited plate space precluded a true head-to-head comparison. Future experiments should include matched-coating controls and ensure more rigorous batch-to-batch consistency.

Finally, while these tetramers were designed for downstream use in FACS-based detection and sorting, no assay was performed to explicitly verify tetramerisation. An additional quality control step (eg, native PAGE or gel filtration) would be advisable before proceeding to bait-assisted FACS.

Overall, despite these caveats, this chapter established a robust, scalable workflow for generating functional NF155 and NF186 antigen tetramers. These tools are now poised for downstream use in antigen-specific B-cell detection, sorting, and repertoire analysis – addressing the core objective of identifying and characterising B cells that give rise to pathogenic IgG1 pan-NF^+ autoantibodies. Moreover, the platform described here offers a template for expanding bait-based immunophenotyping to additional peripheral nervous system (PNS) antigens and autoimmune disease targets.

5.7 Summary and future directions

5.7.1 Finalised bait production pipeline

Building on the iterative optimisation described above, this section summarises the finalised and validated workflow for producing biotinylated NF155 and NF186 antigen baits. The pipeline integrates optimised transfection conditions, site-specific enzymatic biotinylation *in vivo*, Ni-NTA purification, and stoichiometric tetramerisation with SA-PE, yielding stable, functionally validated reagents. Transition to HEK293F-based

suspension culture enabled high-yield scale-up, while multiple complementary quality control approaches (Western blotting, ELISA, and competition-based stoichiometry) confirmed antigen integrity and effective biotin incorporation. Together, these constructs now constitute a renewable reagent platform for identifying, isolating, and characterising neurofascin-reactive B cells.

5.7.2 Applications and future experiments

The next step is to apply these tetramerised baits in FACS to detect and isolate circulating antigen-specific B cells in patients with pan-NF^+ autoantibodies. Dual-fluorophore labelling and matched decoy tetramers will enable stringent gating strategies to reduce background signal due to non-specific binding. Sorted cells will then be expanded *ex vivo*, enabling repertoire analysis and monoclonal antibody generation to explore antigen specificity and isotype.

Although time constraints precluded flow cytometry validation during the present work, the pipeline described here now offers a robust and ready-to-implement platform for B-cell capture. Its modular design supports future adaptation to other PNS autoantigens. Future work will focus on confirming stability, tetramerisation, and neurofascin expression in large-scale baits; minimising aggregation; and assessing cross-platform fluorophore compatibility – all directed toward refining antigen-specific B-cell detection and advancing mechanistic insight into the autoimmune nodopathies.

6 Discussion

6.1 Overview of key findings

This thesis investigated the origins and characteristics of pan-neurofascin (pan-NF) antibodies in a rare and severe subtype of autoimmune nodopathy (AN). Using a sequential experimental strategy combining *in vitro* stimulation, single-cell sorting, monoclonal antibody (mAb) production, and development of novel antigen "baits" for future antigen-specific enrichment, I sought to characterise the autoreactive B-cell responses that may drive this condition.

First, I established and optimised a peripheral blood mononuclear cell (PBMC) culture system capable of generating antibody-secreting cells (ASCs) and IgG output from both healthy donors and pan-NF AN patients. Extended culture duration significantly enhanced IgG production, while sCD40L had no statistically significant additive effect in 6-day cultures. However, its inclusion in the final protocol was supported by its proven ability to promote robust B-cell activation in downstream single-cell systems, as well as increased IgG output in 14-day cultures in the absence of TNFα and IFNγ, thus providing a reliable platform for subsequent B-cell interrogation. Bulk sorting revealed that memory B-cell bulk cultures exhibited the highest levels of IgG and IgM secretion.

Second, I applied single-cell sorting and sequencing to isolate individual $CD27^{+}IgD^{-}$ B cells from a pan-NF^{+} patient, identifying rare clones with reactivity to both NF155 and NF186 isoforms. Notably, several culture supernatants of these clones displayed clear antigen-specific binding in live cell-based assays (CBAs), despite minimal or absent somatic hypermutation (SHM) as would have been expected based on their switched

memory B-cell surface marker phenotype. Although initial mAbs were generated from two $CD27^{+}IgD^{-}$ memory B cell clones expressing IgG heavy chain transcripts, 4G2 and 5A6, these exhibited low or absent binding to neurofascin in recombinant form. Retrospective re-screening of the corresponding single-cell supernatants revealed that these wells had robust IgM reactivity, and IgM reactivity against NF155 and/or NF186 was found at approximately a four-times higher incidence than IgG across the 480 original single-cell supernatants. Nanopore sequencing confirmed that clone 5A6 expressed transcripts for both IgG and IgM heavy chains, suggesting co-expression or recent class switching. Most other neurofascin-reactive clones exhibited reactivity in either the IgM or IgG isotype, but not both, and pan-NF reactivity was found only in IgM^{+} autoreactive clones (2/13). Furthermore, binding was much stronger to both NF155 and NF186 when clones 4G2 and 5A6 were expressed as IgM mAbs versus IgG1 mAbs. However, this may have reflected the naturally higher avidity conferred by the pentameric structure of IgM,[43] rather than inherently higher affinity at the single Fab level, and the implications for pathogenicity require further investigation. Regardless, these findings indicate that early neurofascin-reactive clones may predominantly secrete IgM, and that class-switched IgG versions can retain reduced or altered binding, supporting a model of class switching occurring outside of extensive affinity maturation.

Third, I developed and validated a recombinant antigen bait system targeting both NF155 and NF186, with encouraging results. This suggests that specific enrichment of neurofascin-reactive B cells from peripheral blood will be possible in future. Following a series of optimisations in protein expression, biotinylation, and tetramerisation, the bait constructs were shown to successfully capture pan-NF^{+} antibodies from patient

sera. This platform will hopefully provide a sensitive method for interrogating the autoreactive B-cell compartment in pan-NF AN and will establish a foundation for future compartmental and longitudinal studies.

6.2 Mechanisms of tolerance failure and B-cell origins

The presence of neurofascin-reactive B cell clones which can be induced to differentiate into IgM antibody-secreting cells (subsequently referred to as "IgM NF-reactive B cells") in this patient, alongside IgG1-dominant autoantibody profiles in serum from all 8 pan-NF AN patients screened in our cohort, highlights the potential complexity and heterogeneity of B-cell tolerance mechanisms in this condition. While a small number of autoreactive clones from the patient studied here expressed both IgM and IgG transcripts, most neurofascin-reactive clones exhibited reactivity in only one isotype. This pattern may reflect dysregulation at multiple levels of B-cell development – potentially involving both central and peripheral tolerance checkpoints – or represent distinct developmental routes driven by microenvironmental or inflammatory cues.

A number of possible mechanisms may underlie these observations. First, failures in central tolerance, such as impaired clonal deletion or receptor editing in the bone marrow, could allow autoreactive B cells to enter the peripheral circulation, explaining the presence of IgM autoantibodies. Second, peripheral checkpoints at the new emigrant and naïve B-cell stages may be compromised, enabling the persistence, activation, and class switching of clones that would ordinarily be silenced or deleted. Third, it is plausible that extrafollicular activation pathways, bypassing germinal centre (GC) selection altogether, may preferentially generate IgM^+ autoreactive B cells in this setting. This possibility is supported by recent findings from Rohrbacher et al (2024),

who observed that polyclonal stimulation of PBMCs from anti-NF155 and anti-CNTN1 patients elicited stronger IgM responses compared to controls, alongside antigen-specific IgG secretion in certain patients.[74] These data suggest that autoreactive memory B cells with IgM- or IgG-secreting potential may persist in peripheral blood despite immunotherapy, indicating partial tolerance failure and functional heterogeneity within the autoreactive compartment.

The absence of significant SHM in the neurofascin-reactive clones recovered from this patient, despite their $CD27^{+}IgD^{-}$ surface phenotype, further supports a model in which these cells may have arisen through GC-independent pathways. However, this interpretation must be approached with caution. It is increasingly recognised that $CD27^{+}IgD^{-}$ memory-like B-cell populations can include cells from extrafollicular responses, particularly under conditions of strong innate immune activation, such as viral infection or systemic inflammation.[113–115] Importantly, the single-cell culture conditions used in this work did not include Resiquimod (a Toll-like receptor-7 (TLR7) agonist), but instead utilised a T cell-like stimulation cocktail consisting of membrane-bound CD40L (mCD40L), B-cell activating factor (BAFF), interleukin (IL)-2, IL-4, and IL-21. This combination is known to support B-cell proliferation, survival, and class switching in a T-dependent manner.[116–119] Therefore, the predominance of IgM secretion among autoreactive clones is unlikely to be an artefact of innate activation and instead may reflect intrinsic properties of the B-cell compartment in this patient or early developmental arrest in class-switch capacity.[118–121]

Alternatively, these findings may also reflect partial or inefficient class switching, despite the presence of switching-promoting cytokines such as IL-4 and IL-21. It

remains possible that neurofascin-specific B cells initiated GC entry but did not undergo full rounds of proliferation, class switching, or selection before being sampled or reactivated in culture. Differences in cytokine exposure, T-cell help, or local immunological context – factors not fully recapitulated *in vitro* – could all influence SHM and isotype distribution.

Taken together, these findings suggest that autoreactive B cells in pan-NF AN may emerge through non-canonical pathways, potentially involving early tolerance failure and extrafollicular/GC-independent class switching. Whether these responses are antigen-driven, influenced by molecular mimicry, or shaped by systemic immune dysregulation remains to be determined. Future work examining the immunophenotype and clonal relationships of neurofascin-reactive B cells in both peripheral and lymphoid compartments may help clarify the development of these clones, as well as their potentially pathogenic role in driving disease.

6.3 The role of autoantibody isotype and subclass

The contrast between IgG1-dominant autoantibodies in this patient's serum and the predominance of IgM-secreting neurofascin-reactive clones isolated from single-cell cultures underscores a potential compartmentalisation of autoreactive B-cell responses. Serum positivity for both NF155- and NF186-reactive IgG1 strongly suggests the existence of class-switched, affinity-matured B cells that may reside in lymphoid tissues or inflamed sites such as peripheral nerves, which were not sampled directly in this work. The peripheral blood and PBMC-derived cultures used here may preferentially reflect circulating precursors, memory-like populations, or B cells activated extrafollicularly with limited exposure to classical GC architecture.

The identification of clones such as 5A6, which expressed both IgM and IgG heavy chain transcripts, suggests the possibility of ongoing or recent class switching. Such dual expression may reflect new emigrant B cells undergoing switching *in vivo*, or could be artefactually preserved *in vitro* due to the simultaneous expansion of related clonal variants under polyclonal stimulation. However, the presence of IgM pan-NF^+ autoantibodies in the sera of the rest of the pan-NF AN cohort screened, including the patient whose B cells were cultured and analysed here, suggest the presence of IgM neurofascin-reactive clones *in vitro* was not purely an artefact. This finding raises the possibility that some of the IgM^+ autoreactive clones isolated represent the immediate precursors of pathogenic $IgG1^+$ B cells. However, the fact that most autoreactive clones secreted either IgM or IgG, but not both, argues for potential functional divergence between isotype compartments. This may reflect either temporally distinct activation stages or the emergence of separate autoreactive lineages that respond to different stimuli, supported by the diverse V/D/J gene usage observed across the three IgG^+ autoreactive clones sequenced thus far. However, further clonal lineage analysis of autoreactive clones in this context will clarify this in future.

The higher abundance of IgM-reactive clones compared to IgG (approximately four-fold) *in vitro* might initially suggest an overrepresentation of early or naïve-like autoreactive populations. However, phenotypic analysis of peripheral B-cell subsets in this patient did not show enrichment of immature B cells relative to a healthy control (Figure 29). In fact, switched and unswitched memory populations were more prevalent in the patient, suggesting prior antigen exposure or broader immune activation. This implies that the dominance of IgM-secreting clones observed in culture does not necessarily reflect naïve B-cell origins, but may reflect isotype-specific

compartmentalisation, a pattern increasingly supported by recent findings in AN cohorts. For example, Rohrbacher et al (2024) used IL-2 plus TLR7/8 stimulation to identify three distinct PBMC secretion patterns in AN: (i) inducible IgG4 secretion in $NF155^+$/$CNTN1^+$/$Caspr1^+$ patients with rituximab-responsive disease; (ii) non-secretion despite high serum titre in a minority of $NF155^+$ IgG4 cases, suggesting long-lived plasma cell dominance; and (iii) no inducible secretion in monophasic IgG4/3 pan-NF patients, implying an acute plasmablast response without formation of autoantigen-specific memory B cells.[74] In contrast, here the IgG1 pan-NF phenotype has been investigated, revealing a circulating memory B-cell pool that was unexpectedly dominated by IgM-secreting clones, many with low or absent SHM. These findings suggest that IgG1 pan-NF AN may retain a rudimentary memory compartment – a subclass-specific divergence not apparent in the IgG4 cases studied by Rohrbacher and colleagues.

This subclass-stratified contrast has important diagnostic and therapeutic implications. Whereas IgG4 pan-NF may benefit from plasma-cell-directed therapies (eg, bortezomib or daratumumab) due to the absence of neurofascin-specific memory B cells,[74] the presence of IgM and complement-activating IgG1 in IgG1 pan-NF argues for combined complement blockade and B-cell targeting. Together, these studies suggest that subclass may reflect fundamentally distinct B-cell developmental trajectories that may guide precision immunotherapy in AN.

The predominance of IgM reactivity in this IgG1 pan-NF AN case, corroborated by both monoclonal reconstruction and retrospective serum screening, likely reflects intrinsic limitations in the autoreactive B-cell repertoire, rather than experimental bias

or naïve cell enrichment. Despite the use of T cell-like stimulatory conditions known to support memory B-cell activation and class switching, a predominance of IgM production persisted, suggesting incomplete or inefficient switching. These observations align with emerging subclass-specific models of autoreactivity, in which IgG1 pan-NF AN maintains a rudimentary memory compartment not seen in IgG4 pan-NF AN.[74]

This subclass-divergent architecture may have functional implications. IgM mAbs derived from neurofascin-reactive clones demonstrated stronger antigen binding than their corresponding IgG1 versions, despite identical variable regions. While this might imply superior antigen recognition, it is more likely attributable, at least in part, to the higher avidity of pentameric IgM, which can compensate for lower individual Fab affinities by multivalent binding. This property may allow even low-affinity antibodies to exert pathogenic effects *in vivo*, particularly if antigen density or conformational accessibility is favourable. However, it remains unclear whether IgM contributes directly to tissue damage in pan-NF AN, or instead serves as a marker of an early, possibly tolerised, precursor population. In future studies, it would be informative to generate monomeric versions of the IgM mAbs characterised here to directly compare their binding strength to both NF155 and NF186 against their native pentameric forms as well as their IgG1 counterparts. Such experiments could help disentangle the relative contributions of multivalency and constant region structure to neurofascin reactivity.

Furthermore, the lack of pan-NF reactivity among IgG^+ clones, despite serum positivity for both NF155 and NF186, raises important questions about epitope specificity, subclass restriction, and selection pressures during B-cell maturation. Among the IgM^+ neurofascin-reactive clones, a minority demonstrated dual reactivity to both isoforms,

whereas the IgG clones identified were specific for only one, with minimal, if any, cross-reactivity. This could reflect stochastic light-chain pairing during B-cell development, as different light chains can significantly alter epitope recognition and engagement even within identical heavy-chain frameworks.

Alternatively, the observed differences may arise from intrinsic structural differences between antibody isotypes. Unlike monomeric IgG, pentameric IgM possesses 10 antigen-binding sites and can bind with high avidity to repetitive or conformational epitopes, even when individual Fab affinities are modest. This multivalency may allow IgM to bind both NF155 and NF186 despite subtle structural differences between the two isoforms. In contrast, IgG antibodies rely on higher monovalent affinity and exhibit a more rigid Fab-Fc geometry, which may constrain epitope accessibility or reduce the breadth of antigen recognition. Furthermore, although class switching preserves the variable region, the change in constant region framework can subtly alter Fab conformation and paratope positioning. Thus, even in the absence of SHM, class switching from IgM to IgG may functionally restrict epitope engagement by altering antibody geometry or flexibility. These findings suggest that the breadth of neurofascin reactivity may not only depend on the B-cell receptor (BCR) sequence, but also on structural properties conferred by the antibody isotype itself.

Further insights into the isotype and subclass usage of neurofascin-reactive clones were provided by CBA-based subclass screening of single-cell culture supernatants. Notably, both IgM and IgG1 were detected in the 4G2 well, consistent with the dual reactivity observed in both mAb formats. In contrast, for 5A6 and 3G2, IgG1 and IgG2 were not detected, despite successful reconstruction of recombinant IgG1 mAbs in the case of

5A6 with both kappa and lambda light chains. These IgG1 mAbs retained reactivity to their targets, albeit with markedly reduced apparent binding strength compared to their IgM counterparts. This suggests that class switching to IgG1 in these clones may preserve basic antigen specificity while diminishing avidity or altering binding conformation. Importantly, IgG3 and IgG4 could not be tested due to limited supernatant availability, leaving open the possibility that additional subclass usage may have gone undetected. These findings raise the possibility that some IgM-reactive B cells may undergo class switching to IgG *in vivo* while retaining autoreactivity, albeit with altered binding characteristics. The functional impact of such isotype transitions, particularly on antigen affinity, stability of binding, and effector function, warrants further structural and kinetic study, especially given the predominance of IgG1 subclass antibodies in patient serum. Likewise, generating IgG3 and/or IgG4 subclass versions of the mAbs generated for this thesis could help determine the role of the autoantibody constant region in shaping both antigen binding properties – such as avidity, accessibility, and epitope engagement – and functional immunopathology, like complement activation and Fcγ receptor binding.

Taken together, these findings suggest that neurofascin reactivity may originate in an IgM^+, minimally mutated compartment, with a subset undergoing class switching to IgG, either in the periphery or within lymphoid structures not sampled here. The differential antigen binding, isotype distribution, and reactivity breadth between these populations raise important questions about the temporal and anatomical dynamics of autoreactive B-cell responses in pan-NF AN. Future work assessing clonal lineage relationships and sampling secondary lymphoid organs, as well as bone marrow, cerebrospinal fluid (CSF), or nerve tissue may help determine whether pan-NF IgG1

antibodies represent evolved descendants of circulating IgM precursors or arise through distinct developmental trajectories.

6.4 Technical and methodological considerations

This work achieved significant progress in isolating and characterising autoreactive B cells in pan-NF AN, but several methodological constraints must be acknowledged.

First, the reliance on PBMCs alone, without access to CSF, peripheral nerve, lymphoid tissue, or bone marrow, likely limited the sampling of autoreactive B cells. Autoreactive clones may be enriched in inflamed or compartmentalised sites, such as lymph nodes or inside the blood-nerve barrier, that were inaccessible in this work. Circulating cells may not fully reflect the complete diversity or maturation state of the autoreactive repertoire.

Second, cryopreserved samples were used for all functional and phenotypic assays. While done for practical reasons of fresh sample availability and timing constraints, and viability post-thaw was generally acceptable, subtle effects on subset recovery and activation potentially, especially for fragile or antigen-experienced populations, cannot be excluded. As discussed in Chapter 3, the possibility that cryopreservation contributed to the absence of detectable antigen-specific immunoglobulin in some cultures remains a relevant interpretative consideration.

The *in vitro* stimulation protocol, though effective at inducing ASC differentiation and immunoglobulin secretion in bulk cultures utilising Resiquimod, was restricted to a single cytokine combination for single-cell cultures (mCD40L, BAFF, IL-2, IL-4, IL-21) due to previous success with this cytokine combination in a single-cell format. This precluded systematic comparisons across activation pathways. Notably, one of the pan-

NF AN patient-derived bulk sort experiments did incorporate a cytokine cocktail that included IL-1β, TNFα, and IL-21, which enabled the detection of neurofascin-reactive IgG production from sorted switched memory B cells. While promising, this was only tested in a limited format, and the broader impact of such cytokines on autoreactive clone activation remains to be fully characterised.

Although sCD40L addition to R848 and IL-2 in short-term bulk cultures did not yield a statistically significant increase in IgG secretion, it was retained in the finalised culture protocol. This decision was based on its demonstrated effectiveness in promoting ASC formation and IgG secretion in previous B-cell studies.[91,92] While sCD40L was not required for short-term IgG induction after 5-6 days of culture, evidence for its role in sustaining B-cell differentiation over extended culture periods and in single-cell applications supported its continued use.

Another constraint was sequencing strategy. Sanger sequencing with IgG-biased primer sets was applied to a limited subset of clones, and while Nanopore sequencing compensated for this, it was only applied to autoreactive clones and not non-autoreactive negative controls that had been used for comparison. As discussed in Chapter 4, this may have underrepresented dual-expressing or non-class-switched clones in the non-autoreactive population, and limited the ability to comprehensively reconstruct clonal relationships or perform lineage tracing. The failure to recover a productive heavy chain sequence from clone 3G2 exemplifies the vulnerability of low-yield sequencing pipelines to dropout and interpretive loss.

Another important limitation is that only $CD27^{+}IgD^{-}$ memory B cells were ultimately single-cell sorted and tested for autoreactivity from a pan-NF AN patient. This strategy

was chosen to enrich for class-switched memory populations, but it carried two important caveats. First, it excluded other potentially relevant B-cell subsets – such as new emigrant, mature naïve, unswitched memory, and ASC/plasmablast subpopulations – that may harbour distinct autoreactive phenotypes. Second, although $CD27^{+}IgD^{-}$ gating is commonly used to approximate switched memory B cells, the sorting panel did not include other isotype-specific surface markers (eg, IgM or IgG), due to constraints on fluorochrome availability and panel complexity. This introduces the possibility that non-switched or incompletely switched cells may have been misclassified as switched memory B cells, particularly in the setting of atypical or dysregulated class-switching. Future studies using either expanded sorting panels or antigen-specific baits could help more precisely map autoreactivity across B-cell subsets, while allowing for flexible post-sort phenotyping.

While the recombinant antigen bait system was ultimately validated and used successfully in proof-of-principle assays, early steps in bait development were complicated by protein quantification errors and inconsistent NF186 expression. The chronic overestimation of bait concentration using Nanodrop, discussed in Chapter 5, likely contributed to weak ELISA signals and limited confidence in early readouts. However, these issues were addressed through improved workflows, and binding of the final large-scale preparations to patient autoantibodies was confirmed via ELISA, though definitive neurofascin expression in the large-scale baits still remains to be confirmed by Western blot. The above considerations underscore the value of this antigen bait system – unlike subset-specific sorting strategies, bait-based enrichment enables subpopulation-agnostic capture of autoreactive B cells while still allowing phenotypic resolution at the time of sorting. In this way, baits can provide a more

inclusive view of the autoreactive repertoire across compartments and could help define the full cellular architecture of autoreactive responses in pan-NF AN.

Finally, retrospective CBA analysis revealed that many early experiments should have included antigen-specific IgM screening, a choice initially made to conserve supernatant for IgG-based assays. As noted at the end of Chapter 3, this likely led to an underrepresentation of relevant autoreactive clones, and future workflows should systematically incorporate screening for multiple antibody isotypes.

Together, these limitations do not undermine the key findings of this work, but rather highlight the importance of continued technical refinement. More extensive multi-compartment sampling and enrichment for autoreactive clones enabled by antigen baits in additional patients, high-throughput isotype-inclusive sequencing, and expanded stimulation panels may substantially enhance the resolution and generalisability of future investigations into autoreactive B-cell ontogeny in autoimmune neuropathies.

6.5 Clinical and scientific implications

6.5.1 Clinical relevance of IgM autoantibodies and complement activation

This study reveals a nuanced isotype landscape in pan-NF AN, with IgG1 autoantibodies dominating in serum[12,27] while IgM-reactive clones emerged predominantly *in vitro*. Previous work has demonstrated that pan-NF^{+} antibodies, particularly IgG1 and IgG3, can mediate complement-dependent injury at the node of Ranvier, causing paranodal disorganisation and axonal damage.[7,120] This reinforces complement activation as a central pathogenic mechanism, distinguishing IgG1 pan-NF AN from less severe, IgG4-dominated nodopathies such as NF155^{+} AN.

The detection of neurofascin-reactive IgM^+ clones in single-cell cultures, although not directly linked to nerve or tissue damage in this work, raises important questions about IgM's potential pathogenicity. While prior studies have not implicated IgM in pan-NF AN, its high avidity and intrinsic complement-fixing capacity suggest that it could play a role, particularly in early disease stages or extrafollicular immune responses. Alternatively, the predominance of IgM *in vitro* may reflect selective expansion of specific subsets under T cell-like stimulation, rather than physiological dominance *in vivo*. Further studies are needed to assess *in vivo* presence, effector function, and clinical correlates of IgM pan-NF^+ autoantibodies.

The presence of both IgM and complement-activating IgG subclasses supports the potential utility of complement-targeted therapies (eg, eculizumab, ravulizumab, C1q inhibitors), especially in patients with histopathological or serological evidence of complement-mediated pathology. This work also highlights the limitations of IgG-only diagnostic platforms. Expanding neurofascin autoantibody testing to include IgM, potentially with high-affinity antigen baits which bind their targets more reliably via ELISA (a 1-day assay, versus a 3-day assay using CBA) versus their commercial counterparts, may increase diagnostic sensitivity and provide insights into disease stage and immunological activity.

6.5.2 Scientific insights into B-cell tolerance and autoimmunity

The coexistence of IgM and IgG neurofascin autoantibodies suggests a breakdown in immune tolerance. The predominance of IgM-secreting neurofascin-reactive clones among recovered neurofascin-reactive cells, coupled with a lack of SHM in many IgG^+ clones, supports a model in which germline-encoded or minimally mutated autoreactive

B cells escape central tolerance and expand through extrafollicular or GC-independent pathways.[59,107–110,121,122]

These patterns resemble those observed in other antibody-mediated autoimmune diseases such as neuromyelitis optica (NMOSD) and N-methyl-D-aspartate receptor (NMDAR)-antibody encephalitis, where tolerance defects at multiple checkpoints permit autoreactive B-cell survival. In both conditions, studies have shown that disease-driving antibodies can derive from B cells with minimal or no SHM, suggesting a bypass of the GC reaction. [91,92,111,127] For instance, in NMOSD, pathogenic aquaporin-4 (AQP4)-specific antibodies were found to originate from naïve or early activated B cells with low SHM burden, consistent with extrafollicular maturation pathways.[92,111] Similarly, in Sjögren's syndrome and rheumatoid arthritis, autoreactive clones with low SHM have been reported.[45,112–114] This convergence across diseases supports the notion that incomplete GC participation, or the bypassing of affinity maturation entirely, may be a shared feature of some pathogenic autoreactive responses. In the context of pan-NF AN, the findings here may therefore reflect an early and potent breach of tolerance, allowing germline or near-germline clones to participate in autoreactivity before undergoing extensive diversification.

However, the findings here could alternatively reflect transient activation states, or experimental biases linked to *in vitro* stimulation, and must be interpreted within that framework. Importantly, the identification and sequencing of pan-NF-specific IgM clones in this work will enable targeted exploration of their complement-fixing capacity, epitope specificity, and fate during class switching in future. These results underscore the need for future clonal lineage analyses to determine whether class-

switched autoreactive B cells represent evolved progeny of IgM^+ precursors or arise through distinct developmental routes.

6.5.3 Implications for diagnosis and therapeutic intervention

From a diagnostic perspective, the dominant IgG1 autoantibody profile in serum, together with the presence of rare but antigen-reactive IgM-producing clones identified in culture and confirmed by mAb reconstruction, underscores the need for more granular autoantibody testing. Isotype-resolved assays, particularly in early or ambiguous clinical presentations, may increase diagnostic accuracy and reveal otherwise undetected immune activity.

Therapeutically, these findings reinforce the potential rationale for complement inhibition in pan-NF AN, while raising the possibility that IgM-mediated mechanisms may be relevant in early disease or relapse. Given IgM's strong complement-fixing potential and multivalency, its role in amplifying or initiating autoimmune injury warrants further exploration. Conversely, its presence may represent an early or abortive stage of autoreactive B-cell activation, suggesting a therapeutic window of early intervention.

The low levels of SHM observed in recovered autoreactive clones also supports a model of extrafollicular or incomplete GC responses, indicating tolerance failure may occur before full maturation. This insight could guide strategies aimed at modulating B-cell activation thresholds, eg, via BAFF/a proliferation-inducing ligand (APRIL) or CD40L blockade. In addition, the antigen bait platform described here offers a robust method to track and characterise autoreactive B cells, enabling monitoring of disease activity, treatment response, and clonal dynamics.

These findings also support a rationale for combining therapeutic strategies that target both extrafollicular activation pathways and early tolerance defects, rather than relying solely on broad-spectrum immunosuppression. Agents that inhibit CD40-CD40L interactions, TLR7 signalling, or BAFF/APRIL-mediated B-cell survival may suppress the activation and persistence of autoreactive clones in extrafollicular compartments. Simultaneously, complement inhibitors can mitigate downstream effector damage. Such rational combinations may ultimately allow for tailored, mechanism-specific interventions that reduce off-target immunosuppression while maximising efficacy.

6.5.4 Implications for other forms of AN

The immunological mechanisms characterised here may have broader implications for other types of AN. While pan-NF AN is defined by a rapidly progressive and treatment-resistant clinical course, correlating with potent effector functions of IgG1 and IgG3 antibodies including complement fixation and Fcγ receptor engagement, other nodopathies – particularly those involving antibodies against CNTN1, Caspr1, or NF155 – are typically associated with the IgG4 subclass and tend to follow a more indolent trajectory, thought to reflect their limited pro-inflammatory capacity.[1,4,6] However, this dichotomy may oversimplify the immunopathological spectrum of AN, as highlighted by several key findings in the work presented here.

A particularly notable observation is that all 8 pan-NF AN patients (13/13 serum samples) screened demonstrated neurofascin-specific serum IgM autoantibodies, whereas only 3 of 6 CNTN1 AN patients (3/19 serum samples) exhibited detectable IgM reactivity (section 4.8). This disparity suggests that IgG1 pan-NF AN may arise from an earlier, more extrafollicular stage of autoreactive B-cell activation, where class

switching is incomplete and GC maturation may be bypassed. This interpretation is supported by multiple lines of evidence from this thesis: neurofascin-specific B cells in the pan-NF AN patient studied here displayed transcriptional signatures of IgM memory, limited SHM, and co-expression of IgM and IgG transcripts from the same clones. Additionally, recombinant IgM mAbs bound NF155 and NF186 more strongly than their IgG1-switched counterparts, despite sharing identical variable regions, highlighting the functional relevance of multivalency in low-mutation autoreactive responses.

By contrast, CNTN1 AN appears to be dominated by more class-switched and possibly GC-derived responses, with a known predominance of IgG4 autoantibodies and far lower rates of IgM reactivity.[1] This suggests that different AN subtypes may reflect immunologically distinct paths to pathogenic autoimmunity: IgG1 pan-NF AN through rapid, possibly T-independent B-cell activation with preserved IgM production, and CNTN1/Caspr1 AN through slower, T-dependent GC responses with more complete class switching and tolerance editing. These mechanistic differences may account not only for the contrasting clinical phenotypes and treatment responses, but also for differences in long-term outcomes and relapse profiles across AN subtypes.

These findings also point to limitations in current diagnostic frameworks. While current assays typically detect IgG binding to nodal/paranodal antigens using cell-based or ELISA platforms, they do not routinely distinguish between isotypes at the point of testing. Given the high prevalence and superior binding avidity of IgM autoantibodies observed in pan-NF AN here, routine screening for IgM across AN may improve diagnostic sensitivity, particularly in patients with rapidly progressive neuropathies or

atypical serologies. Furthermore, the tools developed in this work, such as biotinylated NF155/NF186 antigen baits and single-cell BCR analysis pipelines, could be extended to study other AN subtypes, enabling direct comparison of B-cell clonal architectures, subclass distributions, and effector mechanisms.

In sum, the immunological findings described in this thesis support the notion that the nodopathies do not form a homogeneous disease group, but rather represent a spectrum of related syndromes underpinned by potentially divergent pathways of autoreactive B-cell activation. The near-universal IgM reactivity found in the pan-NF AN patients in our cohort, coupled with evidence for extrafollicular class switching and restricted clonal mutation, define a mechanistically distinct phenotype that stands in contrast to more classically studied IgG4-dominant nodopathies. Recognising and characterising these distinctions will be essential for future efforts to personalise treatment strategies, refine diagnostic criteria, and better understand the immunobiology of nodal/paranodal autoimmune disease.

6.6 Future directions

This thesis has laid the groundwork for advancing the understanding of pan-NF AN, identifying novel immunological mechanisms, and developing targeted diagnostic and therapeutic tools. Building on these findings, several critical avenues emerge for future investigation.

6.6.1 Comprehensive characterisation of autoreactive B-cell populations

Expanding the characterisation of autoreactive B-cell populations is a priority. Incorporating samples from CSF, lymphoid tissues, peripheral nerves, and bone marrow

would help capture compartmentalised autoreactive B cells that are not fully represented in peripheral blood. Employing antigen-specific enrichment tools such as the NF155 and NF186 tetramers developed in this work, combined with advanced flow cytometry and single-cell sequencing, would allow for detailed phenotypic and functional profiling of these rare populations. This would enable comparisons across anatomical niches and developmental stages, potentially uncovering site-specific drivers of pathogenicity. Longitudinal studies tracking the dynamics of autoreactive B cells over the disease course and in response to therapies could illuminate the mechanisms underlying relapse and persistence.

6.6.2 Refining *in vitro* and *in vivo* models of pathogenicity

To better recapitulate the *in vivo* environment and facilitate mechanistic studies, refinement of *in vitro* models is warranted. Human induced pluripotent stem cell (iPSC)-derived peripheral neuron co-cultures will offer an opportunity to assess the pathogenic potential of autoantibodies, including IgM and IgG isotypes. These systems would allow real-time evaluation of neurofascin-specific antibody-induced nerve injury, including complement activation, demyelination, and axonal degeneration, while providing a platform for testing therapeutic interventions. Testing reactivity of patient-derived mAbs on teased nerve fibres, as well as incorporating them into complementary passive transfer experiments in animal models, could validate the pathogenic relevance of findings and support preclinical therapeutic testing. These systems should also include subclass-matched IgG and monomeric IgM mAb variants to dissect the functional impact of isotype structure on pathogenesis.

6.6.3 Dissecting tolerance breakdown and isotype switching mechanisms

The predominance of IgM-reactive clones and limited SHM reported in this thesis point to a critical potential role for early tolerance checkpoints and extrafollicular activation pathways in disease pathogenesis. To build on these insights, future research should apply clonal lineage tracing across multiple B-cell subsets to resolve whether IgM and IgG autoreactivity derive from shared precursors or arise independently. Future research should also focus on delineating the molecular signals – such as TLR7/9 stimulation, BAFF signalling, cytokine profiles, and chronic antigen exposure – that drive the selection and persistence of autoreactive B cells. Investigating the epitope specificity, polyreactivity, and affinity profiles of both IgM and IgG autoantibodies using polyreactivity assays, domain-swapped constructs, and surface plasmon resonance could provide insight into how pathogenic autoreactivity emerges and evolves. Understanding the interplay between IgM and IgG responses will clarify whether IgM acts as an early-stage mediator of pathology or a precursor to class-switched autoreactive populations.

6.6.4 Advancing diagnostics and therapeutic strategies

The identification of IgM-class autoantibodies highlights the need to expand diagnostic assays to include both IgG and IgM neurofascin autoantibody detection. The antigen baits developed in this work, once optimised, could form the basis of sensitive and specific diagnostic platforms. Serial monitoring of autoreactive B-cell populations and isotype profiles, particularly in patients undergoing B-cell depletion therapy, may provide biomarkers predictive of relapse or therapeutic response. Moreover, future diagnostic approaches could couple bait-based enrichment with single-cell RNA and

BCR sequencing to provide a dynamic immunological snapshot of disease activity and therapeutic response.

Therapeutically, the combination of antigen-specific B-cell depletion strategies with early tolerance-restoring interventions may prove more effective than broad-spectrum immunosuppression. The use of baits not only as investigative tools but potentially as vehicles for selectively targeting and eliminating autoreactive B cells represents an innovative potential translational direction. In parallel, modulation of extrafollicular B-cell responses, including blockade of TLR7 signalling or cytokines such as IL-21, could be combined with B-cell-directed therapies to better address GC-independent pathways of autoreactive B-cell emergence in pan-NF AN.

7 Conclusion

This thesis has investigated the origins and characteristics of IgG pan-neurofascin (pan-NF) antibodies in a severe type of autoimmune nodopathy (AN), addressing fundamental questions about immune tolerance and autoreactive B-cell development. Through a comprehensive series of experiments, including peripheral blood mononuclear cell (PBMC) culture optimisation, single-cell sequencing, monoclonal antibody generation, and antigen bait development, I have demonstrated that neurofascin-reactive B cells and their antibody products exhibit features consistent with peripheral tolerance defects, often involving germinal centre (GC)-independent pathways, while central tolerance defects remain a plausible contributing factor.

The identification of neurofascin-155 (NF155)- and/or NF186-specific B-cell clones of both IgM and IgG isotypes, with limited somatic hypermutation (SHM) and evidence of incomplete class switching, suggests a complex interplay of early B-cell activation and tolerance disruption. In particular, the detection of class-switched IgG^+ autoreactive clones with minimal SHM, alongside transcriptional co-expression of IgM and IgG heavy chains in some clones, supports a model of atypical post-GC peripheral tolerance enforcement. Although GC selection was not globally impaired in the patient studied, it remains plausible that autoreactive clones were excluded from GCs but escaped deletion or silencing at subsequent peripheral checkpoints. The absence of IgD expression among these clones suggests at least transient GC exposure, favouring a scenario in which extrafollicular reactivation and class switching occurred without full affinity maturation.

Although definitive evidence for central tolerance breach is lacking, the presence of IgM-secreting ASCs with little or no SHM raises the possibility that early-stage B cells may have evaded clonal deletion or receptor editing in the bone marrow and bypassed GC engagement altogether. Confirming this will require analysis of less mature B-cell subsets, such as new emigrant/transitional B cells, immediately after bone marrow egress. In parallel, clonal lineage tracing will be essential to determine whether IgM^+ and IgG^+ autoreactive populations share developmental origins or arise through distinct trajectories. The latter would indicate independent tolerance breaches at both central and peripheral checkpoints.

The development and validation of biotinylated NF155 and NF186 antigen baits also represent an important technical advance, offering a platform for the enrichment and phenotypic characterisation of neurofascin-reactive B cells. This tool will enable high-resolution mapping of the autoreactive repertoire across tissues, disease stages, and treatment conditions, with significant implications for both diagnostics and mechanistic studies.

While this work advances our understanding of the humoral mechanisms underlying pan-NF AN, it also highlights key areas for future investigation. The precise molecular and immunological triggers that precipitate tolerance failure in these patients remain elusive, and the environmental or genetic factors that may influence B-cell selection and survival in the periphery warrant deeper exploration. Furthermore, the predominance of IgG1 subclass antibodies raises questions about Fc-mediated effector functions, such as complement activation and Fcγ receptor engagement, and their role in nerve injury.

In conclusion, this thesis supports a model in which peripheral tolerance checkpoints, particularly those regulating post-GC selection and extrafollicular responses, are functionally impaired in IgG1 pan-NF AN, with central tolerance defects remaining a possibility. The integration of molecular, cellular, and functional analyses within this work provides a robust foundation for future research into targeted immunotherapies and biomarker development for AN. Ultimately, these findings underscore the importance of precise dissection of B-cell immunobiology in neuroimmune disease and open new avenues for stratified, mechanism-informed clinical intervention.

8 Appendix

8.1 List of primers

8.1.1 Primers for reverse transcription for Sanger sequencing

Name	RT Primer Sequences (5' to 3')
CH5	CCTCTCACCAACTTTCTTGTCC

8.1.2 Primers for nested PCRs for Sanger sequencing – PCR1

Name	Chain	Primer Sequences (5' to 3')
CHG1	IgG Heavy	GTTGTCCACCTTGGTGTTGCTGG
VHL1 mod	IgG Heavy	CCATGGACTGSACCTGGAG
VHL2 mod	IgG Heavy	ATGGACATACTTTGYTCCAC
VHL3	IgG Heavy	CCATGGAGTTKGGGCTGAGCTGG
VHL4 mod	IgG Heavy	ATGAAACAYCTGTGGTTCTT
VHL5	IgG Heavy	ATGGGGTCAACCGCCATCCT
CK1	Kappa	ACACTCTCCCCTGTTGAAGCTCTT
VKL1 mod	Kappa	CTCAGCTCCTGGGGCTYC
VKL2 mod	Kappa	CTGCTCAGCTCYTGGGGC
VKL3	Kappa	GGAARCCCCAGCDCAGC
VKL4	Kappa	CTCTGTTGCTCTGGATCTCTG
VKL5	Kappa	GGGGTCCCAGGTTCACCTCCTC
CL1	Lambda	TGAACATTCTGTAGGGGCCAC

VLL1 mod	Lambda	CCTCTCCTCCTSACCCTCCTC
VLL2 mod	Lambda	CTCCTCACTCAGGRCACAG
VLL3 mod	Lambda	ATGGCCTGGAYCCCTCTCCTBCT
VLL4a mod	Lambda	CTCCTCCTCCACTGCACAG
VLL4b	Lambda	TGGCCTGGGTCTCCTTCTACCTAC
VLL569	Lambda	ATGGCCTGGRCTCCTCTCCTYCTC
VLL710	Lambda	ATGGCCTGGRCTCCTCTCCTYCTG
VLL8	Lambda	ATGGCCTGGATGATGCTTCTCCTC

8.1.3 Primers for nested PCRs for Sanger sequencing – PCR2

Name	**Chain**	**Primer Sequences (5' to 3')**
CPEC VH1/5/7	IgG Heavy, IgM Heavy	CTTTTTCTAGTAGCAACTGCAACCGGTGTACATT CCGAGGTGCAGCTGGTGCAG
CPEC VH2	IgG Heavy, IgM Heavy	CTTTTTCTAGTAGCAACTGCAACCGGTGTACATT CCCAGGTCACCTTGAAGGAG
CPEC VH3	IgG Heavy, IgM Heavy	CTTTTTCTAGTAGCAACTGCAACCGGTGTACATT CTGAGGTGCAGCTGGTGGAG
CPEC VH4	IgG Heavy, IgM Heavy	CTTTTTCTAGTAGCAACTGCAACCGGTGTACATT CCCAGGTGCAGCTGCAGGAG
CPEC VH3-23	IgG Heavy, IgM Heavy	CTTTTTCTAGTAGCAACTGCAACCGGTGTACATT CTGAGGTGCAGCTGTTGGAG
CPEC VH4-34	IgG Heavy, IgM Heavy	CTTTTTCTAGTAGCAACTGCAACCGGTGTACATT CCCAGGTGCAGCTACAGCAGTG
CPEC VH1–18/69	IgG Heavy, IgM Heavy	CTTTTTCTAGTAGCAACTGCAACCGGTGTACATT CCCAGGTTCAGCTGGTGCAG

(silent mut)		
CPEC VH1-45/1-58	IgG Heavy, IgM Heavy	CTTTTTCTAGTAGCAACTGCAACCGGTGTACATTCCCAGATGCAGCTGGTGCAG
CPEC VH1–24	IgG Heavy, IgM Heavy	CTTTTTCTAGTAGCAACTGCAACCGGTGTACATTCCCAGGTCCAGCTGGTACAG
CPEC VH3–9/30/33	IgG Heavy, IgM Heavy	CTTTTTCTAGTAGCAACTGCAACCGGTGTACATTCTGAAGTGCAGCTGGTGGAG
CPEC VH6–1	IgG Heavy, IgM Heavy	CTTTTTCTAGTAGCAACTGCAACCGGTGTACATTCCCAGGTACAGCTGCAGCAG
CPEC VH4–39	IgG Heavy, IgM Heavy	CTTTTTCTAGTAGCAACTGCAACCGGTGTACATTCCCAGCTGCAGCTGCAGGAG
CPEC VH3–33/11/30	IgG Heavy, IgM Heavy	CTTTTTCTAGTAGCAACTGCAACCGGTGTACATTCTCAGGTGCAGCTGGTGGAG
3’ CgCH reverse Tiller	IgG Heavy, IgM Heavy	GGAAGGTGTGCACGCCGCTGGTC
CPEC VK1	Kappa	CTTTTTCTAGTAGCAACTGCAACCGGTGTACATTCTGACATCCAGATGACCCAGTC
CPEC VK1-9/1-13	Kappa	CTTTTTCTAGTAGCAACTGCAACCGGTGTACATTCAGACATCCAGTTGACCCAGTCT
CPEC VK1D-43/1-8	Kappa	CTTTTTCTAGTAGCAACTGCAACCGGTGTACATTGTGCCATCCGGATGACCCAGTC
CPEC VK2	Kappa	CTTTTTCTAGTAGCAACTGCAACCGGTGTACATGGGGATATTGTGATGACCCAGAC

CPEC VK2-28/2-30	Kappa	CTTTTTCTAGTAGCAACTGCAACCGGTGTACATG GGGATATTGTGATGACTCAGTC
CPEC VK3-11/3D-11	Kappa	CTTTTTCTAGTAGCAACTGCAACCGGTGTACATT CAGAAATTGTGTTGACACAGTC
CPEC VK3-15/3D-15	Kappa	CTTTTTCTAGTAGCAACTGCAACCGGTGTACATT CAGAAATAGTGATGACGCAGTC
CPEC VK3-20/3D-20	Kappa	CTTTTTCTAGTAGCAACTGCAACCGGTGTACATT CAGAAATTGTGTTGACGCAGTCT
CPEC VK4-1	Kappa	CTTTTTCTAGTAGCAACTGCAACCGGTGTACATT CGGACATCGTGATGACCCAGTC
3' Ck49 4-516 Reverse	Kappa	GTGCTGTCCTTGCTGTCCTGCT
CPEC VL1	Lambda	CTTTTTCTAGTAGCAACTGCAACCGGTTCCTGGG CCCAGTCTGTGCTGACKCAG
CPEC VL2	Lambda	CTTTTTCTAGTAGCAACTGCAACCGGTTCCTGGG CCCAGTCTGCCCTGACTCAG
CPEC VL3	Lambda	CTTTTTCTAGTAGCAACTGCAACCGGTTCTGTGA CCTCCTATGAGCTGACWCAG
CPEC VL4/5	Lambda	CTTTTTCTAGTAGCAACTGCAACCGGTTCTCTCTC SCAGCYTGTGCTGACTCA
CPEC VL6	Lambda	CTTTTTCTAGTAGCAACTGCAACCGGTTCTTGGG CCAATTTTATGCTGACTCAG
CPEC VL7/8	Lambda	CTTTTTCTAGTAGCAACTGCAACCGGTTCCAATT CYCAGRCTGTGGTGACYCAG
3' CL Reverse	Lambda	GGCTTGAAGCTCCTCACTCGAGGGYGGGAACAG AGTG

8.1.4 Primers for cDNA removal from mRNA beads for Nanopore sequencing

Name	Chain	RT Primer Sequences (5' to 3')
IgM_R_nano	IgM	ACTTGCCTGTCGCTCTATCTTCACGTC
IgG_R_nano	IgG	ACTTGCCTGTCGCTCTATCTTCGTCAA
IgKappa_R_nano	Kappa	ACTTGCCTGTCGCTCTATCTTCACTCT
IgLambda_R_nano	Lambda	ACTTGCCTGTCGCTCTATCTTCTCCAC
F_nano_amp	All	TTTCTGTTGGTGCTGATATTGC

8.2 Cloning vector sequences

8.2.1 IgG1

A pTwist CMV hIgG1 vector (Twist Bioscience) was used for heavy chain components. pTwist CMV hIgK and hIgL2 vectors (Twist Bioscience) were used for kappa and lambda light chain components, respectively. Sequences were confidential and therefore cannot be included here.

8.2.2 IgM

COMPONENT	SEQUENCE
Heavy chain	
Kozak	CCACC
Leader	ATGGGATGGTCATGTATCATCCTTTTTCTAGTAGCAA CTGCAACCGGTGTACATTCT
Light chain	
Kozak	GCCGCCACC
Leader	ATGAGAGCCTGGATCTTTTTCCTGCTGTGCCTGGCTG GGCGCGCCCTGGCC
J chain	

Kozak	GCCGCCACC
Leader	ATGAAGAACCATTTGCTTTTCTGGGGAGTCCTGGCG GTTTTTATTAAGGCTGTTCATGTGAAA
Insert	ATGAAGAACCATTTGCTTTTCTGGGGAGTCCTGGCG GTTTTTATTAAGGCTGTTCATGTGAAAGCCCAAGAA GATGAAAGGATTGTTCTTGTTGACAACAAATGTAAG TGTGCCCGGATTACTTCCAGGATCATCCGTTCTTCCG AAGATCCTAATGAGGACATTGTGGAGAGAAACATCC GAATTATTGTTCCTCTGAACAACAGGGAGAATATCT CTGATCCCACCTCACCATTGAGAACCAGATTTGTGTA CCATTTGTCTGACCTCTGTAAAAAATGTGATCCTACA GAAGTGGAGCTGGATAATCAGATAGTTACTGCTACC CAGAGCAATATCTGTGATGAAGACAGTGCTACAGAG ACCTGCTACACTTATGACAGAAACAAGTGCTACACA GCTGTGGTCCCACTCGTATATGGTGGTGAGACCAAA ATGGTGGAAACAGCCTTAACCCCAGATGCCTGCTAT CCTGACTAA

8.3 Antigen bait sequences

Component	Sequence
NF155 insert (extracellular domain + flexible linker + Avitag + His tag)	GCGATCGCCATGGCCAGGCAGCCACCGCCGCCCTGGGT CCATGCAGCCTTCCTCCTCTGCCTCCTCAGTCTTGGCGG AGCCATCGAAATTCCTATGGATCTGACGCAGCCGCCAA CCATCACCAAGCAGTCAGCGAAGGATCACATCGTGGAC CCCCGTGATAACATCCTGATTGAGTGTGAAGCAAAAGG GAACCCTGCCCCCAGCTTCCACTGGACACGAAACAGCA GATTCTTCAACATCGCCAAGGACCCCCGGGTGTCCATG AGGAGGAGGTCTGGGACCCTGGTGATTGACTTCCGCAG TGGCGGGCGGCCGGAGGAATATGAGGGGGAATATCAG TGCTTCGCCCGCAACAAATTTGGCACGGCCCTGTCCAA TAGGATCCGCCTGCAGGTGTCTAAATCTCCTCTGTGGC CCAAGGAAAACCTAGACCCTGTCGTGGTCCAAGAGGG CGCTCCTTTGACGCTCCAGTGCAACCCCCCGCCTGGAC TTCCATCCCCGGTCATCTTCTGGATGAGCAGCTCCATGG AGCCCATCACCCAAGACAAACGTGTCTCTCAGGGCCAT AACGGAGACCTATACTTCTCCAACGTGATGCTGCAGGA

	CATGCAGACCGACTACAGTTGTAACGCCCGCTTCCACT TCACCCACACCATCCAGCAGAAGAACCCTTTCACCCTC AAGGTCCTCACCAACCACCCTTATAATGACTCGTCCTT AAGAAACCACCCTGACATGTACAGTGCCCGAGGAGTTG CAGAAAGAACACCAAGCTTCATGTATCCCCAGGGCACC GCGAGCAGCCAGATGGTGCTTCGTGGCATGGACCTCCT GCTGGAATGCATCGCCTCCGGGGTCCCAACACCAGACA TCGCATGGTACAAGAAAGGTGGGGACCTCCCATCTGAT AAGGCCAAGTTTGAGAACTTTAATAAGGCCCTGCGTAT CACAAATGTCTCTGAGGAAGACTCCGGGGAGTATTTCT GCCTGGCCTCCAACAAGATGGGCAGCATCCGGCACACG ATCTCGGTGAGAGTAAAGGCTGCTCCCTACTGGCTGGA CGAACCCAAGAACCTTATTCTGGCTCCTGGCGAGGATG GGAGACTGGTGTGTCGAGCCAATGGAAACCCCAAACC CACTGTCCAGTGGATGGTGAATGGGGAACCTTTGCAAT CGGCACCACCTAACCCAAACCGTGAGGTGGCCGGAGA CACCATCATCTTCCGGGACACCCAGATCAGCAGCAGGG CTGTGTACCAGTGCAACACCTCCAACGAGCATGGCTAC CTGCTGGCCAACGCCTTTGTCAGTGTGCTGGATGTGCC GCCTCGGATGCTGTCGCCCCGGAACCAGCTCATTCGAG TGATTCTTTACAACCGGACGCGGCTGGACTGCCCTTTCT TTGGGTCTCCCATCCCCACACTGCGATGGTTTAAGAAT GGGCAAGGAAGCAACCTGGATGGTGGCAACTACCATG TTTATGAGAACGGCAGTCTGGAAATTAAGATGATCCGC AAAGAGGACCAGGGCATCTACACCTGTGTCGCCACCAA CATCCTGGGCAAAGCTGAAAACCAAGTCCGCCTGGAG GTCAAAGACCCCACCAGGATCTACCGGATGCCCGAGG ACCAGGTGGCCAGAAGGGGCACCACGGTGCAGCTGGA GTGTCGGGTGAAGCACGACCCCTCCCTGAAACTCACCG TCTCCTGGCTGAAGGATGACGAGCCGCTCTATATTGGA AACAGGATGAAGAAGGAAGACGACTCCCTGACCATCT TTGGGGTGGCAGAGCGGGACCAGGGCAGTTACACGTG TGTCGCCAGCACCGAGCTAGACCAAGACCTGGCCAAG GCCTACCTCACCGTGCTAGCTGATCAGGCCACTCCAAC TAACCGTTTGGCTGCCCTGCCCAAAGGACGGCCAGACC GGCCCCGGGACCTGGAGCTGACCGACCTGGCCGAGAG GAGCGTGCGGCTGACCTGGATCCCCGGGGATGCTAACA ACAGCCCCATCACAGACTACGTCGTCCAGTTTGAAGAA GACCAGTTCCAACCTGGGGTCTGGCATGACCATTCCAA GTACCCCGGCAGCGTTAACTCAGCCGTCCTCCGGCTGT CCCCGTATGTCAACTACCAGTTCCGTGTCATTGCCATCA ACGAGGTTGGGAGCAGCCACCCCAGCCTCCCATCCGAG

	CGCTACCGAACCAGTGGAGCACCCCCCGAGTCCAATCC TGGTGACGTGAAGGGAGAGGGGACCAGAAAGAACAAC ATGGAGATCACGTGGACGCCCATGAATGCCACCTCGGC CTTTGGCCCCAACCTGCGCTACATTGTCAAGTGGAGGC GGAGAGAGACTCGAGAGGCCTGGAACAACGTCACAGT GTGGGGCTCTCGCTACGTGGTGGGGCAGACCCCAGTCT ACGTGCCCTATGAGATCCGAGTCCAGGCTGAAAATGAC TTCGGGAAGGGCCCTGAGCCAGAGTCCGTCATCGGTTA CTCCGGAGAAGATTATCCCAGGGCTGCGCCCACTGAAG TTAAAGTCCGAGTCATGAACAGCACAGCCATCAGCCTT CAGTGGAACCGCGTCTACTCCGACACGGTCCAGGGCCA GCTCAGAGAGTACCGAGCCTACTACTGGAGGGAGAGC AGCTTGCTGAAGAACCTGTGGGTGTCTCAGAAGAGACA GCAAGCCAGCTTCCCTGGTGACCGCCTCCGTGGCGTGG TGTCCCGCCTCTTCCCCTACAGTAACTACAAGCTGGAG ATGGTTGTGGTCAATGGGAGAGGTGATGGGCCTCGCAG TGAGACCAAGGAGTTCACCACCCCGGAAGGAGTACCC AGTGCCCCTAGGCGTTTCCGAGTCCGGCAGCCCAACCT GGAGACAATCAACCTGGAATGGGATCATCCTGAGCATC CAAATGGGATCATGATTGGATACACTCTCAAATATGTG GCCTTTAACGGGACCAAAGTAGGAAAGCAGATAGTGG AAAACTTCTCTCCCAATCAGACCAAGTTCACGGTGCAA AGAACGGACCCCGTGTCACGCTACCGCTTTACCCTCAG CGCCAGGACGCAGGTGGGCTCTGGGGAAGCCGTCACA GAGGAGTCACCAGCACCCCCGAATGAAGCTACTCCAAC CGCAGCTTACACCAACAACCAAGCGGACATCGCCACCC AGGGCTGGGGTGGCGGTGGCAGTGGTGGCGGAGGGAG CGGCCTGAACGACATCTTCGAGGCCCAGAAGATCGAGT GGCACGAGGTTGGACGTACCAAGCACCACCATCACCAT CACTAA
NF186 insert (extracellular domain + flexible linker + Avitag + His tag)	GCGATCGCCATGGCCAGGCAGCCACCGCCGCCCTGGGT CCATGCAGCCTTCCTCCTCTGCCTCCTCAGTCTTGGCGG AGCCATCGAAATTCCTATGGATCCAAGCATTCAGAATG AGCTGACGCAGCCGCCAACCATCACCAAGCAGTCAGC GAAGGATCACATCGTGGACCCCCGTGATAACATCCTGA TTGAGTGTGAAGCAAAAGGGAACCCTGCCCCCAGCTTC CACTGGACACGAAACAGCAGATTCTTCAACATCGCCAA GGACCCCCGGGTGTCCATGAGGAGGAGGTCTGGGACC CTGGTGATTGACTTCCGCAGTGGCGGGCGGCCGGAGGA ATATGAGGGGGAATATCAGTGCTTCGCCCGCAACAAAT TTGGCACGGCCCTGTCCAATAGGATCCGCCTGCAGGTG TCTAAATCTCCTCTGTGGCCCAAGGAAAACCTAGACCC

	TGTCGTGGTCCAAGAGGGCGCTCCTTTGACGCTCCAGT GCAACCCCCCGCCTGGACTTCCATCCCCGGTCATCTTCT GGATGAGCAGCTCCATGGAGCCCATCACCCAAGACAA ACGTGTCTCTCAGGGCCATAACGGAGACCTATACTTCT CCAACGTGATGCTGCAGGACATGCAGACCGACTACAGT TGTAACGCCCGCTTCCACTTCACCCACACCATCCAGCA GAAGAACCCTTTCACCCTCAAGGTCCTCACCACCCGAG GAGTTGCAGAAAGAACACCAAGCTTCATGTATCCCCAG GGCACCGCGAGCAGCCAGATGGTGCTTCGTGGCATGGA CCTCCTGCTGGAATGCATCGCCTCCGGGGTCCCAACAC CAGACATCGCATGGTACAAGAAAGGTGGGGACCTCCC ATCTGATAAGGCCAAGTTTGAGAACTTTAATAAGGCCC TGCGTATCACAAATGTCTCTGAGGAAGACTCCGGGGAG TATTTCTGCCTGGCCTCCAACAAGATGGGCAGCATCCG GCACACGATCTCGGTGAGAGTAAAGGCTGCTCCCTACT GGCTGGACGAACCCAAGAACCTTATTCTGGCTCCTGGC GAGGATGGGAGACTGGTGTGTCGAGCCAATGGAAACC CCAAACCCACTGTCCAGTGGATGGTGAATGGGGAACCT TTGCAATCGGCACCACCTAACCCAAACCGTGAGGTGGC CGGAGACACCATCATCTTCCGGGACACCCAGATCAGCA GCAGGGCTGTGTACCAGTGCAACACCTCCAACGAGCAT GGCTACCTGCTGGCCAACGCCTTTGTCAGTGTGCTGGA TGTGCCGCCTCGGATGCTGTCGCCCCGGAACCAGCTCA TTCGAGTGATTCTTTACAACCGGACGCGGCTGGACTGC CCTTTCTTTGGGTCTCCCATCCCCACACTGCGATGGTTT AAGAATGGGCAAGGAAGCAACCTGGATGGTGGCAACT ACCATGTTTATGAGAACGGCAGTCTGGAAATTAAGATG ATCCGCAAAGAGGACCAGGGCATCTACACCTGTGTCGC CACCAACATCCTGGGCAAAGCTGAAAACCAAGTCCGCC TGGAGGTCAAAGACCCCACCAGGATCTACCGGATGCCC GAGGACCAGGTGGCCAGAAGGGGCACCACGGTGCAGC TGGAGTGTCGGGTGAAGCACGACCCCTCCCTGAAACTC ACCGTCTCCTGGCTGAAGGATGACGAGCCGCTCTATAT TGGAAACAGGATGAAGAAGGAAGACGACTCCCTGACC ATCTTTGGGGTGGCAGAGCGGGACCAGGGCAGTTACAC GTGTGTCGCCAGCACCGAGCTAGACCAAGACCTGGCCA AGGCCTACCTCACCGTGCTAGCTGATCAGGCCACTCCA ACTAACCGTTTGGCTGCCCTGCCCAAAGGACGGCCAGA CCGGCCCCGGGACCTGGAGCTGACCGACCTGGCCGAG AGGAGCGTGCGGCTGACCTGGATCCCCGGGGATGCTAA CAACAGCCCCATCACAGACTACGTCGTCCAGTTTGAAG AAGACCAGTTCCAACCTGGGGTCTGGCATGACCATTCC

	AAGTACCCCGGCAGCGTTAACTCAGCCGTCCTCCGGCT GTCCCCGTATGTCAACTACCAGTTCCGTGTCATTGCCAT CAACGAGGTTGGGAGCAGCCACCCCAGCCTCCCATCCG AGCGCTACCGAACCAGTGGAGCACCCCCCGAGTCCAAT CCTGGTGACGTGAAGGGAGAGGGGACCAGAAAGAACA ACATGGAGATCACGTGGACGCCCATGAATGCCACCTCG GCCTTTGGCCCCAACCTGCGCTACATTGTCAAGTGGAG GCGGAGAGAGACTCGAGAGGCCTGGAACAACGTCACA GTGTGGGGCTCTCGCTACGTGGTGGGGCAGACCCCAGT CTACGTGCCCTATGAGATCCGAGTCCAGGCTGAAAATG ACTTCGGGAAGGGCCCTGAGCCAGAGTCCGTCATCGGT TACTCCGGAGAAGATTTACCCAGTGCCCCTAGGCGTTT CCGAGTCCGGCAGCCCAACCTGGAGACAATCAACCTGG AATGGGATCATCCTGAGCATCCAAATGGGATCATGATT GGATACACTCTCAAATATGTGGCCTTTAACGGGACCAA AGTAGGAAAGCAGATAGTGGAAAACTTCTCTCCCAATC AGACCAAGTTCACGGTGCAAAGAACGGACCCCGTGTC ACGCTACCGCTTTACCCTCAGCGCCAGGACGCAGGTGG GCTCTGGGGAAGCCGTCACAGAGGAGTCACCAGCACC CCCGAATGAAGCTACTCCAACCGCAGCTCCTCCCACAT TGCCCCCGACTACCGTGGGTGCGACGGGCGCTGTGAGC AGTACCGATGCTACTGCCATTGCTGCCACCACCGAAGC CACAACAGTCCCCATCATCCCAACTGTCGCACCTACCA CCATCGCCACCACCACCACCGTCGCCACAACTACTACA ACCACTGCTGCCGCCACCACCACCACGGAGAGTCCTCC CACCACCACCTCCGGGACTAAGATACACGAATCCGCCC CTGATGAGCAGTCCATATGGAACGTCACGGTGCTCCCC AACAGTAAATGGGCCAACATCACCTGGAAGCACAATTT CGGGCCCGGAACTGACTTTGTGGTTGAGTACATCGACA GCAACCATACGAAAAAAACTGTCCCAGTTAAGGCCCA GGCTCAGCCTATACAGCTGACAGACCTCTATCCCGGGA TGACATACACGTTGCGGGTTTATTCCCGGGACAACGAG GGCATCAGCAGTACCGTCATCACCTTTATGACCAGTAC AGCTTACACCAACAACCAAGCGGACATCGCCACCCAG GGCTGGGGTGGCGGTGGCAGTGGTGGCGGAGGGAGCG GCCTGAACGACATCTTCGAGGCCCAGAAGATCGAGTGG CACGAGGTTGGACGTACCAAGCACCACCATCACCATCA CTAA

8.4 Antigen bait tetramerisation protocol

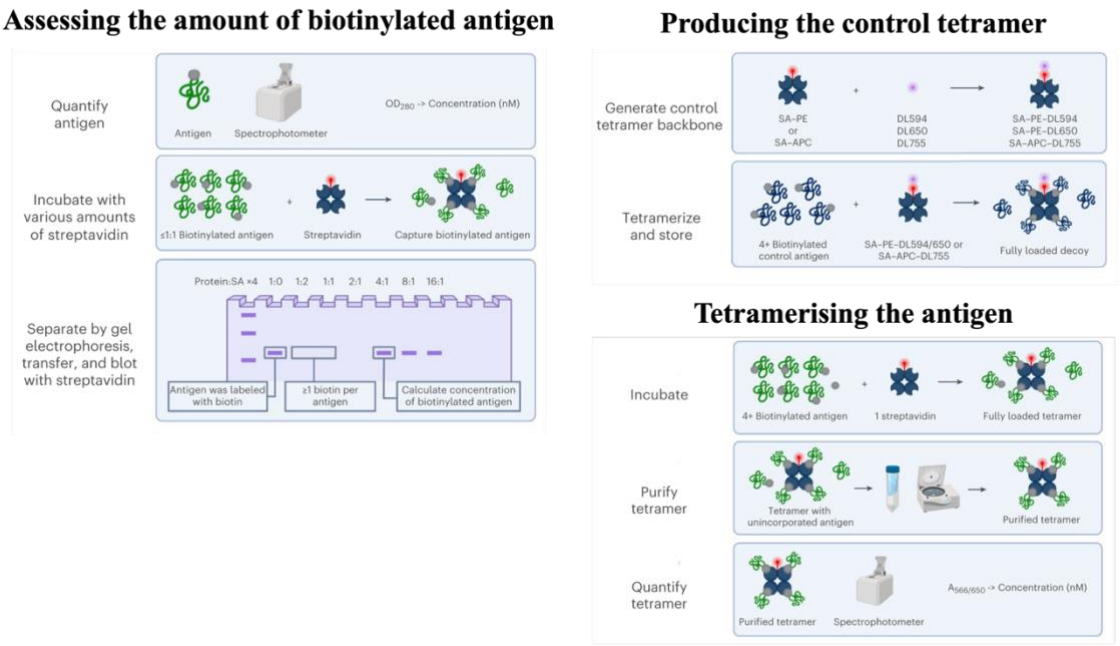

Figure 62: Overview of assessing the amount of biotinylated antigen bait, producing the control tetramer, and tetramerising the antigens. *Adapted from Phelps et al (2024).*[90]

Reference List

1. Johnson, C. B., Fehmi, J. & Rinaldi, S. The immunology and neuropathology of the autoimmune nodopathies. *J Neuroimmunol* 0, 578665 (2025).

2. Fehmi, J. *et al.* IgG1 pan-neurofascin antibodies identify a severe yet treatable neuropathy with a high mortality. *Brain* 1–2 (2020).

3. Jentzer, A. *et al.* IgG4 Valency Modulates the Pathogenicity of Anti–Neurofascin-155 IgG4 in Autoimmune Nodopathy. *Neurol Neuroimmunol Neuroinflamm* 9, 200014 (2022).

4. Dalakas, M. C. Autoimmune Neurological Disorders with IgG4 Antibodies: a Distinct Disease Spectrum with Unique IgG4 Functions Responding to Anti-B Cell Therapies. *Neurotherapeutics* 19, 741–752 (2022).

5. Taieb, G. *et al.* Effect of monovalency on anti-contactin-1 IgG4. *Front Immunol* 14, 1–9 (2023).

6. Querol, L. & Dalakas, M. C. The Discovery of Autoimmune Nodopathies and the Impact of IgG4 Antibodies in Autoimmune Neurology. *Neuroimmunol Neuroinflamm* 12, e200365 (2024).

7. Appeltshauser, L. *et al.* Anti-pan-neurofascin antibodies induce subclass-related complement activation and nodo-paranodal damage. *Brain* 146, 1932–1949 (2023).

8. Koike, H. *et al.* Ultrastructural mechanisms of macrophage-induced demyelination in CIDP. *Neurology* 91, 1051–1060 (2018).

9. Koike, H. & Katsuno, M. Macrophages and Autoantibodies in Demyelinating Diseases. *Cells* 10, 844 (2021).

10. Willison, H. J. & Yuki, N. Peripheral neuropathies and anti-glycolipid antibodies. *Brain* 125, 2591–2625 (2002).

11. Jin, P. H. & Shin, S. C. Neuropathy of Connective Tissue Diseases and Other Systemic Diseases. *Semin Neurol* 39, 651–668 (2019).

12. Pascual-Goñi, E., Caballero-Ávila, M. & Querol, L. Antibodies in Autoimmune Neuropathies: What to Test, How to Test, Why to Test. *Neurology* 103, e209725 (2024).

13. Al-Hakem, H. *et al.* CSF Findings in Relation to Clinical Characteristics, Subtype, and Disease Course in Patients With Guillain-Barré Syndrome. *Neurology* 100, E2386–E2397 (2023).

14. Broers, M. C. *et al.* Clinical relevance of distinguishing autoimmune nodopathies from CIDP: Longitudinal assessment in a large cohort. *J Neurol Neurosurg Psychiatry* 95, 52–60 (2024).

15. Collet, R., Caballero-Ávila, M. & Querol, L. Clinical and pathophysiological implications of autoantibodies in autoimmune neuropathies. *Rev Neurol (Paris)* (2023) doi:10.1016/j.neurol.2023.02.064.

16. Caballero-Ávila, M., Martin-Aguilar, L., Collet-Vidiella, R., Querol, L. & Pascual-Goñi, E. A pathophysiological and mechanistic review of chronic

inflammatory demyelinating polyradiculoneuropathy therapy. *Front Immunol* 16, 1575464 (2025).

17. Appeltshauser, L. *et al.* Antiparanodal antibodies and IgG subclasses in acute autoimmune neuropathy. *Neurology(R) neuroimmunology & neuroinflammation* 7, (2020).

18. Tiller, T. *et al.* Efficient generation of monoclonal antibodies from single human B cells by single cell RT-PCR and expression vector cloning. *J Immunol Methods* 329, 112–124 (2008).

19. Vogelzang, A. *et al.* A Fundamental Role for Interleukin-21 in the Generation of T Follicular Helper Cells. *Immunity* 29, 127–137 (2008).

20. Espéli, M. & Linterman, M. T follicular helper cells: Methods and protocols. *T Follicular Helper Cells: Methods and Protocols* 1–226 (2015) doi:10.1007/978-1-4939-2498-1.

21. Sun, B., Ramberger, M., O'Connor, K. C., Bashford-Rogers, R. J. M. & Irani, S. R. The B cell immunobiology that underlies CNS autoantibody-mediated diseases. *Nature Reviews Neurology* vol. 16 481–492 Preprint at https://doi.org/10.1038/s41582-020-0381-z (2020).

22. Chalayer, E. *et al.* Fc receptors gone wrong: A comprehensive review of their roles in autoimmune and inflammatory diseases. *Autoimmun Rev* 21, 103016–103016 (2022).

23. Tarasenko, T., Dean, J. A. & Bolland, S. FcgammaRIIB as a modulator of autoimmune disease susceptibility. *Autoimmunity* 40, 409–417 (2007).

24. Skokowaa, J., Ali, S. R., Kumar, V., Schmidt, R. E. & Gessner, J. E. The Regulatory FcγR System in Antibody-Mediated Autoimmune Diseases. *Transfusion Medicine and Hemotherapy* 31, 74–82 (2004).

25. Pricop, L. *et al.* Differential modulation of stimulatory and inhibitory Fc gamma receptors on human monocytes by Th1 and Th2 cytokines. *Journal of Immunology* 166, 531–537 (2001).

26. Liu, Y. *et al.* Cytokine-mediated regulation of activating and inhibitory Fcγ receptors in human monocytes. *J Leukoc Biol* 77, 767–776 (2005).

27. Fehmi, J., Scherer, S. S., Willison, H. J. & Rinaldi, S. Nodes, paranodes and neuropathies. *Journal of Neurology, Neurosurgery and Psychiatry* Preprint at https://doi.org/10.1136/jnnp-2016-315480 (2018).

28. Odegard, V. H. & Schatz, D. G. Targeting of somatic hypermutation. *Nat Rev Immunol* 6, 573–583 (2006).

29. Brooks, J. F., Steptoe, R. J. & Steptoe, R. J. The periphery is the dominant site of B-cell deletion in a polyclonal repertoire. *bioRxiv* 2020.03.10.985192 (2020) doi:10.1101/2020.03.10.985192.

30. Franz, B., May, K. F., Dranoff, G. & Wucherpfennig, K. Ex vivo characterization and isolation of rare memory B cells with antigen tetramers. *Blood* 118, 348–357 (2011).

31. Sage, P. T. & Sharpe, A. H. T follicular regulatory cells. *Immunol Rev* 271, 246–259 (2016).

32. Cambier, J. C., Gauld, S. B., Merrell, K. T. & Vilen, B. J. B-cell anergy: from transgenic models to naturally occurring anergic B cells? *Nat Rev Immunol* 7, 633–643 (2007).

33. Gutzeit, C., Chen, K. & Cerutti, A. The enigmatic function of IgD: some answers at last. *Eur J Immunol* 48, 1101–1113 (2018).

34. de Taeye, S. W., Rispens, T. & Vidarsson, G. The Ligands for Human IgG and Their Effector Functions. *Antibodies 2019, Vol. 8, Page 30* 8, 30 (2019).

35. Zhang, L. *et al.* Anti-neurofascin-155 antibody mediated a distinct phenotype of chronic inflammatory demyelinating polyradiculoneuropathy. *J Neurol* 271, 4991–5002 (2024).

36. Hervé *et al.* Unmutated and mutated chronic lymphocytic leukemias derive from self-reactive B cell precursors despite expressing different antibody reactivity. *Journal of Clinical Investigation* 115, 1636–1643 (2005).

37. Parks, A. R. & Peters, J. E. V(D)J Recombination. *Molecular Life Sciences* 1243–1245 (2018) doi:10.1007/978-1-4614-1531-2_170.

38. Christie, S. M., Fijen, C. & Rothenberg, E. V(D)J Recombination: Recent Insights in Formation of the Recombinase Complex and Recruitment of DNA Repair Machinery. *Front Cell Dev Biol* 10, (2022).

39. Shimazaki, N. & Lieber, M. R. Histone methylation and V(D)J recombination. *Int J Hematol* 100, 230–237 (2014).

40. De Villartay, J. P. Congenital defects in V(D)J recombination. *Br Med Bull* 114, 157–167 (2015).

41. Yurasov, S. *et al.* Defective B cell tolerance checkpoints in systemic lupus erythematosus. *Journal of Experimental Medicine* (2005) doi:10.1084/jem.20042251.

42. Ota, M. *et al.* Multimodal repertoire analysis unveils B cell biology in health and immune-mediated diseases. *medRxiv* 2022.01.04.22268769 (2022) doi:10.1136/ard-2023-224421.

43. Tiller, T. *et al.* Autoreactivity in human IgG+ memory B cells. *Immunity* 26, 205–213 (2007).

44. Koelsch, K. *et al.* Mature B cells class switched to IgD are autoreactive in healthy individuals. *J Clin Invest* 117 6, 1558–65 (2007).

45. Corsiero, E., Sutcliffe, N., Pitzalis, C., Bombardieri, M. & Reddy, J. Accumulation of Self-Reactive Naïve and Memory B Cell Reveals Sequential Defects in B Cell Tolerance Checkpoints in Sjögren's Syndrome. *PLoS One* 9, (2014).

46. Kumar, S. *et al.* Developmental bifurcation of human T follicular regulatory cells. *Sci Immunol* 6, (2021).

47. Chen, Z. & Wang, J. H. Signaling control of antibody isotype switching. *Adv Immunol* 141, 105–164 (2019).

48. Vlachiotis, S. & Abolhassani, H. Transcriptional regulation of B cell class-switch recombination: the role in development of noninfectious complications. *Expert Rev Clin Immunol* 18, 1145–1154 (2022).

49. Dauba, A. *et al.* The immunoglobulin heavy chain super enhancer controls class switch recombination in developing B cells. *Dental science reports* 14, (2024).

50. Castleman, M. J. *et al.* Phenotypical and Functional Characterization of Unswitched Memory B cells verses Switched during SARS-CoV-2 Infection. *Journal of Immunology* 210, 75.15-75.15 (2023).

51. Mikelov, A. *et al.* Memory persistence and differentiation into antibody-secreting cells accompanied by positive selection in longitudinal BCR repertoires. *Elife* 11, (2022).

52. Claireaux, M. *et al.* Deep profiling of B cells responding to various pathogens uncovers compartments in IgG memory B cell and antibody-secreting lineages. *Sci Adv* 11, 1331 (2025).

53. Broketa, M. & Bruhns, P. Single-Cell Technologies for the Study of Antibody-Secreting Cells. *Front Immunol* 12, (2022).

54. Rivas, J. R. *et al.* Peripheral VH4+ plasmablasts demonstrate autoreactive B cell expansion toward brain antigens in early multiple sclerosis patients. *Acta Neuropathol* 133, 43–60 (2017).

55. Christopher, M. A., Johnson, S. N., Griffin, J. D. & Berkland, C. J. Autoantigen Tetramer Silences Autoreactive B Cell Populations. *Mol Pharm* 17, 4201–4211 (2020).

56. Jiao, L. *et al.* Efficacy of low dose rituximab in treatment-resistant CIDP with antibodies against NF-155. *J Neuroimmunol* 345, 577280 (2020).

57. Dalakas, M. C. Autoimmune Neurological Disorders with IgG4 Antibodies: a Distinct Disease Spectrum with Unique IgG4 Functions Responding to Anti-B Cell Therapies. *Neurotherapeutics* 1, 1–12 (2022).

58. Sun, B. *et al.* Permissive central tolerance plus defective peripheral checkpoints licence pathogenic memory B cells in CASPR2-antibody encephalitis. *bioRxiv* 2025.01.14.631703 (2025) doi:10.1101/2025.01.14.631703.

59. Meffre, E. & O'Connor, K. C. Impaired B-cell tolerance checkpoints promote the development of autoimmune diseases and pathogenic autoantibodies. *Immunological Reviews* vol. 292 90–101 Preprint at https://doi.org/10.1111/imr.12821 (2019).

60. Deguine, J. & Xavier, R. J. B cell tolerance and autoimmunity: Lessons from repertoires. *Journal of Experimental Medicine* 221, (2024).

61. Battram, A. M., Bachiller, M. & Martín-Antonio, B. Senescence in the Development and Response to Cancer with Immunotherapy: A Double-Edged Sword. *International Journal of Molecular Sciences 2020, Vol. 21, Page 4346* 21, 4346 (2020).

62. Jenks, S. A. *et al.* Distinct Effector B Cells Induced by Unregulated Toll-like Receptor 7 Contribute to Pathogenic Responses in Systemic Lupus Erythematosus. *Immunity* 49, 725-739.e6 (2018).

63. Cowan, G. J. M. *et al.* In Human Autoimmunity, a Substantial Component of the B Cell Repertoire Consists of Polyclonal, Barely Mutated IgG+ve B Cells. *Front Immunol* 11, 395–395 (2020).

64. Martinez-Martinez, L. *et al.* Anti-NF155 chronic inflammatory demyelinating polyradiculoneuropathy strongly associates to HLA-DRB15. *J Neuroinflammation* 14, (2017).

65. Ogata, H. *et al.* Unique HLA haplotype associations in IgG4 anti-neurofascin 155 antibody-positive chronic inflammatory demyelinating polyneuropathy. *J Neuroimmunol* 339, (2020).

66. Cheekati, M. & Murakhovskaya, I. Anti-B-Cell-Activating Factor (BAFF) Therapy: A Novel Addition to Autoimmune Disease Management and Potential for Immunomodulatory Therapy in Warm Autoimmune Hemolytic Anemia. *Advances in Cardiovascular Diseases* 12, 1597–1597 (2024).

67. Uppin, V. *et al.* CAR-T cell targeting three receptors on autoreactive B cells for systemic lupus erythematosus therapy. *J Autoimmun* 151, 103369–103369 (2025).

68. Kleyer, A. *et al.* Op0069 sequential b cell/t cell therapy to re-induce humoral immune tolerance in acpa-positive rheumatoid arthritis (tolera): first results from phase 2, open label, randomized controlled trial comparing rituximab and

abatacept with rituximab alone. 83.2-83 (2024) doi:10.1136/ANNRHEUMDIS-2024-EULAR.4932.

69. Li, Y. *et al.* Structural insights into immunoglobulin M. *Science (1979)* 367, 1014–1017 (2020).

70. Goldberg, B. S. & Ackerman, M. E. Antibody-mediated complement activation in pathology and protection. *Immunol Cell Biol* 98, 305–317 (2020).

71. Wang, B. *et al.* Regulation of antibody-mediated complement-dependent cytotoxicity by modulating the intrinsic affinity and binding valency of IgG for target antigen. *MAbs* 12, (2020).

72. Appeltshauser, L. *et al.* Case report: target antigen and subclass switch in a patient with autoimmune nodopathy. *Front Immunol* 15, 1475478 (2024).

73. Napodano, C. *et al.* Immunological Role of IgG Subclasses. *Immunol Invest* 1–18 (2021) doi:10.1080/08820139.2020.1775643.

74. Rohrbacher, S. *et al.* Different Patterns of Autoantibody Secretion by Peripheral Blood Mononuclear Cells in Autoimmune Nodopathies. *Neurol Neuroimmunol Neuroinflamm* 11, e200295 (2024).

75. Stengel, H. *et al.* Anti-pan-neurofascin IgG3 as a marker of fulminant autoimmune neuropathy. *Neurol Neuroimmunol Neuroinflamm* 6, (2019).

76. Xu, Q. *et al.* Characteristics of Anti-Contactin1 Antibody-Associated Autoimmune Nodopathies With Concomitant Membranous Nephropathy. *Front Immunol* 12, 759187 (2021).

77. Ratelade, J. *et al.* Involvement of antibody-dependent cell-mediated cytotoxicity in inflammatory demyelination in a mouse model of neuromyelitis optica. *Acta Neuropathol* 126, 699–709 (2013).

78. Duan, T., Smith, A. J. & Verkman, A. S. Complement-independent bystander injury in AQP4-IgG seropositive neuromyelitis optica produced by antibody-dependent cellular cytotoxicity. *Acta Neuropathol Commun* 7, 112 (2019).

79. Querol, L. *et al.* Rituximab in treatment-resistant CIDP with antibodies against paranodal proteins. *Neurol Neuroimmunol Neuroinflamm* 2, e149 (2015).

80. Querol, L. *et al.* Neurofascin IgG4 antibodies in CIDP associate with disabling tremor and poor response to IVIg. *Neurology* (2014) doi:10.1212/WNL.0000000000000205.

81. Willison, H. J., Jacobs, B. C. & van Doorn, P. A. Guillain-Barré syndrome. *The Lancet* 388, 717–727 (2016).

82. Yuki, N. & Hartung, H.-P. Guillain–Barré Syndrome. *New England Journal of Medicine* 366, 2294–2304 (2012).

83. Querol, L. *et al.* Antibodies against peripheral nerve antigens in chronic inflammatory demyelinating polyradiculoneuropathy. *Scientific Reports 2017 7:1* 7, 1–9 (2017).

84. Delmont, E. *et al.* Autoantibodies to nodal isoforms of neurofascin in chronic inflammatory demyelinating polyneuropathy. *Brain* 140, 1851–1858 (2017).

85. Cortese, A. *et al.* Antibodies to neurofascin, contactin-1, and contactin-associated protein 1 in CIDP: Clinical relevance of IgG isotype. *Neurol Neuroimmunol Neuroinflamm* 7, E639 (2020).

86. Chu, V. T. & Berek, C. The establishment of the plasma cell survival niche in the bone marrow. *Immunol Rev* 251, 177–188 (2013).

87. Fels, M. *et al.* Report of a fulminant anti-pan-neurofascin-associated neuropathy responsive to rituximab and bortezomib. *Journal of the Peripheral Nervous System* 26, 475–480 (2021).

88. Cornelis, R., Chang, H. D. & Radbruch, A. Keeping up with the stress of antibody production: BAFF and APRIL maintain memory plasma cells. *Curr Opin Immunol* 71, 97–102 (2021).

89. Subas Satish, H. P. *et al.* NAb-seq: an accurate, rapid, and cost-effective method for antibody long-read sequencing in hybridoma cell lines and single B cells. *MAbs* 14, (2022).

90. Phelps, A. *et al.* Production and use of antigen tetramers to study antigen-specific B cells. *Nat Protoc* 19, 727–751 (2024).

91. Makuch, M. *et al.* N-methyl-D-aspartate receptor antibody production from germinal center reactions: Therapeutic implications. *Ann Neurol* 83, 553–561 (2018).

92. Wilson, R. *et al.* Condition-dependent generation of aquaporin-4 antibodies from circulating B cells in neuromyelitis optica. *Brain* 141, 1063–1074 (2018).

93. Rodríguez, Y. *et al.* Chronic inflammatory demyelinating polyneuropathy as an autoimmune disease. *Journal of Autoimmunity* vol. 102 8–37 Preprint at https://doi.org/10.1016/j.jaut.2019.04.021 (2019).

94. Wolbert, J., Cheng, M. I., Meyer Zu Horste, G. & Su, M. A. R E V I E W Deciphering immune mechanisms in chronic inflammatory demyelinating polyneuropathies. *Reference information: JCI Insight* 5, (2020).

95. Rizzo, F. R. *et al.* Tumor Necrosis Factor and Interleukin-1 β Modulate Synaptic Plasticity during Neuroinflammation. *Neural Plasticity* vol. 2018 Preprint at https://doi.org/10.1155/2018/8430123 (2018).

96. O'Carroll, S. J. *et al.* Pro-inflammatory TNFaα and IL-1β differentially regulate the inflammatory phenotype of brain microvascular endothelial cells. *J Neuroinflammation* 12, (2015).

97. Mendiola, A. S. & Cardona, A. E. The IL-1β phenomena in neuroinflammatory diseases. *Journal of Neural Transmission* vol. 125 781–795 Preprint at https://doi.org/10.1007/s00702-017-1732-9 (2018).

98. Hashiguchi, M., Asatsuma-Okumura, T. & Iwai, Y. Interleukin 21 promotes IgG1+ plasma cell differentiation instead of class switching to IgE via Blimp1 expression. *Eur J Immunol* 54, (2024).

99. Ettinger, R. *et al.* IL-21 induces differentiation of human naive and memory B cells into antibody-secreting plasma cells. *J Immunol* 175, 7867–7879 (2005).

100. Pan, Z. *et al.* Peripheral Blood Lymphocyte Subsets and Heterogeneity of B Cell Subsets in Patients of Idiopathic Inflammatory Myositis with Different Myositis-specific Autoantibodies. *Inflammation* 48, (2025).

101. Polak, J. *et al.* Single-cell transcriptomics combined with proteomics of intrathecal IgG reveal transcriptional heterogeneity of oligoclonal IgG-secreting cells in multiple sclerosis. *Front Cell Neurosci* 17, 1189709 (2023).

102. Berti, A. *et al.* Circulating autoreactive proteinase 3+ B cells and tolerance checkpoints in ANCA-associated vasculitis. *JCI Insight* 6, e150999 (2021).

103. Wangriatisak, K. *et al.* The expansion of activated naive DNA autoreactive B cells and its association with disease activity in systemic lupus erythematosus patients. *Arthritis Res Ther* 23, 1–11 (2021).

104. Pollmann, R. *et al.* Identification of Autoreactive B Cell Subpopulations in Peripheral Blood of Autoimmune Patients With Pemphigus Vulgaris. *Front Immunol* 10, (2019).

105. Malkiel, S. *et al.* Checkpoints for Autoreactive B Cells in the Peripheral Blood of Lupus Patients Assessed by Flow Cytometry. *Arthritis Rheumatol* 68, 2210–2220 (2016).

106. Trezise, S. *et al.* An arrayed CRISPR screen of primary B cells reveals the essential elements of the antibody secretion pathway. *Front Immunol* 14, (2023).

107. Sertorio, M., Amarachintha, S., Wilson, A. & Pang, Q. Loss of Fancc Impairs Antibody-Secreting Cell Differentiation in Mice through Deregulating the Wnt Signaling Pathway. *J Immunol* 196, 2986–2994 (2016).

108. Ascs, E. *et al.* 203 Follicular B cell derived CD21lo B cells are immediate precursors to autoreactive extrafollicular ASCs. *Lupus Sci Med* 11, A13.1-A13 (2024).

109. Fichtner, M. L. *et al.* Affinity maturation is required for pathogenic monovalent IgG4 autoantibody development in myasthenia gravis. *J Exp Med* 217, (2020).

110. Bien, C. G. *et al.* Anti-contactin-associated protein-2 encephalitis: relevance of antibody titres, presentation and outcome. *Eur J Neurol* 24, 175–186 (2017).

111. Cotzomi, E. *et al.* Early B cell tolerance defects in neuromyelitis optica favour anti-AQP4 autoantibody production. doi:10.1093/brain/awz106.

112. Menard, L., Samuels, J., Ng, Y. S. & Meffre, E. Inflammation-independent defective early B cell tolerance checkpoints in rheumatoid arthritis. *Arthritis Rheum* (2011) doi:10.1002/art.30164.

113. Glauzy, S. *et al.* Defective Early B Cell Tolerance Checkpoints in Sjögren's Syndrome Patients. *Arthritis and Rheumatology* (2017) doi:10.1002/art.40215.

114. Samuels, J., Ng, Y. S., Coupillaud, C., Paget, D. & Meffre, E. Impaired early B cell tolerance in patients with rheumatoid arthritis. *Journal of Experimental Medicine* (2005) doi:10.1084/jem.20042321.

115. Kristyanto, H. *et al.* Multifunctional, Multivalent PIC Polymer Scaffolds for Targeting Antigen-Specific, Autoreactive B Cells. *ACS Biomater Sci Eng* 8, 1486–1493 (2022).

116. Brooks, J. F., Liu, X., Davies, J. M., Wells, J. W. & Steptoe, R. J. Tetramer-based identification of naïve antigen-specific B cells within a polyclonal repertoire. *Eur J Immunol* 48, 1251–1254 (2018).

117. Hurtado, C. *et al.* Altered B cell phenotype and CD27+ memory B cells are associated with clinical features and environmental exposure in Colombian systemic lupus erythematosus patients. *Front Med (Lausanne)* 9, (2022).

118. Nevalainen, T. *et al.* CD27- IgD- B cell memory subset associates with inflammation and frailty in elderly individuals but only in males. *Immunity & Ageing* 16, 1–9 (2019).

119. Seifert, M. *et al.* Functional capacities of human IgM memory B cells in early inflammatory responses and secondary germinal center reactions. *Proc Natl Acad Sci U S A* 112, 201416276 (2015).

120. Robinson, M. J. *et al.* BAFF, IL-4 and IL-21 separably program germinal center-like phenotype acquisition, BCL6 expression, proliferation and survival of CD40L-activated B cells in vitro. *Immunol Cell Biol* 97, 826–839 (2019).

121. Jin, H. & Malek, T. R. Redundant and unique regulation of activated mouse B lymphocytes by IL-4 and IL-21. *J Leukoc Biol* 80, 1416–1423 (2006).

122. Ettinger, R. *et al.* IL-21 Induces Differentiation of Human Naive and Memory B Cells into Antibody-Secreting Plasma Cells. *Journal of Immunology* 175, 7867–7879 (2005).

123. Karnell, J. L. & Ettinger, R. The interplay of IL-21 and BAFF in the formation and maintenance of human B cell memory. *Front Immunol* 3, 2–2 (2012).

124. Appeltshauser, L. & Doppler, K. Pan-Neurofascin autoimmune nodopathy – a life-threatening, but reversible neuropathy. *Curr Opin Neurol* 36, 394–401 (2023).

125. Getahun, A., Smith, M. J. & Cambier, J. C. Mechanisms of Peripheral B Cell Tolerance. *Encyclopedia of Immunobiology* 1, 83–91 (2016).

126. Kinnunen, T. *et al.* Specific peripheral B cell tolerance defects in patients with multiple sclerosis. *J Clin Invest* 123, 2737 (2013).

127. Wenke, N. K. *et al.* N-methyl-D-aspartate receptor dysfunction by unmutated human antibodies against the NR1 subunit. *Ann Neurol* 85, 771–776 (2019).